UNIVERSITY OF SOUTHAMPTON

FACULTY OF MEDICINE, HEALTH & LIFE SCIENCES

School of Biological Sciences

Interaction of a Membrane Protein with its Surrounding Lipid Bilayer: Studies with the Mechanosensitive Channel MscL

by

Andrew M Powl

A thesis presented for the degree of
Doctor of Philosophy

Biochemistry & Molecular Biology December 2004

UNIVERSITY OF SOUTHAMPTON

ABSTRACT

FACULTY OF MEDICINE, HEALTH & LIFE SCIENCES
SCHOOL OF BIOLOGICAL SCIENCES

Doctor of Philosophy

INTERACTION OF A MEMBRANE PROTEIN WITH ITS SURROUNDING LIPID BILAYER: STUDIES WITH THE MECHANOSENSITIVE CHANNEL MscL

By Andrew Michael Powl

Mechanosensitive (MS) channels open in response to membrane stretch. All organisms require the ability to detect mechanical stimuli and MS conductances have been characterised in a diverse range of cells, reflecting the importance of these channels in many physiological processes. The most studied of the MS channels is the bacterial mechanosensitive ion channel of large conductance, MscL. Interactions between the lipid bilayer and MscL are particularly important since MscL opens on increasing tension in model systems containing just lipid and MscL, so that membrane tension must be transduced directly from the lipid molecules to the protein. Key to understanding how stretching of the lipid bilayer leads to opening of MscL is understanding how MscL interacts with the lipid bilayer. Site directed mutagenesis and fluorescence spectroscopy were used to define how the MscL channel interacts with the lipid bilayer that surrounds it in the membrane. Single Trp-containing mutants of *Mycobacterium tuberculosis* MscL were reconstituted into lipid bilayers of defined composition. Fluorescence emission maxima were used to identify the transmembrane region of MscL in bilayers of dioleoylphosphatidylcholine (di(C18:1)PC) and the levels of fluorescence quenching by brominated lipid gave lipid binding constants for MscL in the vicinity of the Trp groups. Introducing a lysine residue into the central pore of MscL generated a gain of function phenotype, thereby allowing the lipid-protein interactions of both the open and closed channel to be determined. Preferential binding was observed with phosphatidylcholines possessing fatty acyl chains with a length of C16 for the closed channel and C14 for the open channel, suggesting the open channel has thinned by 4 Å. All lipid head groups bind equally well to MscL on the periplasmic side of the membrane. In contrast, anionic lipids bind with significantly greater affinity on the cytoplasmic side of MscL, with two classes of binding site involving the conserved charge cluster Arg-98, Lys-99 and Lys-100. This binding site is broken up when the channel forms an open structure.

Contents

CONTENTS

CHAPTER 2: GENERAL MATERIALS AND METHODS

LIST OF TABLES

Chapter 7: Characterisation of the Open MscL Channel

LIST OF FIGURES

Chapter 1: General Introduction

Chapter 2: General Materials and Methods

Chapter 3: Fluorescence and the Properties of Trp Residues

Chapter 4: Characterisation of MscL: Binding of Phospholipids to MscL as a Function of Phospholipid Structure

Chapter 5: Determining the Hydrophobic Thickness of MscL

Chapter 6: Lipid Head Group Interactions with TbMscL

Chapter 7: Characterisation of the Open MscL Channel

ACKNOWLEDGMENTS

First and foremost I would like to thank Tony for his excellent supervision during my time at Southampton. Not only is he a brilliant mentor but also a friend. He helped me achieve my potential as a PhD student and develop as a person, for which I will be eternally grateful... oh, and he helped with the English too! A huge thanks also go to Malcolm for getting me started in the 'black art' of molecular biology, for offering advice, being great fun to work with and for bringing interesting cakes back from his visits up tut north!

Thanks to all the members of the AGL/JME group, and of course, the rest of lab 4061 for being such an interesting bunch of people to work with. Within the group I would especially like to thank Barbara for looking after me while I found my lab feet, thanks also go to Sanjay, John(y-boy) (my partner in crime), Trish and Liz. I should also like to thank Nicki-nickster, in addition to the numerous people from around the department and building who shared their expertise, encouraged and supported me.

To my friends, you're all fantastic. Thank you for making my time at Soton really enjoyable, alleviating the stress and keeping me sane (?!?), especially while I was writing up (in no particular order): Krys, Mich 1 & 2 (you can argue who is which!) Adam, Rob, Sarah, Vezza, Gaz, Sam, Kate-bush, 'Ki-Ki' Kim, Owen, Andy 'Penn-dulum' & Charlie-warlie. Good luck guys, you all deserve to do well ☺.

To my family, the biggest THANK YOU of all. To my big bro' Alastair, thank you for 'paving the way'. To my Dad, thank you for your support during my earlier days at Soton, and thanks to Auntie Janet for your lovely letters and help when times were tight. Lastly, to my super Mum, thanks for always encouraging and believing in me, being brave enough to read my work (despite it probably appearing as scientific gobbledygook to you), financial support and travelling hundreds of miles at a moments notice to visit and bring me food parcels - you're a star '☆'.

ABBREVIATIONS

BSA	Bovine serum albumin
bp	Base pair
CD	Circular dichroism
CMC	Critical micelle concentration
$C_{12}E_8$	Dodecylpoly(ethyleneglycolether)$_8$
di(C12:0)PC	Didodecylphosphatidylcholine
di(C14:1)PC	Dimyristoylphosphatidylcholine
di(C16:1)PC	Dipalmitoleoylphosphatidylcholine
di(C18:1)PA	Dioleoylphosphatidic acid
di(C18:1)PC	Dioleoylphosphatidylcholine
di(C18:1)PE	Dioleoylphosphatidylethanolamine
di(C18:1)PG	Dioleoylphosphatidylglycerol
di(C18:1)PS	Dioleoylphosphatiodylserine
di(Br_2C18:0)PC	1,2-di(9,10-dibromostearoyl) phosphatidylcholine
di(C20:1)PC	Dieicosenoylphosphatidylcholine
di(C22:1)PC	Dierucoylphosphatidylcholine
di(C24:1)PC	Dinervonylphosphatidylcholine
DDM	*n*-Dodecyl-β-D-maltoside
DMSO	Dimethyl sulphoxide
DSS	Disuccinimidyl suberate
EGTA	Ethyleneglycol-bis(β-aminoethylether)-N,N,N',N'-tetraacetic acid
ESR	Electron spin resonance
FET	Fluorescence energy transfer
GOF	Gain of function
Hepes	N-(2-hydroxyethyl)piperazine-N'-(2-ethyanesulphonic acid)
IANBD	N-((2-(iodoacetoxy)ethyl)-N-methyl)amino-7-nitroben-2-oxa-1,3-diazole
IPTG	Isopropyl-β,D-thiogalactopyranoside
kB	kilo base pair
kDa	kilo Daltons
LDAO	N,N-Dimethyldodecylamine-N-oxide
LOF	Loss of function
MS	Mechanosensitive
MscL	Mechanosensitive ion channel of large conductance

NBD	N-methyl amino-7-nitroben-2-oxa-1,3-diazole
OG	*n*-Octyl β-D-glucopyranoside
PAGE	Polyacrylamide gel electrophoresis
PBS	Phosphate buffered saline
PC	Phosphatidylcholine
PCR	Polymerase chain reaction
PE	Phosphatidylethanolamine
PG	Phosphatidylglycerol
PS	Phosphatidylserine
SDS	Sodium dodecyl sulphate
TAE	Tris-acetate ethylenediamine tetraacetic acid
TCEP	Tri(2-carboxyethyl)phosphine hydrochloride
TEMED	N,N,N',N'-tetraetylmethylene diamine
tetra(C18:1)CL	Tetraoleoylcardiolipin
TLC	Thin-layer chromatography
TM	Transmembrane
Triton X-100	t-Octylphenoxypolyethoxyethanol

Standard three letter amino acid and element abbreviations are used.

Chapter 1:

General Introduction

1 GENERAL INTRODUCTION

1.1 Membranes

Membranes separate cells from their external environment by forming a highly selective permeability barrier; membranes also separate the organelles within cells. This allows the cell to regulate the transfer of material between intracellular and extracellular locations and create distinct microenvironments in order for highly specialised reactions to occur.

Membranes are complex structures, largely composed of lipids and proteins with a smaller contribution from membrane conjugated carbohydrates (Berg et al., 2002); only the lipid and protein components are fundamental to the mechanics of a working membrane. These membrane building blocks adopt the structure of a fluid mosaic, in which lipids are arranged to form an asymmetric bimolecular layer approximately 60 Å thick, with the hydrophobic domains of proteins embedded within the lipid bilayer, while the hydrophilic domains of these proteins project from the bilayer surface (Figure 1.1) (Singer and Nicholson, 1972).

The relative proportions of lipid and protein that make up a given membrane vary considerably among species, cell types and even among the organelles within each cell (Table 1.1). Furthermore, the membrane composition may be altered in response to environmental influences and in the case of animal cells, in response to diet (Gould et al., 1987; Ingraham et al., 1987). Despite large variations in their composition, biological membranes are fluid under physiological conditions, enabling both lipids and untethered proteins to diffuse rapidly within the lateral plane of the membrane (Cullis et al., 1996). Overall, the organisation of the membrane into large, dynamic structures, allows the bilayer to continually change shape, offer an extensive source of functional diversity, and hence, evolve with the needs of the cell.

1.2 Membrane Lipids

Lipids are the primary structural components of biological membranes and are responsible for the formation of the membrane matrix, establishing compartments, and creating the permeability barrier. They are amphipathic species, containing both polar and apolar domains, and each lipid may be formed from a large range of hydrophobic fatty acyl chains, in combination with a diverse range of hydrophilic polar head groups. Therefore, a membrane has the potential to contain 1000 or more different lipid species, each with their own distinct physiochemical properties. Despite huge diversity, membrane lipids may be classified into three main constituent groups: phospholipids; glycolipids; and sterols (Berg et al., 2002).

1.2.1 *Phospholipids*

Phospholipids constitute the major lipid component of biological membranes, and can be further subdivided into phosphoglycerides and sphingomyelins. The simplest phosphoglyceride, phosphatidic acid, consists of a glycerol-3-phosphate backbone esterified with two fatty acyl chains (Figures 1.2 and 1.3). The fatty acyl chains are normally unbranched and contain an even number of carbon atoms of between C14 and C24 in length (Table 1.2). However, the two acyl chains may differ in length and the glycerol *sn*-1 position is normally occupied by a saturated chain, whereas the *sn*-2 position is occupied by an unsaturated fatty acid in a *cis* configuration (McKee and McKee, 1999). The *cis* double bond creates a kink within the acyl chain, which prevents tight packing of the chains, and ultimately enhances membrane fluidity.

Phosphatidic acid is the simplest of the phosphoglycerides. Esterification of the phosphate group to the hydroxyl group of one of a number of alcohols expands the lipid diversity further (Dowhan and Bogdanov, 2002). Phospholipids are classified with respect to their alcohol moiety (Figure 1.3).

Sphingomyelins differ from phosphoglycerides in that they are derived from a sphingosine backbone, which contains its own long unsaturated hydrocarbon tail in addition to a second fatty acyl chain linked via the sphingosine amide bond. The

head group is formed by esterification of the sphingosine hydroxyl group with a phosphoryl choline (Figure 1.2) (Alberts et al., 2002).

1.2.2 *Glycolipids*

Glycolipids are sugar containing lipids. When the lipid backbone is derived from sphingosine, they are also known as the glycosphingolipids. However, glycolipids differ from sphingomyelins in that they contain no esterified phosphate, but instead contain either a monosaccharide, disaccharide, or oligosaccharide linked to the sphingosine hydroxyl group via an O-glycosidic bond (Figure 1.2) (McKee and McKee, 1999).

1.2.3 *Sterols*

Sterols are complex molecules containing four fused carbon rings. The major sterol found in eukaryotic membranes is cholesterol (Figure 1.2). The large sterol ring intercalates perpendicular to the plane of the membrane, with the hydrophobic chain buried within the bilayer matrix (McKee and McKee, 1999). Despite the amphipathic nature of cholesterol, this lipid is unable to form membrane bilayers on its own, and the amount of cholesterol in mammalian membranes never exceeds 50 mole % of the total membrane lipid composition. Cholesterol is an important regulatory component of membrane fluidity, while hydrogen bonding of the hydroxyl group on cholesterol to the phospholipid backbone immobilises the lipid interface, effectively decreasing membrane deformability and permeability, and at higher concentrations has the ability to inhibit phase transitions (Alberts et al., 2002).

1.3 Lipid Phase

Lipids form the bilayer matrix and offer mechanical stability to the membrane. They achieve their structural role through spontaneous aggregation into highly cooperative, ordered structures known as lipid phases when in an aqueous environment. This process is driven by the hydrophobic effect, whereby the hydrocarbon chains of lipids disrupt the highly organised hydrogen bonded structure of water (Tanford, 1980). In

order to reduce this disruption, the hydrocarbon chains associate together, effectively minimising the total surface area exposed to water, while the polar lipid head groups interact favourably with the aqueous phase (Dowhan and Bogdanov, 2002).

The transition from lipid monomer to an ordered structure containing many lipid molecules depends upon a broad range of factors that include hydration, temperature, lipid concentration, ionic strength of the aqueous phase, and the physical properties or geometric 'shape' of the lipid (Cullis et al., 1996). The shape is the main factor that determines the structure of the self-associated phase formed, and refers to a number of characteristic features possessed by each lipid that includes the size and polarity of the head group, in relation to the size and saturation state of the hydrophobic fatty acyl chains (Table 1.3) (Cullis et al., 1996). Depending upon the lipids present, aggregates can include lamellar, hexagonal, or cubic phases (Figure 1.4). Within these structures the acyl chains are sequestered away from the aqueous phase, maximising van der Waals interactions, while the polar head groups form hydrogen bonds and electrostatic interactions with water. Therefore, each phase results from a balance between the hydrophobic effect, geometric packing constraints, and intra- and intermolecular interactions (Seddon and Templer, 1995).

The most common lipid in mammalian membranes, phosphatidylcholine (PC), has a cylindrical shape, since the surface area occupied by the head group region is similar to that occupied by the acyl chains. Cylindrical shaped lipids best organise into lamellar bilayers (Figure 1.4 and Table 1.3) (Dowhan and Bogdanov, 2002). The lamella phase is normally liquid crystalline under physiological conditions due to the fatty acyl chains being unsaturated. In contrast, fatty acyl chains are packed into highly ordered structures in the gel phase. The temperature at which the phase transition occurs increases with fatty acyl chain length and is reduced by the presence of *cis* double bonds, since *cis* double bonds introduce kinks into the chain, making close packing of the fatty acyl chains more difficult (Lee, 1983). Transition from the gel to the liquid crystalline phase is accompanied by a large lateral expansion, a decrease in the thickness of the bilayer and a small increase in the total volume occupied by the lipid molecules (Cullis et al., 1996).

Lipids with a small surface area in relation to their acyl chains are cone shaped (Table 1.3). These lipids arrange into large three-dimensional rod-like structures with the polar head groups surrounding an aqueous centre, while the acyl chains project outwards. The surface of the rod is hydrophobic, allowing an infinite number of rods to pack together to form a hexagonal structure, termed the hexagonal H_{II} phase (Figure 1.4) (Lee, 2000). In contrast, lipids with head groups that occupy a greater surface area than their acyl chains have a geometric shape analogous to an inverted cone (Table 1.3). Such shapes pack together to adopt a non-bilayer micelle structure, whereby the head groups are exposed to, and interact with the aqueous phase, while the acyl chains orientate towards the centre. Micelles also organise into two-dimensional tubular arrays, termed the hexagonal H_I phase. The space between micelle cylinders is separated by an unbroken aqueous phase (Figure 1.4) (Seddon and Templer, 1995). H_I phase forming lipids generally include those with ionised head groups, since these lipids experience charge-repulsion from neighbouring ionised lipids. The charge-repulsion effectively increases the size of the head group by preventing close association of the lipids (Cullis et al., 1996). Correspondingly, lysophospholipids containing only a single acyl chain will also have a head group size which exceeds that of the acyl chain, and therefore these lipids also adopt a micellar structure (van Voorst and de Kruijff, 2000).

The most structurally complex lipid phase is that formed by lipids with three-dimensional cubic symmetry, termed the cubic phase. These assemblies can be further subdivided into two distinct families: bicontinuous and micellar cubic phases both of which may exist as either normal (type I) or inverted (type II) cubic phases (Seddon and Templer, 1995). The bicontinuous phase consists of a highly curved bilayer folded into a regular pattern of two separated, but intertwined labyrinths, formed by a continuous network of lipid and an interconnecting network of aqueous channels. The water within these channels is able to exchange with the bulk aqueous phase (Figure 1.4) (Epand, 1998). In the micellar cubic phase, micelle aggregates are packed with cubic symmetry and water is trapped inside the structure, unable to exchange with bulk aqueous phase (Landau and Rosenbusch, 1996).

1.4 Lipid Polymorphism

A given cell or organelle contains a diverse range of lipids and lipid shapes, but the membrane predominantly adopts the bilayer structure or lamellar phase. The lamellar phase is the phase of choice for biological systems, as it is the only phase capable of forming sealed structures and maintaining a permeability barrier (Dowhan and Bogdanov, 2002). Surprisingly, 40 mole % of the total membrane lipid content may be non-bilayer forming lipids that prefer the hexagonal H_{II} arrangement e.g. phosphatidylethanolamine (PE), or in the case of certain species such as *Escherichia coli* these values are higher (75 mole %). However, lipids that favour non-bilayer phases can be stabilised into bilayer arrays by the presence of 10-50 mole % of lipids that prefer to adopt a bilayer structure (Cullis et al., 1996).

The levels of non-bilayer lipids in a membrane are tightly regulated, and non-bilayer species are believed to have important functional roles by creating membrane diversity, serving as signalling molecules, altering the structural and thermodynamic properties of the membrane, and modulating the function of proteins either embedded or interacting with the bilayer (de Kruijff, 1997; Epand, 1998; Lee, 1998; Simidjiev et al., 2000; Lee, 2004). It has been suggested that the ability of non-bilayer lipids to exert large affects on the lateral pressure profile of a membrane could also be important (Cullis et al., 1996).

1.5 Lateral Pressure Profile

When a lipid bilayer is formed and reaches a state of equilibrium, the net lateral pressure forces acting over the thickness of the entire bilayer is approximately zero to give a stable planar structure (Ben-Shaul, 1995; Lee, 2004). However, at different depths within the bilayer there are localised and nonuniform pressures, which give the bilayer a lateral pressure profile (van Voorst and de Kruijff, 2000). These localised pressure regions originate from two distinct areas within the membrane, the negative surface tension created at the hydrophilic/hydrophobic interface and a second, broadly distributed, positive pressure, resulting from the conformational entropy of the acyl chains, and to a lesser degree head group repulsions (Marsh, 1996). The

negative interfacial tension drives the bilayer to close up and exclude water, effectively minimising the area occupied by each lipid molecule. However, the disordered lipid acyl chains make a large and opposite contribution to the bilayer, which prevents close packing of the lipids (Figure 1.5) (Seddon, 1990). These two distinct pressure regions are normally equal and opposite, and hence cancel each other out. Although the lateral pressures cannot be measured directly, molecular models predict that the size or charge of the head group, level of unsaturation and position of the *cis* double bond(s) greatly influences and alters the pressure profile (Cantor, 1999).

As described in Section 1.4, non-bilayer lipids in isolation normally adopt their preferred phase, or lowest free energy configuration corresponding to highly curved structures. However, when present in the heterogeneous environment of a biological membrane, those lipids that readily adopt the lamellar phase force non-bilayer lipids to adopt planar arrays, resulting in curvature strain or a 'frustrated' bilayer state (Bezrukov, 2000). Depending upon the non-bilayer lipids present, the bilayer may experience either positive or negative curvature strain of its bilayer leaflets (Figure 1.5) (Epand, 1998). The frustrated bilayer has lipid packing defects that results in a less uniform lateral pressure profile, with the potential to generate distinct and localised pressured forces in the membrane bilayer corresponding to many hundreds of atmospheres (Figure 1.5) (Cantor, 1997b). Therefore, non-bilayer species within the membrane result in changes in lateral bulk pressures, which could in turn, be transmitted to all species contained within the membrane including integral membrane proteins (Cantor, 1997a). This has the potential to influence and interfere with conformational changes of membrane proteins, and thereby greatly affect membrane protein functioning within the membrane milieu (van Voorst and de Kruijff, 2000).

1.6 Membrane Proteins

Protein forms the largest component by weight of many types of membranes (Table 1.1). They are responsible for providing membrane specialism, by regulating the transfer of material into and out of the cell and ultimately allowing the membrane

enclosed space to become a dynamic system. Membrane proteins are classified into two main groups according to their structural relationship to the membrane, the integral and the peripheral proteins (Figure 1.1) (McKee and McKee, 1999).

1.6.1 *Peripheral Membrane Proteins*

Peripheral, or membrane associated proteins are located on the surface of the membrane. They are anchored to the bilayer surface by either associating with integral membrane proteins or with lipids and bind to the membrane via one or a combination of the following interactions, calcium bridging, hydrogen bonding, hydrophobic interactions, and weak electrostatic interactions. However, all these interactions are non-covalent and easily disrupted, which allows peripheral membrane proteins to be easily released from the membrane surface through relatively mild treatments that leave the membrane intact, such as changes in pH or ionic strength (Alberts et al., 2002).

1.6.2 *Integral Membrane Proteins*

Integral membrane proteins are amphipathic in nature possessing both hydrophilic and hydrophobic regions. The latter regions are composed predominately of hydrophobic amino acid residues that traverse the membrane and interact with the acyl chains of lipids. The hydrophilic domains of integral membrane proteins are exposed to water on either side of the membrane, where they act to anchor the protein within the bilayer. Good van der Waals contacts are generally achieved between membrane lipids and integral membrane proteins, with lipid chains sometimes binding into distinct grooves formed on the surface of the protein. Interactions between lipid head groups and proteins can sometimes be very specific or can be non-specific, involving charged and hydrogen bonding interactions with the protein (Lee, 2003; Lee, 2004). Unlike peripheral membrane proteins, removal and isolation of integral membrane proteins from the membrane requires complete disruption of the bilayer with detergents (Garavito and Ferguson-Miller, 2001).

The energetic cost of transferring a peptide bond from water into a nonpolar environment is about 25 kJ mol^{-1} when not hydrogen-bonded, compared with the much lower value of about 2.5 kJ mol^{-1} when hydrogen-bonded (Roseman, 1988).

Therefore, although hydrophobic residues are required to span the bilayer, the polar backbone of the polypeptide chain must also be satisfied as it can not simply pass straight through the hydrophobic membrane interior, due to the high energy barrier incurred by exposing the polar backbone regions to the hydrophobic membrane interior. Instead the polypeptide chain adopts a repeating conformation, either as an α-helix or as a β-barrel (Figure 1.6). The whole process is driven by the necessity of the polypeptide backbone to form a hydrogen bonded structure (Mall et al., 2002). In the α-helix the polypeptide chain becomes tightly coiled, with the polar backbone forming the inner part or core of the helix and stabilised by an extensive array of hydrogen bonds between all the main-chain NH and CO groups. The hydrophobic side chains in the transmembrane α-helices extend out from the rod-like structure in a helical array. The β-sheet is a more extended structure and is stabilised by hydrogen bonds between NH and CO groups in adjacent and/or different polypeptide strands, which may run in the same or opposite direction (Berg et al., 2002).

1.7 Osmosis

The selective permeability barrier formed by the lipid bilayer allows rapid and spontaneous diffusion of water molecules (10^{-2}-10^{-4} cm s^{-1}) into and out of the cell, while preventing the movement of many biological molecules across the membrane (Cullis et al., 1996). However, nutrients and ions can be selectively taken up through membrane proteins and become concentrated within the cell. This creates a concentration gradient and results in an osmotic pressure difference ($\Delta\Pi$) across the cell membrane; water molecules will then spontaneously transfer from the extracellular environment into the cell, in order to equilibrate the chemical potential of the water (Morris, 1978). The movement of water into the cell increases the cell volume and generates turgor pressure on the membrane; under normal conditions turgor pressure is 1-5 atm for Gram-negative bacteria and 15-25 atm for Gram-positive bacteria (Csokna, 1989), and provides the driving force behind bacterial cell growth and expansion (Booth and Louis, 1999). However, under severe hypoosmotic stress, turgor pressure ultimately has the potential to lyse the cell unless the osmotic gradient is regulated in some way.

1.8 Osmoregulation in Bacteria

One of the most fundamental of homeostatic processes in a prokaryotic organism is the ability to regulate the osmotic pressure across the cytoplasmic membrane. Following an increase in the osmolarity of the medium, water diffuses out of the cells causing the cell volume to decrease. Following a decrease in the osmolarity of the medium, passive influx of water into the cell will increase turgor and ultimately lyse the cells. However, bacteria compensate for shifts to the external osmolarity of the medium through the activation of numerous channels and transporters that, in turn, adjust a pool of low molecular weight solutes (osmolytes), and hence regulate turgor pressure and maintain osmostasis (Table 1.4) (Booth and Louis, 1999; Wood et al., 2001; Poolman et al., 2004)

1.8.1 *Hyperosmotic Stress*

Bacteria counteract hyperosmotic stress by accumulating compatible solutes by uptake and/or synthesis of specific osmolytes, termed osmoprotectants, that can be accumulated to high levels without affecting vital cell processes (Bremer and Krämer, 2000); accumulation of compatible solutes occurs in proportion to the osmolarity of the surrounding medium (Wood et al., 2001). Osmoprotectants prevent shrinking of the cell and stimulate the rate of growth of hyperosmotically stressed bacteria, by allowing the cell to maintain turgor (Poolman and Glaasker, 1998). Osmoprotectants commonly include amino acids (glutamate, proline), polyols and sugars (glycerol, treahalose), and quaternary ammonium compounds (glycine betaine, carnitine) (Wood, 1999). Osmoprotectants can be synthesised *de novo*, in an active process tightly regulated at the level of transcription (Csokna, 1989). However, the most rapid response to hyperosmotic shock involves the activation of solute transporters already present in the membrane (Poolman et al., 2004), which accumulate osmoprotectants from exogenous sources that include those released from other hypoosmotically shocked cells, decaying microbes, and mammalian excretions (Wood, 1999). The accumulation of neutral or zwitterionic compatible solutes is often associated with the displacement of ionic solutes such as potassium and glutamate from the cell, with no overall change in osmotic potential. This is because

neutral solutes are more favourable to protein stability than ionic solutes; in most bacterial species glycine betaine is the osmoprotectant of choice (Poolman and Glaasker, 1998).

The ATP-binding cassette transporter OpuA (Table 1.4), is the main osmoregulated transporter for quaternary compounds in *Lactococcus lactis* and has been studied in great detail (van der Heide et al., 2001; Poolman et al., 2004). OpuA, the sequence homologue of ProU from *E. coli*, protects the organism against hyperosmotic stress via the transport of glycine betaine against its chemical gradient, in an active process that requires two molecules of ATP (Wood, 1999; Poolman et al., 2004). The osmosensing mechanisms of OpuA was originally proposed to be regulated by distortions in the lipid bilayer, for example, membrane ruffling (van der Heide and Poolman, 2000). However, it has now been shown to be dependent on electrostatic interactions between the protein and anionic lipids. It is suggested that changes in osmotic strength, associated with the flux of water, leads to a change in the ionic strength at the internal surface of the membrane, which, in turn, alters anionic lipid-protein interactions and leads to activation of the transporter. Although activity was found to be chain length dependent, with a maximum at C18, changing the chain length of the phosphatidylcholine in mixtures with di(C18:1)PG did not affect the activation threshold (van der Heide et al., 2001).

The BetP transporter has a similar function to OpuA but is unrelated in structure (Table 1.4); it catalyses the symport of glycine betaine with two sodium ions. Changes in osmotic strength and therefore interfacial ionic strength, may have a similar affect on BetP as on OpuA, since the activation threshold of BetP shifts to higher osmolarities when the fraction of di(C18:1)PG in the membrane is increased (Rübenhagen et al., 2000). Furthermore, the intracellular C-terminal domain of BetP is composed of 23 amino acid residues with a net charge of approximately +10, which would facilitate interaction of the C-terminal domain with the anionic membrane surface (Poolman et al., 2004). Removal of the C-terminal domain renders the transporter constitutively active and insensitive to intracellular potassium ion concentrations (Peter et al., 1998; Rübenhagen et al., 2001), thus implicating the C-terminal domain in the sensory mechanism of BetP (Wood, 1999).

The data obtained with OpuA and BetP argue against the bulk properties of the bilayer being important for activation. Instead the osmosensing 'switch' for these transporters in response to hyperosmotic shock, appears to be the result of changes in osmotic strength as a result of changes in cell volume. This, in turn, leads to a change in the ionic strength at the membrane surface, and hence to altered anionic lipid-protein interactions (van der Heide et al., 2001; Poolman et al., 2004).

1.8.2 *Hypoosmotic Stress*

Following a shift to a medium of low osmolarity, bacteria release ions (mainly potassium), small metabolites and osmoprotectants, in order to dissipate the excess turgor pressure. The efflux of potassium and osmoprotectants, triggered by osmotic downshock, occurs at very high rates and has been reported in *E. coli* and *Salmonella typhimurium*; the extent of solute loss is related to the severity of the hypoosmotic shock (Ingraham et al., 1987; Csonka, 1989; Glaasker et al., 1996). The efflux of solutes does not severely damage the cells, since reaccumulation of glycine betaine is observed when the osmolarity of the medium is raised to the level before hypoosmotic shock (Bremer and Krämer, 2000). Electrophysiological studies with the cytoplasmic membranes of *Eubacteria* and *Archaea* have revealed the presence of mechanically gated channels (Table 1.4) with high levels of conductance (Berrier et al., 1996; Le Dain et al., 1998). The high rates and the nonspecificity of these channels led Berrier et al. (1992) to propose that the mechanically gated channels may be the exit pathway for solutes during hypoosmotic shock, since gadolinium inhibited both mechanosensitive channels and the efflux of metabolites (such as lactose and ATP) from osmotically shocked cells (Berrier et al., 1992).

1.9 Mechanosensation

Mechanosensation is the ability to detect mechanical stimuli applied to a cellular membrane. Mechanosensitive channels were first observed in chick skeletal muscle in 1984, using patch-clamp electrical recordings (Guharay and Sachs, 1984). However, all organisms require the ability to detect mechanical force and this is reflected in the diverse range of cells where mechanosensitive conductances have

been characterised, which include neurones, oocytes, muscle, heart, kidney, blood, lens, plant roots and leaves and microorganisms (Sackin, 1995; Sukharev et al., 1997). Although the role of mechanosensitive channels is to transduce a pressure force, the response elicited is cell and organism specific, and mechanosensitive channels have roles in many important physiological processes, including hearing, balance, touch, cardiovascular and renal regulation, geotropism and osmoregulation (Hamill and McBride, 1993; Hamill and Martinac, 2001). In mammalian cell types, mechanosensitivity not only involves interaction with the membrane, but also components of the cytoskeleton, whereas in bacterial systems these channels are activated by interaction with the membrane alone. Therefore, although eukaryotes and prokaryotes mechanosensitive channels are different, bacterial channels provide a simplified model system from which findings can be applied to their eukaryotic homologues.

1.10 Mechanosensitive Channels

The discovery of a bacterial, non-selective mechanosensitive channel, based on patch-clamp electrical recordings of giant *E. coli* spheroplasts in 1987, provided the most viable option for characterising mechanosensation, due to the amenability of *E. coli* to genetic manipulation and molecular biological techniques (Martinac et al., 1987). The protein (MscL) and subsequently gene (*mscL*) responsible for these conductances was successfully isolated and cloned, and shown to regulate turgor pressure upon hypoosmotic stress of this organism by releasing solutes and other small cytoplasmic components, while maintaining cell viability (Berrier et al., 1992; Sukharev et al., 1994). Confirmation of the pressure activated pathway came from patch clamp studies in which mechanical pressure or suction has been applied to a membrane patch and been seen to open mechanosensitive channels (Martinac et al., 1987; Berrier et al., 1989; Sukharev et al., 1994; Häse et al., 1995). Patch clamp studies with reconstituted MscL membranes exhibited channel activation, confirming that only lipid and protein (the mechanosensitive channel) are required (Sukharev et al., 1994). Lysolipids also activate MscL, but only when added to one surface of the bilayer, an effect that is thought to occur via an affect on the intrabilayer lateral

pressures profile (Perozo et al., 2002b), thereby confirming their activation via the membrane and not by some form of cytoskeletal interaction (Martinac et al., 1990).

Further studies revealed a number of distinct and unique conductances activated by membrane stretch that differed from patch to patch. Furthermore, native *E. coli* membranes had complex electrical activity (Berrier et al., 1989; Sukharev et al., 1993), with different conductances corresponding to distinct proteins located in the cell membrane of *E. coli*, which could be grouped into three subfamilies based on their single channel conductances: mini conductance, 0.4 nS (MscM); small conductance, 1 nS (MscS); and large conductance, approximately 3 nS (MscL), with the smallest channel being activated first and at lower levels of membrane pressure (Berrier et al., 1996).

E. coli cells are thought to contain only one or two functional copies of MscM per cell, whereas the abundance of MscS and MscL in a given bacterium is known to be around 20-30 per cell for MscS and five per cell for MscL (Stokes et al., 2003). Mechanosensitive channels exhibit some of the largest ion conductances recorded to date, in the range of 10^8 to 10^9 ions s^{-1} (Poolman et al., 2004). MscL appears to have no selectivity, expect for size of the solute (Berrier et al., 2000; Anishkin et al., 2003). However, MscM is believed to display a slight preference for cations over anions (Berrier et al., 1989), while MscS displays a slight preference for anions over cations, and in addition to mechanosensitivity, also demonstrates voltage dependence, with an increased open probability with membrane depolarisation (Martinac et al., 1987). The MscS homologue, MscK does not exhibit ion selectivity, but requires a high external cation concentration to gate, the role of the high external cation concentration not being completely understood (Li et al., 2002).

The genes responsible for the production of MscK, MscS, and MscL channels have been identified; however no gene has yet been described for MscM (Edwards et al., 2004). The presence of more than one channel in *E. coli* suggests redundancy, while also highlighting the importance of these channels. Redundancy was confirmed through *E. coli* knockout mutants $MscK^-$, $MscS^-$, and $MscL^-$ (Levina et al., 1999). Single mutants show no phenotypic difference from wild type when subjected to low

osmolarity media. However, the double mutant, MscS$^-$ and MscL$^-$ exhibited greater than 10-fold loss of cell viability when exposed to the same media.

Experiments with the *E. coli* knockout mutant MscL$^-$ have shown that removing MscL has no effect on the levels of release of glutamate and glycine betaine (Ajouz et al., 1998). However, deletion of the *mscL* gene does prevent the release of thioredoxin, and severely impaired the release of elongation factor Tu (EF-Tu) and DnaK; all these proteins are cytoplasmic proteins, the levels of which increase during hyperosmotic shock, and all are known to be excreted during hypoosmotic shock (Ajouz et al., 1998; Berrier et al., 2000). Furthermore, mutations in MscL that create a channel that opens more easily, have revealed that during osmotic downshock a higher level of cytoplasmic potassium is released from cells expressing the mutant channel than from cells expressing wild type MscL (Blount et al., 1997). Although these data support a role for MscL in the response to hypoosmotic shock, the release of osmoprotectants appears not to be mediated by MscL; instead the mechanosensitive channels, MscM, MscS and MscK may be responsible for the rapid efflux of compatible solutes (Ajouz et al., 1998). Experiments measuring the release of osmoprotectants from the *E. coli* knockout mutant MscS$^-$ appear not to have been carried out.

The presence of multiple channels is therefore considered a fail-safe or back-up mechanism, where MscL has functional analogy to an over-flow system and is only activated during acute and extreme turgor pressure, when MscM, MscK and MscS alone are unable to relieve sufficient turgor (Sukharev et al., 1994). Furthermore, the presence of multiple channels allow a graded response to different types of osmotic stress, allowing appropriate relief from turgor, in contrast to an all-or-none response that could potentially put the cell at a metabolic disadvantage (Berrier et al., 1996; Sukharev, 2000).

1.11 Mechanosensitive Channel of Large Conductance, MscL

The *E. coli* mechanosensitive channel isolated by Martinac et al. (1987) and the gene cloned by Sukharev et al. (1993) was shown to encode the mechanosensitive channel

of large conductance (MscL). To date, eight MscL homologues have been cloned and characterised by electrophysiological techniques (Moe et al., 1998), and an additional 30 homologues from all three phylogenetic domains have been identified (Martinac and Kloda, 2003). These channels are believed to function as pressure-valves, due to the ability of heterologous expressed MscL to retain their mechanosensitivity when expressed in *E. coli* and other bacterial strains lacking native MscL (Moe et al., 1998; Nakamaru et al., 1999).

Multiple sequence alignment indicates a good overall level of similarity for all regions, with membrane spanning domains exhibiting strong conservation (Figure 1.7). In particular, transmembrane helix one (TM1) is the most highly conserved region among all MscL family members, whereas the cytoplasmic loop region is the most variable (Moe et al., 1998). From sequence alignments, mechanosensitive channels of large conductance can be divided into at least five different subfamilies (Maurer et al., 2000). The largest subfamily, containing 13 members, includes the *E. coli* MscL (EcMscL). However, *Mycobacterium tuberculosis* MscL (TbMscL) belongs to a smaller subfamily that only has 37 % homology with EcMscL (Figure 1.8).

1.12 Structure of MscL

The X-ray crystallographic structure of the *M. tuberculosis* MscL homologue (TbMscL) was resolved in the closed state to 3.5 Å (Chang et al., 1998). X-ray crystallography revealed the protein to exist as a homopentamer, with an overall length of 85 Å and diameter of 50 Å (Figure 1.9). The structure can be divided into two major domains: membrane spanning (~50 Å) and cytoplasmic (~35 Å) domains.

The crystal structure confirms the topology of MscL elucidated from previous experiments by Blount et al. (1996c) and Arkin et al. (1998), illustrating that each monomer possesses two transmembrane α-helices. The inner transmembrane α-helix (TM1) from each MscL subunit starts in the cytoplasm and crosses the membrane to form a vase-like pore lined by several polar and charged residues (T25, T28, T32, T35, K33, and T35 in TbMscL). The pore alters in diameter from approximately 18

Å at the periplasmic face to 2 Å at the channel constriction, the latter formed by a ring of valines (Figure 1.10).

The second transmembrane α-helix (TM2) returns to the cytoplasm across the membrane to form the lipid facing helix. Both transmembrane α-helices (TM1 and TM2) are titled approximately 28° with respect to the bilayer normal and have a single helix contact point, with a crossing angle of 135° within the same subunit. Each TM1 helix has an additional three contacts with helices from the two neighbouring monomers, two with the two adjacent TM1 helices (crossing angles -43°) the third being with an adjacent TM2 helix (crossing angle 169°) (Chang et al., 1998).

Bowie (1997) has shown that the most common helix-packing angle in transmembrane proteins is approximately 20°. A crossing angle of 20° creates a large contact interface between the two helices, favouring helix interactions, this mode of packing is referred to as knobs-into-holes or ridges-into-grooves packing. However, a consequence of the relatively steep packing angles observed in MscL transmembrane α-helices would be limited ridges-into-grooves contact between membrane helices (Chothia et al., 1981). Reduced contact between helices may be expected to facilitate helix-helix rearrangements associated with mechanotransduction, and the formation of a large open pore.

The crystallisation of the closed channel provides a strong framework for site directed mutagenesis, structure-function and molecular modeling studies. However, it is important to note that the structure is incomplete, since the side chains of residues I56, L57, R58, I59, L97, K100, Q105, and R118 are absent. Furthermore, the extreme amino terminus (10 residues) and carboxyl terminus (39 residues) of TbMscL are not resolved in the structure. This is unfortunate, since the amino terminal residues are predicted to form amphipathic helices (S1), which are thought to have important roles in the formation of a second hydrophobic gate (Sukharev et al., 2001b), while the cytoplasmic helical bundle (S3) may provide stability to the open conformation, and function as a size-exclusion filter to the cytoplasmic entrance of the pore (Anishkin et al., 2003).

1.13 Channel Gates

In order to understand the gating properties of MscL, random and site directed mutagenesis have been employed to probe and alter the gating kinetics of the channel (Blount et al., 1996c; Ou et al., 1998; Yoshimura et al., 1999; Maurer and Dougherty, 2003; Bartlett et al., 2004). Two mutational phenotypes have been observed for MscL: gain of function (GOF) mutants that result in the channel opening either spontaneously or at lower tension thresholds than the wild type protein, and loss of function (LOF) mutants, where gating is completely abolished or greater tension is required to gate the channel than the wild type. GOF, or leaky mutants exhibit reduced growth rates due to an inability to retain solutes and therefore maintain turgor pressure, an effect reversed by growing some of these mutants in high solute medium (Yoshimura et al., 1999).

Mutational studies using the EcMscL homologue have shown that channel gating is most sensitive to mutagenesis at the narrowest region of the pore, a region composed of five valines located above five glycines (Gly-22 and Val-23), one pair being provided by each TM1 α-helix. Using sequence alignments, these residues have been mapped onto the high resolution structure of the TbMscL homologue and shown to be equivalent to residues Ala-20 and Val-21 (Figure 1.10). Hydrophobic substitutions at Gly-22 in EcMscL generated cells with a LOF phenotype, whereas hydrophilic substitutions decreased the threshold pressure, generating GOF phenotypes (Yoshimura et al., 1999). These data suggest that the primary gate in the TbMscL channel is maintained through hydrophobic interactions between the five valine residues, and five glycine residues in the EcMscL homologue.

Detailed analysis of patch clamp data suggests that the MscL channel passes through a series of at least five subconducting states before reaching the open state (Sukharev et al., 1999b). A thermodynamic analysis of the tension sensitivity of EcMscL predicted that the channel expands to around two-thirds of its open pore size before actually opening, suggesting the presence of additional gates in MscL (Sukharev et al., 2001b). It has been suggested that a second gate could be formed from either the S1 or S3 helices (Sukharev et al., 2001a; Anishkin et al., 2003).

The S1 helical bundle is absent from the crystal structure of MscL. These S1 helices have high sequence homology with all the other MscL homologues (Figure 1.7), and it is thought that five phenylalanines (F10-EcMscL and F8-TbMscL, Figure 1.8) may combine to form a second hydrophobic gate (Sukharev et al., 2001a). Deletion of the extreme amino terminus (EcMscLΔ2-11) up to and including the S1 helical bundle results in the loss of MscL activity, suggesting the importance of this region (Blount et al., 1996a; Blount et al., 1996c). The possible role of S1 helices was investigated experimentally, using single and double cysteine mutants located on S1 alone, or S1 and M2 helices (Sukharev et al., 2001a). Cross-linking S1 segments (F10C-EcMscL) to each other in the closed channel prevents opening of the channel, whereas cross-linking the I3C:I96C-EcMscL channel in the open state impedes channel closure. Despite the LOF phenotype observed with deletion mutants, random mutation of S1 helices has failed to alter channel gating kinetics or produce any phenotypic differences from wild type protein under normal conditions, in contrast to mutations in TM1 that consistently alter the channel kinetics (Ou et al., 1998; Maurer and Dougherty, 2003).

The carboxyl terminal (S3) domains are also conserved within the MscL family, and the crystal structure of MscL revealed a cytoplasmic helical bundle. However, in the high resolution structure the S3 helices are formed with hydrophobic groups facing the outside while charged residues are orientated towards the centre, and this is unlikely physiologically given that the S3 helical bundle is located in the aqueous environment of the cytoplasm. It is possible that the S3 domain takes up an unusual structure in the crystal structure because of the acidic crystallisation conditions (pH 3.0) (Chang et al., 1998; Anishkin et al., 2003). Instead, the helical S3 bundle has been modelled with aliphatic residues located on the inside of the bundle, and molecular dynamic simulations with the modified S3 helical bundle predicted higher stability for this conformation (Anishkin et al., 2003). Complete removal of the carboxyl terminal domain (EcMscLΔ110-136) did not cause loss of MscL activity, but instead increased the probability that the channel would occupy a subconducting state (Blount et al., 1996a; Anishkin et al., 2003). Furthermore, subjecting *E. coli* knock-out strain MJF465 expressing EcMscLΔ110-136 to an *in vivo* hypoosmotic stress, triggered the released of larger amounts of ATP than in wild type controls, and removal of an additional six residues EcMscLΔ104-136 abolished channel activity

(Blount et al., 1996a). Therefore, these data indicate that the bundle-like assembly of cytoplasmic helices may provide stability to the open conformation, while also functioning as a size-exclusion filter at the cytoplasmic entrance to the pore, preventing loss of essential metabolites (Anishkin et al., 2003).

Unlike ion channels with high selectivity, for example, the potassium channel KcsA (Doyle et al., 1998), the external, periplasmic loop of MscL (S2) that connects transmembrane α-helices (TM1 and TM2) in MscL is poorly conserved, and the crystal structure revealed that the loop region does not enter the channel. Furthermore, cleavage of the periplasmic loop (S2) did not alter channel conductance although, channel mechanosensitivity was increased, triggering channel opening at lower membrane pressures (Ajouz et al., 2000). Theses data suggests that packing of TM helices is sufficient to maintain channel structure and mechanosensitivity, while the loop serves as a spring that resists channel opening and promotes channel closure.

1.14 Gating Mechanism

The channel is tightly closed and absolutely non-leaky under normal conditions, and does not open until the membrane tension reaches a value close to the membranes lytic threshold (8-12 dyne cm^{-1}) (Betanzos et al., 2002). The estimated free energy (ΔG) for opening MscL is 46.3 kJ mol^{-1} (Sukharev et al., 1999b), and this high energy barrier prevents channel gating under normal conditions (Yoshimura et al., 2001). However, when open, MscL exhibits the largest channel conductance of any ion channel characterised to date, with a nonselective conductance of approximately 3 nS (Batiza et al., 1999). *In vitro* sieving experiments and conductivity measurements suggest that the open state of MscL may reach 30-40 Å in diameter (Cruickshank et al., 1997; Sukharev et al., 1999b). In addition, osmotically shocking *E. coli* cells *in vivo* triggers the release of thioredoxin, a 12 kDa protein, further supporting the formation of a large pore in the active state (Ajouz et al., 1998).

The X-ray crystallographic structure of the *E. coli* MscS channel has been solved in the open state to 3.9 Å (Bass et al., 2002). X-ray crystallography reveals the protein to exist as a homoheptamer, with an overall length of 120 Å and diameter of 80 Å

(Figure 1.11). The open pore size in the structure of the channel is approximately 11 Å, consistent with the channel conductance of 1 nS reported for this channel (Berrier et al., 1996; Blount, 2003). The resolved structure is also consistent with genetic and biochemical analyses, and confirms that MscS can be divided into two major domains, the membrane spanning domain (~50 Å), which contains three TM α-helices per monomer, and the cytoplasmic domain (70 Å), which forms a large chamber (Bass et al., 2002; Miller et al., 2003a).

The cytoplasmic domains of both MscS and MscL are thought to provide stability to the open structures and function as selectivity filters (Anishkin et al., 2003; Schumann et al., 2004). The pore-lining helices in MscS and MscL channels are tilted by approximately 30° with respect to the membrane normal. However, the cross-sectional areas generated by these arrangements are different for the two channels, due to the different oligomeric states of the channels (Perozo and Rees, 2003).

Unfortunately, the two structures of MscS and MscL in the open and closed states respectively, are thought to represent two different mechanisms for detecting bilayer tension, and are considered structurally too distinct to provide useful insight into the possible mechanism of channel gating (Miller et al., 2003b; Perozo and Rees, 2003). However, what is certain, is that MscL must undergo large conformational rearrangements in order to move from a closed channel of approximately 2 Å in diameter, to one with an open pore diameter of 30-40 Å (Batiza et al., 1999; Sukharev et al., 2001b; Perozo et al., 2002a). Furthermore, kinetic data reveals the presence of a number of subconducting states, as the channel goes from the closed to open state (Figure 1.12), consistent with a sequence of conformational changes, rather than one large change in the proteins tertiary structure (Sukharev et al., 1999b; Biggin and Sansom, 2001; Perozo et al., 2002b).

Electron spin resonance (ESR) spectroscopy and site directed spin labelling studies with EcMscL have suggested that, upon reaching a fully open state, TM1 helices flatten by 15° away from the bilayer normal while also shifting approximately 13 Å away from the axis. In addition, TM2 moves in unison with TM1, while also flattening by 17° towards the bilayer (Perozo et al., 2002b). This concerted rearrangement of transmembrane helices is also supported by crosslinking

experiments, where the helix contact points between TM1 and TM2 helices of neighbouring subunits were shown to remain constant throughout channel gating, confirming that both transmembrane helices tilt in unison (Betanzos et al., 2002).

Based upon molecular dynamic simulations, biochemical, and electrophysical data, TM1 and TM2 helices are thought to undergo large rearrangements with gradual increases in inter-helical tilt angles upon increasing bilayer tension (Figure 1.13), causing an iris-like expansion and reduction in the length of the pore as the channel enters one of the many intermediate states (Gullingsrud et al., 2001; Sukharev et al., 2001b; Betanzos et al., 2002; Perozo et al., 2002b; Colombo et al., 2003). The transmembrane α-helices (TM1 and TM2) move in unison and continue to move radially away from the pore's axis, an effect that results in the primary hydrophobic gate on TM1 (residues Gly-22 and Val-23) being broken (Kong et al., 2002; Perozo et al., 2002a,b). The second gate formed by the S1 helical bundle remains closed, and therefore the channel enters a closed-expanded state (Figure 1.13). As turgor pressure increases and the membrane reaches its lytic threshold, the S1-TM1 linker becomes fully stretched, thereby transferring the tension directly to the S1 helical bundle and breaking the second hydrophobic gate. S1 helices swing back towards the pore periphery, and dock with the pore wall and the channel is open (Figure 1.13). The cytoplasmic helical bundle (S3) remains associated in the cytoplasm, forming a size-exclusion filter providing stability to the open conformation (Anishkin et al., 2003).

Membrane	Percentage Mass by Weight		
	Lipid	**Protein**	**Carbohydrate**
Chloroplast inner membrane	30	70	-
Endoplasmic reticulum	27	62	10
Golgi complex	26	64	10
Mitochondrion:			
outer membrane	45	55	trace
inner membrane	22	78	-
Nuclear envelope	32	66	2
Plasma membranes:			
amoeba	42	54	4
liver cells	36	54	10
myelin	79	18	3
red blood cells	43	49	8

Table 1.1 Comparison of cell and organelle membrane composition. The amounts of lipid, protein and carbohydrate are approximate values per dry weight. Taken from Lotan and Nicholson (1981).

Common Name	Structure	Abbreviation
	Saturated Fatty Acids	
Lauric	$CH_3(CH_2)_{10}COOH$	12:0
Myristic	$CH_3(CH_2)_{12}COOH$	14:0
Palmitic	$CH_3(CH_2)_{14}COOH$	16:0
Stearic	$CH_3(CH_2)_{16}COOH$	18:0
Arachidic	$CH_3(CH_2)_{18}COOH$	20:0
Behenic	$CH_3(CH_2)_{20}COOH$	22:0
Lignoceric	$CH_3(CH_2)_{22}COOH$	24:0
	Unsaturated *cis* Fatty Acids	
Palmitoleic	$CH_3(CH_2)_5CH{=}CH(CH_2)_7COOH$	$16{:}1^{\Delta 9}$
Oleic	$CH_3(CH_2)_7CH{=}CH(CH_2)_7COOH$	$18{:}1^{\Delta 9}$
Linoleic	$CH_3(CH_2)_3(CH_2CH{=}CH)_2(CH_2)_7COOH$	$18{:}2^{\Delta 9,12}$
α-Linolenic	$CH_3(CH_2CH{=}CH)_3(CH_2)_7COOH$	$18{:}3^{\Delta 9,12,15}$
Arachidonic	$CH_3(CH_2)_3(CH_2{=}CHCH)_4(CH_2)_3COOH$	$20{:}4^{\Delta 5,8,11,14}$

Table 1.2 Examples of fatty acids commonly found in membrane lipids. The number on the left of the colon is the number of carbon atoms; the number on the right of the colon represents the number of double bonds, while the superscript denotes the placement of the double bond. Adapted from McKee and McKee (1999).

Geometric Shape	Phase	Amphiphile Example
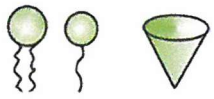 Inverted Cone	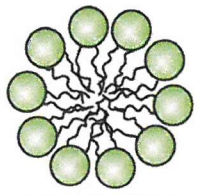 Micelle (H_I)	Lysophosphatidylcholine Lysophosphatidylethanolamine Oleic Acid Stearic Acid Detergents
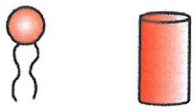 Cylindrical	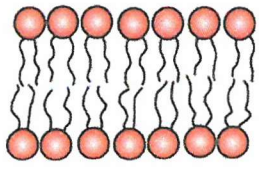 Lamellar	Phosphatidylcholine Sphingomyelin Phosphatidylserine Phosphatidylglycerol Cardiolipin Phosphatidylinositol Phosphatidic acid
 Cone	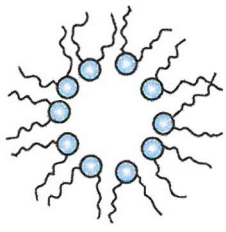 Hexagonal (H_{II})	Phosphatidylethanolamine Cardiolipin + Ca^{2+} Phosphatidic acid + Ca^{2+} Phosphatidic acid < pH 3.0 Phosphatidylserine < pH 4.0

Table 1.3 Geometric shapes and their associated aggregated structures, for a selection of amphipathic molecules. Adapted from Cullis et al. (1996).

Name	Type of System	Function
	Hyperosmotic Stress	
BetP	Na^+ electrochemical gradient	Uptake of glycine betaine
EnvZ	Sensor kinase	Regulation of expression of OmpC and OmpF
KdpD	Sensor kinase	Regulation of expression of P-type K^+-ATPase
OpuA	ABC transporter	Uptake of glycine betaine
ProP	H^+ proton motive force	Uptake of proline
	Hypoosmotic Stress	
MscK	Mechanosensitive	Efflux of osmolytes
MscL	Mechanosensitive	Efflux of osmolytes
MscS	Mechanosensitive	Efflux of osmolytes

Table 1.4 Bacterial channels and transporters associated with maintaining osmostasis. Modified from Poolman et al. (2002).

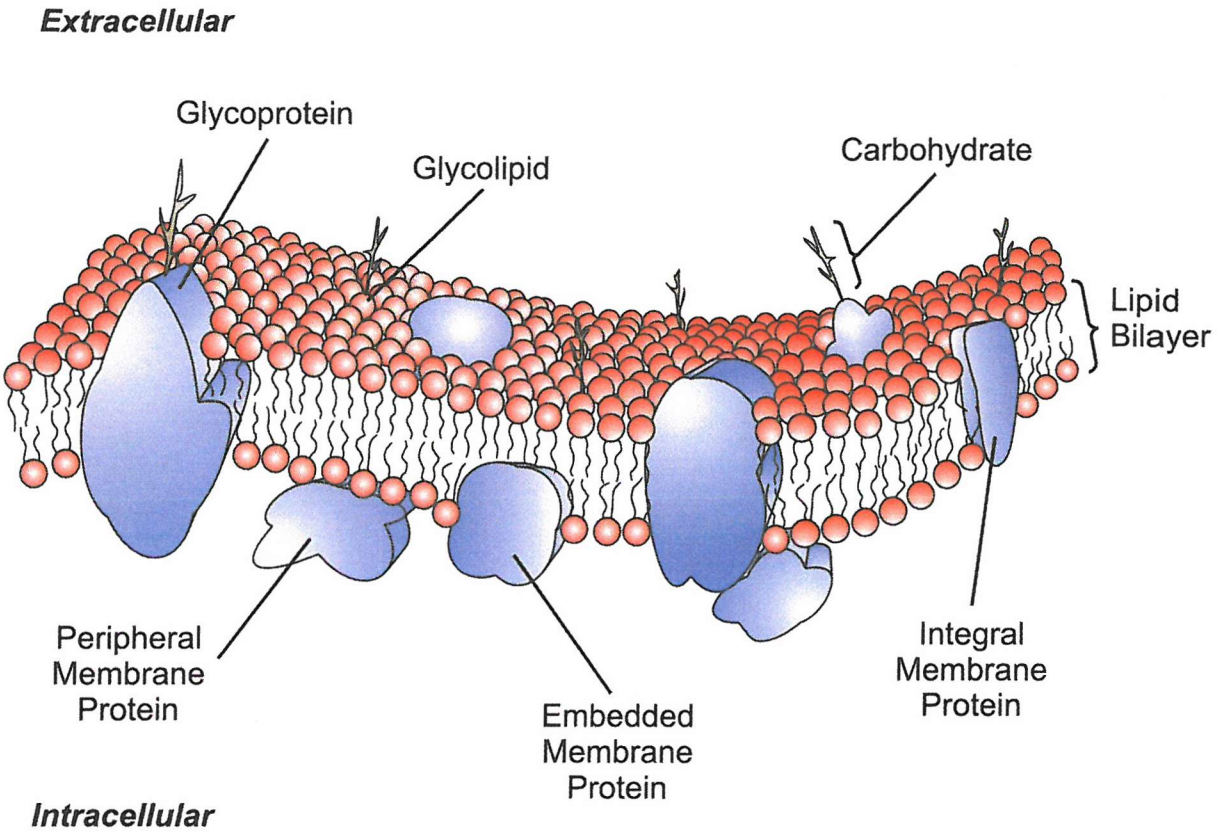

Figure 1.1 The fluid mosaic model of the biological membrane. The phospholipid bilayer is shown with proteins either embedded or traversing the bilayer. Both membrane lipids and untethered proteins diffuse within the lateral plane of the membrane. Peripheral membrane proteins are shown on the intracellular leaflet, either directly interacting with the lipid surface or with the integral membrane proteins. Glycoproteins and glycolipids are also shown associated with the external leaflet of the bilayer.

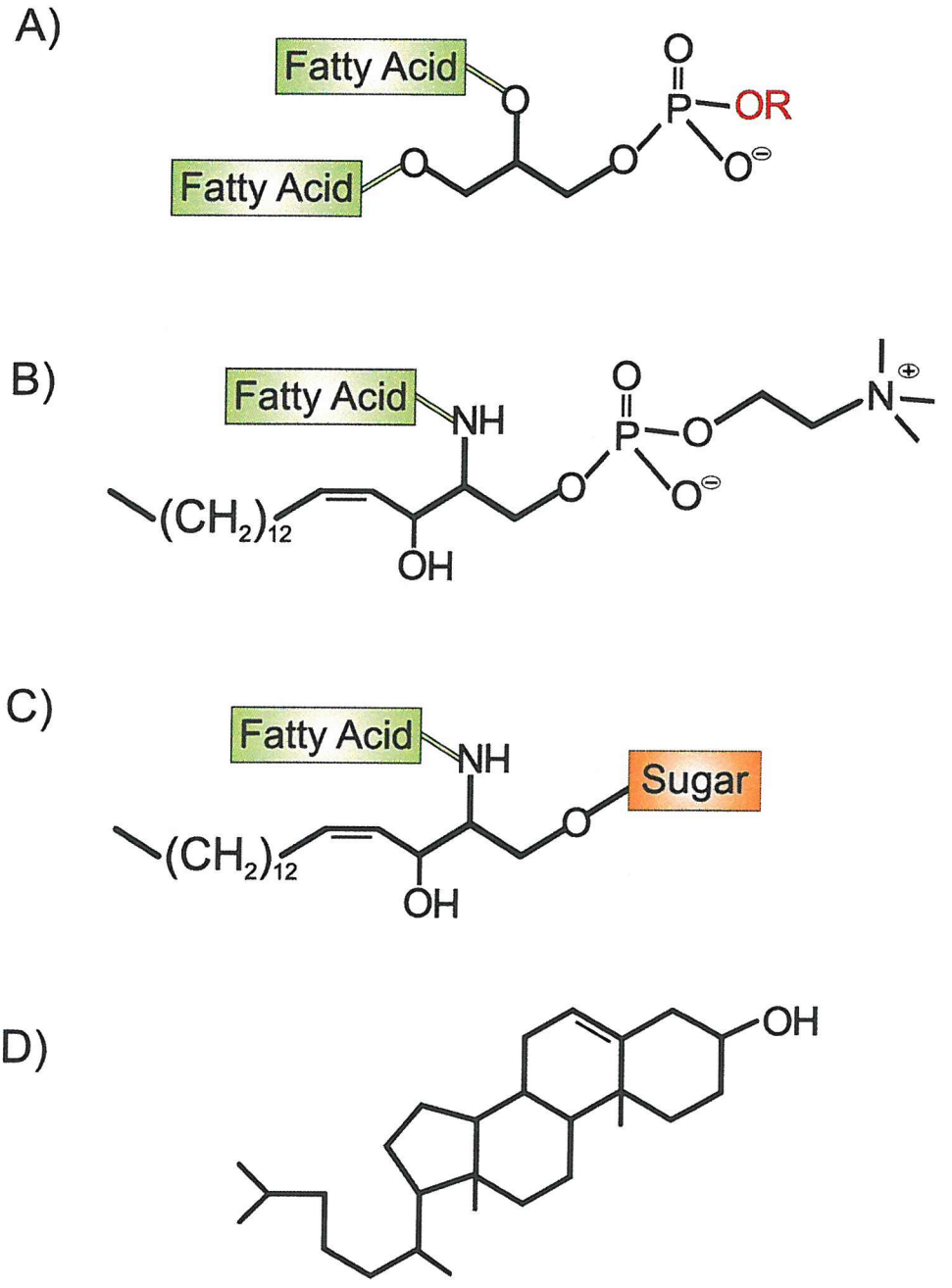

Figure 1.2 The structural components of a phosphoglyceride (**A**); sphingomyelin (**B**) and glycolipid (**C**). The structure of the sterol, cholesterol (**D**) is also shown.

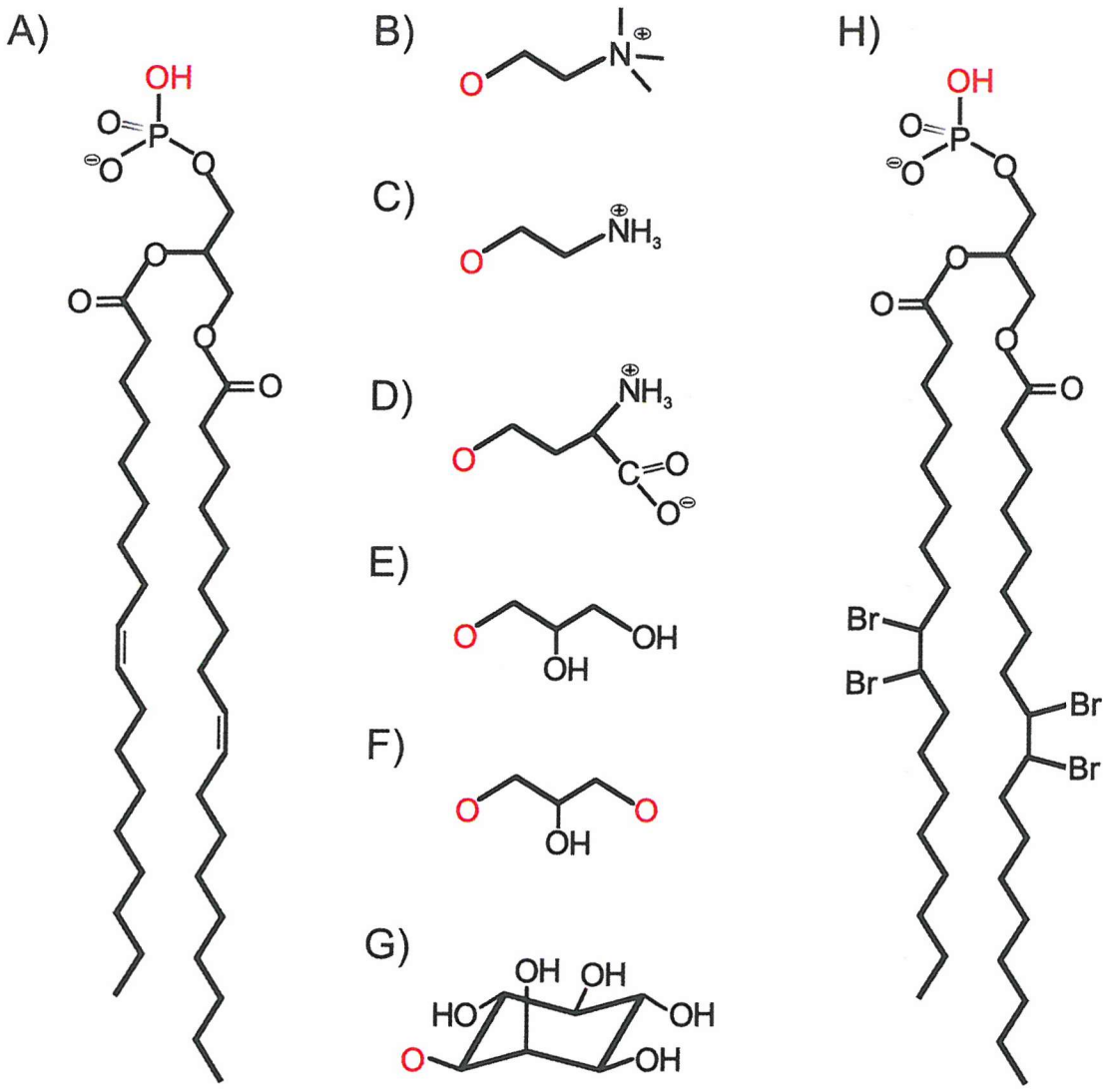

Figure 1.3 Components of the glycero-3-phospho lipids. The simplest phosphoglyceride, phosphatidic acid (1,2-dioleoyl-sn-glycero-3-phosphatidic acid) is shown in full (A). The lipid is formed from a glycerol backbone with two fatty acid chains covalently linked at the *sn*-1 and *sn*-2 positions, and a phosphate at the *sn*-3 position. Substitution of the phosphate, with any of the alcohol groups shown above (B-G), results in the formation of: (B), phosphatidylcholine; (C), phosphatidyethanolamine; (D), phosphatidylserine; (E), phosphatidylglycerol; (F), cardiolipin; and (G), phosphatidylinositol. The structure of 1,2-di(9,10-dibromostearoyl)-sn-glycero-3-phosphatidic acid (H) is also shown. Adapted from Dowhan and Bogdanov (2002).

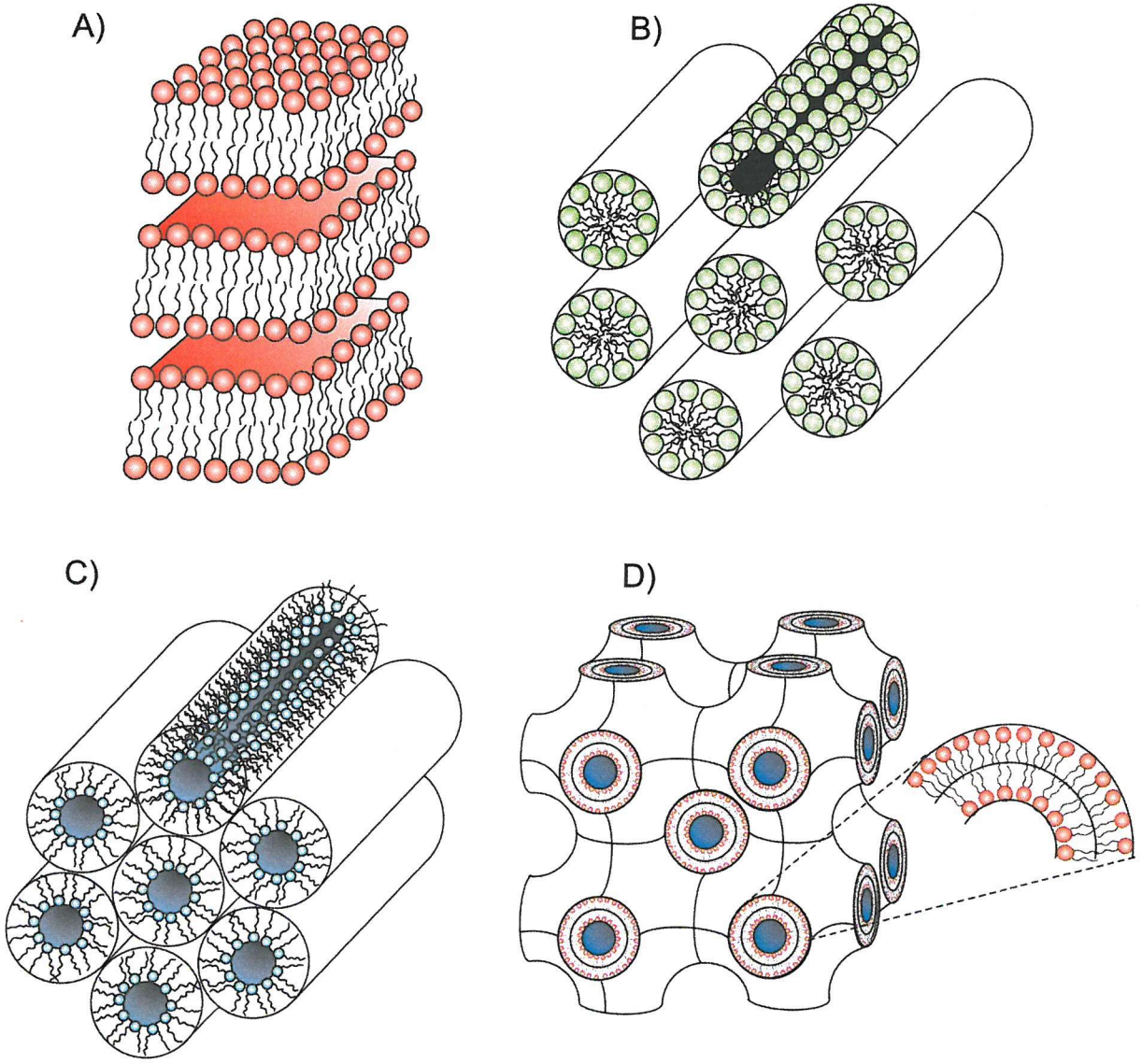

Figure 1.4 Examples of fluid phase lipid aggregated structures: (A), lamellar; (B), hexagonal (H_I); (C), hexagonal (H_{II}); and (D), cubic (bicontinuous). Adapted from Seddon and Templer (1995).

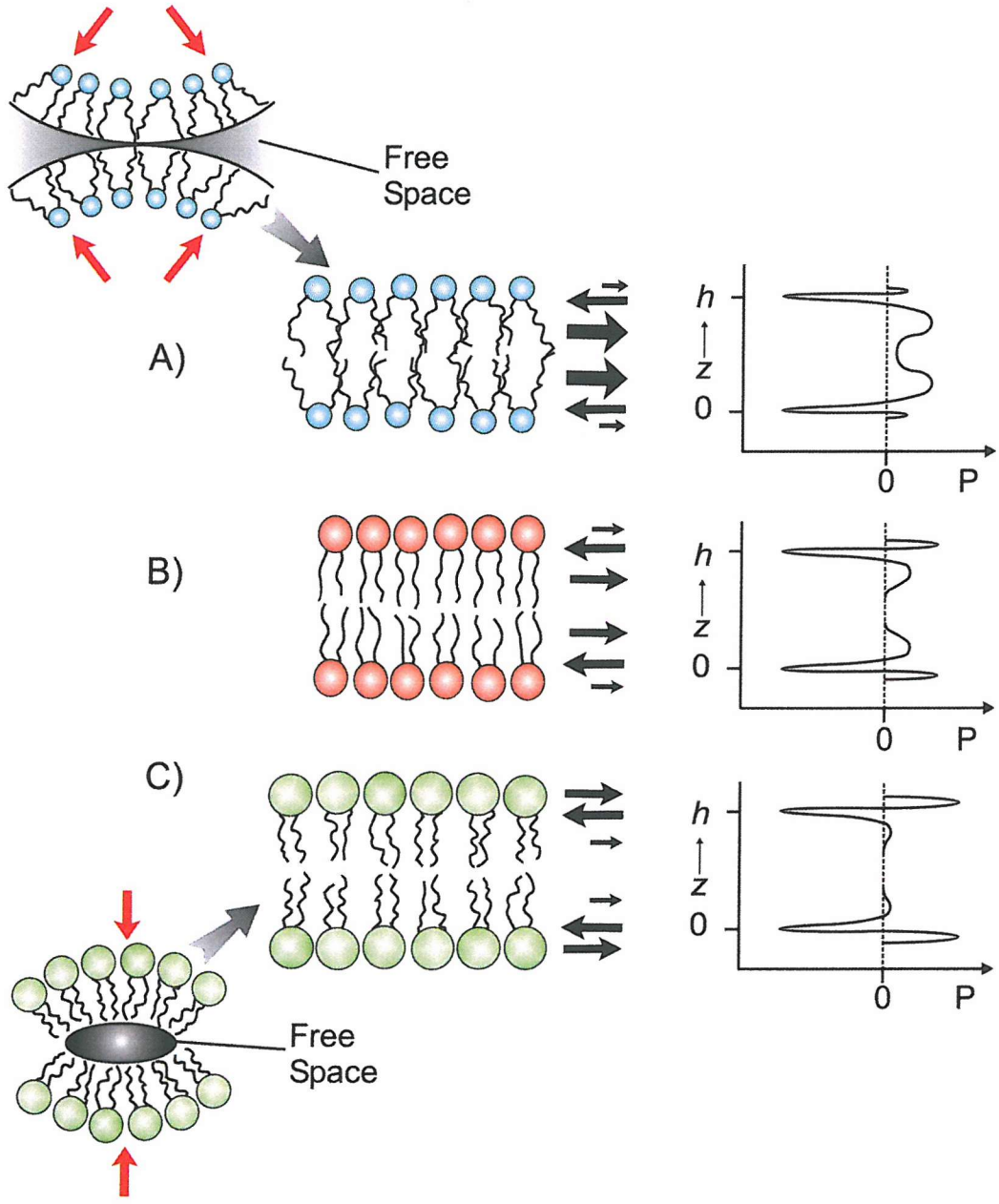

Figure 1.5 Schematic representation of the lateral pressure profile (P) at different depths (z) within a single component bilayer. When a lamellar membrane forms (B), the cylindrically shaped lipids have little or no spontaneous curvature and the net lateral pressure forces acting over the entire bilayer thickness (h) is approximately zero. Non-bilayer, conical shaped lipids (A) normally adopt H_{II} structures that have higher negative spontaneous curvature. Forcing these lipids into flat bilayer structures creates a 'frustrated bilayer' with greater pressures within the acyl chain area. In contrast, inverted cone shaped lipids (C) that adopt H_I structures, have greater positive spontaneous curvature. When these lipids are forced into planar bilayers, they generate higher pressures at the head group region and very little in the acyl chain area. Adapted from Seddon (1990), Cantor (1997a), and Bezrukov (2000).

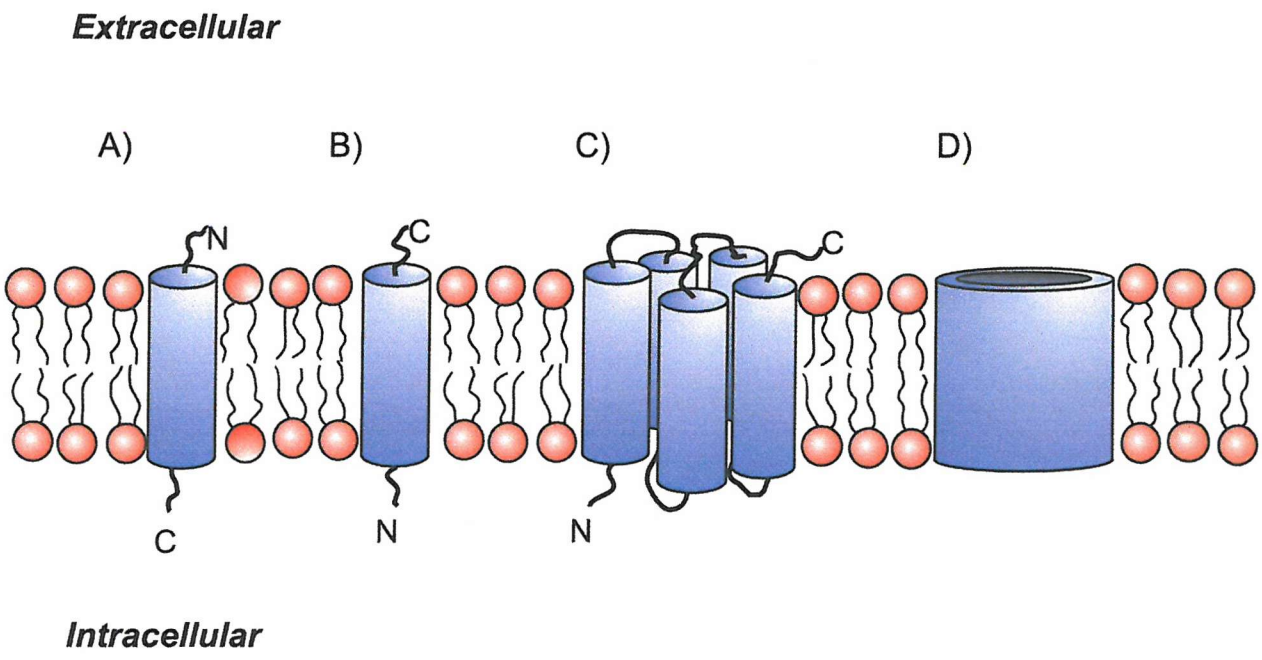

Figure 1.6 Types and topologies of integral membrane proteins. Transmembrane proteins may penetrate and traverse the lipid bilayer in number of ways, which include: single-pass, bitopic α-helical proteins (A and B) that can be further subdivided into: (A), type I, with the carboxyl C-terminus located intracellularly; (B), type II, with the amino N-terminus located intracellularly; or (C), multi-pass, polytopic membrane proteins; and (D), closed β-sheet configuration (β-barrel).

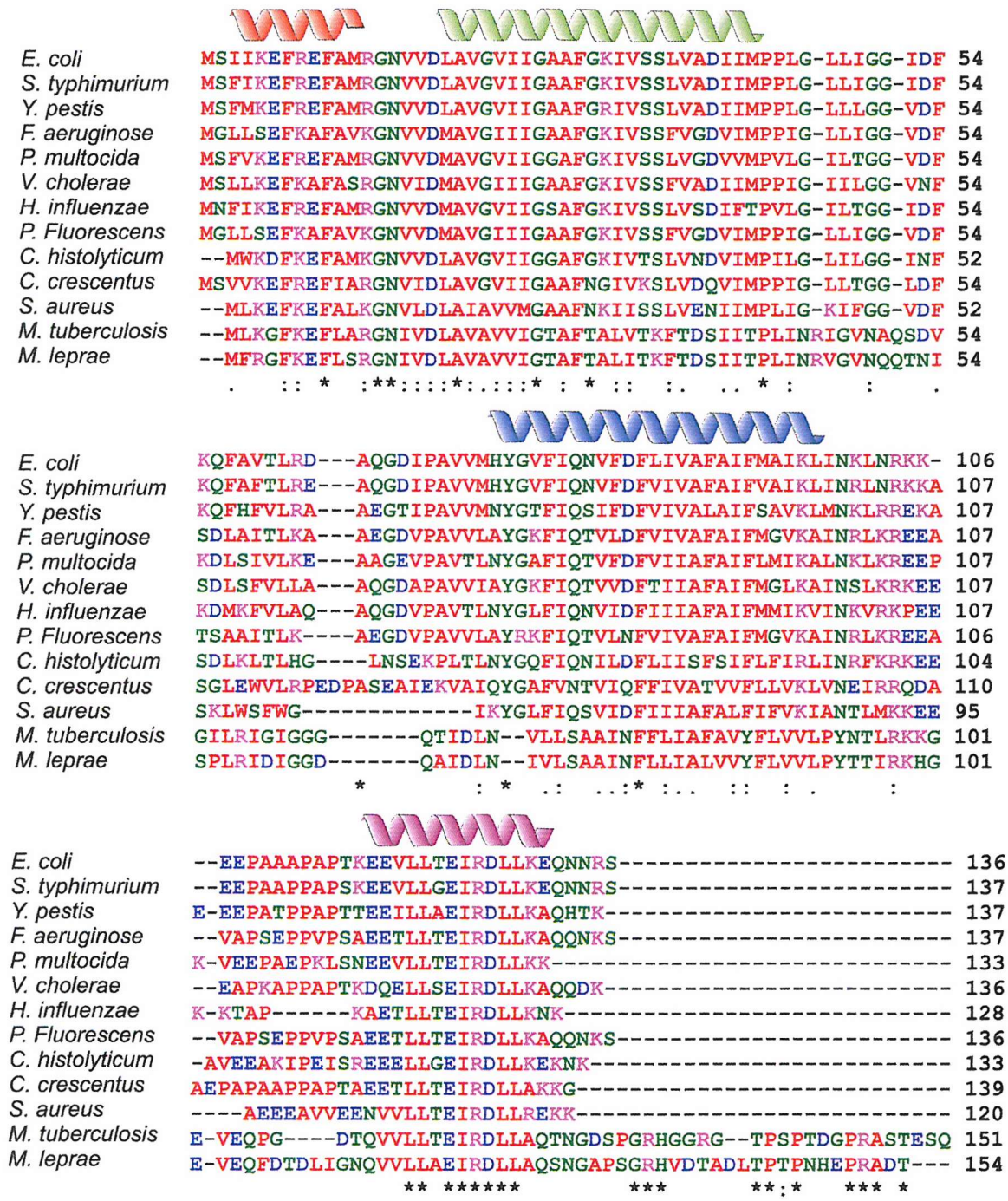

Figure 1.7 Multiple sequence alignment of 13 homologues of the MscL family. The position of the α-helices are indicated above the sequence alignment and correspond to: S1 (red); TM1 (green); TM2 (blue); and the cytoplasmic helices S3 (purple). The alignment was carried out using DbClustal Output available at EMBI (Thompson et al., 2000).

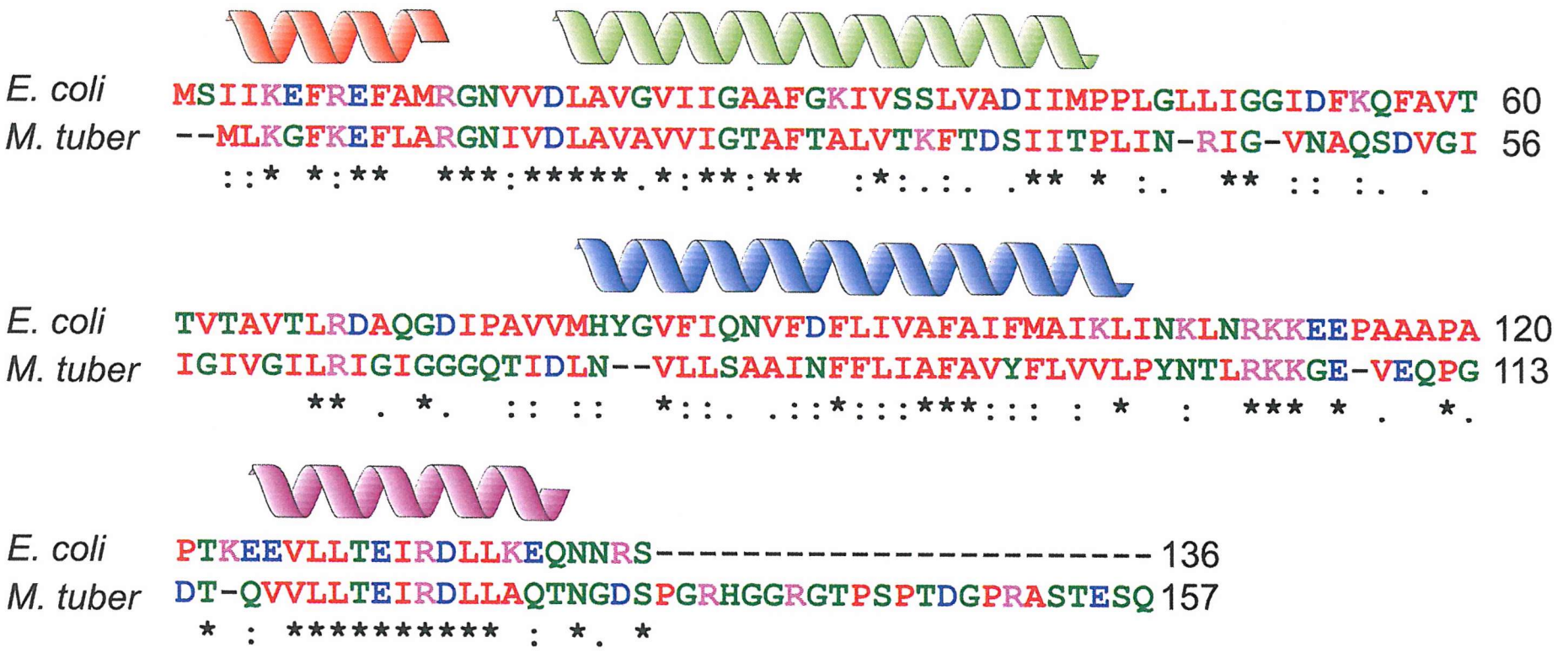

Figure 1.8 Pair-wise sequence alignment of the *E. coli* and *M. tuberculosis* MscL channels. Most notable is the high degree of sequence homology in S1 (red), TM1 (green), TM2 (blue) and the S3 helix (purple). Loop regions between TM1 and TM2 and also between TM2 and S3 are less conserved. The position of S1 is taken as that postulated by Sukharev et al. (2001b). The positions of TM1 and TM2 are determined from a combination of ESR (Perozo et al., 2001) and scanning Trp mutagenesis data (Chapter 5). The location of S3 was determined using data from Anishkin et al. (2003). The alignment was carried out using DbClustal Output available at EMBI (Thompson et al., 2000).

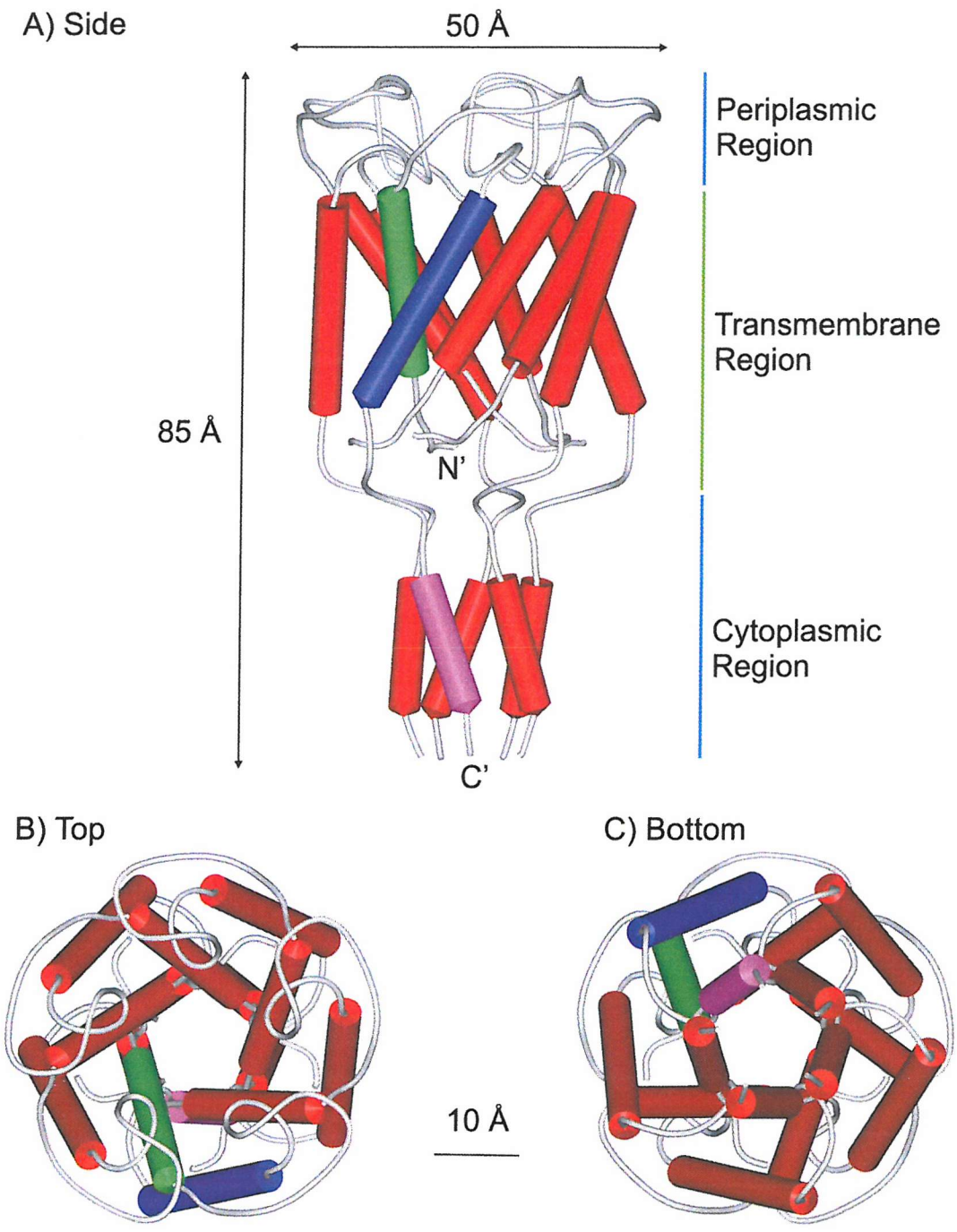

Figure 1.9 Schematic representations of the mechanosensitive channel of large conductance from *M. tuberculosis*, viewed from: (A), side; (B), top; and (C), bottom. The channel is a homopentamer, with a five-fold axis of symmetry. Each monomer contains two transmembrane helices and a single cytoplasmic helix (S3, purple). The inner helix (TM1, green) of each subunit starts in the cytoplasm and crosses the membrane to form the channel pore. The second helix (TM2, blue) returns to the cytoplasm across the membrane to form the membrane facing helix. Both transmembrane helices (TM1 and TM2) are titled approximately 28° with respect to the membrane normal. PDB file 1MSL.

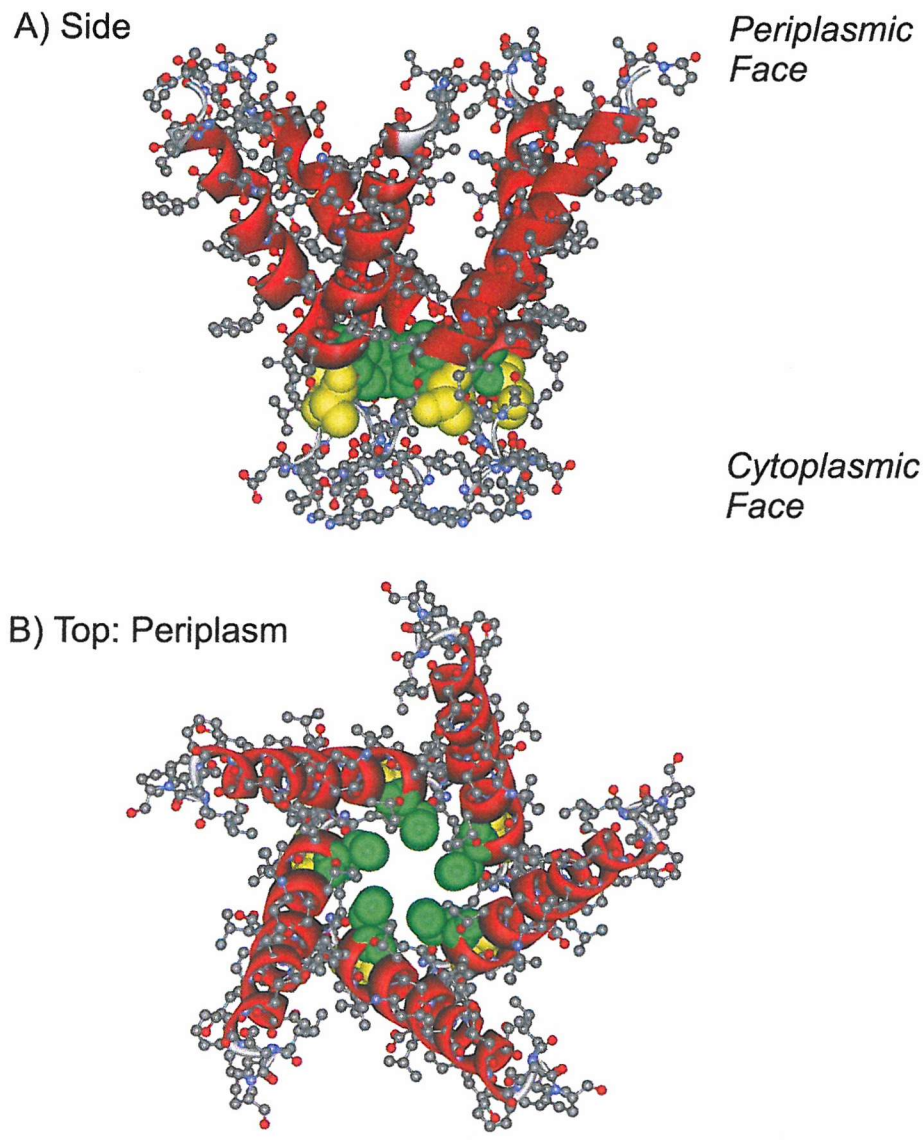

Figure 1.10 Ball and stick and ribbon representation of the five identical pore-forming, inner transmembrane helices (TM1) from the closed structure of TbMscL (residues 14 to 41 shown). The TM1 helix starts in the cytoplasm and crosses the membrane to form the permeation pathway. The vase-like pore alters in diameter from approximately 18 Å at the periplasmic face to 2 Å at the channel constriction, the latter formed by a ring of valines (Val-21, shown in Corey-Pauling-Koltun representation and highlighted green), above a ring of alanines (Ala-20, shown in CPK and highlighted yellow).

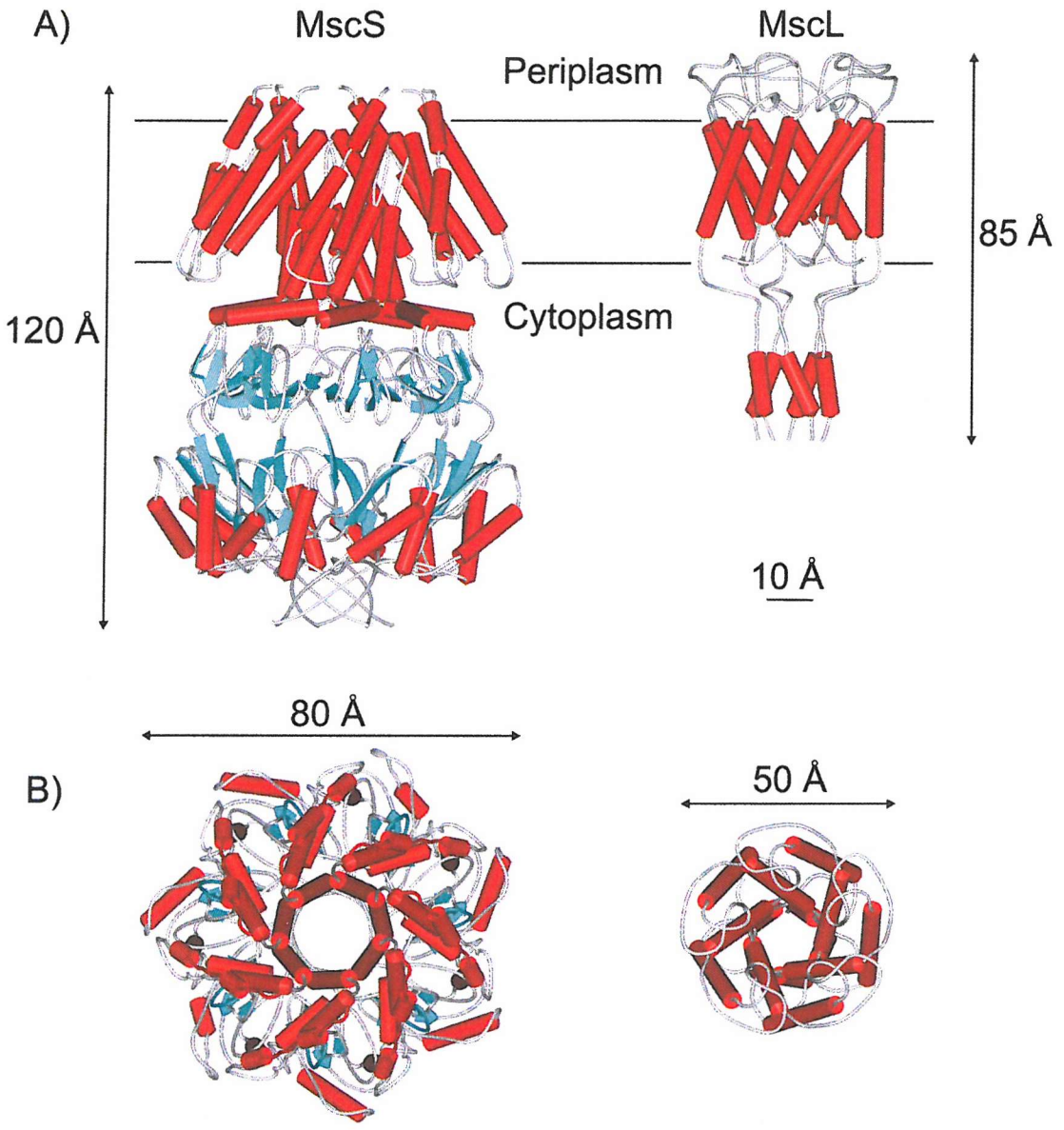

Figure 1.11 Structures of the MscS and MscL mechanosensitive channels. The channels are viewed from: (A), the membrane; and (B), the periplasmic surface. The two mechanosensitive channels have very little overall structural homology. The open MscS channel is a homoheptamer, with each monomer consisting of 286 residues, containing a mixture of both α-helical and β-sheet components, three transmembrane α-helices and a large cytoplasmic domain. In contrast, the closed MscL channel is a much smaller homopentamer, with each monomer consisting of 157 residues (136 in EcMscL) and containing only α-helical components, two transmembrane α-helices and a small cytoplasmic helical bundle. The transmembrane α-helices of both MscS and MscL are tilted by around 30° with respect to the bilayer normal; the cytoplasmic domains of both channels are thought to form selectivity filters. PDB files 1MXM and 1MSL.

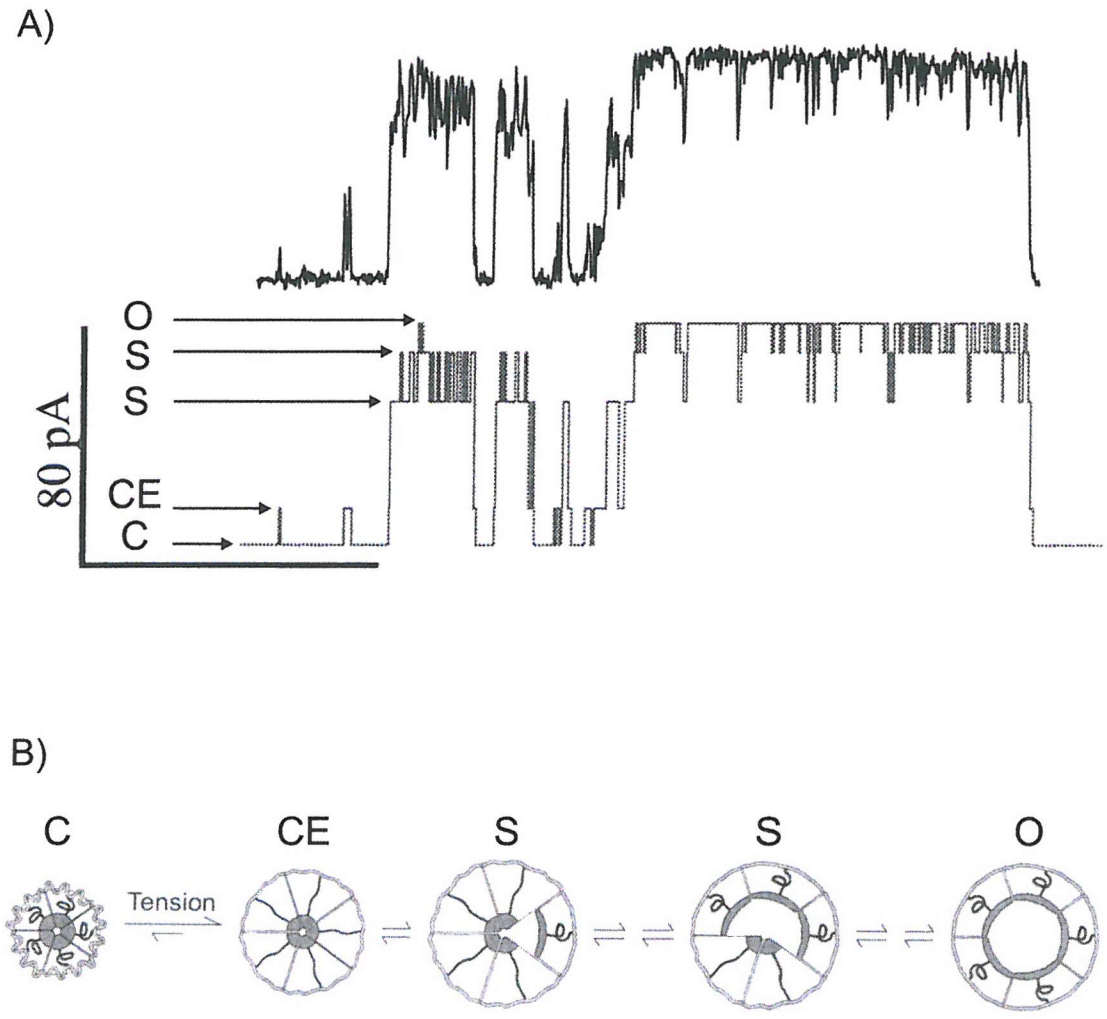

Figure 1.12 Gating kinetics of a single MscL channel of *Escherichia coli*. A), top panel shows a patch clamp trace highlighting the multiple subconducting states; bottom panel represents an idealisation of the above patch clamp trace. B) schematic representation of the gating mechanism. In both A) and B) the nomenclature is as follows: C, closed; CE, closed-expanded; S, subconducting; and O, open state of the channel. Adapted from Sukharev et al. (1999) and Sukharev et al. (2001a).

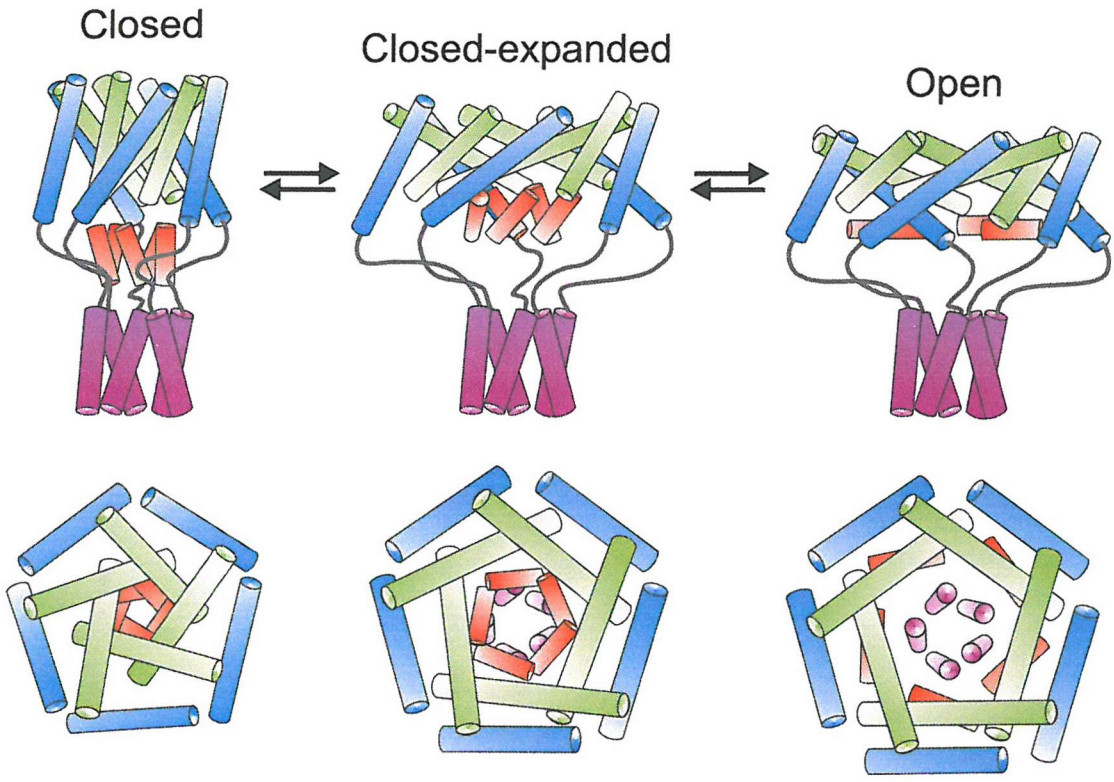

Figure 1.13 Cartoon representation of the MscL channel gating mechanism, based upon molecular dynamic simulations and ESR data obtained from experiments with the EcMscL channel. The channel is viewed from the side and the cytoplasmic surface of the membrane in each of the above pictures. Under bilayer tension, TM1 (green) and TM2 (blue) helices undergo large movements with gradual increases in inter-helical tilt angles, causing an iris-like expansion of the pore, resulting in the primary hydrophobic gate on TM1 being broken, generating a closed-expanded state. As membrane tension increase, further sliding and flattening of TM1 and TM2 occurs, and at the lytic threshold of the membrane the S1-TM1 linker is maximally stretched, thereby directly transferring tension to the S1 helical bundle (red) and breaking the second hydrophobic gate, triggering the S1 helices to dock with the pore wall, the channel becoming fully open. The S3 helical bundle (purple) remains associated in the cytoplasm throughout the gating process. Modified from Sukharev and Anishkin (2004) and Sukharev and Guy (2004).

Chapter 2:

General Materials & Methods

2 GENERAL MATERIALS AND METHODS

2.1 Materials

All chemicals were obtained from Sigma or BDH with the following exceptions:

Anatrace, Anagrade®

n-Octyl-β-D-glucopyranoside (Octylglucoside)

Calbiochem, Ultrol® Grade

N-(2-hydroxyethyl)piperazine-N'-(2-ethyanesulphonic acid) (Hepes)
1,3-diaza-2,4-cyclopentadiene (Imidazole)
Tris

Difco

Bacto Yeast Extract
Bacto-agar
Bactotryptone

Millipore

Nitrocellulose disc filters (0.025 μm)

National Diagnostics

ProtoGel (30 % (w/v) acrylamide: 0.8 % (w/v) bis-acrylamide)

New England Biolabs

BamHI
ClaI
NdeI
NheI
SalI
XhoI

Pharmacia

Agarose (NA Grade)

Promega

DpnI
Pfu DNA Polymerase
T4 DNA Ligase enzyme
Wizard® DNA clean-up system
Wizard® PCR preps DNA purification system
Wizard® *Plus* Minipreps DNA purification system

Sartorius

Sterile disposable 0.22 μm filters

2.2 Methods

2.2.1 Microbiological Techniques

2.2.1.1 Sterilisation

Growth media, solutions, pipette tips, microfuge and PCR tubes were sterilised by autoclaving at 120 °C, 15 lbs.sq.inch for 20 min, unless otherwise stated. Antibiotic stock solutions (ampicillin 100 mg ml^{-1}; chloramphenicol 25 mg ml^{-1} and kanamycin 25 mg ml^{-1}) were sterilised by filtration through sterile 0.22 µm filters and stored at -20 °C.

2.2.1.2 Media

2.2.1.2.1 *Luria-Bertani (LB) Medium*

5 g	Bacto Yeast Extract
10 g	Bactotryptone
10 g	NaCl

The solution was made to a final volume of 1 l with distilled water and the pH was adjusted to 7.2 before autoclaving.

2.2.1.2.2 *LB Agar*

1.5 % Bacto-agar was added to 300 ml of LB medium before being autoclaved. Growth media was left to cool to 50 °C before adding sterile antibiotic solutions. Final concentrations were 100 µg ml^{-1} ampicillin; 25 µg ml^{-1} chloramphenicol and 25 µg ml^{-1} kanamycin.

2.2.1.2.3 *SOB Medium*

5 g	Bacto Yeast Extract
20 g	Bactotryptone
1.98 g	$MgCl_2$
2.46 g	$MgSO_4$
0.58 g	NaCl

10 ml of 250 mM KCl was added to approximately 950 ml of analytical grade water containing the above compounds. The pH was adjusted to 6.8 with HCl and then made up to a final volume of 1 l with distilled water before autoclaving.

2.2.1.2.4 *SOC Medium*

SOB medium was autoclaved and left to cool to approximately 60 °C before adding 20 ml of 1 M sterile-filtered glucose.

2.2.1.3 Transformation Buffer

0.17 g	$CaCl_2$
1.86 g	KCl
0.30 g	PIPES

The solution was made up to a final volume of 90 ml with analytical grade water and the pH was adjusted to 6.8. 10 ml of 55 mM $MnCl_2$ solution was added before autoclaving.

2.2.1.4 *Escherichia coli* Strains

Strain	Genotype	Source
BL21(DE3)pLysS	F⁻ *ompT hsdS* (r_B^-, m_B^-) *gal dcm* λ(DE3) [pLysS Cam^r]	Novagen
GM3819	F⁻ *thr*-1 *araC14 leuB6*(Am) Δ(*gpt-proA)62 lacY1 tsx-33* qsr'⁻ *glnV44*(AS) *galK2*(Oc) λ⁻ *Rac-0 hisG4*(Oc) *rfbD1 mgl-51 rpsL31*(Str^r) Δ*dam-16*::Kan^r *kdgK51 xylA5 mtl-1 argE3*(Oc) *thi-1*	*E. coli* Genetic Stock Centre, Yale University
M15 [pREP4]	nal^s str^s rif^s *lac*⁻ *ara*⁻ *gal*⁻ *mtl*⁻ F'⁻ *recA*⁺ *uvr*⁺ *lon*⁺ [pREP4 Kan^r]	Qiagen
MJF465	F⁻ *rha thi gal lacZ* Δ*mscL*::Cam^r Δ*mscS* Δ*mscK*::Kan^r	Levina et al. (1999)
XL-1 Blue	*recA1 endA1 gyrA96 thi*-1 *hsdR17 supE44 relA1 lac* [F' *proAB* $lacI^q$ΔM15 Tn10(Tet^r)]	Novagen

Strain BL21(DE3)pLysS was used for the high level protein expression of biologically active TbMscL. *E. coli* M15 carrying the repressor plasmid (pREP4) was used to express biologically active EcMscL. GM3819 DNA adenine methylase (Dam) knock out strain was used to generate non-methylated plasmid for DNA manipulation with Dam sensitive restriction enzyme *ClaI*. XL-1 Blue *E. coli* were used for the repair and replication of mutated plasmid DNA. Stain MJF465, lacking mechanosensitive ion channels, was used for an *in vivo* channel function assay following transfection with plasmid containing the *mscL* gene.

2.2.1.5 Vectors

The *EcmscL* gene was cloned into expression vector pQE-32 (Qiagen; Figure 2.1) using restriction sites *BamHI* and *SalI* and generously donated by Professor B. Martinac. Insertion of *EcmscL* into pQE-32 creates a recombinant protein with a hexapeptide His tag at the N-termini, and protein expression is under the control of a T5 promoter.

TbMscL has been cloned into expression vector pET-19b (Novagen; Figure 2.2) using restriction sites *NdeI* and *BamHI*, and kindly donated by Professor D. C. Rees. Insertion of the *TbmscL* gene into the multiple cloning site adds a decapeptide His tag at the N-terminus and puts the *TbmscL* gene under the control of a T7 promoter. Vectors pQE-32 and pET-19b contain strong promoters and are located on the *lac* operator element, allowing high levels of inducible protein expression; pREP4 and pLysS provide a means of tight regulation for the plasmids respectively.

2.2.1.6 Glycerol Permastocks

For long-term storage of *E. coli* strains and transformants, 10 ml of antibiotic-containing LB cultures were inoculated with a single colony and grown for 16 h at 37 °C. Stationary phase cultures (1 ml) were transferred to a sterile cryovial containing 500 µl of glycerol and mixed by inversion. Cryovials were immediately snap-frozen in liquid nitrogen and stored at -80 °C until use.

2.2.2 DNA TECHNIQUES

2.2.2.1 Plasmid DNA Extraction

Plasmid DNA template was obtained using the Promega Wizard® *Plus* Miniprep DNA purification system. 5 ml of antibiotic-containing LB cultures were inoculated with a single colony and grown for 16 h at 37 °C. Cells were harvested by centrifugation at 3000 rpm for 10 min on a Heraeus Labofuge 400e, and plasmid

DNA was extracted from the pellet as directed by the manufacturer's instructions. Plasmid DNA was run on a 1 % (w/v) agarose gel and the concentration determined by measuring the optical density at 260 nm.

2.2.2.2 Measurement of DNA Concentration

Plasmid DNA concentrations were measured by UV spectroscopy. The absorbance of DNA was recorded in a quartz cuvette on a U-2001 Spectrophotometer (Hitatachi) at 260 nm. Absorbance readings were corrected for background light scatter by subtracting the absorbance of the quartz cuvette with a suitable blank. An absorbance of 1.0 corresponds to a DNA concentration of 50 g ml^{-1}. Sample purity was assessed by measuring the absorbance ratio at 260:280 nm. Pure DNA has a 260:280 ratio of 1.8.

2.2.2.3 Ethanol Precipitation of DNA

Plasmid DNA purified using the Promega Wizard® *Plus* Miniprep DNA purification system was precipitated out of solution for sequencing by MWG Biotech. 10 µl of 3 M sterile-filtered sodium acetate (pH 5.1) was added to 5 µg plasmid DNA. 200 µl of ice-cold sterile-filtered ethanol was added to the mixture followed by incubation on ice for a further 30 min. The sample was centrifuged at 10,000 rpm for 20 min in an Eppendorf centrifuge 5415C. Sample supernatant was removed and the pellet resuspended in 1 ml of ice-cold sterile-filtered 70 % (v/v) ethanol. The sample was centrifuged as before for 10 min, and the supernatant was again removed and discarded. Microfuge tubes containing precipitated DNA were loosely covered with foil and allowed to air-dry for 2 h at room temperature.

2.2.2.4 Restriction Enzyme Digest

All restriction digests were performed in 10 µl, 50 µl and 150 µl volumes according to the manufacturer's recommendations. The digest products were separated by

agarose gel electrophoresis as described in Section 2.2.2.5.4 and visualised under UV light to confirm digestion was complete and ensure DNA fragments were the correct size.

2.2.2.5 DNA Gel Electrophoresis

2.2.2.5.1 *50 x TAE*

57.1 ml	Acetic Acid
1.9 g	Na EDTA
242 g	Tris

Distilled water was added to 1 l and the pH was adjusted to 8.0. The buffer was diluted 1:50 with distilled water for use.

2.2.2.5.2 *Loading Buffer*

30 mg	Bromophenol blue
3 ml	Glycerol
1 ml	10 x TAE buffer

Distilled water was added to 10 ml.

2.2.2.5.3 *Ethidium Bromide*

100 mg ethidium bromide was dissolved in 10 ml analytical grade water.

2.2.2.5.4 *Agarose Gel Electrophoresis of DNA*

Agarose 1 % (w/v) (in 1 x TAE) was melted and ethidium bromide was added to a final concentration of 0.5 μg ml^{-1} before pouring into a horizontal gel tank. DNA samples were mixed 4:1 with loading buffer and loaded into a set gel. 2 μl of either 1 kB or 100 bp ladder (Tables 2.1 and 2.2 respectively) were separated in lanes either

side of the samples. Electrophoresis was carried out at 120 V for approximately 45 min in 1 x TAE, followed by visualisation of the DNA bands using a Gene Genius Bio Imagining System.

2.2.3 MOLECULAR BIOLOGY TECHNIQUES

2.2.3.1 Preparation of Competent Cells

2.2.3.1.1 *Electrocompetent Sure Cells*

10 ml of antibiotic-containing LB cultures were grown for 12-16 h at 37 °C and were used to inoculate 500 ml of LB. Cells were grown at 37 °C in an orbital shaker to an absorbance at 600 nm of between 0.5 and 0.6. Cells were harvested by centrifugation at 4500g for 10 min in a Sorvall RC286 at 4 °C. Culture supernatant was removed and the cell pellet resuspended in 500 ml of cold sterile distilled water. The cells were centrifuged as before and the pellet was resuspended in sterile 10 % (v/v) glycerol and again centrifuged as before. The pellet was washed in sterile 10 % (v/v) glycerol and recentrifuged. The pellet was finally suspended in 2-3 ml of 10 % (v/v) sterile glycerol and aliquoted into 60 µl fractions. These cells were snap-frozen in liquid nitrogen and stored at -80 °C.

2.2.3.1.2 *Ultracompetent Cells*

5 ml of antibiotic-containing LB cultures were grown for 12-16 h at 37 °C and were used to inoculate 250 ml of SOB. Cells were grown for 12 h at 18 °C in an orbital shaker to an absorbance at 600 nm of 0.3 and immediately transferred to ice for 10 min. Cells were harvested by centrifugation at 4500g for 10 min in a Sorvall RC286 at 4 °C. Culture supernatant was removed and the cell pellet was resuspended in 80 ml of ice-cold sterile transformation buffer and kept on ice for a further 10 min. The cells were centrifuged as before and the pellet was resuspended in 10 ml of ice-cold sterile transformation buffer supplemented with 7 % (v/v) sterile-filtered dimethyl sulphoxide (DMSO). The cell suspension was incubated on ice for 10 min and

aliquoted into 100 µl fractions. The cells were snap-frozen in liquid nitrogen and stored at -80 °C.

2.2.3.2 Transformation of Competent Cells

2.2.3.2.1 *Electroporation*

Electroporation provides a high efficiency method of transforming *E. coli* with plasmid DNA. 60 µl of electrocompetent cells were thawed on ice and mixed with 1-10 ng of desalted DNA in a 0.2 cm BioRad sterile electroporation cuvette, followed by incubation on ice for a further 2 min. Transformation was performed using a BioRad *MicroPulser*™ with a voltage of 2.5 kV. 1 ml of SOC medium was immediately added and the cells were then left to recover at 37 °C for 60 min in an orbital shaker. The transformed cells were aliquoted onto antibiotic-containing LB agar plates in the following volumes: 10 µl, 100 µl, and 1000 µl. The cells were spread on the plates using a sterile spreader and then incubated for 12-16 h at 37 °C.

2.2.3.2.2 *Heat-shock*

100 µl of ultracompetent cells were thawed on ice and mixed with 10-100 ng of DNA followed by incubation on ice for a further 30 min. The mixture was then transferred to a 42 °C water bath for 90 s, followed by immediate incubation on ice for a further 2 min. Bacteria were resuscitated by the addition of 1 ml of SOC medium pre-warmed to 42 °C and then left to recover at 37 °C for 60 min in an orbital shaker. The transformed cells were aliquoted onto antibiotic-containing LB agar plates. Transformants were spread on the plates using a sterile spreader followed by incubation at 37 °C for 12-16 h.

2.2.4 EXPRESSION AND PURIFICATION OF MscL

2.2.4.1 Expression of MscL

E. coli BL21(DE3)pLysS transformants carrying the pET-19b plasmid with the *TbmscL* gene or *E. coli* M15 carrying the pQE-32 plasmid with the *EcmscL* gene were grown at 37 °C in 6 l LB medium supplemented with ampicillin (100 μg ml^{-1}) and either chloramphenicol (25 μg ml^{-1} for BL21(DE3)pLysS) or kanamycin (25 μg ml^{-1} for M15). Cells were grown to mid-log phase (absorbance at 600 nm of 0.6) and then induced for 3 h in the presence of isopropyl-β-D-thiogalactopyranoside (1.0 mM). The cells were harvested by centrifugation at 7000g for 15 min in a Beckman Avanti J-20 XPI at 4 °C and the cell pellet was frozen at -20 °C until use.

2.2.4.2 Purification of MscL

The cell pellet was resuspended in PBS buffer (120 ml; 140 mM NaCl, 2.7 mM KCl, 10 mM Na_2HPO_4, 1.8 mM KH_2PO_4, pH 7.2) supplemented with DNase 1 (400 μg ml^{-1}) followed by sonication using a XL-2020 Misonix sonicator (15 cycles; 20 s pulse, 15 s off). The sample was spun at 100,000g for 40 min in a Beckman L7 Ultracentrifuge at 4 °C and the membrane pellet was solubilised in 80 ml PBS containing 40 mM n-octyl-β-D-glucopyranoside (octylglucoside; Anatrace) at 4 °C for 4 h. The sample was spun at 8000g for 20 min in a Beckman J2-HS at 4 °C and the supernatant applied to a Ni-NTA column (5 ml; agarose beads; Qiagen). The Ni-NTA column was coupled to a UV detector (280 nm; Pharmacia) and extensively washed with PBS buffer containing 40 mM OG and 30 mM imidazole (Calbiochem), typically six times the agarose bed volume to ensure all non-specific protein had been removed. MscL was eluted with PBS buffer containing 40 mM OG and 400 mM imidazole (typically two and a half times the agarose bed volume). The sample was snap-frozen in liquid nitrogen and stored at -80 °C until use.

Homogeneity of MscL was assessed by sodium dodecyl sulphate polyacrylamide gel electrophoresis (SDS-PAGE), using the method of Laemmli (1970), and protein

concentrations were estimated using BioRad protein assay as described in Section 2.2.4.4.

2.2.4.3 SDS-Polyacrylamide Gel Electrophoresis of Proteins

Separation of proteins was performed as described by Laemmli (1970) using BioRad mini-gel electrophoresis apparatus as per the manufacturer's instructions. 10 µl of low molecular weight range protein standards (Table 2.3) were separated in lanes either side of the samples for size approximation.

2.2.4.3.1 *Resolving Gel*

	10 %	**12 %**	**15 %**
Acrylamide/bis-acrylamide (30 %/ 0.8 % w/v)	6.70 ml	8.00 ml	9.90 ml
Distilled water	9.46 ml	8.16 ml	6.26 ml
10 % (w/v) SDS	0.20 ml	0.20 ml	0.20 ml
1.5 M Tris-HCl, pH 8.8	3.40 ml	3.40 ml	3.40 ml
25 % (w/v) Ammonium persulphate	0.24 ml	0.24 ml	0.24 ml
TEMED	10 µl	10 µl	10 µl

2.2.4.3.2 *Stacking Gel*

0.6 ml	Acrylamide/bis-acrylamide (30 %/ 0.8 % w/v)
1.7 ml	Distilled water
40 µl	10 % (w/v) SDS
1.6 ml	3.6 M Tris-HCl, pH 8.8
20 µl	25 % (w/v) Ammonium persulphate
4 µl	TEMED

2.2.4.3.3 *5 x SDS Running Buffer*

142.63 g	Glycine
10.00 g	SDS
30.25 g	Tris

Distilled water was added to 1 l. The buffer was diluted 1:5 with distilled water for use.

2.2.4.3.4 *Coomassie Brilliant Blue Stain*

90 ml	Acetic acid
250 mg	Coomassie blue
460 ml	Distilled water
450 ml	Methanol

2.2.4.3.5 *Destain Solution*

375 ml	Acetic acid
3.625 l	Distilled water
1 l	Methanol

2.2.4.3.6 *Sample Buffer*

0.2 mg	Bromophenol blue
1.0 ml	0.5 M Tris-HCl, pH 6.8
2.0 ml	10 % (w/v) SDS
5.3 ml	Distilled water
1.0 ml	Glycerol

2.2.4.4 Measurement of Protein Concentration

Protein concentrations were estimated spectrophotometrically using the BioRad Protein Assay kit, a Coomassie Blue G-250 dye-binding assay largely based upon the Bradford Assay. Bovine serum albumin (BSA; Pierce) standards (2-10 μg ml^{-1}) were prepared in triplicate from a stock solution by dilution into analytical grade water (up to 800 μl). Samples (50 μl) were prepared in triplicate and with two dilution factors in the range 0-1.5 mg ml^{-1}, followed by the addition of analytical grade water (750 μl). BioRad dye reagent (200 μl) was added with mixing, followed by incubation at room temperature for 5 min. Absorbance measurements were recorded at 595 nm using a U-2001 Spectrophotometer (Hitatachi) at 25 °C, and corrected for background light scatter by subtracting the absorbance of a blank containing 800 μl analytical grade water and 200 μl BioRad dye reagent only.

2.2.5 *mscL* MUTAGENESIS

Trp-mutated *mscL* genes were generated from wild type MscL template by two methods: three-stage site directed mutagenesis and the QuickChange™ protocol (Figures 2.3 and 2.4).

2.2.5.1 Three-stage Site Directed Mutagenesis

Mutations were introduced into the *E. coli mscL* (*EcmscL*) gene through a three-stage PCR procedure, modified from Higuchi et al. (1988) that used combinations of Primer 1 with the reverse mismatched primer, and Primer 2 with the forward mismatched primer (Figure 2.3).

2.2.5.1.1 *First Stage PCR*

Reactions were performed in 0.5 ml thin wall PCR tubes, with a final volume of 100 μl. In the first stage PCR, each assay contained 1 μl plasmid template pQE-32:*EcmscL* (150 ng μl^{-1}); 0.8 μl deoxynucleoside triphosphates (25 mM); 2.5 μl (100

ng μl^{-1}) of each oligonucleotide primer (either Primer 1 with the reverse mismatched primer or Primer 2 with the forward mismatched primer (Table 2.4)); 2 µl thermostable *Pfu* DNA Polymerase (3 u μl^{-1}); 10 µl of 10 x *Pfu* DNA Polymerase reaction buffer (200 mM Tris-HCl pH 8.8, 100 mM KCl, 100 mM $(NH_4)_2SO_4$, 20 mM $MgSO_4$, 1.0 % (w/v) Triton X-100, 1 mg ml^{-1} nuclease-free BSA).

PCR cycling reactions were carried out using a Peltier Thermal Cycle PTC-200. Cycle conditions used involved denaturation at 94 °C for 45 s, annealing at 47 °C (melting temperature of primer minus 5 °C) for 45 s, extension at 72 °C for 20 s (allowing 2 min kB^{-1}); each cycle was repeated 30 times. The final cycle contained an additional extension step at 72 °C for 10 min, followed by a holding temperature of 4 °C.

2.2.5.1.2 *Second Stage PCR*

PCR products from the first stage PCR were analysed on a 1 % (w/v) agarose gel (Figure 2.5). Products 1 and 2 were subsequently annealed together through a second stage PCR reaction. The reaction was performed in a 0.5 ml thin wall PCR tube with a final volume of 97.5 µl. 100 ng of each PCR product (1 and 2), were added to 0.8 µl deoxynucleoside triphosphates (25 mM); 2 µl thermostable *Pfu* DNA Polymerase (3 u μl^{-1}); 10 µl of 10 x *Pfu* DNA Polymerase reaction buffer. PCR cycling conditions were the same as previously described with 5 cycles.

2.2.5.1.3 *Third Stage PCR*

In the third stage PCR, 1.25 µl of Primer 1 and Primer 2 (100 ng μl^{-1}) were used to seed further PCR and generate the full-length mutagenised fragment (284 bp). The PCR cycling conditions were the same as previously described with 25 cycles. The 284 bp fragment was purified using the Wizard® PCR preps DNA purification system and analysed on a 1 % (w/v) agarose gel (Figure 2.6).

The 284 bp fragment generated from each mutation was digested with *ClaI* and *SalI* restriction endonucleases (Section 2.2.2.4), producing a 257 bp fragment and purified

using the Wizard® PCR DNA purification system, prior to ligation with *ClaI* and *SalI* digested pQE-32:*EcmscL* (Figure 2.7).

2.2.5.1.4 *Digestion and Extraction of DNA from Agarose Gels*

pQE-32:*EcmscL* (3.88 Kb) was transformed into GM3819 by electroporation (Section 2.2.3.2.1). Transformants were grown and plasmid DNA harvested in the normal manner, using the Wizard® *Plus* Minipreps DNA purification system (Section 2.2.2.1). pQE-32:*EcmscL* was digested with *ClaI* and *SalI* restriction enzymes, and the digest products separated on a 1 % (w/v) agarose gel (Figure 2.8A). *ClaI* and *SalI* digested Plasmid (3.59 Kb) was excised with a sterile scalpel (Figure 2.8B), transferred to a sterile 0.5 ml microfuge tube plugged with siliconised glass wool, and snap-frozen in liquid nitrogen.

The base of the 0.5 ml microfuge tube was punctured with a needle, and placed inside a sterile 1.9 ml microfuge tube, followed by centrifugation at 10,000 rpm for 5 min on an Eppendorf centrifuge 5415C. The eluted DNA was purified with the Wizard® DNA clean-up system, according to the manufacturer's specifications and analysed on a 1 % (w/v) agarose gel (Figure 2.9).

2.2.5.1.5 *Ligation*

Digested and purified plasmid and PCR insert were ligated together to produce a continuous plasmid containing Trp-mutated *mscL*. Ligation reactions were carried out using T4 DNA Ligase enzyme (Promega) and T4 DNA Ligase 10 x buffer (Tris-HCl pH 7.8, 100 mM $MgCl_2$, 100 mM DDT, 10 mM ATP), as specified in the manufacture's instructions; with different molar ratios of vector:insert, and a control containing vector alone. The reactions were performed in 0.5 ml microfuge tubes with a final volume of 20 µl, and incubated at 16 °C for 18 h. Ligation products were dialysed against 10 % (v/v) glycerol using 0.025 µm nitrocellulose disc filters (Millipore) for 20 min prior to electroporation.

2.2.5.1.6 *Selection of Trp-mutated mscL Recombinant E. coli*

To confirm that selected colonies contained constructs with the Trp-mutated recombinants, diagnostic restriction digests were carried out on all samples. The digested DNA was separated by electrophoresis on 1 % (w/v) agarose gels and visualised under ultraviolet light so that recombinants with the correct size inserts could be detected.

Digestion of wild type plasmid with *ClaI-SalI* was designed to remove a cassette corresponding to the TM2-C' end of EcMscL protein. Removing the wild type cassette from wild type plasmid also removes a *XhoI* restriction site. The latter is important, since wild type plasmid contains two *XhoI* restriction sites, therefore a single *XhoI* digest generates a 577 bp fragment (Figure 2.10).

Successful ligation of the Trp-mutated cassette into *ClaI-SalI* digested plasmid, removes one *XhoI* site, and provides a relatively simple screen for the Trp-mutated *EcmscL* (Figure 2.10). Mutated plasmid (1-10 ng) was transformed into 60 µl of electrocompetent M15 cells by electroporation.

2.2.5.2 QuickChange™

Site directed mutagenesis was performed using the QuickChange™ protocol from Stratagene. The QuickChange™ protocol is a widely used technique that only requires a single PCR cloning step and negates the need to subclone the amplified DNA fragments. Mutated *TbmscL* genes were prepared using two complementary synthetic oligonucleotide primers for each mutation introduced (Figure 2.4).

Reactions were performed in 0.5 ml thin wall PCR tubes, with a final volume of 50 µl. Each assay contained 1 µl plasmid template pET-19b:*TbmscL* (50 ng μl^{-1}); 1 µl deoxynucleoside triphosphates (25 mM); 0.3 µl (0.3 pmol) of each of the complementary oligonucleotide primers (Tables 2.5, 2.6, 2.7); 1 µl thermostable *Pfu* DNA Polymerase (3 u μl^{-1}); 5 µl of 10 x *Pfu* DNA Polymerase reaction buffer (200

mM Tris-HCl pH 8.8, 100 mM KCl, 100 mM $(NH_4)_2SO_4$, 20 mM $MgSO_4$, 1.0 % (w/v) Triton X-100, 1 mg ml^{-1} nuclease-free BSA).

PCR cycling reactions were carried out using a Peltier Thermal Cycle PTC-200. Cycle conditions used involved denaturation at 95 °C for 30 s, annealing at 55 °C for 1 min, extension at 68 °C for 13 min (allowing 2 min kB^{-1}); each cycle was repeated 16 times. The final cycle was followed by a holding temperature of 4 °C.

Following mutagenesis, the PCR product (5 µl) was analysed on a 1 % (w/v) agarose gel (Figure 2.11). The native methylated parental DNA templates were digested with 1 µl *DpnI* (Promega) in the presence of 5 µl of 10 x *DpnI* buffer (60 mM Tris-HCl pH 7.5, 500 mM NaCl, 60 mM $MgCl_2$, 10 mM DTT) for 2 h at 37 °C. Mutated plasmid (10-100 ng) was transformed into 100 µl of ultracompetent XL-1 Blue cells by heat-shock (Section 2.2.3.2.4).

2.2.5.3 DNA Sequencing

To confirm successful mutation of the wild type *mscL* template and fidelity of the product, all mutations were confirmed by automated DNA sequencing by MWG Biotech. 5 µg plasmid DNA purified using the Promega Wizard® *Plus* Minipreps DNA purification system was precipitated out of solution by the ethanol precipitation method (Section 2.2.2.3). Samples were sent to MWG Biotech, together with sequencing primers pQE Fwd or T7 promoter primers for EcMscL and TbMscL respectively (Table 2.8).

2.2.5.4 Sequence Analysis

MscL DNA sequences were analysed using Chromas *v*1.45 and sequences were aligned using the programme Blast.

DNA band	Size (kB)
1	12.2
2	11.2
3	10.2
4	9.2
5	8.1
6	7.1
7	6.0
8	5.1
9	4.1
10	3.1
11	2.0
12	1.6
13	1.0
14	0.5
15	0.5
16	0.4
17	0.3
18	0.3
19	0.2
20	0.2
21	0.2
22	0.1
23	0.04

Table 2.1 1 kB DNA ladder used for size and mass approximation of DNA samples. 2 µl of 1 kB ladder (Invitrogen) was separated in lanes either side of the DNA samples on agarose gels.

DNA band	Size (Base Pairs)	DNA Mass (ng)
1	1517	45
2	1200	35
3	1000	95
4	900	27
5	800	24
6	700	21
7	600	18
8	500, 517	97
9	400	38
10	300	29
11	200	25
12	100	48

Table 2.2 100 basepair DNA ladder used for size and mass approximation of DNA samples. 2 µl of 100 basepair ladder (New England Biolabs) was separated in lanes either side of the DNA samples on agarose gels.

Band	Protein	Molecular Weight (kDa)
1	Albumin, bovine serum	66.0
2	Ovalbumin, chicken egg	45.0
3	Glyceraldehyde-3-phosphate Dehydrogenase, rabbit muscle	36.0
4	Carbonic Anhydrase, bovine erythrocytes	29.0
5	Trypsinogen, bovine pancreas	24.0
6	Trypsin Inhibitor, soybean	20.0
7	α-Lactalbumin, bovine milk	14.2
8	Aprotinin, bovine lung	6.5

Table 2.3 Low molecular weight range protein standards used for size approximation of protein samples. 10 µl of low molecular weight range protein standards (Sigma) were separated in lanes either side of the protein samples on SDS-polyacrylamide gels.

Primer	EcMscL Primer Sequence
Primer 1	5'- TATTAATTGGCGGGATCGAT -3'
Primer 2	5'- ACGGTCGTCGACTCAACTGCGGTTATTCTGCTCTTTCAG -3'
I79W Fwd	5'- GTCTTCTGGCAAAACGTCTTTGATTTTCTGATTG -3'
I79W Rev	5'- GACGTTTTGCCAGAAGACAACGTAATGCATC -3'
F85W Fwd	5'- CTTCGATTGGTTGATTGTTGCCTTTGCCATCTTTATG -3'
F85W Rev	5'- CAACAATCAACCAATCGAAGACGTTTTGAATGAAGAC -3'
L86W Fwd	5'- TCGATTTCTGGATTGTTGCCTTTGCCATCTTTATG -3'
L86W Rev	5'- AGGCAACAATCCAGAAATCGAAGACGTTTTGAATGAAGAC -3'
F93W Fwd	5'- GCGATCTGGATGGCGATTAAGCTAATCAACAAAC -3'
F93W Rev	5'- TAATCGCCATCCAGATCGCAAAGGCCACAATCAGAAAATC -3'
N100W Fwd	5'- GCTAATCTGGAAACTGAATCGGAAAAAAGAAG -3'
N100W Rev	5'- GATTCAGTTTCCAGATTAGCTTAATCGCCATAAAG -3'

Table 2.4 Synthetic oligonucleotide primers used in the three-stage site directed mutagenesis procedure of the *EcmscL* gene. Primer 1 was used in combination with the reverse (antisense) Trp mutagenic primer. Primer 2 was used in combination with the forward (sense) Trp mutagenic primer, as outlined in Section 2.2.5.1. Trp mutations are double underlined and conservative codon substitutions are single underlined. Conservative mutations were introduced to prevent secondary structure formation of the oligonucleotide.

Primer	TbMscL Primer Sequence
Q51W Fwd	5'- CCGGATCGGCGTCAACGCGTGGTCAGACGTCGGCATCTTGC -3'
Q51W Rev	5'- GCAAGATGCCGACGTCTGACCACGCGTTGACGCCGATCCGG -3'
T66W Fwd	5'- GATCGGTATCGGCGGTGGGCAGTGGATTGACTTGAACGTCTTG -3'
T66W Rev	5'- CAAGACGTTCAAGTCAATCCACTGCCCACCGCCGATACCGATC -3'
L69W Fwd	5'- GGTCAGACCATTGATTGGAACGTGTTGTTGTCGGCAGC -3'
L69W Rev	5'- GCTGCCGACAACAACACGTTCCAATCAATGGTCTGACC -3'
L73W Fwd	5'- GACTTGAACGTCTTGTGGTCGGCAGCGATCAAC -3'
L73W Rev	5'- GTTGATCGCTGCCGACCACAAGACGTTCAAGTC -3'
I77W Fwd	5'- CTTGTTGTCGGCAGCCTGGAACTTTTTTCTGATCGCGTTCG -3'
I77W Rev	5'- CGAACGCGATCAGAAAAAAGTTCCAGGCTGCCGACAACAAG -3'
F79W Fwd*	5'- GATCAACTGGTTCCTGATTGCGTTCGCGGTGTACTTCC -3'
F79W Rev*	5'- GAACGCAATCAGGAACCAGTTGATCGCTGCCGACAAC -3'
F80W Fwd	5'- GCAGCGATCAACTTTTGGCTAATTGCGTTTGCGGTGTACTTCC -3'
F80W Rev	5'- GGAAGTACACCGCAAACGCAATTAGCCAAAAGTTGATCGCTGC -3'
F84W Fwd	5'- GCGATCAACTTTTTCCTGATTGCGTGGGCGGTGTACTTCCTAG -3'
F84W Rev	5'- CTAGGAAGTACACCGCCCACGCAATCAGGAAAAAGTTGATCGC -3'
Y87W Fwd	5'- CCTGATCGCGTTCGCTGTGTGGTTCCTAGTCGTGCTGCCC -3'
Y87W Rev	5'- GGGCAGCACGACTAGGAACCACACAGCGAACGCGATCAGG -3'
V91W Fwd	5'- CGGTGTACTTCCTAGTCTGGCTGCCCTACAACACAC -3'
V91W Rev	5'- GTGTGTTGTAGGGCAGCCAGACTAGGAAGTACACCG -3'
Y94W Fwd	5'- CCTAGTCGTGCTGCCCTGGAACACACTACGCAAG -3'
Y94W Rev	5'- CTTGCGTAGTGTGTTCCAGGGCAGCACGACTAGG -3'
V103W Fwd	5'- CTACGCAAGAAGGGGGAGTGGGAGCAGCCGGGCGACAC -3'
V103W Rev	5'- GTGTCGCCCGGCTGCTCCCACTCCCCCTTCTTGCGTAG -3'

Table 2.5 Synthetic oligonucleotide primers used in the QuickChange™ site directed mutagenesis procedure of the *TbmscL* gene. Forward (sense) Trp mutagenic primers were used in combination with the complementary reverse (antisense) Trp mutagenic primer, as outlined in Section 2.2.5.2. Trp mutations are double underlined and conservative codon substitutions are single underlined. Conservative mutations were introduced to prevent secondary structure formation of the oligonucleotide. * primer with small overhangs.

Primer	TbMscL Primer Sequence
L69C Fwd	5'- GGTCAGACCATTGATTGTAACGTCTTGTTGTCGGCAGCGATC -3'
L69C Rev	5'- GATCGCTGCCGACAACAAGACGTTACAATCAATGGTCTGACC -3'
Y87C Fwd	5'- CCTGATCGCGTTCGCTGTGTGCTTCCTAGTCGTGCTGCCC -3'
Y87C Rev	5'- GGGCAGCACGACTAGGAAGCACACAGCGAACGCGATCAGG -3'
V91C Fwd	5'- GCGGTGTACTTCCTAGTCTGCCTGCCCTACAACACAC -3'
V91C Rev	5'- GTGTGTTGTAGGGCAGGCAGACTAGGAAGTACACCGC -3'
Y94C Fwd	5'- CCTAGTCGTGCTGCCCTGCAACACACTACGCAAG -3'
Y94C Rev	5'- CTTGCGTAGTGTGTTGCAGGGCAGCACGACTAGG -3'

Table 2.6 Synthetic oligonucleotide primers used in the QuickChange™ site directed mutagenesis procedure of the *TbmscL* gene. Forward (sense) Cys mutagenic primers were used in combination with the complementary reverse (antisense) Cys mutagenic primer, as outlined in Section 2.2.5.2. Cys mutations are double underlined and conservative codon substitutions are single underlined. Conservative mutations were introduced to prevent secondary structure formation of the oligonucleotide.

Primer	TbMscL Primer Sequence
V21K Fwd	5'- GACCTGGCAGTCGCGAAAGTAATTGGCACAGCGTTCACGGC -3'
V21K Rev	5'- GCCGTGAACGCTGTGCCAATTACTTTCGCGACTGCCAGGTC -3'
R98Q Fwd	5'- CCTACAACACACTACAGAAGAAGGGGGAGGTCGAGC -3'
R98Q Rev	5'- GCTCGACCTCCCCCTTCTTCTGTAGTGTGTTGTAGG -3'
K99Q Fwd	5'- CTACAACACACTACGCCAGAAGGGGGAGGTCGAGCAG -3'
K99Q Rev	5'- CTGCTCGACCTCCCCCTTCTGGCGTAGTGTGTTGTAG -3'
K100Q Fwd	5'- CTACAACACACTACGCAAGCAGGGGGAGGTCGAGCAG -3'
K100Q Rev	5'- CTGCTCGACCTCCCCCTGCTTGCGTAGTGTGTTGTAG -3'
R98Q:K99Q Fwd	5'- CCTACAACACACTACAGCAGAAGGGGGAGGTCGAGCAGCC -3'
R98Q:K99Q Rev	5'- GGCTGCTCGACCTCCCCCTTCTGCTGTAGTGTGTTGTAGG -3'
R98Q:K100Q Fwd	5'- CCTACAACACACTACAGAAGCAGGGGGAGGTCGAGCAGCC -3'
R98Q:K100Q Rev	5'- GGCTGCTCGACCTCCCCCTGCTTCTGTAGTGTGTTGTAGG -3'
K99Q:K100Q Fwd	5'- CTACAACACACTACGCCAGCAGGGGGAGGTCGAGCAG -3'
K99Q:K100Q Rev	5'- CTGCTCGACCTCCCCCTGCTGGCGTAGTGTGTTGTAG -3'
R98Q:K99Q:K100Q Fwd	5'- CCTACAACACACTACAGCAGCAGGGGGAGGTCGAGCAGCCG -3'
R98Q:K99Q:K100Q Rev	5'- CGGCTGCTCGACCTCCCCCTGCTGCTGTAGTGTGTTGTAGG -3'

Table 2.7 Synthetic oligonucleotide primers used in the QuickChange™ site directed mutagenesis procedure of the *TbmscL* gene. Forward (sense) charge mutagenic primers were used in combination with the complementary reverse (antisense) charge mutagenic primer, as outlined in Section 2.2.5.2. Residue mutations are double underlined and conservative codon substitutions are single underlined. Conservative mutations were introduced to prevent secondary structure formation of the oligonucleotide.

Primer	Sequence
pQE Fwd	5'- CGGATAACAATTTCACAC -3'
T7 Fwd	5'- TAATACGACTCACTATAGGG -3'

Table 2.8 Synthetic oligonucleotide primers used in the sequencing of *mscL* genes. pQE Fwd can be used in conjunction with any of the Qiagen pQE plasmids, and was used for the sequencing of pQE-32:*EcmscL* samples. T7 Fwd can be used in conjunction with any plasmid containing a T7 promoter, and was used for the sequencing of pET-19b:*TbmscL* samples. Plasmid DNA containing the *EcmscL* and *TbmscL* genes was sequenced prior to site directed mutagenesis to ensure wild type status. Following site directed mutagenesis, mutations were confirmed by DNA sequencing.

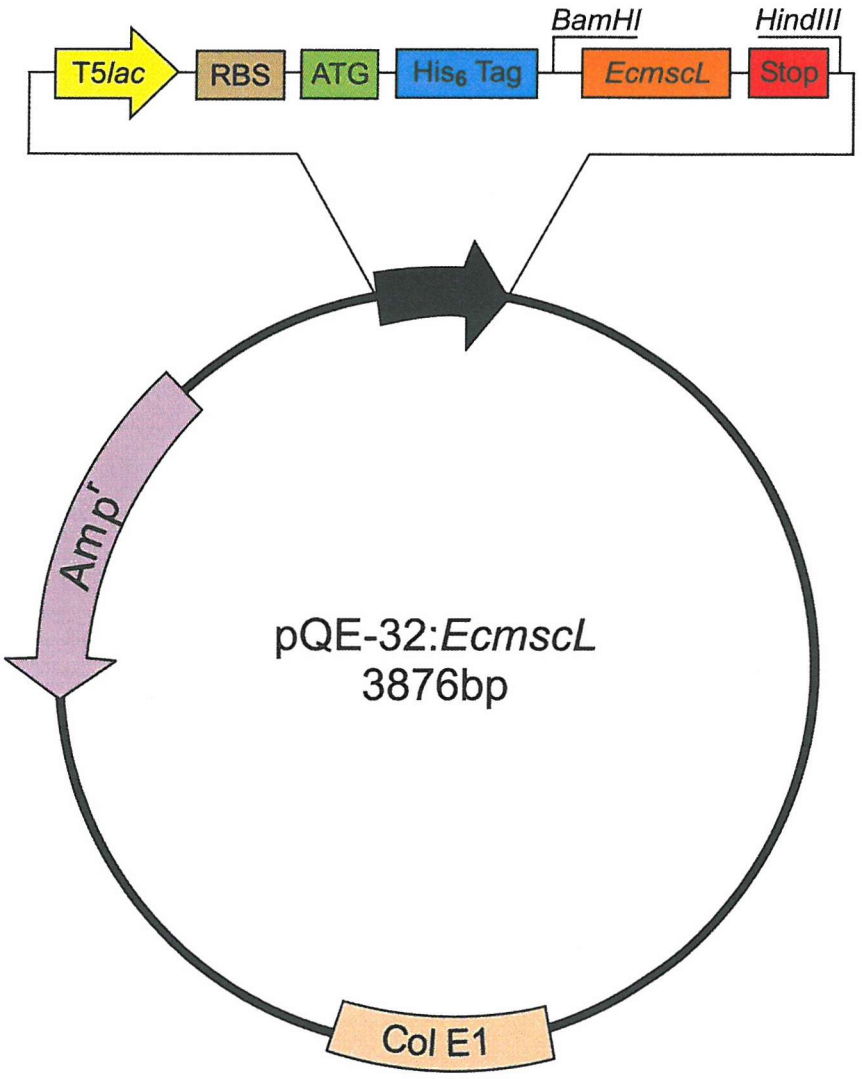

Figure 2.1 pQE-32:*EcmscL* protein expression plasmid (Qiagen). The *EcmscL* gene was cloned into the expression vector pQE-32 using the restriction sites *BamHI* and *HindIII*, generating the recombinant plasmid pQE-32:*EcmscL* and kindly donated by Professor B. Martinac. The *EcmscL* gene is under the control of the T5 promoter and regulated by the *lac* operon. *E. coli* transformants harbouring pQE-32:*EcmscL* were selected by ampicillin resistance.

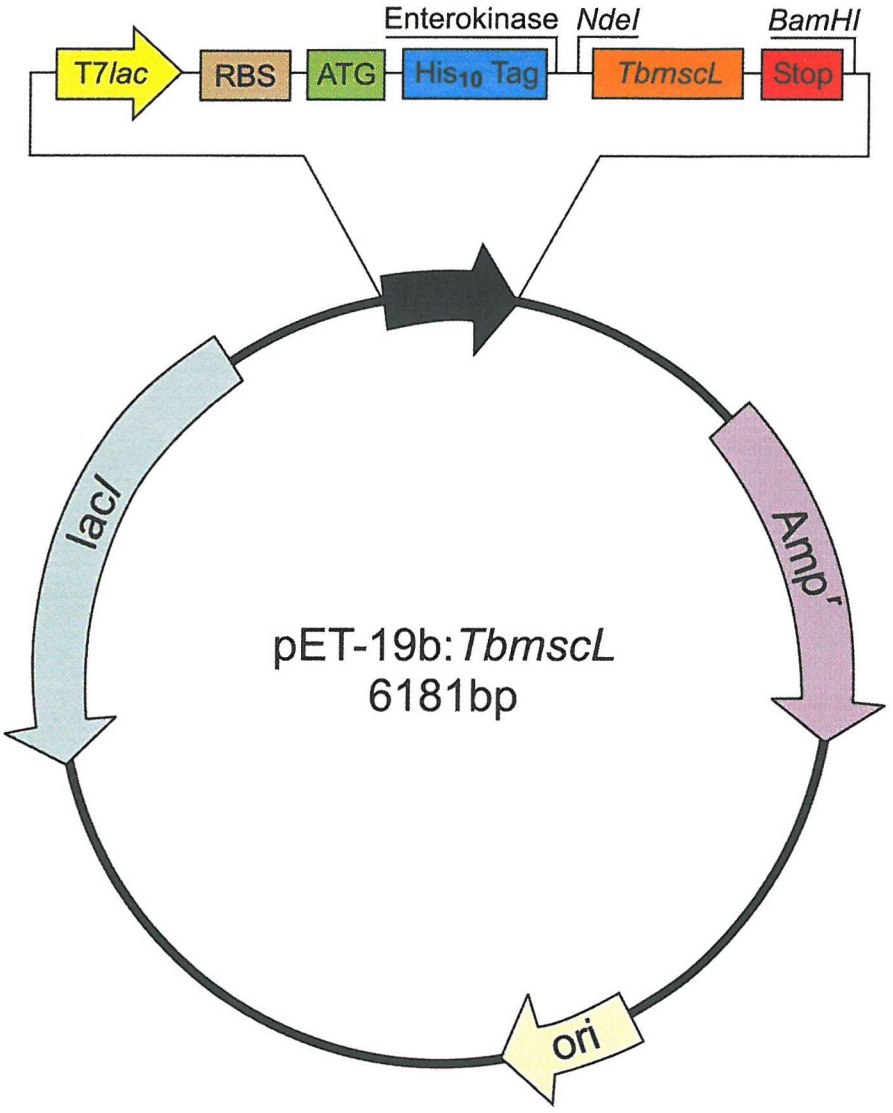

Figure 2.2 pET-19b:*TbmscL* protein expression plasmid (Novagen). The *TbmscL* gene was cloned into the expression vector pET-19b using the restriction sites *NdeI* and *BamHI*, generating the recombinant plasmid pET-19b:*TbmscL* and kindly donated by Professor D. C. Rees. The *TbmscL* gene is under the control of the T7 promoter and regulated by the *lac* operon. *E. coli* transformants harbouring pET-19b:*TbmscL* were selected by ampicillin resistance.

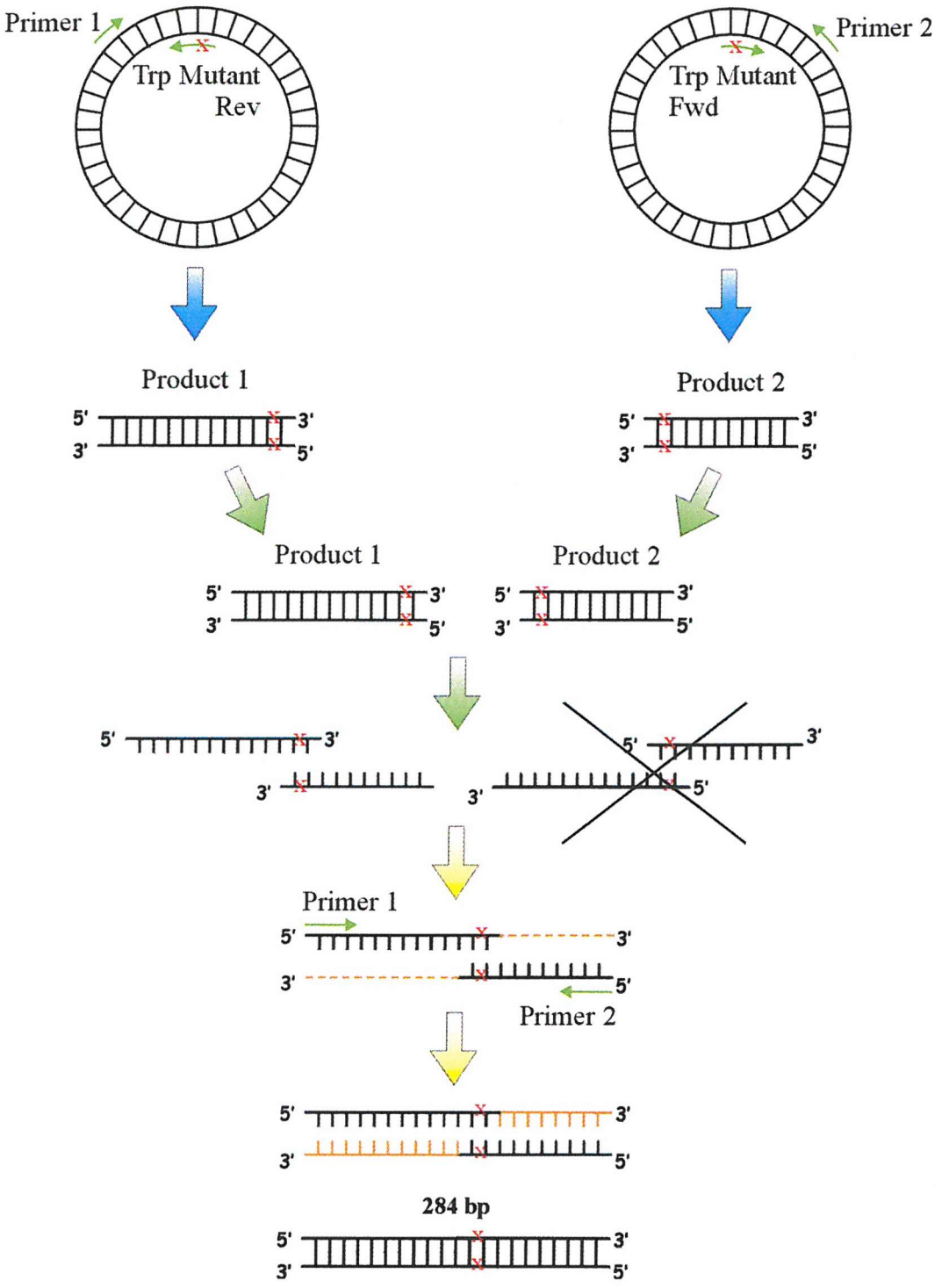

Figure 2.3 Schematic overview of the three-stage site directed mutagenesis protocol used for replacing specific amino acids with Trp in the EcMscL homologue. Wild type template was used in combination with Primer 1 and the reverse mismatched primer, and Primer 2 with the forward mismatched primer to produce two Trp-mutated PCR products 1 and 2 (Table 2.4). The latter were subsequently annealed together through a second round of PCR and finally amplified in the third stage PCR reaction.

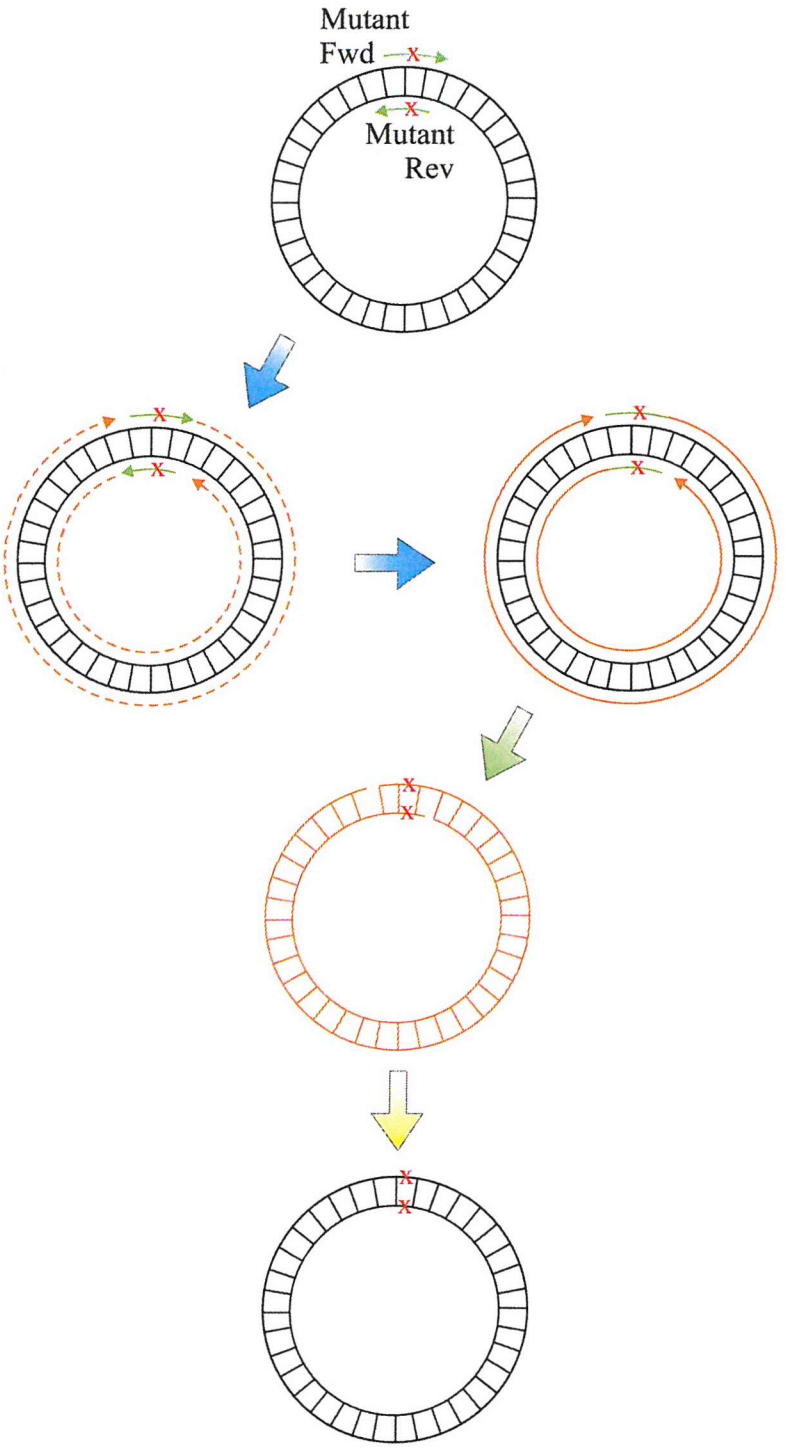

Figure 2.4 Schematic overview of the QuickChange™ protocol from Stratagene used for replacing specific amino acids within the TbMscL homologue. Wild type template was used in combination with two complementary mutagenic primers (Tables 2.5-2.7), to produce nicked circular stranded DNA. The hemimethylated plasmids containing mutated, nonmethylated DNA and methylated, nonmutated parental DNA were subsequently digested with *DpnI*. Nicked, mutagenic dsDNA was repaired by transformation into *E. coli* strain XL-1 Blue.

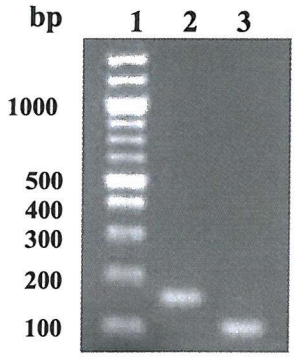

Figure 2.5 Agarose gel of PCR products from the first stage PCR of the three-stage site directed mutagenesis procedure. Lane 1 contains 100 bp ladder (2 µl). Lanes 2 and 3 contain 2 µl of products 1 and 2 respectively.

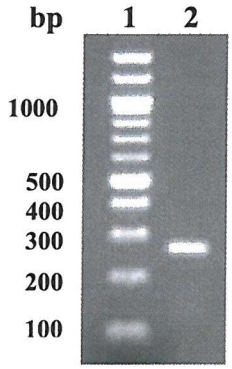

Figure 2.6 Agarose gel of the full-length mutant fragment (284 bp) produced in the third stage of the three-stage site directed mutagenesis procedure. Lane 1 contains 100 bp ladder (2 µl). Lane 2 contains 2 µl full-length Trp-mutated fragment.

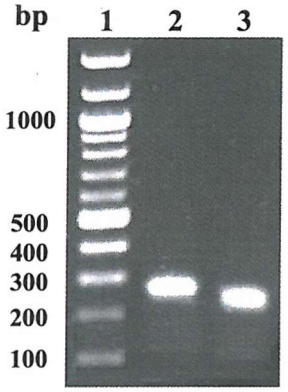

Figure 2.7 Agarose gel of the full-length mutant fragment produced in the third stage of the three-stage site directed mutagenesis procedure, before and after DNA digestion with restriction enzymes *ClaI* and *SalI* and DNA clean-up. Lane 1 contains 100 bp ladder (2 µl). Lane 2 contains full-length Trp-mutated fragment before DNA digest (284 bp) (2 µl). Lane 3 contains the digested and cleaned Trp-mutated fragment (257 bp) (5 µl).

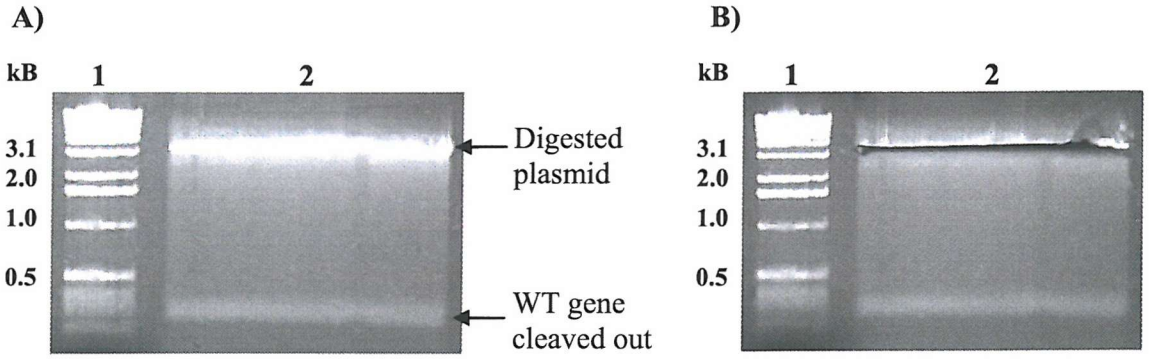

Figure 2.8 Agarose gels of *ClaI* and *SalI* digested WT pQE-32:*EcmscL* before and after DNA extraction from the agarose gel. A) Lane 1 contains 1kB ladder (2 µl) and Lane 2 contains *ClaI* and *SalI* digested plasmid (150 µl). B) Lane 1 contains 1kB ladder (2 µl) and Lane 2 contains *ClaI* and *SalI* digested plasmid (150 µl) following extraction of the plasmid from the agarose gel.

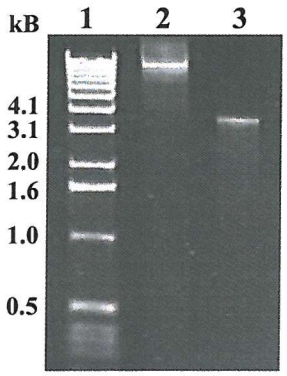

Figure 2.9 Agarose gel of native and *ClaI* and *SalI* digested WT pQE-32:*EcmscL* following extraction of the digested plasmid from the agarose gel and DNA clean-up. Lane 1 contains 1 kB ladder (2 µl). Lane 2 contains native undigested WT pQE-32:*EcmscL* plasmid (2 µl). Lane 3 contains *ClaI* and *SalI* digested plasmid (3.59 kB) after gel extraction and purification (5 µl).

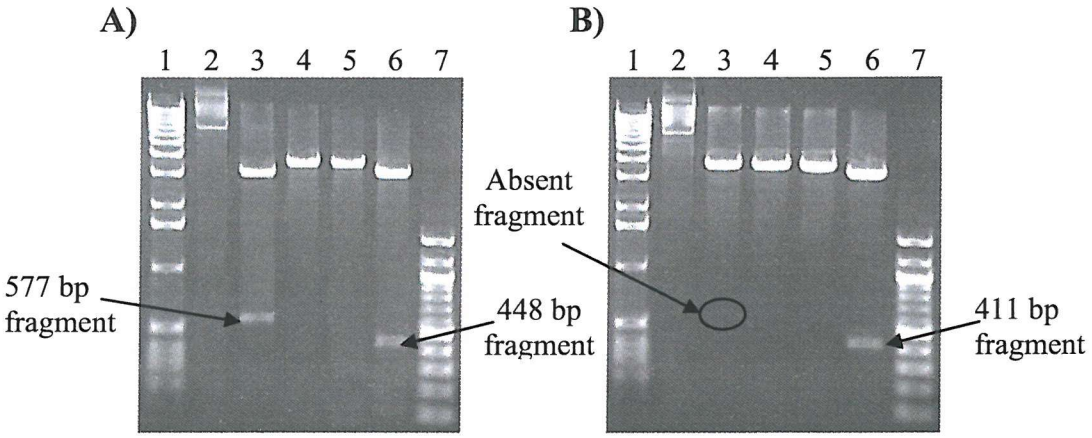

Figure 2.10 Agarose gel of wild type pQE-32:*EcmscL* (A) and Trp-mutated pQE-32:*EcmscL* (B). For both A) and B) Lane 1 contains 1 kB ladder (2 µl); Lane 2 contains uncut plasmid (2 µl); Lane 3 *XhoI* digested plasmid (2 µl); Lane 4 *BamHI* digested plasmid (2 µl); Lane 5 *SalI* digested plasmid (2 µl); Lane 6 *BamHI/SalI* double digested plasmid (2 µl) and Lane 7 contains 100 bp ladder (2 µl).

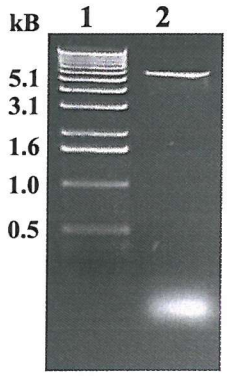

Figure 2.11 Agarose gel of the Trp-mutated plasmid PCR product carried out using the QuickChange™ protocol from Stratagene. Lane 1 contains 1 kB ladder (2 µl). Lane 2 contains Trp-mutated pET-19b:*TbmscL* (5 µl).

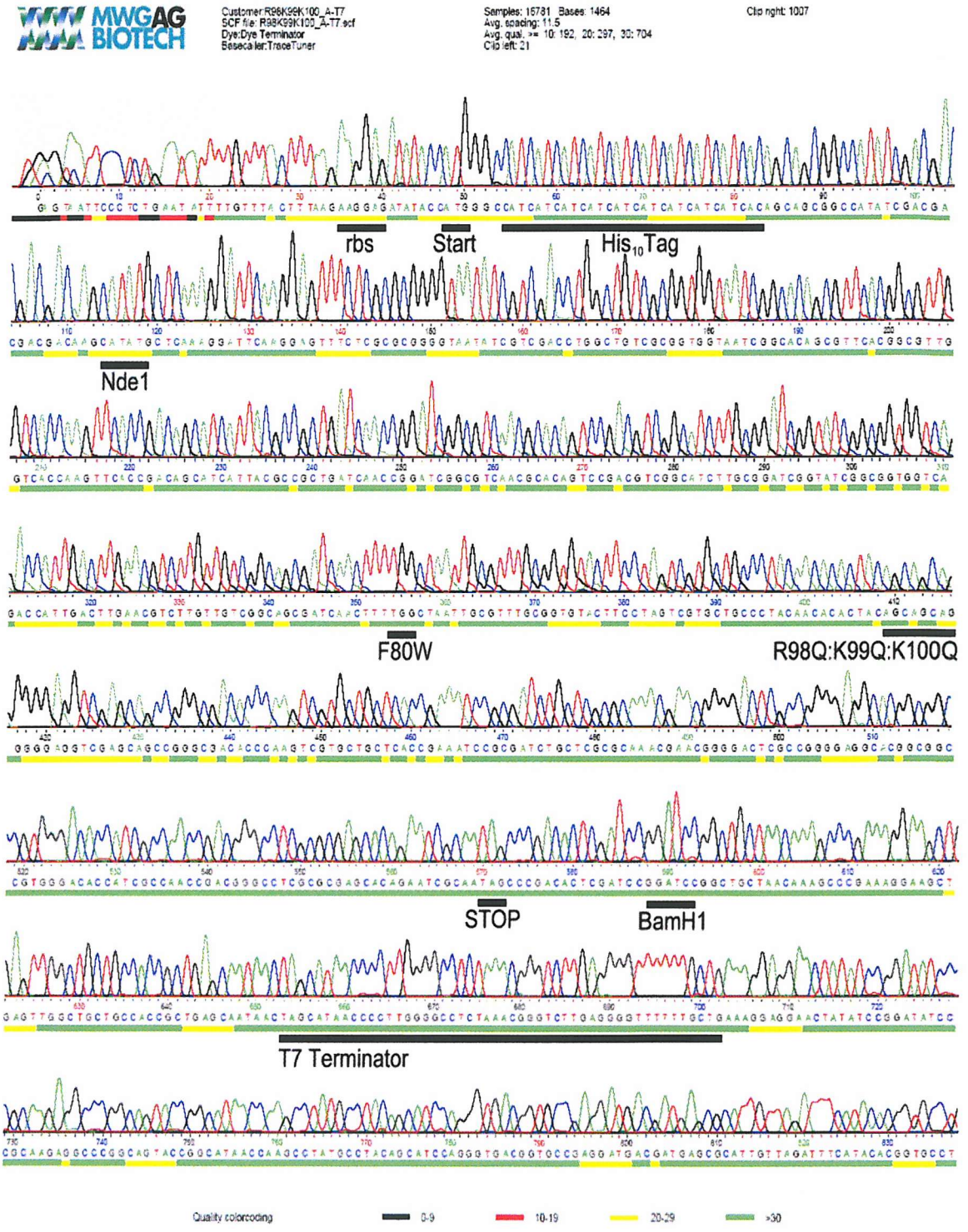

Figure 2.12 Example sequencing trace from MWG. The fidelity of mutated *mscL* products were confirmed by sequence analysis, as described in Section 2.2.5.3. Forward reading frame sequence of F80W:R98Q:K99Q:K100Q-*TbmscL* (sense) amplified using the T7 Fwd promoter primer (Table 2.8). Ribosome binding site (rbs), decapeptide His (His_{10}) tag, start and stop codons, and *NdeI* and *BamHI* restriction sites are labelled. File analysed using Chromas *v*1.45.

Chapter 3:
Fluorescence & the Properties of Trp Residues

3 FLUORESCENCE AND THE PROPERTIES OF TRP RESIDUES

3.1 Introduction

Fluorescence is a highly sensitive and non-invasive technique that can be used to study many aspects of biochemistry involving structure and conformation, reaction pathways and kinetics, and concentrations of ions within cells.

Fluorescence is the process of emission of light following absorption, returning the molecule from an electronically excited state to a ground state, as shown by the Jabłoński diagram (Figure 3.1). Transition of an electron from the ground state (S_0) to a higher energy level (S_1, S_2, etc) following absorption of a photon occurs very rapidly, on a 10^{-15} s time scale. Following promotion of the electron to one of the excited states the electron rapidly returns to the lowest vibrational level, S_1 within 10^{-12} s or less, in a process known as internal conversion, where energy is lost by non-radiative processes (e.g. heat or excited-state reactions). The electron returns from the S_1 exited state to the ground state. The emitted light is of lower energy or longer wavelength than the exciting light due to the loss of energy during internal conversion and further loss of energy as the electron drops to a higher vibrational level of the ground state. This shift in wavelength is commonly referred to as Stokes' shift (Eftink, 1991).

Not all molecules that absorb light emit fluorescence. Fluorescent molecules typically contain conjugated polyaromatic hydrocarbons and of the 20 amino acids usually found in proteins only Phe, Tyr, and Trp contribute to the intrinsic fluorescence of proteins (Figure 3.2). However, the fluorescence emission of proteins that contain all three amino acids is dominated by tryptophan fluorescence, which has the largest extinction coefficient and absorbs at the longest wavelength (Campbell and Dwek, 1986).

The fluorescence quantum yield (Φ_F) is the probability that the exited state electron will return to the ground state by emission of a photon, and hence is an indication of the efficiency of the fluorescence process. Φ_F is dependent on temperature and the

solvent; the energy yield of fluorescence is always less than unity due to non-radiative processes, hence Stokes' losses (Lakowicz, 1999).

The indole nucleus of tryptophan is extremely sensitive to solvent effects, with significant shifts in the emission spectrum to longer wavelengths due to the presence of two excited states. The two excited states, L_a and L_b have similar energies but different polarities; the polarity of L_b is similar to that of the ground state, whereas L_a has a polarity double that of the ground state and is thought to be the main contributor to emission (Ladokhin, 2000). In nonpolar solvents the L_b state is lower in energy than the L_a state, but in polar solvents the imino nitrogen forms an exciplex (becomes hydrogen bonded with the solvent during the excited state), which stabilises the L_a state causing the energy of the L_a state to fall below that of the L_b state (Lakowicz, 1999). Emission occurs from the lowest-energy state, therefore tryptophan fluorescence emission maxima (λ_{max}) in proteins varies over a 40 nm range depending on the dielectric constant of the solvent, and this environmental sensitivity provides a wealth of information about the location of the Trp within a protein or membrane (Ladokhin et al., 2000).

3.2 Fluorescence Quenching

Fluorescence quenching is a process which decreases the intensity of the fluorescence emission by deactivating the excited state by mechanisms other than radiative emission. Quenching can occur by several different mechanisms:

1) static quenching occurs upon formation of a nonfluorescent complex between fluorophore and quencher prior to excitation,

2) dynamic quenching occurs upon diffusive collision of the fluorophore and quencher during the fluorescence lifetime, or

3) energy transfer occurs when the emission spectrum of the fluorophore and absorption spectrum of the quencher overlap.

Static quenching occurs due to the formation of a non-fluorescent ground-state complex, which is immediately returned to the ground state upon absorption of light. Static quenching therefore removes the fluorescence contribution of those fluorophores that are accessible to the quencher, leaving only the fluorescence from those residues that cannot be complexed with quencher (Lakowicz, 1999).

The decrease in fluorescence intensity due to quenching by a collisional event is related to the decrease in fluorescence lifetime and is described by the Stern-Volmer equation:

$$F_o/F = 1 + K_{SV}[Q] = 1 + k_q\tau_o[Q] \qquad \text{Equation 3.1}$$

where F_o and F are the fluorescence intensities in the absence and presence of quencher, respectively, K_{SV} is the Stern-Volmer quenching constant, k_q is the bimolecular quenching constant, τ_o is the lifetime of the fluorophore in the absence of quencher, and [Q] is the quencher concentration. Thus, collisional quenching data are usually presented as a plot of F_o/F versus [Q], with an intercept of 1 on the y-axis and the gradient equal to K_{SV} or $k_q\tau_o$ (Eftink, 1991).

Fluorescence quenching due to a collisional event is a short range effect where the fluorophore and the quencher have to come into contact within the lifetime of the excited state of the fluorophore, which is typically 1 ns. Typically fluorescence quenchers are molecules containing heavy atoms such as iodine or bromine. The mechanisms of the quenching event is uncertain, but is believed to involve the excited triplet state. Quenching by metal ions such as Mn^{2+} probably involves donation of an electron from the fluorophore to the quencher. Trp fluorescence is also quenched by molecules such as acrylamide.

In contrast to collisional quenching, fluorescence energy transfer (FET) between chromophores can occur over much greater distances. The most common form of the energy transfer is the transfer of an excited state singlet electron from a donor to the excited singlet state of an acceptor, with the donor subsequently returning to the ground state. Transfer occurs via a non-radiative process and only occurs when there is overlap between the fluorescence spectrum of the donor and the absorbance spectra

of the acceptor. The overlap integral $J(\lambda)$ expresses the degree of spectral overlap between the donor emission and the acceptor absorption

$$J(\lambda) = (\int_0^\infty F_D(\lambda)\varepsilon_A(\lambda)\lambda^4 \, d\lambda)/(\int_0^\infty F_D(\lambda) \, d\lambda) \qquad \text{Equation 3.2}$$

where $F_D(\lambda)$ is the corrected fluorescence intensity of the donor at wavelength λ, and $\varepsilon_A(\lambda)$ is the extinction coefficient of the acceptor at λ (Lakowicz, 1999). The overlap integral $J(\lambda)$ together with the quantum yield of the donor can be used to calculate R_o, the Förster distance between the donor and acceptor at which the efficiency of energy transfer is 50 %:

$$R_o = 9.78 \times 10^3[\kappa^2 n^{-4} \Phi_D J(\lambda)] \qquad \text{Equation 3.3}$$

where Φ_D is the quantum yield of the donor in the absence of the acceptor, n is the dielectric constant of the medium and κ^2 is a factor describing the relative orientation in space of the transition dipoles of the donor and acceptor, and is assumed to be equal to 2/3 (Lakowicz, 1999). The rate of energy transfer k_T for a single donor-acceptor pair can be written as

$$k_T = (1/\tau_D)(R_o/r)^6 \qquad \text{Equation 3.4}$$

where τ_D is the decay rate of the donor in the absence of the acceptor, r is the distance between the donor and acceptor, and R_o is the Förster distance (Lakowicz, 1999). The efficiency E of energy transfer is given by:

$$E = k_T/(k_T + \tau_D^{-1}) \qquad \text{Equation 3.5}$$

which can be written as

$$E = 1-(F_{DA}/F_D) \qquad \text{Equation 3.6}$$

where F_{DA} and F_D are the fluorescence intensity of the donor in the presence and absence of the acceptor respectively.

3.3 Quenching of Trp Fluorescence by Dibromo molecules

The mechanism of quenching of Trp by bromine is unclear, as it could either be a collisional event or by fluorescence energy transfer, as in Förster energy transfer (Bolen and Holloway, 1990; Zelent et al. 1996). For energy transfer by the Förster mechanism the quencher must absorb light at the wavelengths of Trp emission (Lakowicz, 1999). As shown in Figure 3.3, 2,3-dibromobutane shows significant absorbance centred at a wavelength of 275 nm. To check that this absorbance was not due to impurities of the commercial sample of 2,3-dibromobutane, a spectra was run for 1,2-nonadecene, which showed no absorption over the range studied, and then the 1,2-nonadecene was brominated to give 1,2-dibromononadecane; the 1,2-dibromononadecane showed absorbance centred at 275 nm, as shown for 2,3-dibromobutane shown in Figure 3.3. The small but significant overlap with the emission spectra of Trp shown in Figure 3.3, gives the overlap integral given in Table 3.1. Similarly, the absorption of 1,3-diiodobenzene overlaps Trp emission, with a larger overlap integral. Putting these values of $J(\lambda)$ into the Förster equation (Equation 3.3) gives the values for R_0 in Table 3.1. Clearly the Förster equation is invalid under these conditions; an assumption of the derivation of the Förster equation is that the absorbance and emission dipoles are point dipoles, so that they have no significant size on the distance scale defined by R_0. For a typical donor-acceptor pair, R_0 is ca. 50 Å, and so the size of the donor and acceptor group can indeed by ignored. However, with a calculated R_0 value of 3-13 Å, it is not possible to ignore the finite sizes of the donor and acceptor groups, and values of R_0 calculated for the Förster equation will be underestimates. Thus it is possible that the 'true' values for R_0 for the dibromo-Trp pair would be close to the experimentally estimated valued of 8 Å (Mall et al., 2001), if it were possible to calculate a 'true' theoretical value for R_0. Some evidence in favour of the FET model is present in Chapter 5. On the other had, it is also possible that both collisional quenching and FET contribute to quenching by dibromo compounds (Ladokhin 1999). For the purposes here the important point is that quenching fits to a sixth-power dependence on the distance of separation between the Trp residue and the quencher, and so the equation derived in the literature to describe the distance dependence of FET can be used here to describe the distance dependence quenching by brominated phospholipids.

3.4 The Inner Filter Effect

In dilute solutions or suspensions, fluorescence intensity is linearly proportional to concentration over a limited range of optical densities. However, when the sample absorbance exceeds 0.05 in a cell of 1 cm pathlength, the relationship becomes nonlinear, due to absorption of either the primary or fluorescent radiation by the solution. This is referred to as the inner filter effect. Loss of fluorescence intensity due to absorption of the incident light and that due to absorption of the emitted light are sometimes referred to as the primary and secondary inner filter effects, respectively. Another form of a primary inner filter effect is when a non-fluorescent species or interferent absorbs in the same wavelength range as the fluorophore excitation wavelength, thereby decreasing the radiant power available to excite the fluorophore (Lakowicz, 1999).

3.5 Steady-State Fluorescence Measurements

For Trp fluorescence measurements, typically 250 µl of the sample containing 0.98 µM MscL were diluted into sterile-filtered Hepes buffer (2.75 ml; 20 mM Hepes, 1 mM EGTA, 100 mM KCl, pH 7.2) and incubated at 25 °C. Fluorescence intensities were recorded at 25 °C using an SLM-Aminco 8100 Series Fluorimeter, with an excitation wavelength of 280 nm. Fluorescence emission spectra were measured using a 10 x 10 mm quartz cuvette and recorded between 290 and 400 nm, with slit widths of 4 nm for both excitation and emission. Results were corrected for light scatter by subtracting the emission spectra of an appropriate blank.

Quenching of Trp fluorescence by acrylamide and iodide was measured at an excitation wavelength of 295 nm to minimise the inner filter effect (Figure 3.4), which was corrected for by applying the formula:

$$F_{corr} = F_{obs} \times 10^{\varepsilon 0.5bC} \qquad \text{Equation 3.7}$$

where F_{corr} and F_{obs} are the corrected and observed fluorescence intensities respectively, ε is the excitation coefficient for quencher (acrylamide or iodide) at 295

nm in the units of M^{-1} cm^{-1}, b is the path length of the cuvette in centimetres, and C is the molar concentration of quencher (acrylamide or iodide) in the sample (Lakowicz, 1999). The values of ε measured at 295 nm for acrylamide and iodide were 0.070 and 0.032 M^{-1} cm^{-1} respectively. The emission wavelength was measured at 340 nm to eliminate the interference from the Raman band of water.

A table of correction factors was generated for the SLM-Aminco 8100 Series Fluorimeter. The experimental emission spectrum of L-Trp in Hepes buffer recorded on the instrument was compared with the normalised reference spectrum for Trp published by Landokhin et al. (2000), thereby generating a set of correction factors.

To obtain accurate values for wavelengths of maximum fluorescence emission, intensity corrected fluorescence spectra were fitted to skewed Gaussian curves:

$$F = F_{max} \exp\{-(\ln 2)[\ln(1+2b(\lambda - \lambda_{max})/\omega_\lambda)/b]^2\} \qquad \text{Equation 3.8}$$

where F and F_{max} are the fluorescence intensities at λ and λ_{max} respectively, b is the skew parameter and ω_λ is the peak width at half height (Rooney and Lee, 1986).

3.6 Time-Resolved Fluorescence Measurements

Fluorescence lifetime measurements were recorded at 25 °C using a PTI GL-3300 lifetime fluorimeter equipped with a PTI nitrogen dye laser (10 mM 7-diethylamino-4-methylcumarin (C-460; Sigma)) to excite samples at 478 nm. Measurements were recorded using a 10 x 10 mm quartz cuvette with slit widths of 5 nm for both excitation and emission. The start and end delay were 46 ns and 88 ns respectively and data were collected to a resolution of 10 channels ns^{-1}. Five shots were fired for each channel at a frequency of 10 Hz and an integration time of 50 μs. Averaging of three spectra was used to increase signal-to-noise ratio. Fluorescence decays were fitted to sums of two and three exponentials and the fractional contribution f of each decay time were calculated by applying the formula:

$$f_i = \alpha_i\tau_i/(\sum_j \alpha_j\tau_j) \qquad \text{Equation 3.9}$$

where α_i is the amplitude of the component or preexponential factor, τ_i is the decay time from the excited state, α_j is the amplitude of the all the components and τ_j is the total decay time. The average lifetime, $\bar{\tau}$ was calculate from the equation:

$$\bar{\tau} = (f_1\tau_1) + (f_2\tau_2) + (f_3\tau_3) \qquad \text{Equation 3.10}$$

as described by Lakowicz (1999).

3.7 Fluorescence Analysis of Lipid Quenching

3.7.1 *Annular Lipid Binding Sites*

Quencher-labelled fatty acids and phospholipids are a powerful tool in the study of fluorescent species within membranes. In bilayers, the quencher group can be positioned at different positions along the fatty acyl chain. This allows brominated-lipids to be used to quantify the depth or location of a fluorescent group on a protein within the membrane and allows binding constants for lipids to the membrane protein as a function of lipid structure to be determined.

A complication of the fluorescence quenching method for determining lipid binding constants is that most membrane proteins contain several Trp residues. Therefore, analysis of Trp fluorescence quenching data for membrane proteins generally requires the assumptions to be made that all the Trp residues that are quenched by the quenching lipid are quenched to the same extent, and that all the lipid binding sites close to the quenched Trp residues have equal affinities for the quenching lipid. MscL channels from *Escherichia coli* and *Mycobacterium tuberculosis* contain no Trp residues. We therefore have the opportunity of introducing single Trp residues into regions of interest in the protein. Although the MscL channels are homopentameric, so that the intact channel will contain five Trp residues if one Trp residue is introduced into each monomer, lipid interactions with each monomer in the pentamer will be identical so that the quenching properties of each Trp residue will also be identical.

Fluorescence occurs on a 10^{-9} s time scale, whereas the lateral exchange of lipids within the membrane is slower (10^{-8} s), so that during the fluorescence lifetime, lipids appear to be static entities. This allows a lattice model of quenching to be applied, where the number of brominated-lipids (n) occupying sites close enough to the fluorophore to quench Trp fluorescence can be estimated from the equation:

$$F = F_{min} + (F_o - F_{min})(1 - x_{Br})^n \qquad \text{Equation 3.11}$$

where F_o and F_{min} are the fluorescence intensities of MscL in nonbrominated and brominated lipid respectively, and F is the fluorescence intensity in a phospholipid mixture, when the mole fraction of brominated lipid is x_{Br} (London and Feigenson, 1981; East and Lee, 1982). The level of fluorescence quenching is dependent on the number of lattice sites surrounding a Trp residue (Figure 3.5); the higher the number of lattice sites, the greater the probability of a lattice site being occupied by brominated lipid and the higher the quenching.

The hydrophobic surface of a membrane protein covered with annular lipids is shown in Figure 3.6. The complete surface of the protein is covered by lipid molecules, so that one lipid molecule must leave the surface before another can enter, which can be described in terms of a simple competitive binding of lipids at a number of lattice sites on the protein surface. Measuring fluorescence quenching in mixtures of lipids either with different fatty acyl chain lengths or with different lipid head groups, allows the determination of the binding affinity of one lipid relative to another. At each lattice site there will be an equilibrium between the two different lipid species, given by:

$$PA + B \xleftrightarrow{K} PB + A \qquad \text{Equation 3.12}$$

where PA and PB are protein bound to nonbrominated (A) and brominated lipid (B) respectively and A and B are lipids not bound to the protein. The equilibrium constant is described as:

$$K = ([PB][A])/([PA][B]) \qquad \text{Equation 3.13}$$

where K is the binding constant for the non-brominated lipid relative to the brominated lipid and the square brackets denote concentration in mole per litre of sample. If the non-brominated lipid A binds more strongly to MscL than lipid B, then fluorescence will be high and K is high, as lipid A will have a greater probability of occupying a lattice site and shielding Trp fluorescence from quenching by lipid B. Conversely, if lipid A has lower affinity for MscL, K is low, and the lattice sites will be occupied by lipid B; consequently, Trp fluorescence quenching will be marked. The effect of K on the level of quenching is shown in Figure 3.7.

At a given total concentration of A and B, the fraction of annular sites (f_{Br}) occupied by brominated lipid (B) is given by:

$$f_{Br} = [PB]/([PA]+[PB]) \qquad \text{Equation 3.14}$$

Therefore, fluorescence quenching in a mixture of two lipids fits to the equation:

$$F = F_{min} + (F_o - F_{min})(1 - f_{Br})^n \qquad \text{Equation 3.15}$$

The amount of lipid used in the experiments for determining lipid binding constants is much greater than the amount of protein, the lipid:protein mole ratio being typically 100:1, so that the fraction of lipid bound to the protein is negligible.

$$[B]/[A] = x_{Br}/(1 - x_{Br})$$

and

$$[PB]/[PA] = f_{Br}/(1 - f_{Br})$$

Hence,

$$K = ((1 - f_{Br})(x_{Br}))/((f_{Br}(1 - x_{Br}))$$
$$= (x_{Br} - f_{Br}x_{Br})/(f_{Br} - f_{Br}x_{Br}) \qquad \text{Equation 3.16}$$

and

$$f_{Br} = x_{Br}/(x_{Br} + K(1 - x_{Br}) \qquad \text{Equation 3.17}$$

If there is a single class of annular binding site on the protein, then the same relative binding constant should be obtained from this analysis, whichever of the two lipids in

the mixture is brominated. Thus in a mixture of lipid X and Y, brominated X and non-brominated Y, or non-brominated X and brominated Y, should give the same value for K. If this is not the case, it is evidence for the possible existence of more than more class of site of the protein.

3.7.2 *Lipid Binding to Two Annular Binding Sites*

In determining the lipid binding constants for a protein using Equation 3.15, we assume that all the lipid binding sites close enough to quench the Trp residues have equal affinities for the quenching lipid and that the quenching lipid binds to a single class of annular binding site. However, it is possible that not all the annular sites have equal affinities for all lipids. In Chapter 6, a case will be analysed is which the two sites around a Trp residue from which Trp fluorescence can be quenched ($n = 2$) have different affinities for lipid molecule. In this case, an equation analogous to equation 3.12 has to be written for each site:

$$P^1A + B \xleftrightarrow{K_1} P^1B + A \qquad \text{Equation 3.18}$$

and

$$P^2A + B \xleftrightarrow{K_2} P^2B + A \qquad \text{Equation 3.19}$$

where P^1 and P^2 represent the two sites on the protein.

Equations analogous to Equation 3.17 describe the fraction of brominated lipid binding at site 1 (f_{Br}^1) and site 2 (f_{Br}^2):

$$f_{Br}^1 = x_{Br}/(x_{Br} + K_1(1 - x_{Br})) \qquad \text{Equation 3.20}$$

and

$$f_{Br}^2 = x_{Br}/(x_{Br} + K_2(1 - x_{Br})) \qquad \text{Equation 3.21}$$

and the total fluorescence intensity is given by analogy to Equation 3.15, by

$$F = F_{min} + (F_o - F_{min})(1 - f_{Br}^1)^n(1 - f_{Br}^2)^n \qquad \text{Equation 3.22}$$

This equation assumes that the level of fluorescence quenching resulting from binding of brominated lipid to site 1 will be equal to that for site 2. This seems reasonable, since the distance of separation between the Trp residues and the dibromo groups of the lipids bound to the two sites will be expected to be similar.

Quencher	Hydrophobic Trp		Hydrophilic Trp	
	$J(\lambda)$ (M^{-1} cm^3)	R_o (Å)	$J(\lambda)$ (M^{-1} cm^3)	R_o (Å)
2,3-Dibromobutane	5.71×10^{-20}	3.8	1.35×10^{-20}	3.0
1,3-Diiodobenzene	1.09×10^{-16}	13.3	3.66×10^{-17}	11.1

Table 3.1 Calculated Förster distance for energy transfer from tryptophan to heavy atom, halide quenchers. The overlap integral $J(\lambda)$ was calculated using the data in Figure 3.3 and Equation 3.2. The values of the Förster distance R_o, were calculated using Equation 3.3. The quantum yield (Φ) of Trp was taken as 0.13 (Lakowicz, 1999).

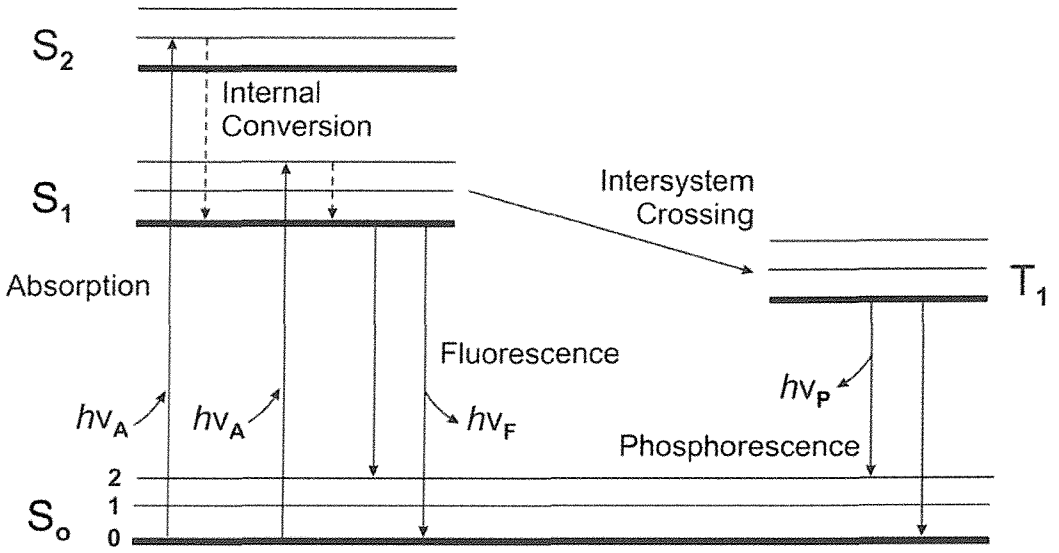

Figure 3.1 Jabłoński diagram showing the energy levels and various processes in an electronically excited molecule. S_o is the singlet ground state and S_1 and S_2 represent the first and second excited singlet energy states respectively. The thinner lines represent the different vibrational energy levels (1, 2, etc.) associated with each of the electronic energy levels (thick lines). The vibrational energy levels of the excited triplet state, T_1 are also shown (Lakowicz, 1999).

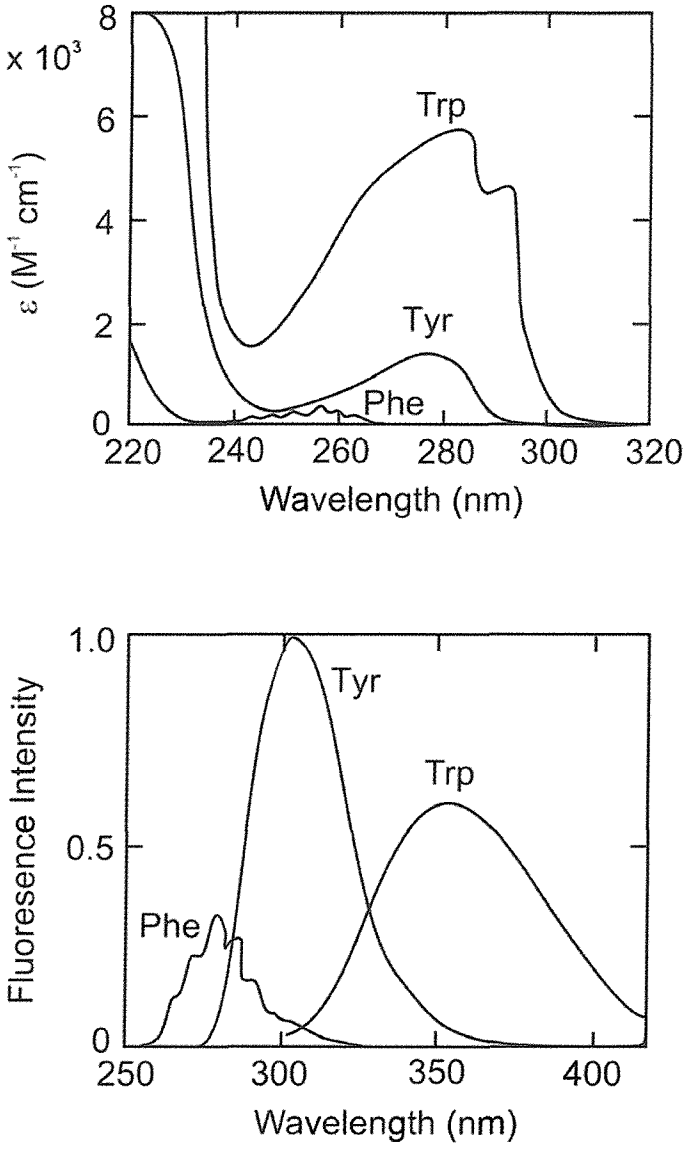

Figure 3.2 Absorption (top) and emission spectra (bottom) of the fluorescent amino acids in aqueous solution at pH 7.0. Trp is the dominant fluorophore absorbing at longer wavelengths and displays a larger extinction coefficient (ε) than the other aromatic residues; energy absorbed by Phe and Tyr is often transferred to Trp residues within the same protein and hence emission spectra are dominated by tryptophan fluorescence (Lakowicz, 1999).

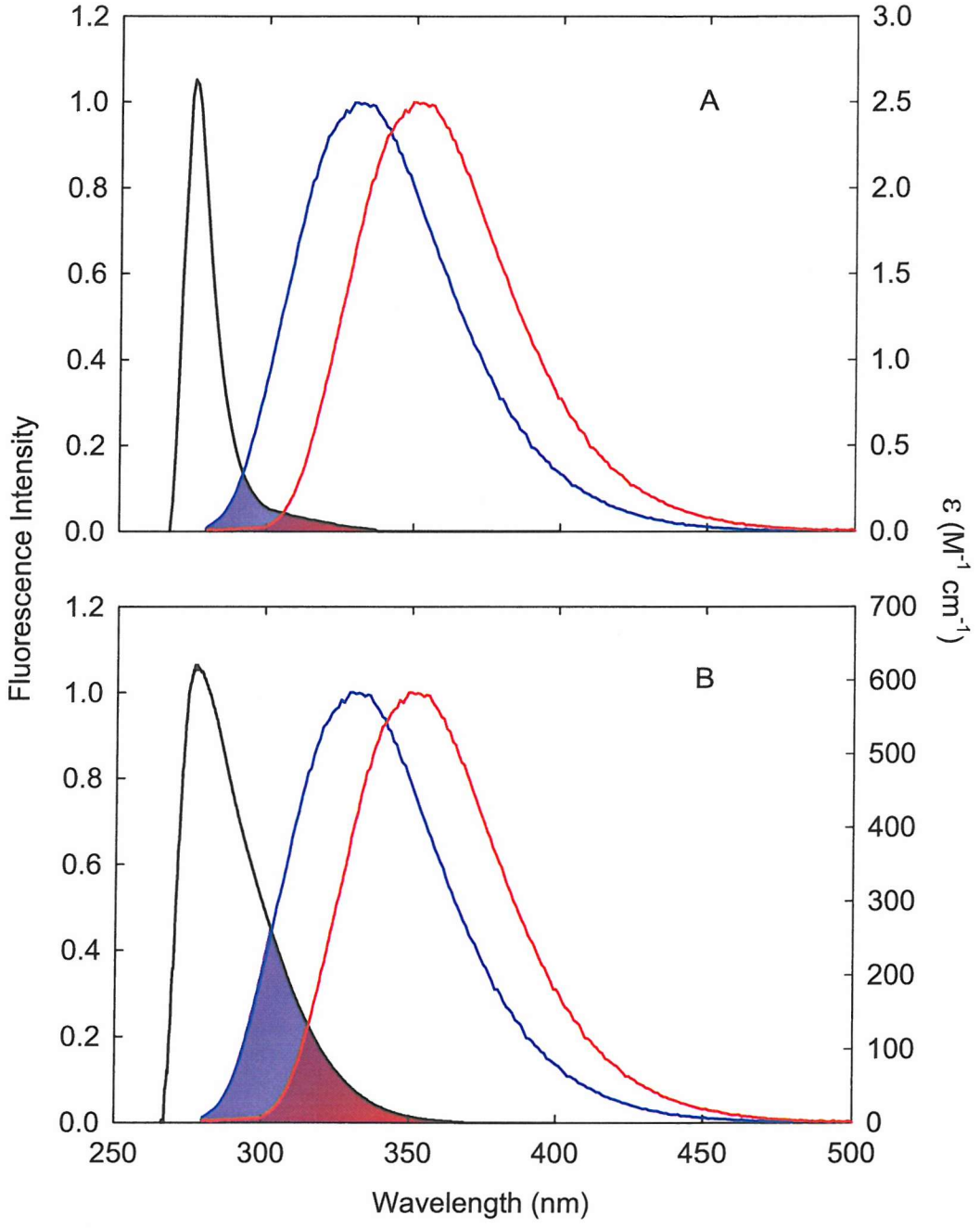

Figure 3.3 Overlap intergral for energy transfer from a tryptophan donor to a dibromo group. The overlap integral $J(\lambda)$ (shaded area) was calculated for Trp in a hydrophilic (red) or hydrophobic environment (blue) in the presence of (A), 2,3-dibromobutane; and (B), 1,3-diiodobenzene. $J(\lambda)$ was calculated using Equation 3.2 and the normalised reference emission spectrum of Trp published by Ladokhin et al. (2000) (left hand axis) to give the values in Table 3.1. The absorbance spectra for 2,3-dibromobutane and 1,3-diiodobenzene (right hand axes) were recorded at 0.3 M and 1 mM solutions, respectively, in decane.

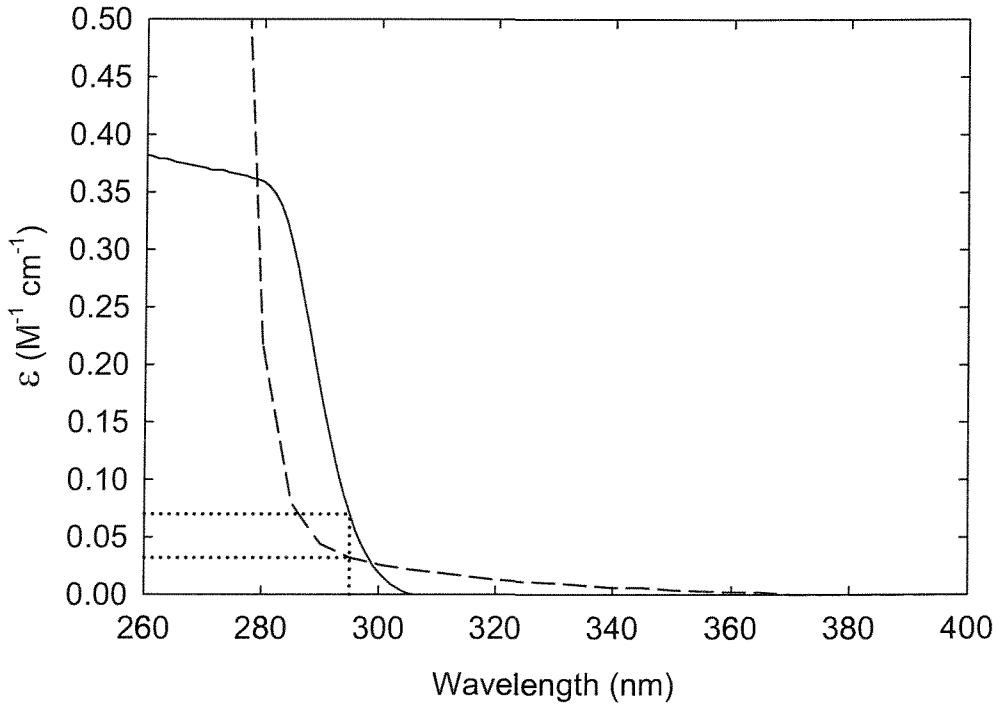

Figure 3.4 Absorption spectra of water soluble-quenchers. The absorption spectra of acrylamide (solid) and iodide (dashed) are shown. Quenching of Trp fluorescence by acrylamide and iodide was measured at an excitation wavelength of 295 nm (dotted) to minimise the inner filter effect. The concentration of the water soluble-quenchers is 1 M. The values of ε^{295} for acrylamide and iodide are 0.070 and 0.032 M^{-1} cm^{-1} respectively.

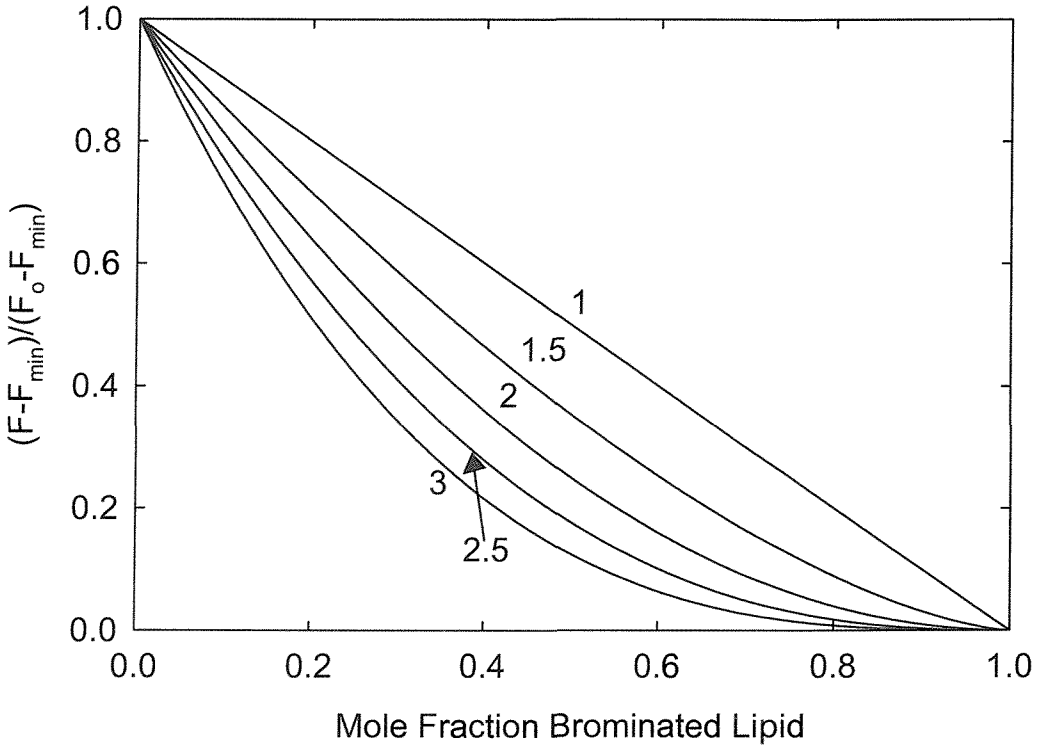

Figure 3.5 Simulated tryptophan fluorescence quenching curves for a transmembrane protein reconstituted into bilayers containing mixtures of a nonbrominated lipid and the corresponding brominated lipid. The level of fluorescence quenching varies with *n*, the number of sites close enough to a Trp residue to result in quenching. The number of sites is indicated on the graph for each line.

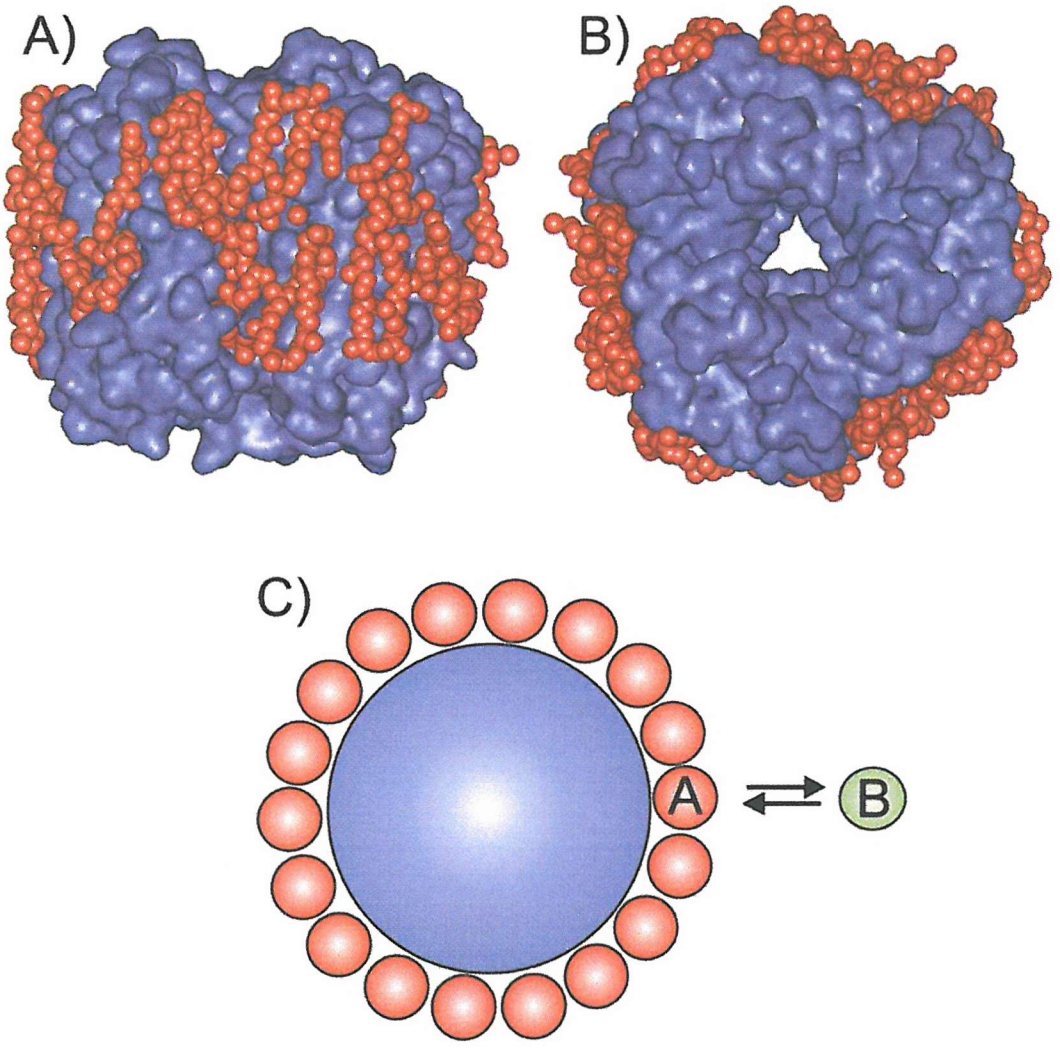

Figure 3.6 The hydrophobic surface of bacteriorhodopsin with associated annular lipids. The high-resolution structure of the protein is viewed from the membrane (A) and extracellular surface of the membrane (B). The protein surface is shown in blue, and those lipids resolved in the structure and forming an annular shell around the circumference of the protein are shown in space-spill and highlighted red. (C) Cartoon representation of (B) with lipid binding sites on the transmembrane surface; exchange of two lipids A and B at a given site on the protein is shown. PDB file 1QHJ.

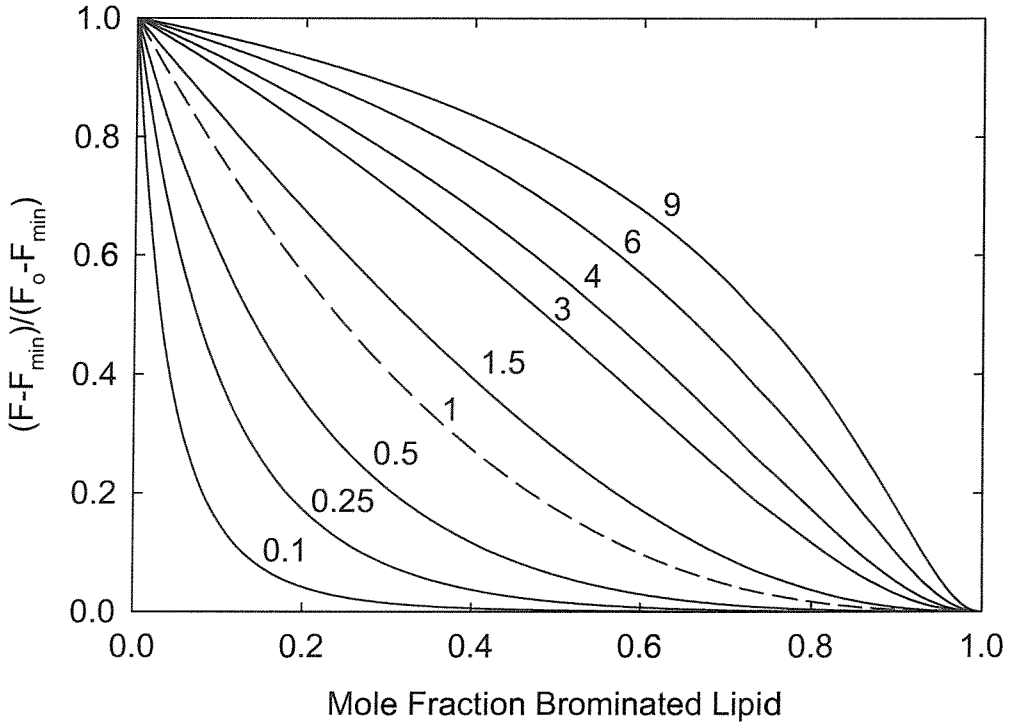

Figure 3.7 Simulated quenching curves of tryptophan fluorescence of MscL in mixtures of phosphatidylcholines and di(Br_2C18:0)PC, at the given mole fraction of di(Br_2C18:0)PC, when the number of lattice sites (*n*) is 2. The level of fluorescence quenching of the protein is dependent on the relative lipid binding constant (K) of MscL for the non-brominated lipid, where the value of K is indicated on each curve. The dotted line is for a relative binding constant of 1. If the non-brominated phospholipid binds more strongly to MscL than di(Br_2C18:0)PC then fluorescence intensity will be high and the curve is located to the right of the dashed line. Conversely, if the non-brominated phospholipid has lower affinity for MscL, the curve is located to the left of the dashed line.

Chapter 4:
Characterisation of MscL as a Function of Phospholipid Structure

4 CHARACTERISATION OF MscL: BINDING OF PHOSPHOLIPIDS TO MscL AS A FUNCTION OF PHOSPHOLIPID STRUCTURE

4.1 Introduction

4.1.1 Lipid-Protein Interactions

Although the bulk of the lipids in the bilayer only interact with other lipid species within the membrane, a significant fraction of the lipids form a layer or shell around the surface of integral membrane proteins, acting as a solvent for the protein (Lee, 2003). Within this shell of lipids the majority of the lipid molecules will interact non-specifically either with the hydrophobic transmembranous surface of the protein or with the polar interfacial regions, and these lipids are termed 'annular' lipids. In addition to the more generalised annular binding sites, specialised interactions may occur between lipid and protein at 'non-annular' sites, such as clefts formed between transmembrane α-helices or at protein-protein interfaces (Simmonds et al., 1982; Lee, 2003). These non-annular lipids may serve as a cofactor, for example, cardiolipin is required in the formation of an active trimer of formate dehydrogenase-N (Jormakka et al., 2002), or the protein could show a preference for a whole class of lipid for example anionic lipids are essential for ion conductivity of KcsA (Valiyaveetil et al., 2002). Alternatively non-annular lipids may have modulatory roles for example, the Ca^{2+}-ATPase has a number of non-annular sites that, when occupied by either phosphatidylinositol or phosphatidylserine, exert distinct regulator effects (Lee, 1998).

In the case of mechanosensitive channels, the ability of these membrane proteins to sense bilayer tension must ultimately be mediated by interactions between the lipid exposed surface of the channel and the surrounding shell of lipids, since MscL can be gated in patch clamp systems containing lipid and MscL as the only protein (Sukharev et al., 1994). Exactly how expansion of the lipid bilayer is 'sensed' by MscL is unclear. Expanding the lipid bilayer will increase the area occupied by each lipid molecule and this could increase the lipid-protein separation, and so weaken van der Waals, hydrogen-bond and charge interactions of the lipid molecule with the

protein. Stretching the lipid bilayer will result in a decrease in hydrophobic thickness for the bilayer and, if the effect is large enough, could favour a conformational change to a state with a decreased hydrophobic thickness. It has also been suggested that a distinct lateral pressure profile exists across the membrane and that changes in shape for a membrane protein would involve doing work against this lateral pressure profile (Cantor, 1999).

As mentioned in Chapter 1, biological membranes contain many diverse lipid species, differing in their head groups and fatty acyl chains; diversity provides many opportunities for lipids to influence and greatly affect membrane protein functioning within the membrane milieu (van Voorst and de Kruijff, 2000). An important property of a lipid bilayer is the thickness of the hydrophobic region, defined by the separation between the lipid carbonyl regions on the two sides of the bilayer. The hydrophobic thickness of the lipid bilayer is expected to match the hydrophobic thickness of any protein embedded in the bilayer, because of the high cost of exposing either fatty acyl chains or hydrophobic amino acids to water (Lee, 2003). All membranes contain both anionic and zwitterionic lipids. The head group exposed surface of MscL is also likely to be sensitive to changes in membrane composition, due to charged lipid head groups and differences in hydrogen bonding potential and hydration of the zwitterionic lipid head groups (Lee, 2004). The head groups and fatty acyl chains of the lipid are also important in determining the phase preference of the lipid (Cullis et al., 1996). Many membrane proteins show a preference for lipid in the liquid crystalline phase over lipid in the gel phase, since the highly ordered rigid structure of the lipid chains in the gel phase will make poorer van der Waals contact with the rough surface of a protein than lipid in the liquid crystalline phase (Lee, 2003).

4.1.2 Chapter 4 Overview

Trp fluorescence spectroscopy is a powerful tool to study the structures of membrane proteins and their interactions with the surrounding lipid bilayer. Many membrane proteins contain several Trp residues that can be used as natural fluorophores. However, the mechanosensitive channels of *Mycobacterium tuberculosis* (TbMscL)

and *Escherichia coli* (EcMscL) contain no Trp residues. This provides a unique opportunity of introducing single Trp residues into regions of interest. The X-ray crystal structure of the TbMscL homologue, together with sequence alignments, secondary structure predictions and hydropathy plots, were used to predict membrane spanning domains and target specific residues in TbMscL and EcMscL for site directed mutagenesis. Lipid-exposed Phe-80 located toward the centre of the second transmembrane α-helix of TbMscL was replaced with Trp. A Trp residue was also introduced into EcMscL at Phe-93, equivalent to Tyr-87 or Phe-88 in TbMscL, both Tyr-87 and Phe-88 in TbMscL being lipid exposed residues located toward the C-terminal end of the second transmembrane α-helix (Figure 4.1). Brominated lipid probes could then be used to quench Trp fluorescence of F80W-TbMscL and F93W-EcMscL channels by the process of heavy atom quenching, allowing specific lipid-protein interactions to be determined. The emission spectrum of Trp is environmentally sensitive and therefore provides additional information about the location of the Trp residue within the lipid bilayer.

To begin to understand how MscL 'senses' bilayer tension we must determine the nature of the shell of lipids surrounding the protein. If the presence of 'non-annular' lipid sites on the protein was established, this could suggest a cofactor or modulatory role for the lipid molecule, whereas the existence of annular binding sites only, would suggest a more generalised method of signal transduction. However, native membranes containing many unique lipid species are far too complex to define precise interactions between protein and a single class of lipid *in vivo*.

4.1.3 Isolation and Purification

Isolation and purification of membrane proteins provides the opportunity to reconstitute these proteins into *in vitro* model bilayer systems containing one or more defined lipid species. Successful purification and isolation of non-denatured and non-aggregated protein from native membranes requires the use of a mild detergent. The detergent disrupts the membrane and protects the hydrophobic domains of the protein from exposure to the hydrophilic environment of the buffer, effectively replacing the

role of the lipids. Solubilisation of purified MscL by an appropriate detergent was central to the purification of non-denatured protein.

The number of detergents available is large, and although detergent molecules vary extensively in their structure, size, and charge, they all are amphipathic. In order to find the most effective detergent to dissolve MscL, a range of detergents including both non-ionic and anionic charged species was tested by measuring the light scatter of MscL as a function of increasing detergent concentration.

4.2 Materials and Methods

All chemicals were obtained from Sigma or BDH with the following exceptions:

Avanti Polar Lipids

1,2-dimyristoleoyl-sn-glycero-3-phosphatidylcholine (di(C14:1)PC)
1,2-dipalmitoleoyl-sn-glycero-3-phosphatidylcholine (di(C16:1)PC)
1,2-dioleoyl-sn-glycero-3-phosphatidylcholine (di(C18:1)PC)
1,2-dieicosenoyl-sn-glycero-3-phosphatidylcholine (di(C20:1)PC)
1,2-dierucoyl-sn-glycero-3-phosphatidylcholine (di(C22:1)PC)
1,2-dinervonyl-sn-glycero-3-phosphatidylcholine (di(C24:1)PC)
1,2-dioleoyl-sn-glycero-3-phosphatdic acid (di(C18:1)PA)
1,2-dioleoyl-sn-glycero-3-phosphatidylethanolamine (di(C18:1)PE)
1,2-dioleoyl-sn-glycero-3-[phospho-rac-(1-glycerol)] (di(18:1)PG)
1,2-dioleoyl-sn-glycero-3-phosphatidylserine (di(C18:1)PS)
1,1'2,2'-tetraoleoyl cardiolipin (tetra(C18:1)CL)

Anatrace, Anagrade®

n-Octyl-β-D-glucopyranoside (Octylglucoside)

Calbiochem, Ultrol® Grade

n-Dodecyl-β-D-maltoside (Dodecylmaltoside)
N-(2-hydroxyethyl)piperazine-N'-(2-ethyanesulphonic acid) (Hepes)
1,3-diaza-2,4-cyclopentadiene (Imidazole)
Mega-9
Octaethylene glycol monodecyl ether ($C_{12}E_8$)

Pierce

Disuccinimidyl suberate (DSS)

4.2.1 *mscL* Mutation

Plasmids containing the *Escherichia coli* and *Mycobacterium tuberculosis mscL* genes were mutated, replacing Phe at position 93 by Trp (F93W) in EcMscL and Phe at position 80 to Trp (F80W) in TbMscL, using the synthetic oligonucleotide primers listed in Tables 2.4 and 2.5 respectively, as outlined in Section 2.2.5.

4.2.2 Protein Expression and Purification

E. coli M15 carrying the pQE-32 plasmid (Qiagen) with the F93W-*EcmscL* gene or *E. coli* BL21(DE3)pLysS transformants carrying the pET-19b plasmid (Novagen) with the F80W-*TbmscL* gene were grown in 6 l Luria broth to mid-log phase (absorbance at 600 nm of 0.6) and then induced for 3 h in the presence of isopropyl-β-D-thiogalactopyranoside (1 mM). MscL was purified as described in Section 2.2.4.

4.2.3 MscL Solubility

The solubility of 80 μg (5.3 nmols) of MscL in 2.5 ml of 0.2 μm filtered Hepes buffer (20 mM Hepes, 1 mM EGTA, 100 mM KCl, pH 7.2 KOH), was recorded at 25 °C using an SLM-Aminco 8100 Series Fluorimeter, with excitation and emission wavelengths of 500 nm. Slit widths of 2 nm were used for both excitation and emission. All solutions were prepared in 0.2 μm sterile-filtered Hepes buffer. The detergents tested included: *n*-octyl β-D-glucopyranoside (OG), Mega-9, cholate, N,N-dimethyldodecylamine-N-oxide (LDAO), *n*-dodecyl-β-D-maltoside (DDM) and dodecylpoly(ethyleneglycolether)$_8$ ($C_{12}E_8$) (Table 4.1). Detergents were titrated into the sample and the light scatter recorded. Results were corrected for background light scatter by subtracting the light scatter of an equivalent sample of detergent in the absence of MscL.

4.2.4 Phosphate Assay

Endogenous lipid co-purified with MscL was extracted with chloroform/methanol, using the procedure of Bligh and Dyer (1959). Lipid phosphorus was determined using a method based on the procedure of Bartlett (1952). All experiments were performed using acid washed glassware to prevent leaching of plasticides. 300 µg (20 nmoles) of MscL was added to a solvent mixture containing chloroform/methanol/water at a final ratio (v/v) of 2:1:1, and left at room temperature for 90 min. The lower solvent layer was pipetted off, and dried down onto the walls of a glass vial in a vacuum dessicator.

The sample was resuspended in 1 ml chloroform, and separated into 25, 75, 150, and 250 µl aliquots. Phosphate standards were prepared from 0.5 mM KH_2PO_4 and contained: 0, 2.5, 5, 10, 15, 20, and 40 nmols of phosphate. Samples and standards were dried down in an oven at 160 °C. 200 µl perchloric acid (60 % w/v) was added to each sample and standard, followed by incubation at 160 °C for a further 60 min in a glass-lined fume cupboard. 1 ml water; 250 µl freshly prepared ammonium molybdate (2.5 % w/v) and 250 µl freshly prepared ascorbic acid (10 % w/v) were added sequentially with mixing, to all samples and standards, followed by incubation at 100 °C for 5 min. Absorbance measurements were recorded at 800 nm using a Hitachi U-2000 Spectrophotometer at 25 °C.

4.2.5 Thin-Layer Chromatography

Lipid present in the MscL sample was separated from the protein and the detergent and identified by TLC using a chloroform/methanol/ethanoic acid/water mixture (25:14:4:2, v/v). 100 µg MscL (5.9 nmols) in PBS buffer containing 40 mM OG was spotted on the TLC plate together with 7.5 µg of the lipid standards in chloroform. Lipid spots were visualised by iodine vapour staining.

4.2.6 Circular Dichroism

CD measurements were recorded at 25 °C using a Jasco J-720 Spectropolarimeter, to a resolution of 0.2 nm with a scan rate of 50 nm min^{-1}. Slit widths of 500 μm and a band width of 1 nm were used. For far-region UV CD measurements, spectra were recorded between 190 and 250 nm, using a 1 mm path length with a response time of 4 s. For near UV CD measurements, spectra were recorded between 250 and 320 nm, using a 5 mm path length with a response time of 4 s. Samples were dialysed against PBS buffer containing 40 mM OG and the final concentration of MscL was 1 mg ml^{-1}. Averaging of nine spectra was used to increase signal-to-noise ratio. Results were corrected for background signals by subtracting the spectra of a sample of OG/PBS buffer in the absence of MscL.

4.2.7 *In vivo* Channel Function Assay

E. coli MJF465 transformants carrying the pET-19b plasmid with the *TbmscL* gene or the pQE-32 plasmid with the *EcmscL* gene were grown in 10 ml of Luria broth medium containing ampicillin (100 μg ml^{-1}) and supplemented with 0.5 M NaCl. Cells were grown in the presence of IPTG (1 mM) for 16 h at 37 °C. Overnight cultures (200 μl) were used to seed fresh cultures (10 ml) in the same medium and grown to mid-exponential phase (absorbance at 600 nm of 0.5). Cells were harvested by centrifugation at 3000 rpm for 10 min on a Heraeus Labofuge 400e. Culture supernatant was removed and the cell pellet resuspended in 1 ml of sterile 0.5 M NaCl solution.

Cultures (30 μl) were diluted 50-fold into six shock solutions of various osmotic strengths. The shock solutions were prepared by mixing sterile 0.5 M NaCl solution containing sterile-filtered ethidium bromide (0.5 μg ml^{-1}) with sterile analytical grade water also containing ethidium bromide (0.5 μg ml^{-1}) in the following ratios: 1:0, 3:2, 2:3 1:4, 1:10, and 0:1. Cells were incubated in the dark for 45 min at room temperature followed by centrifugation at 10,000 rpm for 10 min in an Eppendorf centrifuge 5415C. The supernatant was transferred to a new 1.9 ml microfuge tube and the pellet was resuspended in 1.5 ml sterile analytical grade water containing

ethidium bromide (0.5 μg ml^{-1}). Fluorescence intensities were recorded at 25 °C using an SLM-Aminco 8100 Series Fluorimeter, with an excitation wavelength of 254 nm and emission wavelengths of 632 nm. Slit widths of 4 nm were used for both excitation and emission. Results were corrected for background light scatter by subtracting the emission of a suitable blank.

4.2.8 Preparation of Potassium Cholate

Potassium cholate was prepared by dissolving 48.9 mmols cholic acid in a minimal volume of methanol (140-150 ml) and incubating at 35 °C. Solid KOH (48.9 mmols) was added with mixing to the cholic acid solution and incubated at 35 °C. Potassium cholate was precipitated from the methanol solution by adding an excess of diethyl ether. The solvent was filtered off and the solid dried under vacuum in the dark for 16 h. 15 mM cholate solutions were prepared in 20 mM Hepes, 100 mM KCl, 1 mM EGTA. The pH was adjusted to 7.2 with KOH.

4.2.9 Bromination of Lipid

100 mg of lipid was dissolved in 5 ml of chloroform. Bromine was added drop-wise, until a pale yellow colour persisted. The solvent and excess bromine was removed under vacuum for 30 min and then the lipid was dissolved in 1 ml of chloroform. Brominated lipid was transferred to a glass scintillation vial wrapped in foil, sealed under nitrogen and stored at -20 °C until use. The brominated lipid was diluted 1:5 with chloroform for use as a working stock.

4.2.10 Reconstitution

4.2.10.1 *Dilution Method*

Purified MscL was reconstituted into lipid bilayers by mixing lipid and MscL in cholate, followed by dilution into buffer to decrease the concentration of cholate

below its critical micelle concentration (CMC). For reconstitution into bilayers of a single phospholipid, the required phospholipid (0.47 μmol) was dried from a chloroform solution onto the walls of a thin glass vial. Buffer (400 μl; 20 mM Hepes, 100 mM KCl, 1 mM EGTA, pH 7.2) containing 15 mM cholate was added and the sample was sonicated to clarity in a bath sonicator (Ultrawave). MscL (80 μg) was then added and the suspension incubated at 25 °C for 15 min before use.

For reconstitution into bilayers containing a mixture of two lipids, separate solutions of the two lipids were prepared in cholate-containing buffer as described above. These were then mixed in the appropriate proportions, incubated at 35 °C for 30 min and then mixed with MscL, as described above.

4.2.10.2 *Dialysis Method*

Purified MscL was mixed with lipid and detergent, as previously described for reconstitution of MscL by dilution. After 15 min incubation at 25 °C the sample was transferred to dialysis tubing with a molecular weight cut-off of 7 kDa, and dialysed against 500 ml of buffer (20 mM Hepes, 1 mM EGTA, 100 mM KCl, pH 7.2 KOH) for a total of 10 h at 4 °C with two changes of buffer. Protein concentrations were determined using a combination of BioRad protein assay, and comparison to Trp fluorescence emission intensities when excited at 280 nm.

4.2.11 Characterisation of Reconstituted Sample on a Sucrose Gradient

Gradient centrifugation was used to characterise the reconstituted preparation. Di(C18:1)PC (1.8 μmols) was mixed with rhodamine-labelled di(C18:1)PE (94 nmols) in chloroform and dried onto the walls of a glass vial. The mixture was resuspended in buffer (1.6 ml; 20 mM Hepes, 100 mM KCl, 1 mM EGTA, pH 7.2) containing 15 mM cholate. The sample was sonicated to clarity in a sonication bath (Ultrawave). EcMscL (0.32 mg) was added and the mixture incubated at 25 °C for 15 min. The sample was then dialysed at 4 °C against two lots of buffer (500 ml; 20 mM Hepes, 100 mM KCl, 1 mM EGTA, pH 7.2) for a total of 10 h. Samples of dialysate (1.5 ml) were then loaded onto sucrose gradients containing the following solutions

of sucrose (w/v) in the above buffer: 2.5, 5.0, 10.0, 15.0, 20.0, and 30.0 %; the 30.0 % sucrose solution also contained 0.05 % (w/v) Triton X-100 (Munkonge et al., 1988). Samples were spun at 80,000g for 18 h at 4 °C and then 1.5 ml fractions were collected from the gradients and analysed for lipid and protein by, respectively, absorbance at 570 nm and BioRad protein assay.

4.2.12 Cross-linking of MscL

MscL was cross-linked using disuccinimidyl suberate (DSS; Pierce). MscL (0.34 mg) was mixed with 2 μmols of lipid in cholate buffer and incubated at 25 °C for 15 min. The sample was then dialysed at 4 °C against two lots of buffer (500 ml; 20 mM Hepes, 100 mM KCl, pH 7.2) for 10 h using dialysis tubing with a molecular weight cut-off of 7 kDa. Aliquots of dialysate (100 μl) were cross-linked in the presence of DSS (2.18 mM; added as a stock solution in DMSO) for 30 min at room temperature. Tris (83 mM) was added and the mixture incubated at room temperature for a further 15 min to quench the reaction. MscL (14 μg) was subsequently resolved by 10 % SDS-PAGE using the method of Laemmli (1970).

4.2.13 Steady-State Fluorescence Measurements

Fluorescence intensities were recorded at 25 °C in Hepes buffer for 0.98 μM MscL using an SLM-Aminco 8100 Series Fluorimeter, with an excitation wavelength of 280 nm, as described in Section 3.5.

4.3 Results

4.3.1 Solubilisation of MscL

The solubility of MscL was determined in a range of detergents. The effectiveness of each detergent was assessed by the ability of the detergent to reduce the light scatter of MscL in buffer. The results are shown in Figure 4.2, plotted as a function of increasing detergent concentration. The properties of each detergent used in this study are summarised in Table 4.1.

OG is a non-ionic detergent with a high CMC and the results in Figure 4.2A show that solubilisation is achieved at 21 mM, a value in good agreement with the expected CMC range for this detergent. OG was used as the detergent to solubilise MscL in all the purification procedures, unless otherwise stated. Mega-9 is another non-ionic detergent with a high CMC value comparable to OG (Table 4.1). The results in Figure 4.2A show complete solubilisation within the CMC range of Mega-9. The anionic detergent cholate reduces light scatter at concentrations greater than 10 mM, but does not completely clarify the sample. Another anionic detergent with a low CMC, LDAO successfully solubilised MscL and the results in Figure 4.2B show that solubilisation is achieved at 2 mM, a value well within the CMC range of this detergent. The non-ionic detergent DDM reduces light scatter above 0.1 mM but full solubilisation was only seen at 0.52 mM. The detergent $C_{12}E_8$ has the lowest CMC value tested in these studies and belongs to the non-ionic class of detergents. The results for $C_{12}E_8$ in Figure 4.2B show an appreciable reduction in turbidity, but this reduction is incomplete over the concentration range tested and the concentration of detergent is many times in excess of the CMC value of 0.087 mM.

4.3.2 Phospholipid Content of Purified MscL

EcMscL and TbMscL purified using OG as detergent were analysed for phospholipid content. The levels of phospholipid detected were very small, corresponding to only 0.02 mole of lipid per mole of protein. Similarly, no phospholipids could be detected using thin-layer chromatography (TLC) when EcMscL and TbMscL were purified

using OG, DDM or LDAO as detergent (Figure 4.3). All the lipid standards are located towards the top of the TLC plate. In lane 10 there is a smear located towards the bottom half of the plate, which cannot be explained by the presence of detergent alone, however the top of lane 10 is again clean, confirming that no phospholipids are present (Figure 4.3).

4.3.3 *In vivo* Assay for Function of MscL

An *in vivo* assay was used to show that the mutant MscL channels were functional, using a fluorescence assay to measure levels of release of DNA following osmotic downshock. Wild type and mutant EcMscL and TbMscL were expressed in *E. coli* strain MJF465; strain MJF465 lack endogenous mechanosensitive channels, making them sensitive to osmotic downshock (Section 2.2.1.4; Levina et al., 1999). As shown in Figure 4.4 both the wild type and mutant EcMscL and TbMscL are able to rescue the *E. coli* cells from the effects of osmotic downshock, confirming that introduction of the Trp residues into the channels does not inactivate the channels.

4.3.4 Circular Dichroism (CD) Spectra

The secondary structures of MscL and Trp-mutated MscL were determined by recording CD spectra in OG. As shown in Figure 4.5, CD spectra of both wild type and Trp-mutated EcMscL and TbMscL were very similar. The shape of each individual spectrum is consistent with a protein with a high α-helical content, exhibiting the characteristic minima at 208 and 222 nm and a maximum at 190-195 nm.

4.3.5 Reconstitution of MscL

EcMscL and TbMscL were reconstituted into bilayers of defined composition by mixing the purified protein with phospholipid in buffer with cholate as detergent to give a 100:1 molar ratio of phospholipid to MscL monomer, followed by 12-fold

dilution into buffer to drop the concentration of cholate below its CMC, thereby re-forming large unsealed membrane fragments. Full reconstitution of MscL into lipid bilayers under these conditions was confirmed by using a number of different techniques.

4.3.5.1 *Fluorescence Spectroscopy*

F80W-TbMscL and F93W-EcMscL were reconstituted into bilayers of di(C18:1)PC by mixing in 15 mM cholate followed by a 12-fold dilution to re-form membrane fragments. The emission spectrum for F80W-TbMscL is centred at 321 nm, indicating a very hydrophobic environment for the Trp residue (Figure 4.6). The fluorescence emission maximum for F93W-EcMscL is at 328 nm (Figure 4.6), shifted slightly to longer wavelengths compared to that of F80W-TbMscL. The fluorescence emission spectrum for Trp in water is centred at 350 nm. Reconstitution of F80W-TbMscL into bilayers of di(Br_2C18:0)PC led to quenching of 82 % of the Trp fluorescence of TbMscL (Figure 4.6, Table 4.2). Increasing the dilution factor used to re-form membranes to 60-fold, had no significant effect on the level of fluorescence quenching, and increasing the cholate concentration to 30 mM also had no significant effect (Table 4.2). The level of fluorescence quenching observed using dialysis to remove detergent was the same as that observed using the dilution method (Table 4.2). In di(C18:1)PC increasing or reducing the mole ratio of lipid:MscL to 300:1 or 50:1 respectively, had no affect on the level of fluorescence. However, reducing the ratio further to 25:1 and 15:1 led to a reduction in fluorescence intensity of F80W-TbMscL (Figure 4.7), suggesting that a minimum of ca. 50:1 molar ratio of lipid to MscL monomer is required for successful reconstitution.

4.3.5.2 *Sucrose Density Centrifugation*

The reconstituted MscL was characterised by centrifugation on a discontinuous sucrose gradient. When MscL and lipid are run separately on the gradient, all the MscL is found at the bottom of the gradient and all the lipid is found at the top of the gradient, as shown in Figure 4.8. However, when MscL is mixed with phospholipid in cholate buffer followed by removal of the detergent by dialysis and the dialysate run on the gradient, the results in Figure 4.8 show that MscL is found at the 20-30 %

sucrose interface along with the di(C18:1)PC lipid. Analysis of the phospholipid and protein content for fractions between the 20-30 % interface reveal the molar ratio of lipid to protein in the MscL-containing fraction to be about 60:1, compared to 100:1 in the original mixture. The calculated density of the reconstituted sample was 1.114 g cm^{-3}, consistent with its location at the 20-30 % sucrose interface (Table 4.3).

4.3.5.3 *Cross-linking Studies*

MscL crystallises as a pentamer and cross-linking MscL in the native membrane results in a ladder-like pattern on SDS gels, corresponding to multiples of the monomeric protein up to a pentamer or higher (Blount et al., 1996; Sukharev et al., 1999). SDS gels of EcMscL and TbMscL before cross-linking show the presence of predominantly monomeric species, with small amounts of dimer (Figure 4.9), as previously reported by Chang et al. (1998). Cross-linking EcMscL or TbMscL reconstituted in di(C18:1)PC results in a ladder-like pattern of bands extending up to the pentameric species (Figure 4.9), consistent with MscL retaining its pentameric structure after reconstitution. Reconstitution of TbMscL in short or long-chain phosphatidylcholines or in di(C18:1)PS or di(C18:1)PA also results in a cross-linking pattern consistent with formation of a pentamer (Figure 4.9).

4.3.6 Lipid Phase-transition Studies

F80W-TbMscL was reconstituted into mixture of 90 % di(C14:0)PC or di(C16:0)PC and 10 % of the corresponding chain length brominated phospholipid, using the dilution method. Fluorescence intensities were then recorded as a function of temperature (Figure 4.10). In Figure 4.10 the fluorescence intensity is plotted as F/F_o, where F is the fluorescence intensity at given temperatures and F_o is the maximum fluorescence intensity observed for F80W-TbMscL. The results in Figure 4.10 show an increase in fluorescence intensity with an increase in temperature for F80W-TbMscL reconstituted into mixed bilayers of di(C14:0)PC and di(Br_2C14:0)PC, with the major change being centred around 22 °C. A similar observation is made when F80W-TbMscL is reconstituted into mixed bilayers of di(C16:0)PC and di(Br_2C16:0)PC, with a corresponding increase in fluorescence centred at 38 °C.

Phase transition temperatures for pure di(C14:0)PC and di(C16:0)PC, are 24 and 42 °C respectively (Dixon et al., 1982; Racanksy et al., 1987). At low temperatures, mixture of di(C14:0)PC or di(C16:0)PC and brominated PC will exist as phase separated mixtures, containing gel phase domains enriched in di(C14:0)PC or di(C16:0)PC lipid and liquid crystalline domains enriched in the brominated lipid (East and Lee, 1982). The low fluorescence intensity observed at low temperatures suggests preferential partitioning of MscL into the liquid crystalline domains, where fluorescence will be quenched by the bromine atoms; at higher temperatures, as the gel phase domains melt, the proportion of the liquid crystalline phase lipid in the mixture will increase and partitioning of MscL into the liquid crystalline phase domains will result in less fluorescence quenching as the domains will now contain increased amount of the non-brominated lipid.

4.3.7 Fluorescence Quenching of MscL by Brominated Phospholipids

MscL was reconstituted into bilayer fragments by the dilution method using the detergent cholate, at a molar ratio of lipid-protein of 100:1. Fluorescence quenching curves for F80W-TbMscL and F93W-EcMscL in mixtures of a brominated and the corresponding non-brominated phospholipid were determined and the results are shown in Figure 4.11. The fluorescence intensity is plotted as F/F_o, where F is the fluorescence intensity at intermediate fractions of brominated phospholipid and F_o is the fluorescence intensity when the mole fraction of non-brominated phospholipid is 1. The data shown in Figure 4.11 were fitted to Equation 3.11 using the nonlinear least-squares programme in SigmaPlot, giving the values of n listed in Table 4.4, where n is the number of sites from which Trp fluorescence can be quenched. The values of n are identical within experimental error for all phosphatidylcholines with average values of 2.54 ± 0.15 for F80W-TbMscL and 1.33 ± 0.03 for F93W-EcMscL. The results in Figure 4.11 and Table 4.4 show that fluorescence intensities decrease with increasing mole fraction of brominated lipid.

The maximum levels of fluorescence quenching of F80W-TbMscL in PC and PE are the same within experimental error, as shown by comparison of the data in Figure 4.12 and Figure 4.13. However, the level of quenching shown in Figure 4.12 and

Table 4.5 for F80W-TbMscL and F93W-EcMscL with brominated anionic phospholipids is slightly greater than for the zwitterionic lipids. The *n* values for all phospholipids are very similar except for PA, where the small size of the head group may allow a greater number of lipids to pack around a Trp residue. The value of *n* for tetra(C18:1)PC is approximately half that for the other phospholipids, consistent with this lipid having twice as many chains as the other phospholipids.

4.3.8 Relative Phospholipid Binding Constants for MscL

Fluorescence quenching curves for F80W-TbMscL in mixtures of di(Br_2C18:0)PC and phosphatidylcholines of chain lengths C12, C16, C18, and C24 are shown in Figure 4.13. Fluorescence quenching is slightly more marked in mixtures of di(C12:0)PC and di(Br_2C18:0)PC at intermediate mole fractions of di(Br_2C18:0)PC between 0.2 and 0.8 than in mixtures of di(C18:1)PC and di(Br_2C18:0)PC (Figure 4.13). This shows that di(C12:0)PC binds to TbMscL with a binding constant slightly smaller than that for di(C18:1)PC. In contrast, quenching in mixtures of di(C16:1)PC and di(Br_2C18:0)PC is slightly less at intermediate mole fractions of di(Br_2C18:0)PC than in mixtures of di(C18:1)PC and di(Br_2C18:0)PC, showing that di(C16:1)PC binds slightly more strongly to TbMscL than does di(C18:1)PC. Quenching profiles for other chain length lipids were intermediate between those shown in Figure 4.13. The data for each phospholipid were analysed in terms of Equation 3.15 with a value for *n* of 2.54, thereby providing the relative binding constant (K) for each phospholipid relative to that for di(Br_2C18:0)PC (Table 4.6).

Fluorescence quenching curves were also determined for the reverse experiment in which F80W-TbMscL was reconstituted in mixtures of di(C18:1)PC with brominated phospholipids with chain lengths between C14 and C24 (Figure 4.13). The data were again analysed using Equation 3.15, giving the relative binding constants listed in Table 4.6. The close agreement between the two determinations of relative binding constant gives confidence in the analysis. A corresponding analysis was performed using fluorescence quenching curves for F93W-EcMscL (Figure 4.14), giving the binding constants also listed in Table 4.6.

The relative binding constants are plotted as a function of fatty acyl chain length in Figure 4.15A. The results show that both TbMscL and EcMscL have highest affinity for di(C16:1)PC. The relative binding constants for the MscLs decrease with increasing or decreasing fatty acyl chain length. However, the total change in lipid binding affinity over the C16-C24 range was of 1.5-fold for TbMscL and of three-fold for EcMscL.

Fluorescence quenching curves for F80W-TbMscL in mixtures of phosphatidylcholine and phosphatidylethanolamine or anionic phospholipid are shown in Figures 4.16 and 4.17. The binding constant for di(C18:1)PE relative to di(C18:1)PC is close to 1 (Figure 4.16, Table 4.7). Binding constants for phosphatidylglycerol and phosphatidylserine obtained from experiments with di(C18:1)PC and brominated anionic lipid or from experiments with di(Br_2C18:0)PC and nonbrominated anionic phospholipid are the same (Figure 4.17, Table 4.7), consistent with simple competition between phosphatidylcholines and phosphatidylglycerol or phosphatidylserine for binding to MscL. For cardiolipin, a smaller binding constant was obtained from experiments with mixtures of di(C18:1)PC and tetra(Br_2C18:0)CL than with di(Br_2C18:0)PC and tetra(C18:1)CL (Figure 4.16, Table 4.7), but interpretation of this effect is complicated by the fact that cardiolipin contains four fatty acyl chains compared to the two in phosphatidylcholine. However, for phosphatidic acid, binding constants for phosphatidic acid relative to phosphatidylcholine obtained from experiments with mixtures of di(C18:1)PC and di(Br_2C18:0)PA do not agree with those obtained from experiments with mixtures of di(Br_2C18:0)PC and di(C18:1)PA (Figure 4.17, Table 4.7). The marked quenching observed in mixtures with di(Br_2C18:0)PA suggests that di(Br_2C18:0)PA binds strongly to TbMscL, but the experiments with di(C18:1)PA suggest that di(C18:1)PA is unable to displace di(Br_2C18:0)PC from around TbMscL with the efficiency expected from the experiments with di(Br_2C18:0)PA. Similar observations have been made previously in studies of anionic lipid binding to simple transmembrane α-helices (Mall et al., 1998). The most obvious explanation for this result is that there are two classes of binding sites around MscL for phospholipid, one class of sites showing a higher affinity for phosphatidic acid than the other. Increasing ionic strength leads to a decrease in the relative affinities of both

phosphatidylserine and phosphatidic acid for F80W-TbMscL (Figure 4.17, Table 4.7).

Detergent	Properties	CMC (mM)	Monomer M_r
OG	Non-ionic	20-25	292.4
Mega-9	Non-ionic	19-25	335.5
Cholate	Anionic	13-15	431.0
LDAO	Anionic	1-3	229.4
DDM	Non-ionic	0.17	510.6
$C_{12}E_8$	Non-ionic	0.087	539.1

Table 4.1 Properties of the detergents used to study the solubility of MscL.

Method	F80W-TbMscL F/F_o	F93W-EcMscL F/F_o
15 mM cholate/12-fold dilution	0.18 ± 0.02	0.32 ± 0.01
15 mM cholate/60-fold dilution	0.19 ± 0.04	0.33 ± 0.03
30 mM cholate/12-fold dilution	0.17 ± 0.02	0.33 ± 0.03
30 mM cholate/60-fold dilution	0.18 ± 0.03	0.36 ± 0.06
15 mM cholate/dialysis	0.20 ± 0.01	0.34 ± 0.01

Table 4.2 Effect of method of reconstitution on fluorescence quenching of F80W-TbMscL and F93W-EcMscL by di(Br_2C18:0)PC. F and F_o are fluorescence intensities for MscL reconstituted in di(Br_2C18:0)PC and di(C18:1)PC, respectively. Fluorescence was excited at 280 nm and emission was monitored at 320 nm and 330 nm for F80W-TbMscL and F93W-EcMscL respectively. The molar ratio of lipid to MscL was 100:1.

Sucrose Concentration (%, w/v)	Density (g cm^{-3})
5.0	1.0179
10.0	1.0381
15.0	1.0592
20.0	1.0810
30.0	1.1270

Table 4.3 Sucrose gradient densities of known sucrose concentrations (w/v) used in the characterisation of reconstituted MscL by centrifugation.

Fatty acyl chain	Position of *cis* double bond	F80W-TbMscL		F93W-EcMscL	
		F/F_o	n	F/F_o	n
C14:1	9	0.14 ± 0.01	2.67 ± 0.13	0.24 ± 0.01	1.31 ± 0.06
C16:1	9	0.15 ± 0.01	2.44 ± 0.06	0.26 ± 0.02	1.22 ± 0.07
C18:1	9	0.19 ± 0.01	2.46 ± 0.05	0.34 ± 0.01	1.35 ± 0.02
C20:1	11	0.24 ± 0.02	2.54 ± 0.21	0.43 ± 0.01	1.28 ± 0.07
C22:1	13	0.31 ± 0.02	2.64 ± 0.27	0.51 ± 0.01	1.44 ± 0.09
C24:1	15	0.41 ± 0.01	2.47 ± 0.21	0.61 ± 0.01	1.39 ± 0.03

Table 4.4 Fluorescence quenching of F80W-TbMscL and F93W-EcMscL in brominated phosphatidylcholines as a function of fatty acyl chain length. F_o and F are fluorescence intensities for MscL reconstituted in nonbrominated phospholipid and the corresponding brominated phospholipid respectively, measured at pH 7.2. The value of n is the value obtained by fitting the data in Figure 4.11 to Equation 3.11.

Phospholipid	F80W-TbMscL		F93W-EcMscL	
	F/F_o	n	F/F_o	n
di(C18:1)PC	0.19 ± 0.01	2.46 ± 0.05	0.34 ± 0.01	1.35 ± 0.02
di(C18:1)PE	0.25 ± 0.02	2.59 ± 0.29	0.30 ± 0.02	1.36 ± 0.13
di(C18:1)PS	0.12 ± 0.01	2.95 ± 0.22	0.25 ± 0.01	1.48 ± 0.04
di(C18:1)PG	0.12 ± 0.01	3.12 ± 0.10	0.24 ± 0.01	1.42 ± 0.03
di(C18:1)PA	0.11 ± 0.01	3.62 ± 0.27	0.23 ± 0.01	1.89 ± 0.09
tetra(C18:1)CL	0.09 ± 0.01	1.25 ± 0.02	-	-

Table 4.5 Fluorescence quenching of F80W-TbMscL and F93W-EcMscL in brominated phospholipids as a function of lipid head group. F_0 and F are fluorescence intensities for MscL reconstituted in nonbrominated phospholipid and the corresponding brominated phospholipid respectively, measured at pH 7.2. The value of n is the value obtained by fitting the data in Figure 4.12 to Equation 3.11.

Fatty acyl chain	Relative binding constant measured using di(Br_2C18:0)PC	Relative binding constant Measured using di(C18:1)PC
	TbMscL	
C12:0	0.78 ± 0.08	-
C14:1	1.05 ± 0.10	1.08 ± 0.08
C16:1	1.13 ± 0.11	1.09 ± 0.08
C18:1	1	1
C20:1	0.85 ± 0.07	0.83 ± 0.06
C22:1	0.79 ± 0.08	0.84 ± 0.11
C24:1	0.72 ± 0.05	0.78 ± 0.02
	EcMscL	
C12:0	0.73 ± 0.02	-
C14:1	1.06 ± 0.05	1.13 ± 0.04
C16:1	1.13 ± 0.06	1.35 ± 0.06
C18:1	1	1
C20:1	0.61 ± 0.04	0.83 ± 0.08
C22:1	0.53 ± 0.03	0.70 ± 0.06
C24:1	0.46 ± 0.03	0.65 ± 0.08

Table 4.6 Relative lipid binding constants for F80W-TbMscL and F93W-EcMscL for phosphatidylcholines as a function of fatty acid chain length. Binding constants relative to di(C18:1)PC were calculated from quenching data for F80W-MscL and F93W-EcMscL in mixtures of di(Br_2C18:0)PC with non-brominated lipid or di(C18:1)PC with brominated lipid, at pH 7.2, using values for *n* from Table 4.4.

Phospholipid	[KCl] (mM)	Relative binding constant measured using di(Br_2C18:0)PC	Relative binding constant measured using di(C18:1)PC
di(C18:1)PE	100	1.04 ± 0.07	1.14 ± 0.01
di(C18:1)PG	100	1.87 ± 0.20	1.92 ± 0.12
di(C18:1)PS	26	3.88 ± 0.40	3.57 ± 0.31
	100	1.66 ± 0.16	1.69 ± 0.10
	1000	1.26 ± 0.10	1.37 ± 0.01
di(C18:1)PA	100	1.81 ± 0.21	3.49 ± 0.25
	1000	1.62 ± 0.09	2.44 ± 0.05
tetra(C18:1)CL	100	1.52 ± 0.21	0.96 ± 0.06

Table 4.7 Relative lipid binding constants for F80W-TbMscL as a function of lipid head group. Binding constants relative to di(C18:1)PC were calculated from quenching data for F80W-TbMscL in mixtures of di(Br_2C18:0)PC with non-brominated lipid or di(C18:1)PC with brominated lipid, at pH 7.2, using the values for n given in Table 4.5 for experiments with di(C18:1)PC and n = 2.54 for experiments with di(Br_2C18:0)PC. For tetra(C18:1)CL the mole fraction was calculated based on the number of moles of fatty acyl chains to account for the fact that tetra(C18:1)CL contains four chains and di(C18:1)PC contains two chains, and correspondingly the value for n used in the analysis was consequently double that given in Table 4.5.

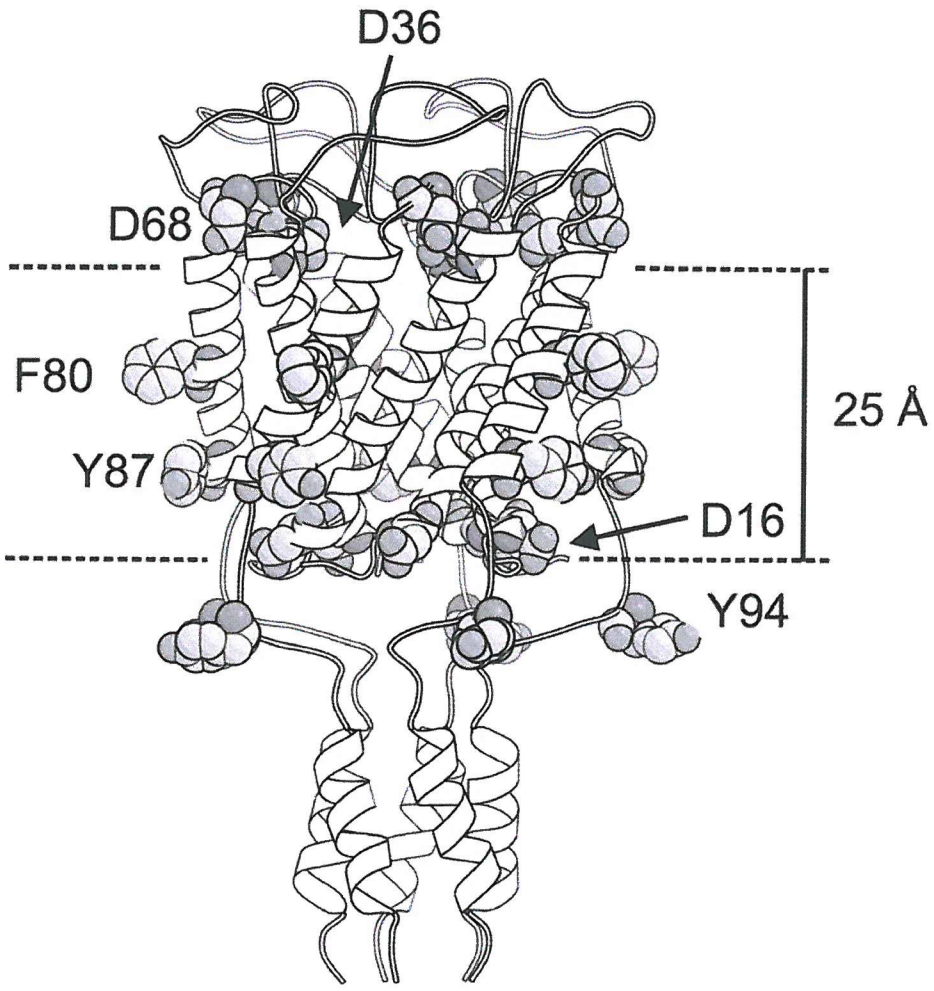

Figure 4.1 Schematic representation of homopentameric TbMscL, viewed from the side. The probable hydrophobic bilayer thickness (See Chapter 5) and putative membrane interfaces, defined by charged residues at positions Asp-16, Asp-36 and Asp-68 are show in CPK format. Phe-80, Tyr-87 and Tyr-94 are also shown. Prepared using Bobscript (Esnouf, 1999) and the coordinates in PDB IMSL.

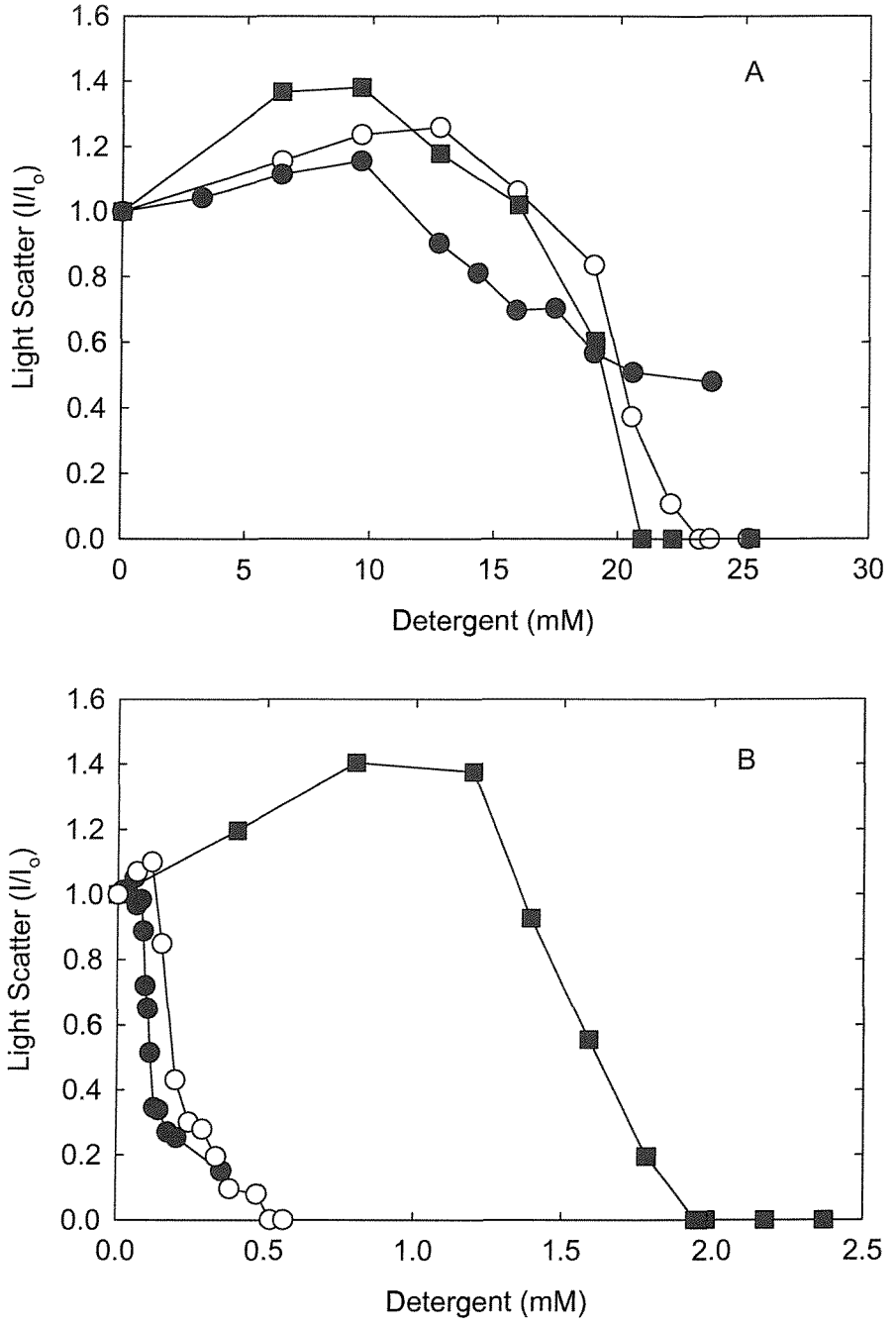

Figure 4.2 Effect of detergents on the solubility of MscL. Light scatter of MscL (1.8 μM) was measured as a function of increasing detergent concentration. A) (●), cholate; (○), Mega-9; and (■), OG. B) (●), $C_{12}E_8$; (○), dodecylmaltoside; and (■), LDAO. The buffer used was 20 mM Hepes, 1 mM EGTA, 100 mM KCl, pH 7.2. The light scatter was recorded at 25 °C using excitation and emission wavelengths of 500 nm, and expressed as I/I_o where I is the intensity in the presence of the given concentration of detergent and I_o is the intensity in the absence of detergent.

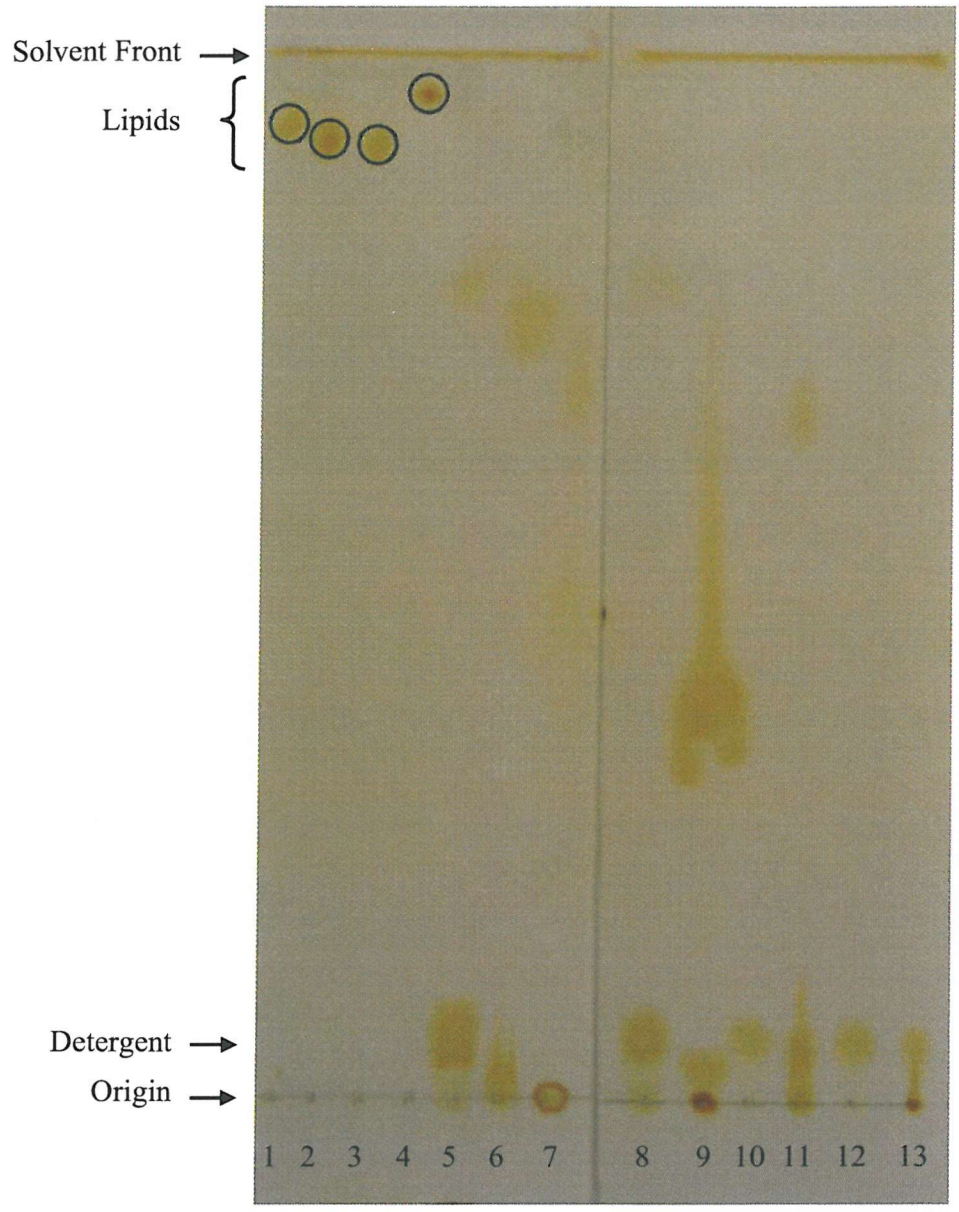

Figure 4.3 Thin layer chromatography was used to identify any lipids associated with EcMscL and TbMscL when purified in OG, DDM or LDAO as detergent. Lanes 1 to 4 contain synthetic lipids standards (10 nmols; Avanti): PA; PE; PG and CL respectively. Lane 5 contains OG buffer; lane 6 contains EcMscL in OG buffer; lane 7 contains TbMscL in OG buffer; lane 8 contains OG/Hepes buffer; lane 9 contains EcMscL in OG/Hepes buffer; lane 10 contains DDM/Hepes buffer; lane 11 contains EcMscL in DDM/Hepes buffer; lane 12 contains LDAO/Hepes buffer and lane 13 contains EcMscL in LDAO/Hepes buffer. EcMscL and TbMscL samples contained 10 nmols of protein. TLC was carried out using a $CHCl_3$/MeOH/CH_3COOH/H_2O system (25:14:4:2, v/v).

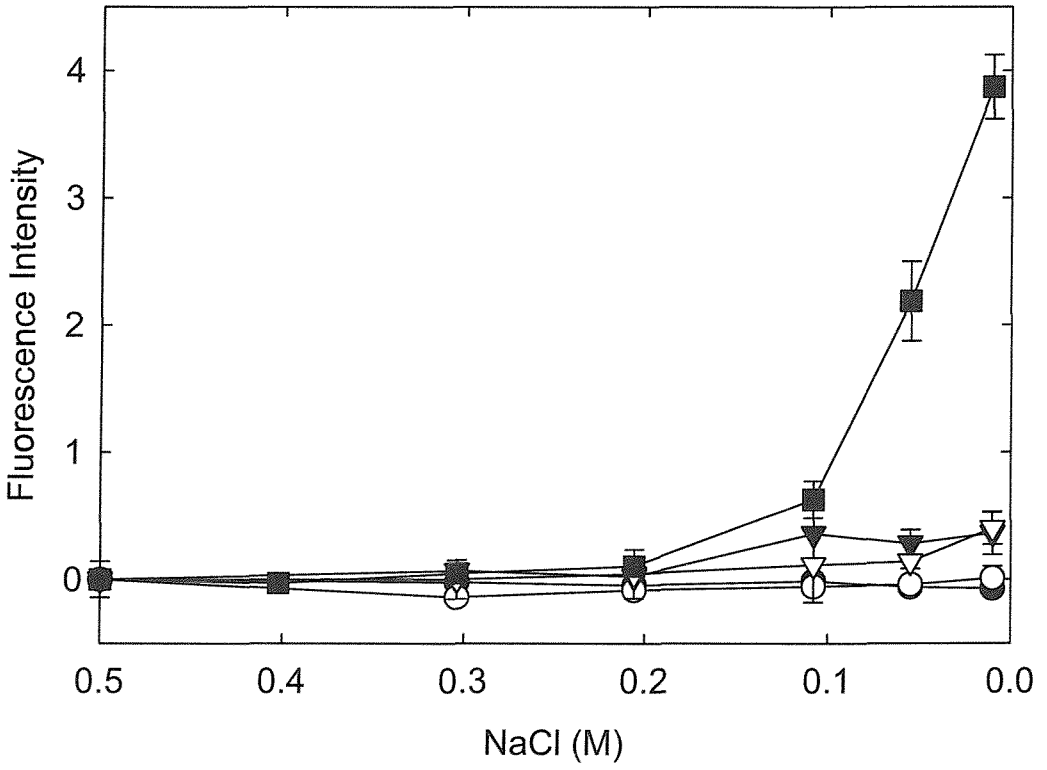

Figure 4.4 *In vivo* assay for function of MscL. Cells were grown in the presence of 0.5 M NaCl to mid-exponential phase, followed by a 50-fold dilution into solutions containing the given concentrations of NaCl, supplemented with 0.5 μg ml^{-1} ethidium bromide. Samples were centrifuged and the fluorescence emission of the supernatant was recorded at 632 nm to assay for released DNA. *E. coli* strain MJF465 (■) and MJF465 expressing: (●), wild type EcMscL; (○), wild type TbMscL; (▼), F93W-EcMscL; and (▽), F80W-TbMscL. Data points are the average of three colonies, the error bars correspond to the standard deviation.

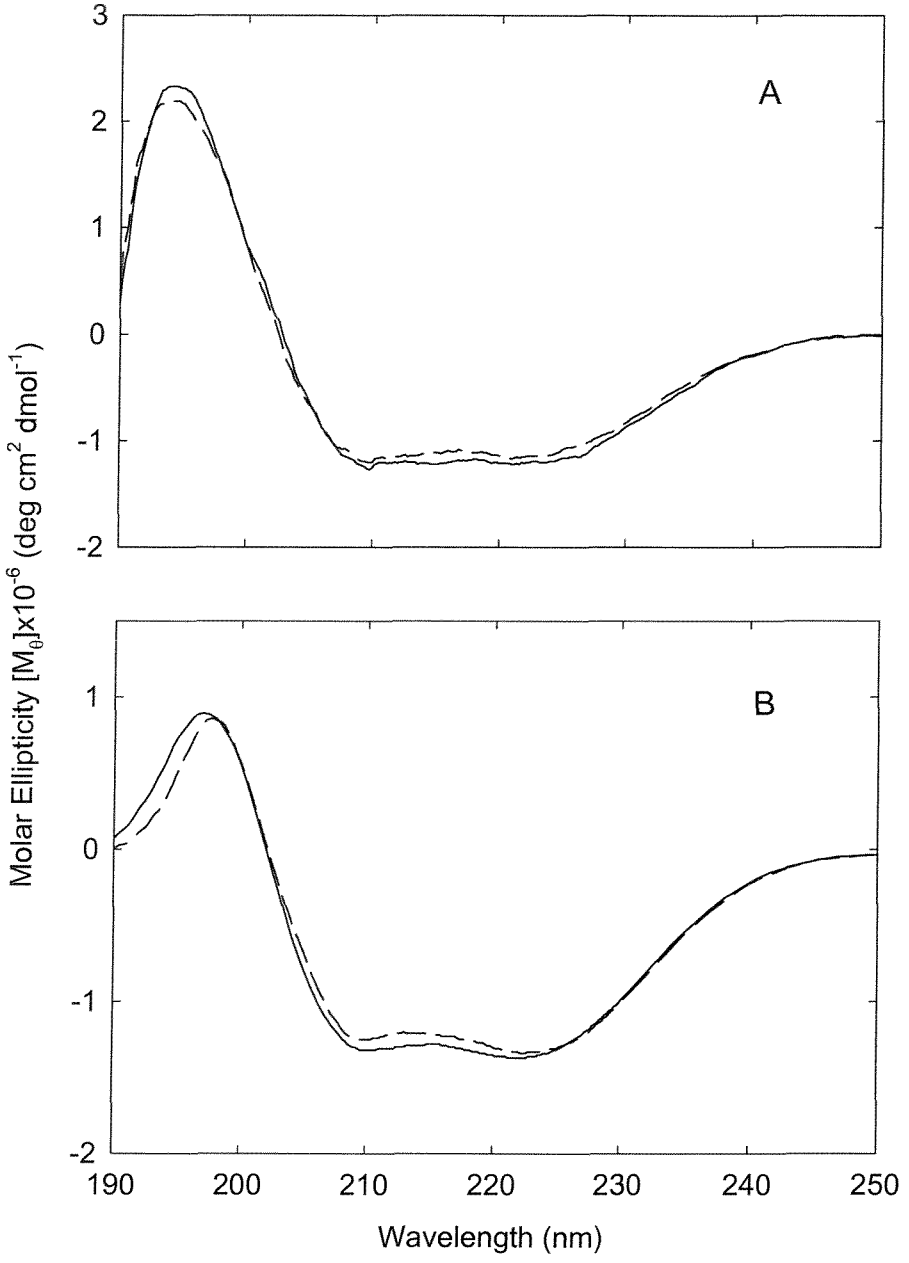

Figure 4.5 Circular dichroism spectra of wild type and Trp-mutated MscL in octylglucoside. The samples contained 1 mg ml^{-1} MscL in PBS buffer containing 40 mM OG and were recorded at 25 °C. (A) Wild type TbMscL (solid line) and F80W-TbMscL (long dashed line). (B) Wild type EcMscL (solid line) and F93W-EcMscL (long dashed line).

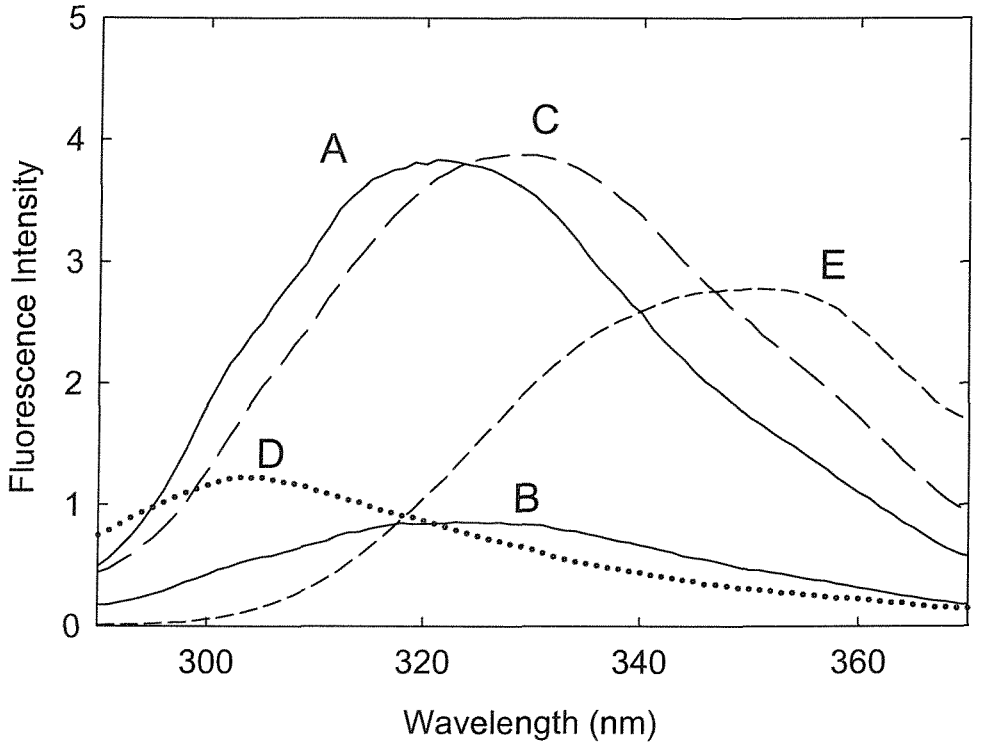

Figure 4.6 Fluorescence emission spectra for F80W-TbMscL and F93W-EcMscL. Fluorescence emission spectra are shown for (A) F80W-TbMscL and (C) F93W-EcMscL reconstituted into bilayers of di(C18:1)PC, and (B) F80W-TbMscL reconstituted into bilayers of di(Br_2C18:0)PC. The emission spectrum (D) of wild type TbMscL reconstituted into bilayers of di(C18:1)PC is also shown. The concentration of MscL was 0.98 μM and the molar ratio of lipid to MscL was 100:1. The emission spectrum of 0.98 μM Trp in buffer is also shown (E). The excitation wavelength was 280 nm and the buffer was 20 mM Hepes, 100 mM KCl, 1 mM EGTA, pH 7.2.

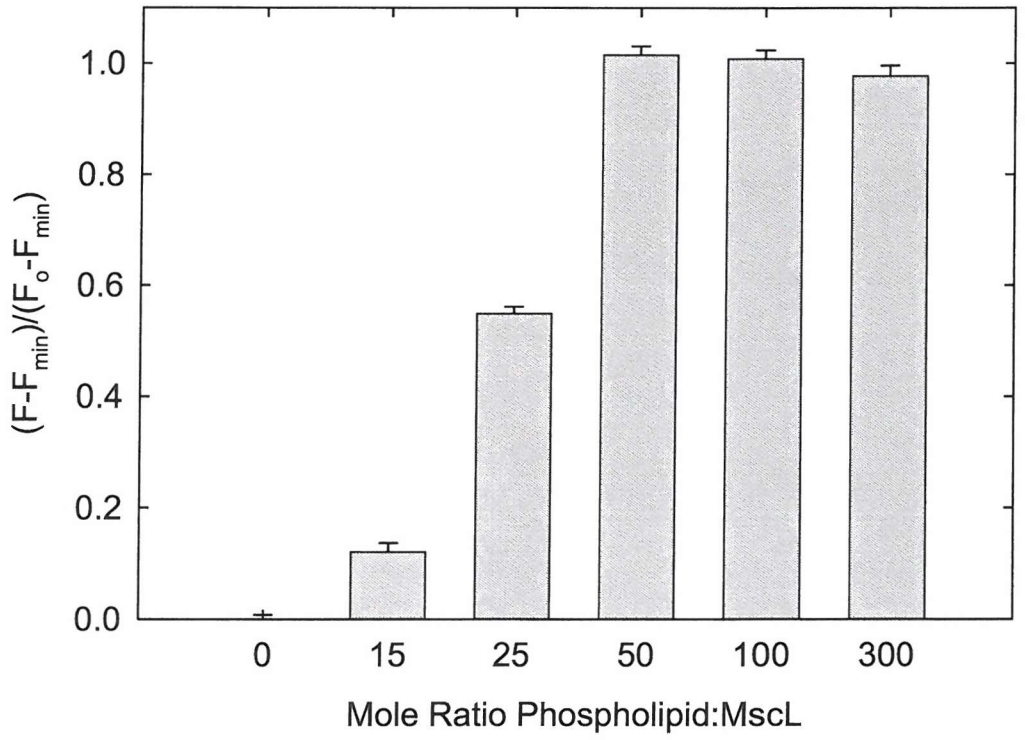

Figure 4.7 Effect of lipid:protein ratio on the relative fluorescence emission for MscL reconstituted with di(C18:1)PC. F and F_o are fluorescence intensities for F80W-TbMscL at a given lipid:protein ratio and 100:1 respectively. F_{min} is the fluorescence intensity for unreconstituted F80W-TbMscL. Fluorescence was excited at 280 nm and emission was monitored at 320 nm. The concentration of MscL was 0.98 μM and the buffer was 20 mM Hepes, 100 mM KCl, 1 mM EGTA, pH 7.2.

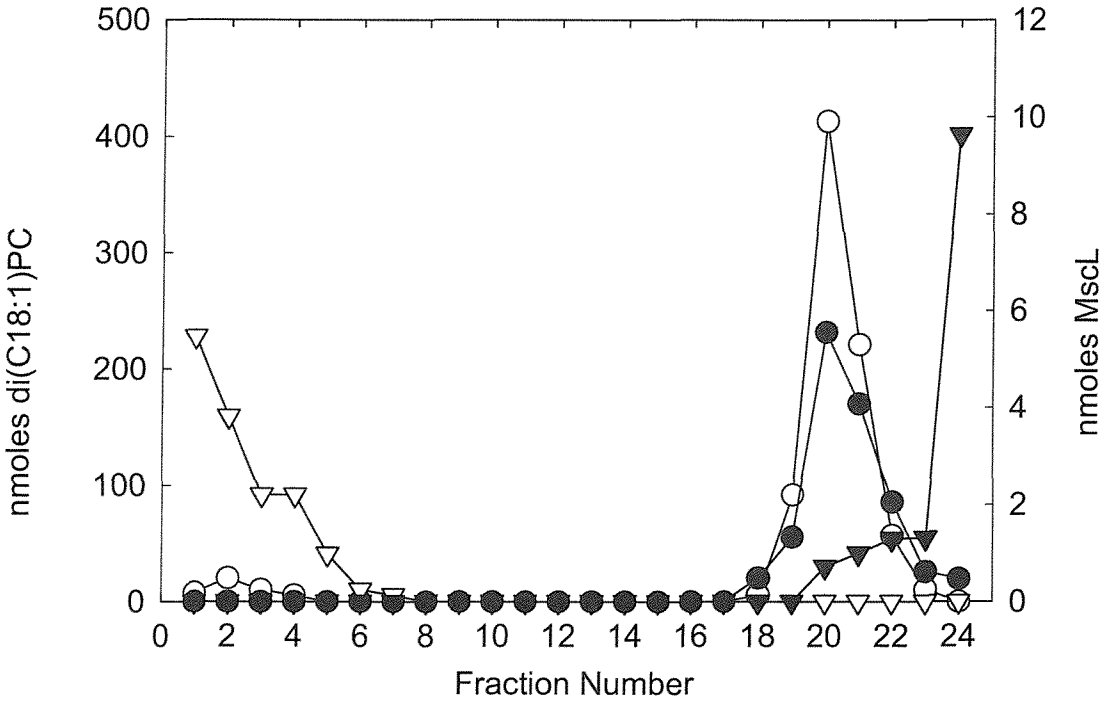

Figure 4.8 Sucrose gradient analysis of reconstituted MscL. A sample of MscL reconstituted with di(C18:1)PC at a lipid to protein molar ratio of 100:1 was separated on a discontinuous sucrose gradient from 30 to 2.5 % (w/v) sucrose. 1.5 ml fractions were taken and analysed for: (○), lipid; and (●), MscL. A sample of (▽), lipid alone and (▼), MscL alone were also analysed employing the same technique and on a separate gradient.

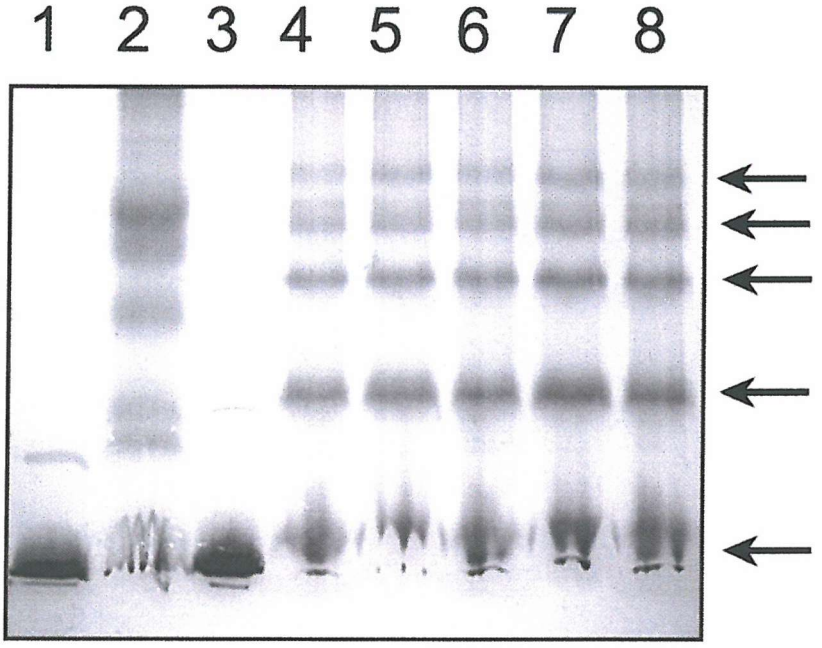

Figure 4.9 10 % Sodium dodecyl sulphate polyacrylamide gel electrophoresis of reconstituted MscL after cross-linking with DSS (2.18 mM) for 30 min at room temperature. Protein bands were visualised by Coomassie brilliant blue staining. Lanes 1 and 3 contain unreconstituted EcMscL and TbMscL respectively, consisting largely of monomeric protein (M_r of 15 and 18.6 kDa for EcMscL and TbMscL respectively) with small amounts of dimeric species. Lane 2 contains cross linked EcMscL following reconstitution in di(C18:1)PC. Lanes 4 to 8 contain cross linked TbMscL following reconstitution into di(C14:1)PC, di(C18:1)PC, di(C24:1)PC, di(C18:1)PS and di(C18:1)PA, respectively. The arrows show the expected positions of monomeric TbMscL and of dimeric, trimeric, tetrameric and pentameric species. In the reconstituted systems the molar ratio of phospholipid to MscL monomer was 100:1.

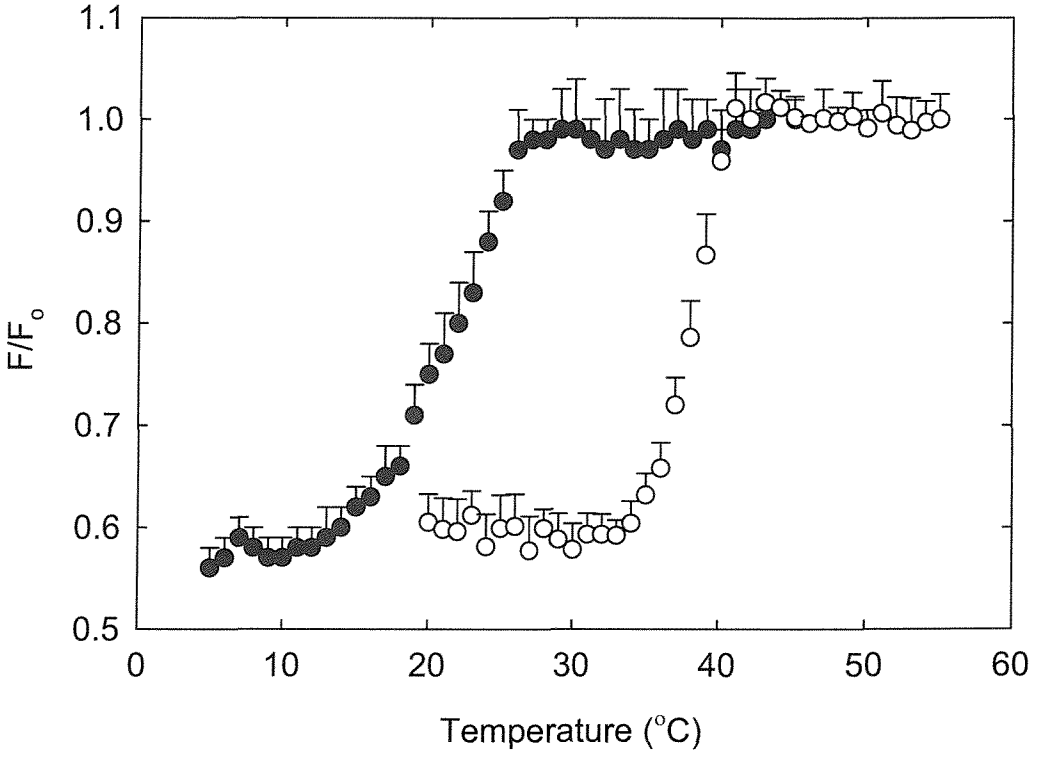

Figure 4.10 Effect of temperature on the fluorescence quenching of F80W-TbMscL. MscL was reconstituted into bilayers containing: (●), di(C14:0)PC with di(Br_2C14:0)PC; and (○), di(C16:0)PC with di(Br_2C16:0)PC and the fluorescence intensities were measured at 320 nm for the given temperatures. The molar ratio of lipid to MscL monomer was 100:1 with a molar ratio of 90:10 for gel phase and liquid crystalline phase lipids respectively. The concentration of MscL was 0.98 μM and the buffer was 20 mM Hepes, 100 mM KCl, 1 mM EGTA, pH 7.2. Data points are the average of fifteen determinations.

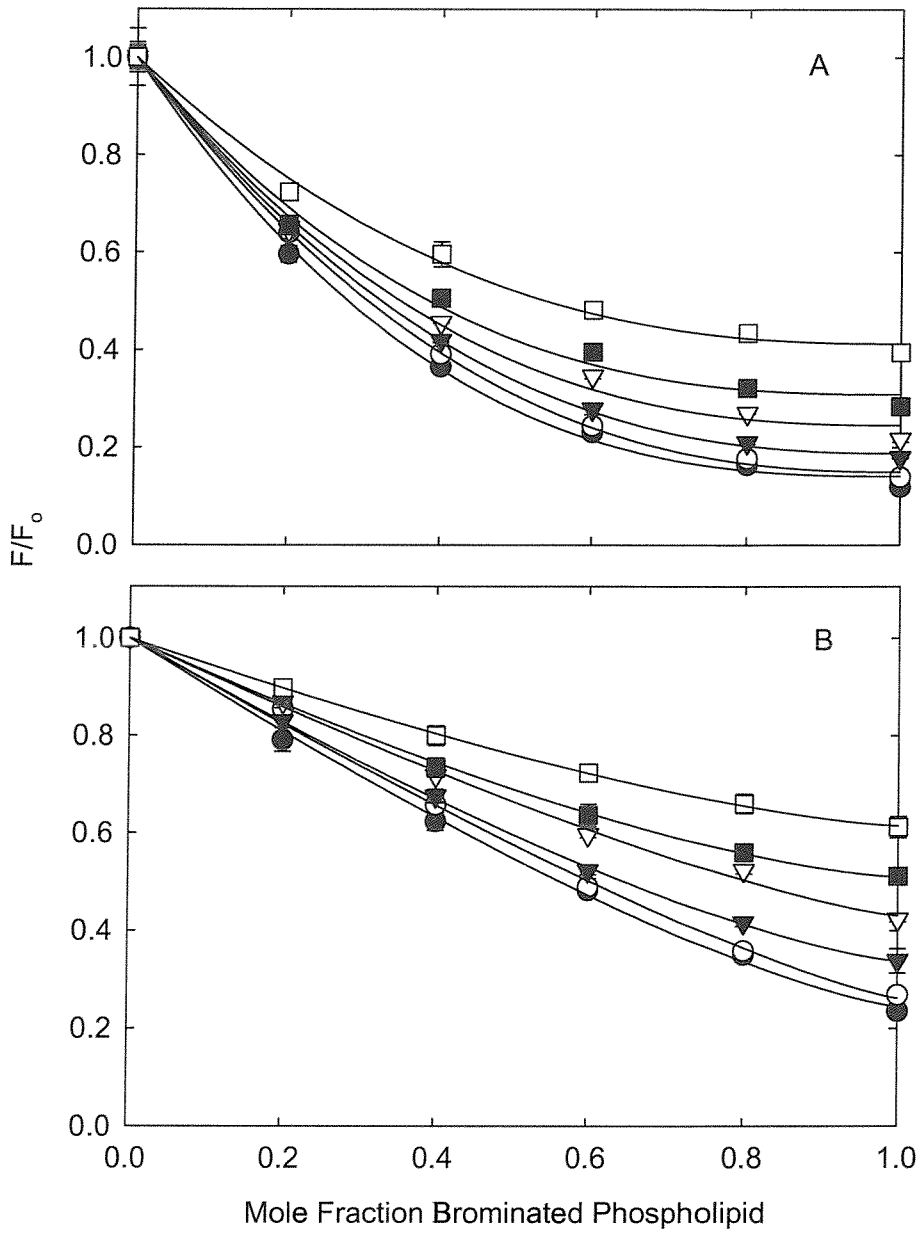

Figure 4.11 Quenching of F80W-TbMscL and F93W-EcMscL fluorescence by brominated phosphatidylcholines as a function of phospholipid chain length. F80W-TbMscL (A) and F93W-EcMscL (B) were reconstituted into bilayers containing mixtures of nonbrominated lipids and the corresponding brominated lipid. Fluorescence intensities are expressed as a fractions of the fluorescence for MscL reconstituted in the nonbrominated lipid. Chain lengths were as follows: (●), C14; (○), C16; (▼), C18; (▽), C20; (■), C22 and (□), C24. The solid lines show fits to Equation 3.11, giving the values for *n* listed in Table 4.4. The concentration of MscL was 0.98 μM, and the molar ratio of lipid to MscL was 100:1. Data points are the average of three determinations.

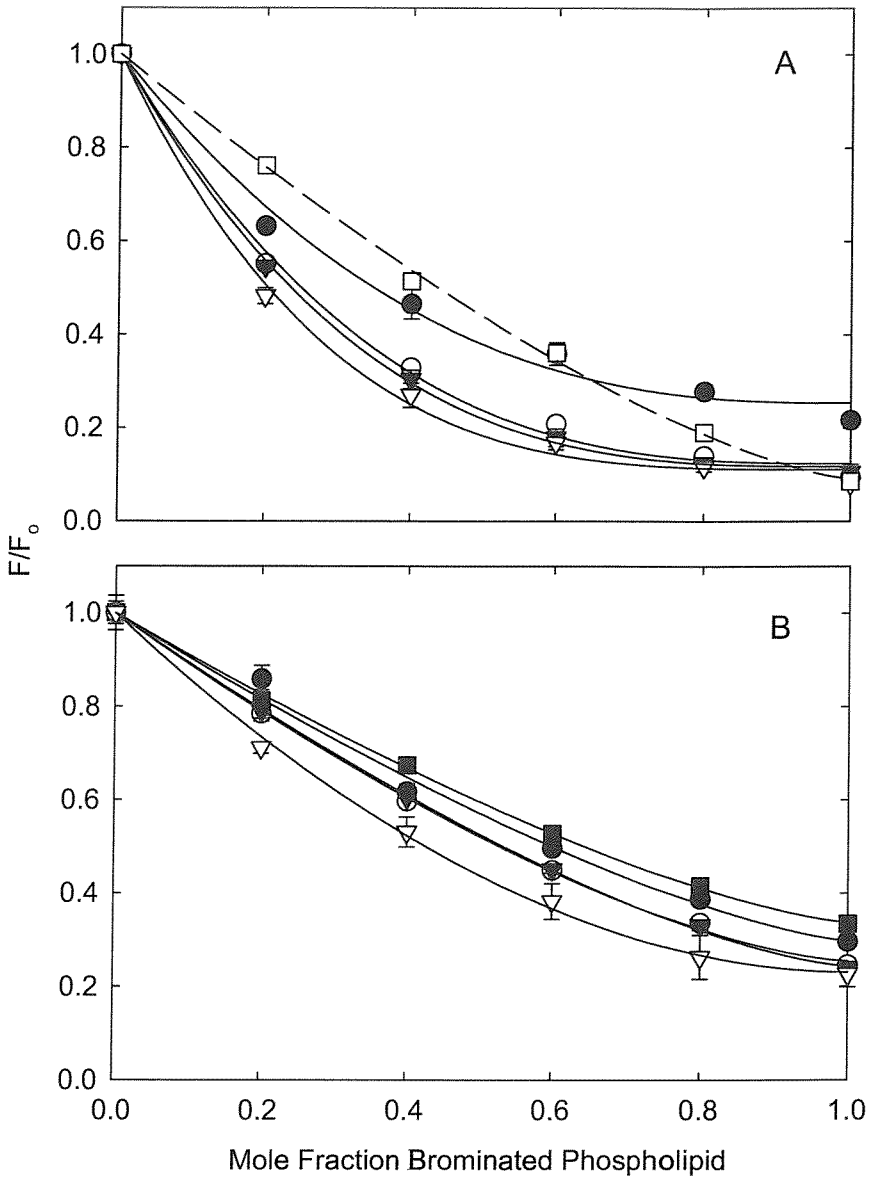

Figure 4.12 Quenching of F80W-TbMscL and F93W-EcMscL fluorescence by brominated phospholipids as a function of phospholipid head group. F80W-TbMscL (A) and F93W-EcMscL (B) were reconstituted into bilayers containing mixtures of nonbrominated lipid and the corresponding brominated lipid, all the lipids having C18 chains. Fluorescence intensities are expressed as a fraction of the fluorescence for F80W-TbMscL reconstituted in the nonbrominated lipid. Lipid head groups were as follows: (●), di(C18:1)PE; (○), di(C18:1)PS; (▼), di(C18:1)PG; (▽), di(C18:1)PA; and (□), tetra(C18:1)CL. Data points are the average of three determinations. The lines show fits to Equation 3.11 giving the values for *n* listed in Table 4.5. The concentration of MscL was 0.98 μM and the molar ratio of lipid to MscL was 100:1.

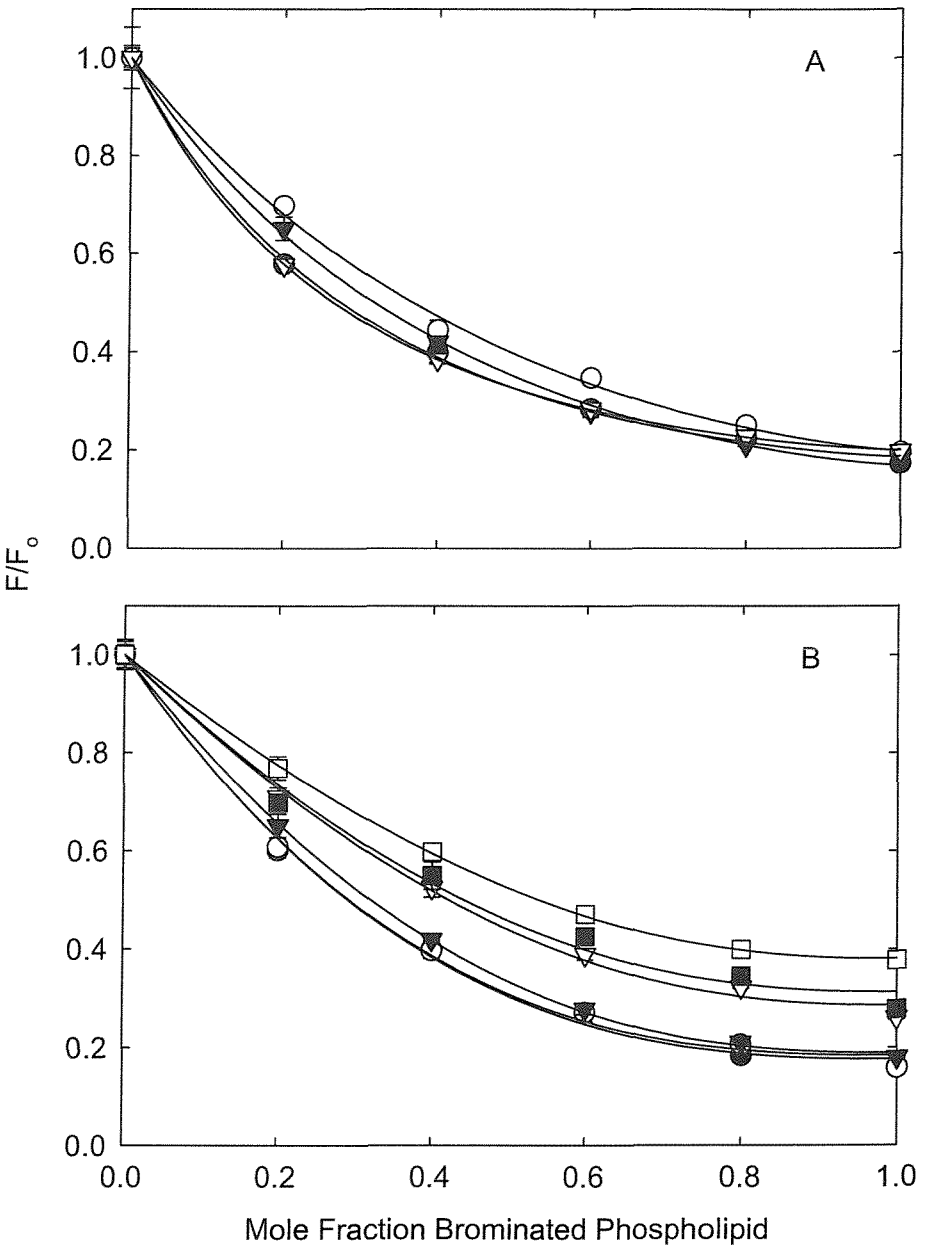

Figure 4.13 Quenching of F80W-TbMscL in mixtures with brominated phosphatidylcholines. (A) F80W-TbMscL was reconstituted into mixtures of di(Br_2C18:0)PC and: (●), di(C12:0)PC; (○), di(C16:1)PC; (▼), di(C18:1)PC; and (∇), di(C24:1)PC. (B) F80W-TbMscL was reconstituted into mixtures of di(C18:1)PC and: (●), di(Br_2C14:0)PC; (○), di(Br_2C16:0)PC; (▼), di(Br_2C18:0)PC; (∇), di(Br_2C20:0)PC; (■), di(Br_2C22:0)PC; and (□), di(Br_2C24:0)PC. Data points are the average of three determinations. The solid lines show best fits to Equation 3.15 giving the relative binding constants listed in Table 4.6.

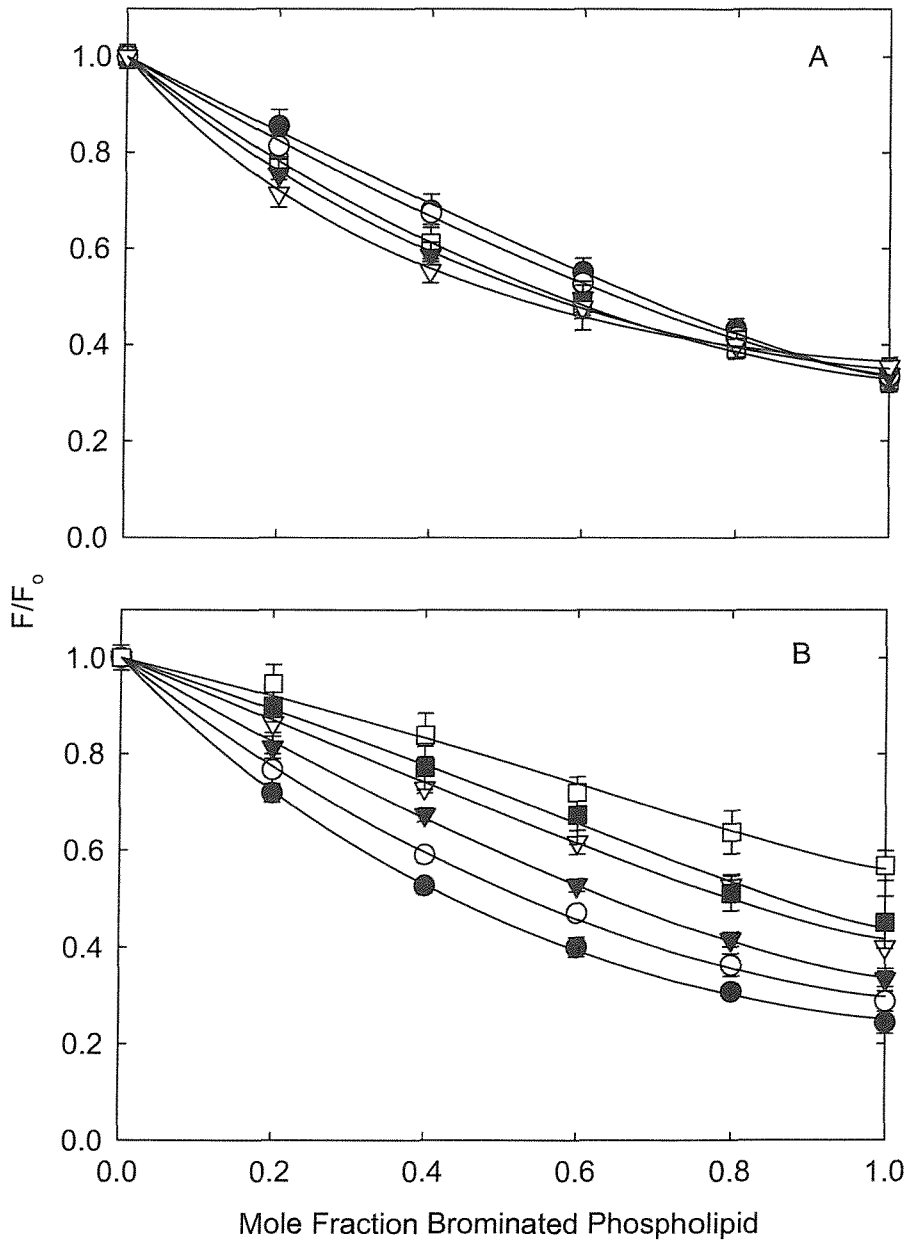

Figure 4.14 Quenching of F93W-EcMscL in mixtures with brominated phosphatidylcholines. (A) F93W-EcMscL was reconstituted into mixtures of di(Br_2C18:0)PC and: (●), di(C12:0)PC; (○), di(C16:1)PC; (▼), di(C18:1)PC; and (▽), di(C24:1)PC. (B) F93W-EcMscL was reconstituted into mixtures of di(C18:1)PC and: (●), di(Br_2C14:0)PC; (○), di(Br_2C16:0)PC; (▼), di(Br_2C18:0)PC; (▽), di(Br_2C20:0)PC; (■), di(Br_2C22:0)PC; and (□), di(Br_2C24:0)PC. Data points are the average of three determinations. The solid lines show best fits to Equation 3.15 giving the relative binding constants listed in Table 4.6.

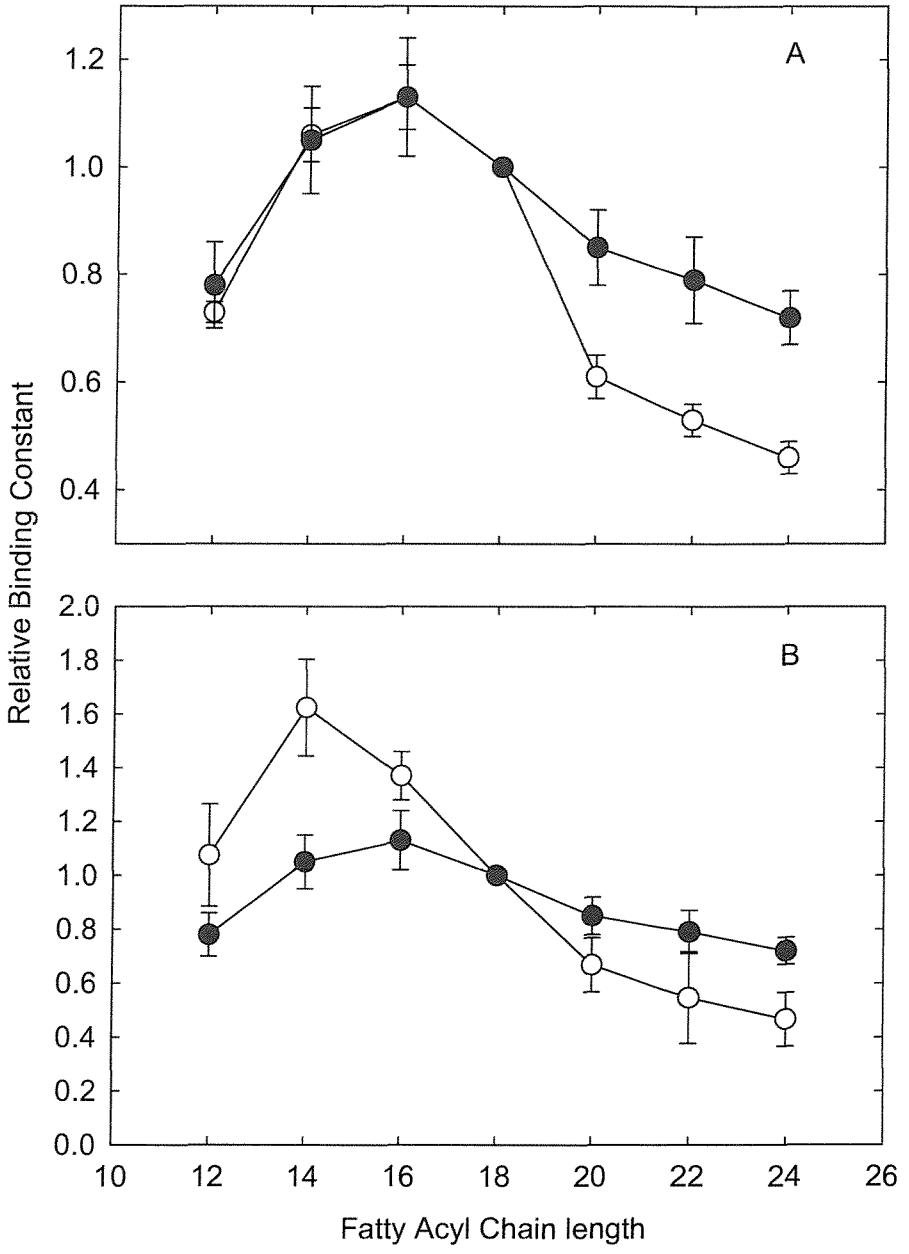

Figure 4.15 The dependence of lipid binding constants on chain length. The chain length dependencies of the binding constants for phosphatidylcholines relative to di(C18:1)PC are plotted for: A) (●), F80W-TbMscL; and (○), F93W-EcMscL (Table 4.6). B) comparison of lipid binding constants for: (●), α-helical protein F80W-TbMscL; and (○), the β-barrel protein OmpF (O'Keeffe et al., 2000).

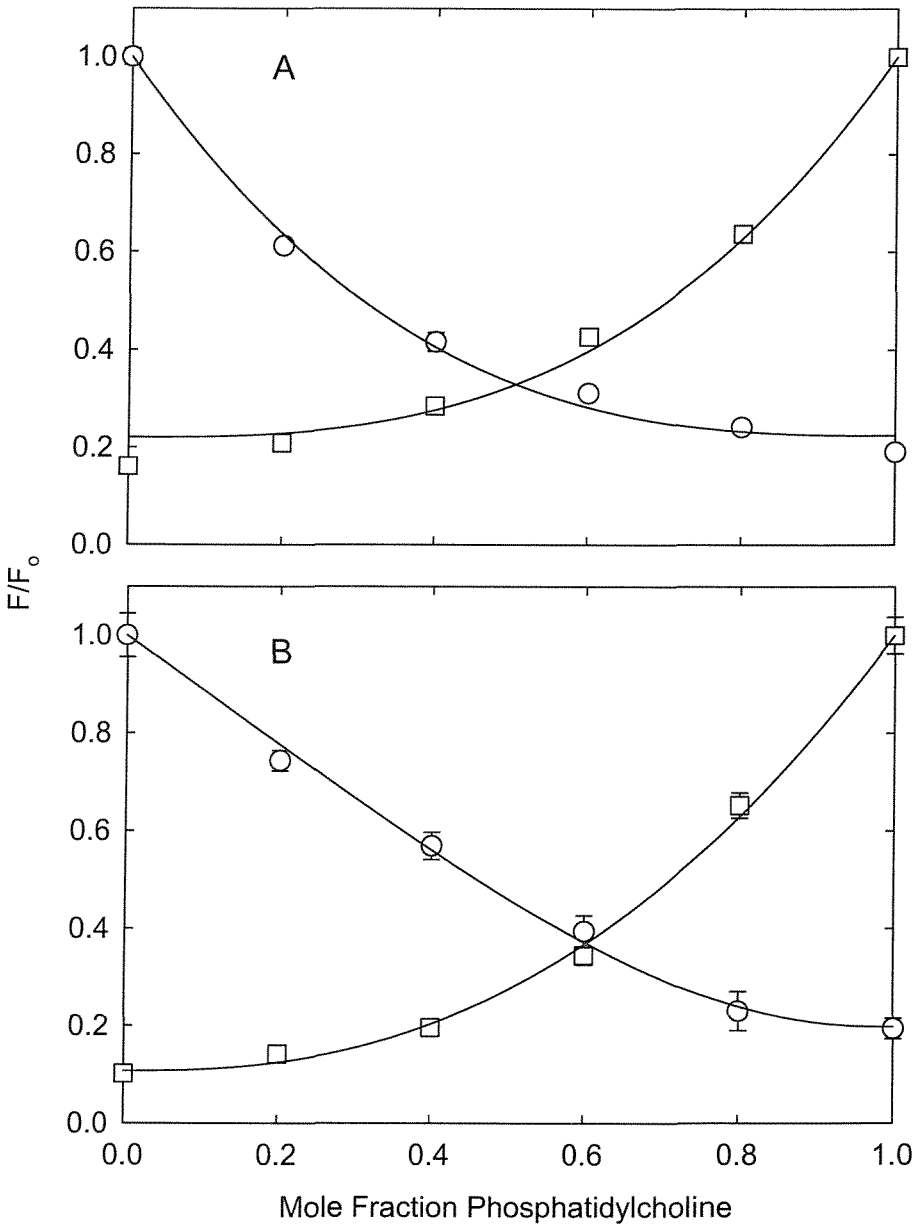

Figure 4.16 Quenching of F80W-TbMscL in mixtures with phosphatidylethanolamine (A) or cardiolipin (B). F80W-TbMscL was reconstituted into mixtures containing di(C18:1)PC and di(Br_2C18:0)PE or tetra(Br_2C18:0)CL (□) or di(Br_2C18:0)PC and di(C18:1)PE or tetra(C18:1)CL (○). Data points are the average of three determinations. The solid lines show best fits to Equation 3.15 giving the relative binding constants listed in Table 4.7. In (B), mole fractions are calculated based on the number of moles of fatty acyl chains to account for the fact that tetra(C18:1)CL contains four chains and di(C18:1)PC contains two chains.

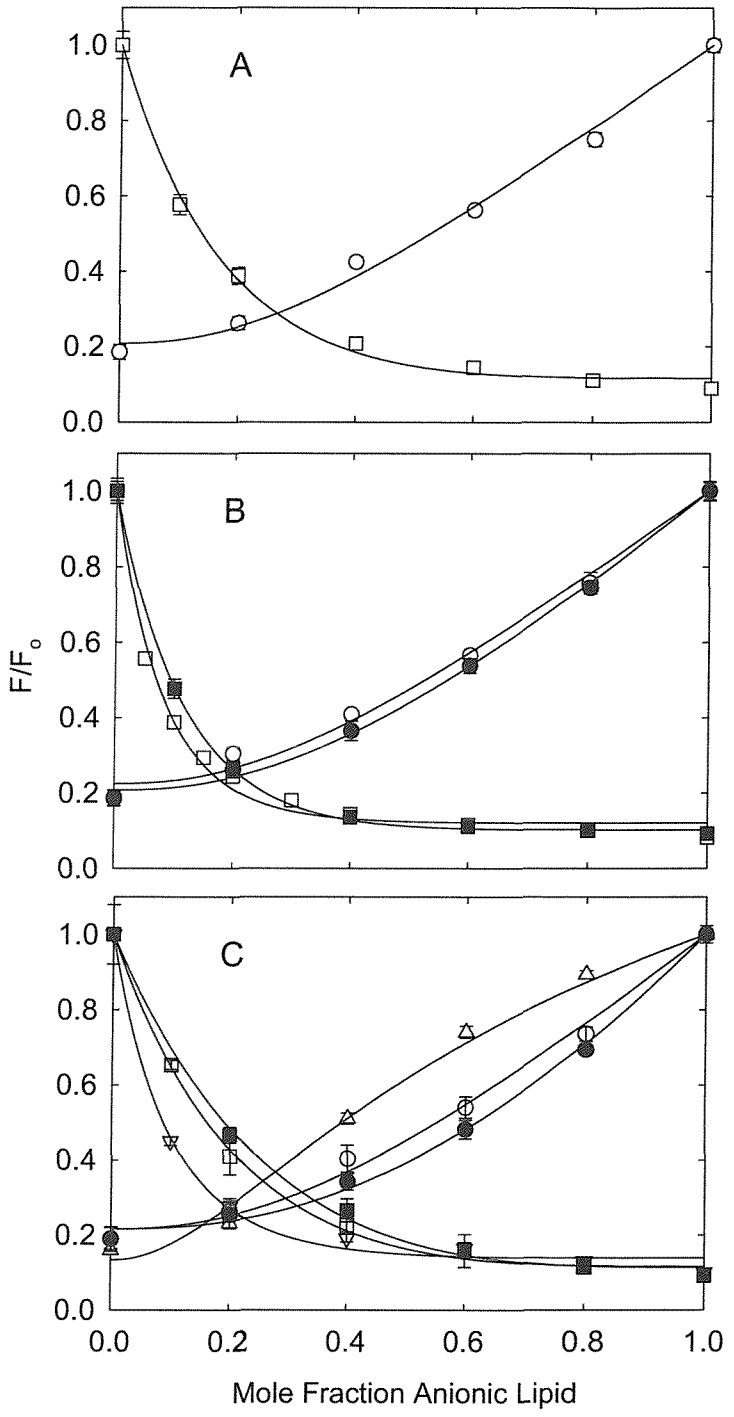

Figure 4.17 Quenching of F80W-TbMscL in mixtures of anionic lipid and phosphatidylcholine. F80W-TbMscL was reconstituted into mixtures containing di(C18:1)PC and brominated anionic phospholipid (□,■,∇), or non-brominated anionic phospholipid and di(Br_2C18:0)PC (○,●,Δ): (A) phosphatidylglycerol; (B) phosphatidic acid; and (C) phosphatidylserine. The concentration of KCl was (∇,Δ) 26 mM, (□,○) 100 mM and (■,●) 1 M. Data points are the average of three determinations. The solid lines show best fits to Equation 3.15 giving the relative binding constants listed in Table 4.7.

4.4 Discussion

4.4.1 Solubilisation of MscL

The ability of a range of detergents to solubilise MscL was investigated. All detergents produced a decrease in light scatter, but varied in their ability to solubilise MscL. OG, Mega-9, and LDAO (Figure 4.2) effectively solubilised MscL at concentrations in good agreement with the CMC value for each detergent. DDM (Figure 4.2) was able to solubilise MscL, but the detergent concentration required to achieve a 100 % solubilised state, was slightly above the CMC. Cholate and $C_{12}E_8$ (Figure 4.2) were apparently less able to solubilise MscL fully over the concentration range tested, but did produce a marked decrease in light scatter.

For protein purification OG was chosen as the detergent of choice, due to the detergents commercial availability, wide use, and high CMC. The latter property allows easy removal of detergent through dilution during the reconstitution process. Although Mega-9 also solubilised MscL and has a high CMC, this detergent precipitates at 4 °C or below, which is not compatible with the purification procedure. Cholate has previously been shown to efficiently solubilised phospholipids at 15 mM (Pilot, 2001) and was used in the reconstitution procedure due to its cheapness. OG was also shown to solubilise phospholipids, but contains fluorescence impurities that contributed a large noise signal to the Trp fluorescence emission spectra.

4.4.2 Endogenous Phospholipid Content of Purified MscL

EcMscL and TbMscL purified using OG, DDM, and LDAO as detergents were analysed for phospholipid content by thin layer chromatography and by phosphate assay, but no phospholipid could be detected. This suggests that neither MscL protein contains high specificity or 'sticky' sites for lipids. In contrast the potassium channel KcsA has been shown to purify from detergent solution with 0.6 mole of phosphatidyl glycerol per mole of KcsA monomer (Valiyaveetil et al., 2002).

4.4.3 *In vivo* Function of Trp-mutated MscL

The results from the *in vivo* channel function assay shown in Figure 4.4 shows that the mutant F80W-TbMscL is able to rescue *E. coli* knock out strain MJF465 from osmotic downshock and is therefore functional. F93W-EcMscL located towards the end of the second transmembrane α-helix was also active in the *in vivo* assay.

4.4.4 Circular Dichroism of Trp-mutated MscL

The CD spectra shown in Figure 4.5 for MscLs in micelles of OG show that the structure of Trp-mutated and wild type MscL are comparable for both TbMscL and EcMscL. Therefore, introduction of Trp residues into the second transmembrane α-helix has not resulted in any large change in the secondary structure of MscL.

4.4.5 Fluorescence Assay

4.4.5.1 *Reconstitution*

Successful reconstitution requires there to be a sufficient molar ratio of lipid to protein in the membrane. Lewis and Engelman (1983) calculated the diameter of a lipid molecule to be 9.4 Å, while the circumference of TbMscL is around 135 Å, so that the number of lipids required to form a single shelled bilayer around the protein can be estimated through simple geometry to be ca. 29 lipid molecules for each MscL pentamer. To ensure complete reconstitution a molar ratio of lipid to MscL monomer of 100:1 was chosen. As shown in Figure 4.7, attempts to reconstitute MscL with di(C18:1)PC at molar ratios of lipid to protein of less than 50:1 resulted in lower than expected Trp fluorescence intensities, but fluorescence intensities did not change with the molar ratios of lipid to protein from 50:1 to 300:1, consistent with successful reconstitution as long as the molar ratio of lipid to protein was greater than 50:1.

The reconstituted membrane was characterised on a discontinuous sucrose gradient as, shown in Figure 4.8, confirming that protein and lipid effectively mix during the

reconstitution procedure. Cross-linking experiments with reconstituted MscLs suggest that TbMscL and EcMscL maintain their pentameric structures in bilayers of phosphatidylcholines with chain lengths between C14-C24 and in bilayers of di(C18:1)PS and di(C18:1)PA, as shown in Figure 4.9, confirming that reconstitution does not denature the protein.

4.4.5.2 *Fluorescence Properties*

The fluorescence emission spectrum of F80W-TbMscL reconstituted in di(C18:1)PC shown in Figure 4.6 shows the Trp residue to be located in a very hydrophobic environment, deep within the membrane as predicted from the position of this residue in the middle of the second transmembrane α-helix (Figure 4.1). Phe-93 in EcMscL was also replaced with a Trp residue; Phe-93 in EcMscL is equivalent to Tyr-87 or Phe-88 in TbMscL (Figures 1.8 and 4.1). The fluorescence emission spectrum for F93W-EcMscL in di(C18:1)PC shown in Figure 4.6 is shifted to slightly longer wavelengths compared to F80W-TbMscL, consistent with a Trp located within the hydrocarbon core of the bilayer, but towards the carbonyl region of the membrane interface (Figure 4.1). MscL is a homopentamer, therefore introduction of a single Trp residue into the monomer results in a channel containing five Trp residues. However, each Trp residue in the pentamer is in an identical position and environment, so that the quenching properties of each Trp residue will also be identical.

Fluorescence quenching by brominated phospholipids was used to confirm that reconstitution had occurred. Quenching of the Trp fluorescence by brominated phospholipids requires either contact between the Trp residue and the dibrominated quencher or close proximity to allow Förster transfer (East and Lee, 1982; Mall et al., 2001). F80W-TbMscL and F93W-EcMscL were reconstituted into lipid bilayers with a molar ratio of lipid to MscL of 100:1, using different concentrations of cholate and various reconstitution methods (Figure 4.11, Table 4.2). A reduction in the fluorescence emission in terms of both F80W-TbMscL and F93W-EcMscL reconstituted in brominated phospholipid compared to reconstitution in non-brominated phospholipid, confirms the protein and lipid components are mixing and successfully reconstituting into bilayer species. Furthermore, increasing the amount

of cholate in the reconstituted system had no significant effect on the level of fluorescence, nor did the method of reconstitution affect the fluorescence emission intensity. These data give confidence that sufficient cholate is present to allow efficient mixing of protein and lipid, and that adequate cholate is removed during reconstitution to allow protein and lipid to form bilayers.

4.4.6 Lipid Binding Affinities for MscL

4.4.6.1 *Chain Length*

Lipid binding constants for phosphatidylcholines with chain lengths between C12-C24 for F80W-TbMscL and F93W-EcMscL are shown in Table 4.6. From this data it can be seen that binding constants vary only by a factor of 1.5-fold for TbMscL and three-fold for EcMscL, with both MscLs exhibiting weak binding affinities for phosphatidylcholines with short or long fatty acyl chains, and greatest affinity for phosphatidylcholine lipid with an acyl chain length of C16. The hydrophobic thickness d of a saturated phosphatidylcholine bilayer is related to its chain length by

$$d = 1.75(n_c - 1) \qquad \text{Equation 4.1}$$

where n_c is the number of carbon atoms in the fatty acyl chain. The thickness of a phosphatidylcholine bilayer with two monounsaturated chains was estimated to be about 2.5 Å less than that of the corresponding phosphatidylcholine with two saturated chains calculated from Equation 4.1 (Lewis and Engelman, 1983). A di(C16:1)PC bilayer will therefore have a hydrophobic thickness of about 24 Å. The fact that di(C16:1)PC is the lipid binding most strongly to MscL suggests that the hydrophobic thickness for MscL is also ca. 24 Å.

Trp and Tyr residues are often located in membrane proteins at the bilayer interface, helping to define the region of the transmembrane α-helices spanning the hydrophobic core of the bilayer (Landolt-Marticorena et al., 1993; Ulmschneider and Sansom, 2001). TbMscL does not contain any Trp residues and only contains two Tyr residues per monomer (Tyr-87 and Tyr-94), both located on the same side of the

membrane (Figure 4.1). However, TbMscL does contain two negatively charged residues that could define the periplasmic interface (Asp-36 and Asp-68) and one that could define the cytoplasmic interface (Asp-16). Asp-16 and Asp-36 are conserved in most MscL channels and although Asp-68 is not conserved, the position is usually occupied by a charged residue or followed by a Trp or Tyr (Figure 1.7). Using these Asp residues to define the bilayer interfaces gives a predicted bilayer thickness of 25 Å, a value in good agreement with the observation that di(C16:1)PC binds with greatest affinity to TbMscL. Furthermore, the *M. tuberculosis* membrane predominately contains phospholipids with acyl chains of C18:1 and C16:0 at the *sn*-1 and *sn*-2 positions respectively (Coren, 1984), corresponding to a native membrane thickness of ca. 26 Å.

In bilayers containing shorter or longer chains than the optimum for a membrane protein there will be a mismatch between the hydrophobic thickness of the protein and that of the lipid bilayer, and to avoid exposure of hydrophobic groups to water, either the protein will distort, the lipid bilayer will distort, or there may be some combination of the two. If the protein acts as a rigid body then the lipids must stretch or compress in order to satisfy the hydrophobic matching conditions. Distortion of the bilayer, either through expansion of short lipids, or compression of long lipids will require energy (Fattal and Ben-Shaul, 1993), which will be reflected in lower binding affinities for these mismatched lipids.

Figure 4.15B shows a comparison of the relative binding constants for TbMscL and the β-barrel protein OmpF. OmpF binds most strongly to di(C14:1)PC (O'Keeffe et al., 2000); OmpF is a bacterial outer membrane protein, and the average chain length of the lipids in the outer membrane are less than those in the inner membrane (Harwood and Russell, 1984). However, the key observation is that the relative lipid binding constants for OmpF show a much greater dependence on chain length than for MscL, with phosphatidylcholines over the C14-C24 range exhibiting a 4-fold change in lipid binding affinity. In comparison, the results in Figure 4.15B for TbMscL show a much smaller 1.5-fold change in binding affinity over the same range of PC chain lengths.

Since OmpF is a rigid, β-barrel protein, hydrophobic matching is presumably achieved by distortion of the lipid bilayer around the protein, with relatively little distortion of the protein itself. The smaller chain length dependence of lipid binding to MscL therefore suggests that hydrophobic matching for MscL involves distortion of MscL as well as distortion of the lipid bilayer. ESR studies with spin-labelled EcMscL suggest that reconstitution of EcMscL into bilayers of short chain length lipids does indeed result in a change in conformation, although not as large a change as seen between closed and open states of the channel (Perozo et al., 2002b). The ability of transmembrane α-helices to tilt within the plane of the bilayer suggests MscL would readily alter its conformation to match bilayer thickness, and therefore supports the observed binding affinities for TbMscL for different chain length phosphatidylcholines.

4.4.6.2 *Head Groups*

The relative binding constants for F80W-TbMscL and phospholipids with different head groups relative to di(C18:1)PC are shown in Table 4.7. There is no selectivity between di(C18:1)PE and di(C18:1)PC, with both phospholipids binding equally well to F80W-TbMscL. A similar observation has been made with OmpF (O'Keeffe et al., 2000), although for Ca^{2+}-ATPase PE was shown to bind with half the affinity of PC (East and Lee, 1982). PE is an unusual lipid favouring the H_{II} phase when in isolation (Dowhan and Bogdanov, 2002) and would be expected to alter the lateral pressure profile of the membrane, an affect translated to the protein (Cantor, 1997b; Epand, 1998). The equal binding affinities for di(C18:1)PE and di(C18:1)PC to F80W-TbMscL is surprising, given that a change in bilayer tension or hydrogen bond potential are believed to influence gating of the channel (Elmore and Dougherty, 2001; Perozo et al., 2002b). A molecular dynamic simulation of TbMscL, suggests that the cytoplasmic domain of the protein undergoes a conformational change upon transition from a PC to PE bilayer, with certain lipid-protein contacts favoured in one conformation but not the other (Elmore and Dougherty, 2003). These simulations suggest that the equal binding affinities observed experimentally for di(C18:1)PE and di(C18:1)PC to F80W-TbMscL could be the result of a compensatory mechanism, in which the protein changes its structure and therefore interactions with the bilayer as the mole ratio of di(C18:1)PC:di(C18:1)PE changes.

Binding constants for di(C18:1)PG and di(C18:1)PS to TbMscL are about two-fold greater than that for di(C18:1)PC in the presence of 100 mM KCl (Table 4.7). The relative binding constant for di(C18:1)PS decreases with increasing ionic strength, being close to 1 in 1 M KCl (Table 4.7), suggesting a large charge component in the anionic lipid-protein interaction.

Results for phosphatidic acid are significantly different from those observed with the other anionic phospholipids (Table 4.7). The quenching data shown in Figure 4.17 for phosphatidic acid, is consistent with two classes of binding sites on TbMscL for di(C18:1)PA, the affinity for di(C18:1)PA being about double that for di(C18:1)PC at one class of sites but 3.5-fold greater at the second class of sites (Table 4.7). The effects of ionic strength are much smaller on the binding of phosphatidic acid than on the binding of phosphatidylserine (Table 4.7), suggesting that interactions other than charge interactions are important in the binding of the small phosphatidic acid head group to TbMscL.

The major membrane lipids of the *Mycobacteria* are the anionic phospholipids cardiolipin and phosphatidylinositolmannosides, with the zwitterionic phospholipid phosphatidylethanolamine making up about a third of the total phospholipid (Coren, 1984). Thus, given the slightly stronger binding of anionic than zwitterionic phospholipids to TbMscL (Table 4.7), the majority of the lipids surrounding TbMscL in the native membrane are likely to be anionic phospholipids.

4.4.6.3 *Lipid Phase*

The relative affinity of MscL for gel and liquid crystalline phase lipid was determined by measuring the fluorescence intensity of F80W-TbMscL as a function of temperature in mixtures of di(Br_2C18:0)PC with di(C14:0)PC and di(C16:0)PC (Figure 4.10). At low temperatures, mixtures of di(C14:0)PC or di(C16:0)PC and brominated PC exist as two phase separated mixtures, containing gel phase domains enriched in di(C14:0)PC or di(C16:0)PC lipid and liquid crystalline domains enriched in the brominated lipid; at higher temperatures, as the gel phase domains melt, the proportion of the liquid crystalline phase lipid in the mixture will increase (East and

Lee, 1982). The phase transition temperatures were centred at 22 and 38 °C for di(C14:1)PC and di(C16:1)PC with MscL respectively. The slightly lower temperature reported with MscL than the pure lipid, is consistent with a model where the protein disrupts the highly organised lattice formed by the gel phase lipids.

Chapter 5:

Determining the Hydrophobic Thickness of MscL

5 DETERMINING THE HYDROPHOBIC THICKNESS OF MscL

5.1 Introduction

The structures and stabilities of integral membrane proteins are determined, in part, by the extent to which the protein is buried within the bilayer matrix and therefore, the interaction with the surrounding lipid bilayer (White et al., 2001) (Figure 5.1); lipid and protein components of the membrane must have co-evolved to allow the integral membrane protein to function within the lipid bilayer, while not compromising membrane structure (Lee, 2003). One important property of a lipid bilayer is its hydrophobic thickness, defined, for a bilayer of a glycerolphospholipid, as the distance between the glycerol backbone regions of the lipid molecules on the two sides of the bilayer.

5.1.1 Structure of the Phospholipid Bilayer

The liquid crystalline phase of a bilayer of dioleoylphosphatidylcholine has been characterised using a combination of X-ray and neutron diffraction methods at low hydration (Figure 5.2) (Wiener and White, 1992). The time-averaged Gaussian distribution profiles provide an estimate of the degree of thermal motion along the bilayer normal. The most rigid part of the bilayer corresponds to the glycerol backbone region, and thermal motion increases with increasing distance from the glycerol backbone. Atom density profiles show water penetration up to the backbone carbonyl groups only, while the hydrophobic thickness of the hydrocarbon core between these two regions is approximately 30 Å at low hydration (White et al., 2001). Not only are biological membranes complex thermally disordered structures, but the presence of many different lipid species results in a fluctuating hydrophobic thickness of the membrane around the protein.

5.1.2 Transmembrane Proteins

The hydrophobic thickness of an intrinsic membrane protein is expected to match that of the surrounding lipid bilayer, due to the high cost of exposing hydrophobic groups to water (Tanford, 1980; Sackmann, 1984). Any potential mismatch between the hydrophobic thickness of a membrane protein and the hydrophobic thickness of the lipid bilayer could be overcome by stretching or compressing the fatty acyl chains of the lipids surrounding the protein, through distortion of the membrane protein, or by some combination of the two (Marsh, 1993; Sprong et al., 2001; White et al., 2001); distortion of the protein could lead to loss of activity of the protein (Lee, 2003).

The hydrophobic thickness of a membrane protein can be determined directly from the crystal structure in those few cases where the crystal structure contains several resolved lipid molecules (Lee, 2003). However, the crystal structure of MscL, as with most integral membrane proteins, does not include resolved lipid molecules and the hydrophobic thickness of the protein and how the protein sits in the membrane has then to be deduced indirectly.

The majority of integral membrane proteins penetrate and cross the lipid bilayer as one or more α-helices (von Heijne, 1994); a stretch of 20 hydrophobic amino acid residues is generally required to traverse a lipid bilayer with a hydrophobic thicknesses of 30 Å, when the α-helix is parallel to the membrane normal. However, transmembrane helices commonly cross the membrane at an angle of approximately 20° to the bilayer normal, and this requires an additional two residues to span the bilayer (Bowie, 1997; Lee, 2003).

5.1.3 Analysis of Transmembrane Regions in Proteins

The distribution of amino acid residues in α-helical-type membrane spanning segments have been analysed and shown to be non-random; that is, specific residues have positional preference, as summarised in Figure 5.3 for bitopic type I transmembrane proteins. The core of a transmembrane α-helix contains predominately hydrophobic residues with aliphatic side chains (Landolt-Marticorena

et al., 1993). The extreme ends of transmembrane helices contain polar or charged residues, both positive and negatively charged residues. These unpaired charged groups are almost exclusively located in the head group region of the bilayer or fully exposed to the aqueous phase, due to the high cost of burying charged residues within the hydrocarbon core of the lipid bilayer (about 37 kJ mol^{-1} for Lys) (Engelman et al., 1986; Lee, 2003). Lys and Arg residues contain long flexible side chains of hydrophobic segments linked to a charged terminal group and so these residues can be located within the hydrophobic core of the helix, while their charged amino groups snorkel to the surface of the membrane, thereby satisfying both the aliphatic and charged moieties of their side chains (Strandberg and Killian, 2003). Aromatic residues Tyr and Trp are found primarily at the ends of transmembrane α-helices. These are located preferentially at the lipid-water interface because of their amphipathic nature (de Planque et al., 2002; Lee, 2003). It has been proposed that these aromatic residues have a functional analogy to floats/buoys on either side of the fluid lipid bilayer, serving to fix the helix within the bilayer (Landolt-Marticorena et al., 1993; Ulmschneider and Sansom, 2001). However, the function of these groups appears to be redundant in the presence of charged residues at the ends of the transmembrane helices (Clark et al., 2003).

When determining the location of a bilayer around a membrane protein using the amino acid sequence and structure, complications arise from the facts that transmembrane α-helices often extend beyond the likely position of the lipid bilayer, that transmembrane α-helices usually have to span the lipid head group region as well as the hydrophobic core of the bilayer, and that the ends of transmembrane α-helices may not be well defined because of the need to provide suitable hydrogen bonding partners for residues at the ends of the helices.

5.1.4 Chapter 5 Overview

Two experimental techniques will be used to determine the hydrophobic thickness of MscL. The first makes use of the environmental sensitivity of Trp fluorescence emission (Lakowicz, 1999). The second method makes use of the environmental sensitivity of the fluorescence of Cys residues labelled with N-((2-

(iodoacetoxy)ethyl)-N-methyl)amino-7-nitroben-2-oxa-1,3-diazole (IANBD) (Shepard et al., 1998). Wild type TbMscL and EcMscL channels do not contain any Trp or Cys residues; therefore site directed mutagenesis was used to introduce single Trp and Cys residues into the lipid-exposed face of transmembrane α-helix 2 (TM2) (Figure 5.4). The fluorescent properties of each reporter group together with the accessibility of the Trp groups to lipid-soluble and water-soluble quenchers could then be used to determine the location of the residues within the membrane.

5.2 Materials and Methods

All chemicals were obtained from Sigma or BDH with the following exceptions:

Avanti Polar Lipids

1,2-dimyristoleoyl-sn-glycero-3-phosphatidylcholine (di(C14:1)PC)
1,2-dioleoyl-sn-glycero-3-phosphatidylcholine (di(C18:1)PC)
1,2-dinervonyl-sn-glycero-3-phosphatidylcholine (di(C24:1)PC)
1,2-dioleoyl-sn-glycero-3-phosphatdic acid (di(C18:1)PA)
1,2-dioleoyl-sn-glycero-3-phosphatidylethanolamine (di(C18:1)PE)
1,2-dioleoyl-sn-glycero-3-[phospho-rac-(1-glycerol)] (di(18:1)PG)
1,2-dioleoyl-sn-glycero-3-phosphatidylserine (di(C18:1)PS)

Anatrace, Anagrade®

n-Octyl-β-D-glucopyranoside (Octylglucoside)

Calbiochem, Ultrol® Grade

N-(2-hydroxyethyl)piperazine-N'-(2-ethyanesulphonic acid) (Hepes)
1,3-diaza-2,4-cyclopentadiene (Imidazole)

Molecular Probes

N-((2-(iodoacetoxy)ethyl)-N-methyl)amino-7-nitroben-2-oxa-1,3-diazole (IANBD)

5.2.1 *mscL* Mutation

The pET-19b plasmid containing the *Mycobacterium tuberculosis mscL* (*TbmscL*) gene was used as a template for site directed mutagenesis, using the QuickChange™ protocol, as outlined in Section 2.2.5.2. Residues on the lipid-exposed face of the second transmembrane α-helix (TM2), together with a number of solvent-exposed flanking residues (Figure 5.4), were mutated to Trp or Cys using the synthetic oligonucleotide primers listed in Tables 2.5 and 2.6 respectively. Similarly, the pQE-32 plasmid containing the *Escherichia coli mscL* (*EcmscL*) gene was used as a template for site directed mutagenesis, using the three-stage mutagenesis protocol, as outlined in Section 2.2.5.1. Residues along the lipid-exposed face of TM2 were mutated to Trp using the synthetic oligonucleotide primers listed in Table 2.4. MscL is a homopentamer, therefore introduction of a single Trp or Cys residue into the monomer results in a channel containing five Trp or Cys residues all in identical positions and environments.

5.2.2 Bioassay

5.2.2.1 *In vivo Channel Function Assay*

E. coli MJF465 transformants carrying the pET-19b plasmid with the *TbmscL* gene were grown in 10 ml of Luria broth medium containing ampicillin (100 μg ml^{-1}) and chloramphenicol (25 μg ml^{-1}) supplemented with NaCl to a final concentration of 0.4 M. Cells were grown for 16 h at 37 °C in an orbital shaker and used to seed fresh cultures (10 ml) that were grown in the presence of IPTG for 4 h. Cells were harvested by centrifugation at 3000 rpm for 10 min on a Heraeus Labofuge 400e. Culture supernatant was removed and the cell pellet resuspended in sterile 0.4 M NaCl solution to produce a concentration of cells equivalent to an apparent absorbance at 600 nm of 5.

Cultures (30 μl) were diluted 60-fold into either 0.4 M NaCl solution containing sterile-filtered ethidium bromide (0.5 μg ml^{-1}) or analytical grade water also containing ethidium bromide (0.5 μg ml^{-1}). Cells were incubated in the dark for 45

min at room temperature followed by centrifugation at 8000g for 10 min. The supernatant was assayed for the amount of released DNA. Fluorescence intensities were recorded at 25 °C using an SLM-Aminco 8100 fluorimeter, with an excitation wavelength of 254 nm and emission wavelength of 632 nm. Slit widths of 4 nm were used for both excitation and emission. Results were corrected for background light scatter by subtracting the emission of a suitable blank.

5.2.2.2 *Growth Curve Studies*

E. coli BL21(DE3)pLysS transformants carrying the pET-19b plasmid with the *TbmscL* gene were grown in 10 ml of Luria broth medium containing ampicillin (100 μg ml^{-1}) and chloramphenicol (25 μg ml^{-1}) for 16 h at 37 °C in an orbital shaker. Overnight cultures (1 ml) were used to seed fresh cultures (50 ml) and grown at 37 °C in an orbital shaker. Cultures were induced with 1 mM IPTG upon reaching early-log phase (absorbance at 600 nm of 0.2). Following induction, absorbance readings were recorded every 20 min at 600 nm using a U-2001 Spectrophotometer (Hitatachi) at 25 °C.

5.2.3 Protein Expression and Purification

E. coli BL21(DE3)pLysS transformants carrying the pET-19b plasmid (Novagen) with the mutated *TbmscL* gene or *E. coli* M15 carrying the pQE-32 plasmid (Qiagen) with the mutated *EcmscL* gene were grown in 6 l Luria broth to mid-log phase (absorbance at 600 nm of 0.6) and then induced for 3 h in the presence of isopropyl-β-D-thiogalactopyranoside (1 mM). MscL was purified as described in Section 2.2.4.

5.2.4 Labelling of Cys-TbMscL Mutants

Cys-containing mutants of TbMscL were labelled with N-((2-(iodoacetoxy)ethyl)-N-methyl)amino-7-nitroben-2-oxa-1,3-diazole (IANBD; Molecular Probes). TbMscL (225 μM) was incubated in the presence of IANBD (3.6 mM; added as a stock solution in DMSO) in PBS buffer (350 μl; 140 mM NaCl, 2.7 mM KCl, 10 mM

Na_2HPO_4, 1.8 mM KH_2PO_4, pH 7.2) containing tri(2-carboxyethyl)phosphine hydrochloride (TCEP) (3 mM) for 1.5 h at 25 °C, followed by removal of unreacted label on a G-25 Sepharose column. Nanoelectrospray mass spectrometry (LCT™ orthogonal acceleration-TOF instrument; Micromass) was used to confirm a 1:1 molar ratio of labelling of TbMscL by IANBD and the absence of any cross-linked dimers of TbMscL as described in Section 5.2.5. The labelling efficiency was also confirmed using an $\varepsilon_{478\ nm}$ of 25,000 M^{-1} for N-methyl amino-7-nitroben-2-oxa-1,3-diazole (NBD).

5.2.5 Mass Spectrometry

The masses of intact TbMscL proteins were measured for labeled and unlabeled samples. Mass spectrometry was performed using an LCT™ (Micromass) orthogonal acceleration time-of-flight mass spectrometer fitted with a nano electrospray source. NBD-labelled TbMscL protein (15 µl; 32 pmol μl^{-1}) was mixed with an equal volume of a methanol/ethanoic acid mixture (44:1 v/v). The samples (5 µl) were loaded into borosilicate capillaries that had been drawn to a fine tip using a micro electrode puller (Narishige; Tokyo) and sputter coated with gold/palladium. Data were recorded in the positive ion mode over the 500-2500 m/z range using the following instrument settings: capillary 1200 V, sample cone 38 V, extraction cone 9 V and source temperature of 50 °C, desolvation gas flow 700-800 l h^{-1} and cone gas flow 100-200 l h^{-1}. Typically, 100 spectra were combined and multiply charged peaks were deconvoluted using the maximum entropy algorithm MaxEnt™ (Micromass) to give relative molecular mass spectra over the 16,000-40,000 Da range at 1 Da resolution. Spectra were externally calibrated using horse heart myoglobin spectra recorded under identical conditions immediately after each sample.

5.2.6 Reconstitution

Purified TbMscL was reconstituted into lipid bilayers by mixing lipid and TbMscL in cholate, followed by dilution into buffer to decrease the concentration of cholate below its critical micelle concentration, as described in Section 4.2.10.1.

5.2.7 Steady-State Fluorescence Measurements

Trp fluorescence was recorded for 0.98 μM MscL in buffer (20 mM Hepes, 100 mM KCl, 1 mM EGTA, pH 7.2) at 25 °C, using an SLM 8100 fluorimeter, with excitation at 280 nm, as described in Section 3.5. Fluorescence of NBD-labelled TbMscL was recorded for 0.5 μM TbMscL with excitation at 478 nm. Values for wavelengths of maximum fluorescence emission intensity were determined by fitting corrected fluorescence spectra to skewed Gaussian curves (Section 3.5).

Quenching of Trp fluorescence by the water-soluble quencher acrylamide was studied by addition of an aliquot of a freshly prepared stock solution of acrylamide (1M) in Hepes buffer (20 mM Hepes, 100 mM KCl, 1 mM EGTA, pH 7.2) to TbMscL (0.98 μM). Quenching by iodide was studied by addition of an aliquot of a freshly prepared stock solution of the quencher potassium iodide (KI) (1M) in buffer (100 mM $Na_2S_2O_3$, 20 mM Hepes, 1 mM EGTA, pH 7.2) to TbMscL (0.98 μM) in buffer (100 mM $Na_2S_2O_3$, 20 mM Hepes, 1 mM EGTA, pH 7.2) containing KCl at a concentration chosen so that the total concentration KI + KCl was maintained constant at 0.91 M. Fluorescence quenching by acrylamide and iodide was measured at an excitation wavelength of 295 nm and corrected for the inner filter effect, as described in Section 3.5. Because MscL is present in the form of unsealed membrane fragments, the quencher will be able to gain access to both sides of the membrane.

5.2.8 Time-Resolved Fluorescence Measurements

Fluorescence lifetime measurements were recorded at 25 °C using a PTI GL-3300 lifetime fluorimeter equipped with a PTI nitrogen dye laser, with excitation at 478 nm (Section 3.6).

5.3 Results

5.3.1 Bioassays for Function of TbMscL

5.3.1.1 *Osmotic Downshock*

An osmotic downshock assay was used to show that the mutated TbMscL channels were functional, by measuring the levels of release of DNA following hypoosmotic stress. WT and mutant TbMscL were expressed in *E. coli* strain MJF465 lacking mechanosensitive channels, making them sensitive to hypoosmotic stress (Section 2.2.1.4). As shown in Figure 5.5, both the WT and mutant *TbmscL* genes are able to rescue the *E. coli* cells from the effects of hypoosmotic stress following induction of TbMscL production with IPTG, confirming that introduction of the Trp or Cys residues into the channels does not inactivate the channels. *E. coli* expressing V91W-TbMscL, but not V91C-TbMscL channel show a level of DNA release slightly higher than the basal level observed with the WT channel; however, the level of DNA release recorded for hypoosmotically stressed MJF465 *E. coli* lacking mechanosensitive ion channels is much greater, confirming that V91W-TbMscL is still active. However, since it is likely that only a few copies of active MscL channels (ca. five per bacterium) are required to protect a cell from osmotic downshock, and since in these experiments the mutated MscL was over expressed from the pET-19b plasmid that contains a strong T7 promoter, it is possible that the tension required to open the mutated MscL was higher than normal. To minimise the level of over expression, the experiments were performed for 4 hours after induction. It was found with wild type TbMscL that 2 hours after induction, insufficient MscL was produced to protect the cells from downshock. Effects of osmotic downshock were also tested on cells grown for 18 h without induction, in the hope that the level of basal expression of wild type TbMscL that cannot be suppressed by the lack of inducer around be sufficient to protect the cells from osmotic downshock, but this was found not to be the case.

5.3.1.2 *Growth Curve Assay*

Gain of function mutants were detected by a reduced rate of growth of *E. coli* expressing the *TbmscL* genes, following induction of TbMscL production with IPTG from an inducible plasmid. Figure 5.6 shows the growth profiles of *E. coli* expressing mutated TbMscL. In Figure 5.6A all growth curves, including expression of WT-TbMscL are clustered in a group at the top of the graph confirming that growth rates are unaffected by expression of the mutant TbMscL channels. In Figure 5.6B the growth curves are again clustered close to that for wild type TbMscL, suggesting the mutants retain WT-TbMscL channel gating properties. Mutants V91C and Y94C (Figure 5.6B) show a slightly reduced rate of growth following induction with IPTG. The reduction in growth rate is not as marked as those reported for severe gain of function mutants by Yoshimura et al. (1999), suggesting that V91C and Y94C are forming closed channels that could be slightly easier to open than the WT channel. In addition, the relative expression levels of these mutant channels was not shown not be affected when examined on sodium dodecyl sulphate polyacrylamide gels (data not shown).

5.3.2 Expression of Mutant TbMscL

Following DNA sequencing and confirmation of the fidelity of the mutated *mscL* genes, 6 l cultures of *E. coli* transformants carrying the pET-19b plasmid with the mutant *TbmscL* genes or pQE-32 plasmid with the Trp mutated *EcmscL* genes were expressed and purified in OG detergent, in the same manner as WT protein. All Trp mutants of TbMscL run predominantly as monomeric species, with small amounts of dimer on sodium dodecyl sulphate polyacrylamide gels (Figure 5.7); all were in the expected range for the full length TbMscL channel. A similar analysis was performed for the Trp mutants of the EcMscL channels; again, all ran as predominantly monomeric species (data not shown). In Figure 5.7 comparable expression of Trp mutant channels is shown; equal volume (5 µl) of pooled and purified protein from each 6 l preparation was loaded onto the gel. Expression of Q51W, T66W and F80W to V103W are equivalent to expression of the WT channel; however, Trp mutations clustered to the periplasmic side of TM2: L69W, L73W, I77W and F79W show a reduced level of protein expression. However, the ability of

L69W, L73W, I77W and F79W channels to rescue *E. coli* strain MJF465 from the effects of hyperosmotic stress (Figure 5.5), or the rate of growth of *E. coli* expressing these mutant channels (Figure 5.6A) was unaffected, suggesting that the channels are likely to be in the closed configuration during all the fluorescence measurements.

5.3.3 Labelling of Cys-TbMscL Mutants with NBD

The Cys mutants L69C, Y87C, V91C and Y94C-TbMscL, following purification, ran predominantly as dimers (M_r 37.3 kDa), rather than monomers (M_r 18.6 kDa) on sodium dodecyl sulphate polyacrylamide gels (data not shown). The dimeric state of the protein was confirmed for L69C-TbMscL, through mass spectrometry (Figure 5.8A). The dimer presumably resulted from formation of a disulphide bond and therefore, prior to labelling of the Cys-containing mutants of TbMscL with IANBD, the mutant proteins were reduced in the presence of TCEP to generate monomeric species (Figures 5.8B and 5.9). Following labelling of Cys-TbMscL mutants with NBD, mass spectrometry was again used to confirm a 1:1 labelling ratio (Figures 5.8C and 5.9), and an increase in molecular mass for each mutant of 291 Da, corresponding to the NBD group. The M_r for each of the Cys-TbMscL mutants were predicted to be 18592, 18606 and 18542 Da for L69C, V91C and Y87C or Y94C mutations respectively, using the Peptide Mass algorithm on the ExPasy server. The M_r for each Cys-TbMscL mutant recorded by mass spectrometry were 18649, 18663 and 18599 Da for L69C, V91C and Y87C or Y94C mutations respectively; all these values are 57 Da greater than the estimated M_r and can be explained by the presence of a complex between TbMscL monomer and Ni^{2+} ion.

5.3.4 Fluorescence Spectroscopy

TbMscL was reconstituted into bilayers of defined composition to give a 100:1 molar ratio of phospholipid to TbMscL monomer. Using this procedure, Trp mutants of TbMscL were reconstituted into bilayers of di(C18:1)PC and the intensity corrected emission spectra (Figure 5.10) were fitted to skewed Gaussian curves to give the values in Table 5.1. A similar analysis was performed for Trp mutants of TbMscL reconstituted into long and short chain phosphatidylcholines (Table 5.1) and also in phospholipid bilayers of chain length C18, containing different lipid head groups

(Table 5.2). In all reconstitutions of Trp mutants of TbMscL with phosphatidylcholines, F80W-TbMscL shows the greatest blue shift (320 nm), suggesting that F80 in TbMscL is located in a very hydrophobic environment. Emission maxima (λ^{max}) for residues either side of F80 show progressive red shift towards the ends of the helix, representing movement of these residues towards a more polar environment (Figure 5.11). F79W is unusual in that the λ^{max} of this residue does not follow the trend. λ^{max} for F79W is red shifted to 332 nm in all reconstitutions, despite being only 1 residue along the helix from F80 in TbMscL.

Trp mutants of EcMscL were also reconstituted into phosphatidylcholine bilayers of chain lengths C14, C18, and C24 to give a 100:1 molar ratio of phospholipid to protein. The intensity corrected emission spectra (data not shown) were fitted to skewed Gaussian curves to give the values in Table 5.3. In all reconstitutions of Trp mutants of EcMscL with phosphatidylcholines, L86W-EcMscL shows the greatest blue shift (326 nm), suggesting that L86 in EcMscL is buried deep within the hydrophobic bilayer core. Emission maxima (λ^{max}) for residues either side of L86 are red shifted, consistent with movement of these residues towards a more polar environment (Figure 5.12). The λ^{max} of F85W-EcMscL does not follow the trend and is red shifted to 333 nm in all reconstitutions, despite being only 1 residue along the helix from L86 in EcMscL, as observed for *M. tuberculosis* residues F79W and F80W.

Ladokhin et al. (2000) established a linear relationship between the wavelength of maximum emission and the spectral width of fluorescence emission from a single Trp residue. The observation of a fairly constant peak width for the mutants (Tables 5.1-5.3) suggests that the mutated MscLs adopt one major conformational state in all reconstitutions with the phospholipids.

5.3.5 Fluorescence Quenching of Trp-TbMscL

Trp mutants of TbMscL were reconstituted into bilayers of di(C18:1)PC and the fluorescence emission was quenched by a number of water-soluble and membrane-soluble quenchers, allowing the location of the Trp-reporter group within the membrane to be determined.

5.3.5.1 *Brominated Lipids*

1,2-di(9,10-dibromostearoyl)phosphatidylcholine was used to quench fluorescence from the lipid phase. Brominated compounds are effective quenchers of Trp fluorescence, and in the brominated phospholipid di(Br_2C18:0)PC, the dibromo group will be located some 7 Å from the bilayer surface on either side of the membrane (Lakowicz, 1999; Williamson et al., 2002). Fluorescence quenching curves for TbMscL mutants in mixtures of di(Br_2C18:0)PC and di(C18:1)PC were determined and the results are shown in Figure 5.13. The fluorescence intensity is plotted as F/F_o, where F is the fluorescence intensity at intermediate fractions of brominated phospholipid and F_o is the fluorescence intensity when the mole fraction of non-brominated phospholipid is 1. The results shown in Figure 5.13 show that, as expected, fluorescence intensities decrease with increasing mole fraction of brominated lipid in the bilayer.

The data were fitted to Equation 3.11 using the nonlinear least-squares programme in SigmaPlot, giving the values of *n* listed in Table 5.4. F80W-TbMscL is taken as the centre of the transmembrane α-helix and has a value of *n* of around 2.4 (Figure 5.14). This value is consistent with the values of *n* of 2.30 and 2.70 reported for reconstituted peptides Ac-KKGL_7WL_9KKA-amide and Ac-KKGL_{10}WL_{12}KKA-amide respectively, which also contain Trp residues located in the centre of the bilayer (Mall et al., 2000), and with the value of *n* of 2.50 reported for the β-barrel protein OmpF where the Trp residue is also located in the centre of the bilayer (O'Keeffe et al., 2000). The value of *n* for Trp residues either side of F80W gradually decrease to around 1.60 as the position of the Trp reporter group approaches the bilayer interface. This value is again consistent with the value of 1.69 reported for the K^+ channel KcsA that contains Trp residues exclusively located at the bilayer interfaces (Williamson et al., 2002).

The highest level of quenching in bilayers of di(Br_2C18:0)PC is observed for F84W, the level of quenching decreasing for Trp residues further from this position, reaching a plateau at about L73W on the periplasmic side of the membrane, quenching of L69W being equal to that of V91W on the cytoplasmic side (Figures 5.13 and 5.18A).

Quenching of Trp fluorescence for F79W by di(Br_2C18:0)PC is lower than expected when compared with residues I77W and F80W. The fact that significant quenching is observed for Q51W, T66W and V103W, three residues located in region of the protein outside the hydrophobic core of the lipid bilayer, is consistent with a Förster energy transfer mechanism for quenching, as described in Sections 3.2 and 3.3.

5.3.5.2 *Lipid-soluble Quencher*

The Stern-Volmer plots for quenching of Trp fluorescence in TbMscL mutants in bilayers of di(C18:1)PC with the lipid-soluble quencher 1,2-diiodobenzene were determined and the results are shown in Figure 5.15. The fluorescence intensity is plotted as F_o/F, where F_o is the fluorescence intensity when the mole fraction of di(C18:1)PC is 1 and F is the fluorescence intensity at the given mole fractions of 1,2-diiodobenzene. Quenching by the lipid-soluble quencher 1,2-diiodobenzene shows a decrease in efficiency from L69W to T66W, consistent with an interfacial location for L69W, with the level of quenching of L69W being between that for V91W and Y94W. Quenching of F79W is again lower than expected (Figures 5.15 and 5.18B).

5.3.5.3 *Water-soluble Quenchers*

The locations of the Trp residues introduced into TbMscL were also monitored in bilayers of di(C18:1)PC, in the presence of water-soluble quenchers. Acrylamide is a small molecule that quenches fluorescence in a neutral environment, whereas iodide is an ion that quenches fluorescence in a cationic environment. The size of the iodide ion can limit the amount of quenching, even in an ideal environment for the quencher. In addition, iodide must be kept in the I^- form due to the ability of I_2 to readily enter the hydrophobic regions of membranes (Lakowicz, 1999).

The Stern-Volmer plot for TbMscL mutants in bilayers of di(C18:1)PC with acrylamide were determined and the results are shown in Figure 5.16. The fluorescence intensity is plotted as F_o/F, where F_o is the fluorescence intensity in the absence of quencher and F is the fluorescence intensity at intermediate concentrations of quencher. The results in Figure 5.16 show that fluorescence quenching was

linearly dependent on acrylamide concentration. Quenching by acrylamide shows a profile the inverse of that with di(Br_2C18:0)PC, the lowest level of quenching being observed for F80W (Figures 5.16 and 5.18A). The 42 % quenching observed for L69W with 0.25 M acrylamide compares to the ca. 40 % quenching by 0.24 M acrylamide for Trp residues at the ends of a model transmembrane α-helix in a lipid bilayer (Caputo and London, 2003). The levels of quenching for V91W and Y94W are equal to that observed for L69W (Figure 5.18A). Quenching of F79W by acrylamide is higher than expected, however the quenching profile still follows the inverse profile of quenching by di(Br_2C18:0)PC as observed with the other Trp mutants (Figure 5.18A).

The Stern-Volmer plot for quenching of the Trp fluorescence of TbMscL mutants in bilayers of di(C18:1)PC with iodide were determined and the results are shown in Figure 5.17. The fluorescence intensity is plotted as F_o/F, where F_o is the fluorescence intensity in the absence of quencher and F is the fluorescence intensity at intermediate concentrations of quencher. The results in Figure 5.17 show that fluorescence quenching was linearly dependent on iodide concentration. Quenching by iodide ion shows a more complex profile on Trp position than seen with acrylamide, but quenching is again low for F80W, with a marked increase in quenching between L69W and T66W and between V91W and V103W, consistent with Leu-69 and Val-91 being close to the interface (Figure 5.18B). Y87W quenches more than expected with iodide for a residue buried within the bilayer; Y87 in TbMscL is located close to the positive charge on the guanidinium group of R11, which could effectively increase the concentration of iodide within the microenvironment of this residue. Trp fluorescence from F79W also shows a higher level of quenching with iodide than expected, but is consistent with the level of quenching observed with acrylamide (Figure 5.18).

5.3.6 NBD-labelled TbMscL

The fluorescence emission of the NBD group is sensitive to solvent polarity (Shepard et al., 1998). Both fluorescence emission maximum and fluorescence lifetimes vary with dielectric constant in mixtures of dioxane/water (Figure 5.19), being particularly

sensitive over the range 2 to 40 characteristic of the lipid head group region (Pérochon et al., 1992).

NBD-labelled mutants of TbMscL were reconstituted into bilayers by mixing phospholipid and labelled protein in buffer containing 15 mM cholate as detergent to give a 100:1 molar ratio of phospholipid to protein, followed by dilution to reform bilayers. The emission spectra for NBD-labelled TbMscL in di(C18:1)PC (Figure 5.20) were fitted to skewed Gaussian curves to give the parameter values listed in Table 5.10. The time-resolved fluorescence intensity decays for NBD-labelled TbMscL in di(C18:1)PC (Figure 5.21) were fitted to sums of two and three exponentials (Tables 5.8 and 5.9) to give the parameters values listed in Table 5.10. A similar analysis was performed for Cys-mutant TbMscL reconstituted into di(C14:1)PC and di(C24:1)PC phosphatidylcholines (Tables 5.8 and 5.9).

The data obtained for labelled TbMscL was compared with that for the NBD label in dioxane-water mixtures (Figure 5.19) to obtain estimates of dielectric constant in the vicinity of the labelled residue. The dielectric constant estimated from the fluorescence emission maximum for labelled L69C is slightly different from that estimated from the fluorescence lifetime, but both estimates are consistent with an interfacial location for Leu-69, the dielectric constant being slightly greater than the value of 2 expected for the hydrophobic core of the bilayer but much less than the value of 80 characteristic of water (Table 5.10). The estimated dielectric constants for labelled V91C and Y94C are slightly smaller and larger respectively than that for L69C, again consistent with the cytoplasmic end of the hydrophobic domain of TbMscL being located between Val-91 and Tyr-94, close to Val-91.

TbMscL Mutant	Fatty Acyl Chain							
	C12:0		C14:1		C18:1		C24:1	
	λ^{max} (nm)	ω (nm)	λ^{max} (nm)	ω (nm)	λ^{max} (nm)	ω (nm)	λ^{max} (nm)	ω (nm)
Q51W	332.7 ± 0.2	60.7 ± 0.2	335.3 ± 0.1	56.7 ± 0.2	335.7 ± 0.1	57.2 ± 0.2	335.1 ± 0.1	56.9 ± 0.2
T66W	336.1 ± 0.3	67.8 ± 0.4	338.4 ± 0.2	60.8 ± 0.4	338.5 ± 0.2	61.5 ± 0.3	339.6 ± 0.2	61.0 ± 0.3
L69W	333.4 ± 0.3	62.7 ± 0.4	332.7 ± 0.1	53.0 ± 0.1	332.8 ± 0.1	53.1 ± 0.1	332.3 ± 0.1	53.4 ± 0.2
L73W	328.3 ± 0.1	51.5 ± 0.2	330.7 ± 0.1	52.9 ± 0.2	331.2 ± 0.1	53.7 ± 0.2	331.5 ± 0.1	53.4 ± 0.2
I77W	327.2 ± 0.2	51.7 ± 0.2	329.0 ± 0.1	50.8 ± 0.1	330.2 ± 0.1	51.9 ± 0.1	330.1 ± 0.1	51.7 ± 0.2
F79W	333.1 ± 0.1	52.5 ± 0.2	331.9 ± 0.1	53.2 ± 0.1	332.1 ± 0.1	52.9 ± 0.1	333.0 ± 0.1	53.6 ± 0.2
F80W	320.1 ± 0.1	42.9 ± 0.2	322.3 ± 0.1	46.3 ± 0.1	321.0 ± 0.1	44.1 ± 0.2	322.8 ± 0.2	45.8 ± 0.3
F84W	324.7 ± 0.1	47.0 ± 0.1	324.5 ± 0.1	46.0 ± 0.2	323.5 ± 0.0	47.0 ± 0.1	323.5 ± 0.0	47.0 ± 0.1
Y87W	327.3 ± 0.1	46.9 ± 0.1	326.8 ± 0.1	46.4 ± 0.1	326.8 ± 0.1	47.1 ± 0.1	325.6 ± 0.1	49.0 ± 0.2
V91W	330.7 ± 0.1	49.2 ± 0.1	330.6 ± 0.1	49.4 ± 0.1	330.7 ± 0.1	50.0 ± 0.1	331.6 ± 0.1	51.7 ± 0.2
Y94W	335.0 ± 0.1	52.8 ± 0.1	334.5 ± 0.1	52.1 ± 0.1	334.4 ± 0.1	52.7 ± 0.1	335.1 ± 0.1	53.8 ± 0.1
V103W	344.6 ± 0.2	62.6 ± 0.3	344.1 ± 0.2	59.6 ± 0.2	343.4 ± 0.2	59.4 ± 0.2	343.5 ± 0.2	59.7 ± 0.3

Table 5.1 Fluorescence properties of Trp mutants of TbMscL reconstituted with phosphatidylcholines. λ^{max} and ω are the wavelengths of maximum emission and the peak width at half height respectively, determined by fitting intensity corrected fluorescence emission spectra to Equation 3.8.

TbMscL Mutant	Phospholipid PC		PE		PG		PS		PA	
	λ^{max} (nm)	ω (nm)	λ^{max} (nm)	ω (nm)	λ^{max} (nm)	ω (nm)	λ^{max} (nm)	ω (nm)	λ^{max} (nm)	ω (nm)
Q51W	335.7 ± 0.1	57.2 ± 0.2	335.5 ± 0.1	56.6 ± 0.2	334.8 ± 0.1	58.5 ± 0.2	334.2 ± 0.1	58.0 ± 0.2	333.7 ± 0.1	57.0 ± 0.1
T66W	338.5 ± 0.2	61.5 ± 0.3	338.9 ± 0.2	61.5 ± 0.3	337.8 ± 0.2	64.6 ± 0.4	338.1 ± 0.2	63.8 ± 0.3	343.4 ± 0.3	72.2 ± 0.5
L69W	332.8 ± 0.1	53.1 ± 0.1	330.1 ± 0.1	52.2 ± 0.2	332.8 ± 0.1	53.3 ± 0.2	332.3 ± 0.1	52.8 ± 0.2	332.7 ± 0.1	52.4 ± 0.1
L73W	331.2 ± 0.1	53.7 ± 0.2	332.1 ± 0.1	52.0 ± 0.1	331.2 ± 0.1	53.9 ± 0.2	330.5 ± 0.1	53.3 ± 0.2	331.5 ± 0.1	52.0 ± 0.1
I77W	330.2 ± 0.1	51.9 ± 0.1	329.4 ± 0.1	50.3 ± 0.1	330.8 ± 0.1	52.4 ± 0.2	330.1 ± 0.1	52.0 ± 0.2	330.7 ± 0.1	51.4 ± 0.1
F79W	332.1 ± 0.1	52.9 ± 0.1	331.7 ± 0.1	51.7 ± 0.2	332.5 ± 0.1	53.6 ± 0.2	332.0 ± 0.1	53.3 ± 0.2	332.3 ± 0.1	52.1 ± 0.1
F80W	321.0 ± 0.1	44.1 ± 0.2	321.9 ± 0.1	44.2 ± 0.2	320.9 ± 0.1	42.3 ± 0.2	321.1 ± 0.1	40.8 ± 0.2	320.9 ± 0.1	43.2 ± 0.2
F84W	323.5 ± 0.0	47.0 ± 0.1	323.5 ± 0.0	47.0 ± 0.1	323.5 ± 0.0	47.0 ± 0.1	323.5 ± 0.0	47.0 ± 0.1	323.5 ± 0.0	47.0 ± 0.1
Y87W	326.8 ± 0.1	47.1 ± 0.1	326.5 ± 0.1	46.8 ± 0.1	326.5 ± 0.1	47.0 ± 0.1	326.4 ± 0.1	46.7 ± 0.1	326.9 ± 0.1	46.3 ± 0.1
V91W	330.7 ± 0.1	50.0 ± 0.1	330.2 ± 0.1	49.2 ± 0.1	329.6 ± 0.1	49.4 ± 0.1	329.3 ± 0.1	48.9 ± 0.1	329.4 ± 0.1	48.3 ± 0.1
Y94W	334.4 ± 0.1	52.7 ± 0.1	333.6 ± 0.1	51.9 ± 0.1	333.8 ± 0.1	52.2 ± 0.1	333.3 ± 0.1	51.5 ± 0.1	332.2 ± 0.1	49.9 ± 0.1
V103W	343.4 ± 0.2	59.4 ± 0.2	342.7 ± 0.1	58.5 ± 0.2	342.7 ± 0.2	59.5 ± 0.2	342.5 ± 0.2	59.5 ± 0.2	342.5 ± 0.1	58.8 ± 0.2

Table 5.2 Fluorescence properties of Trp mutants of TbMscL reconstituted with 1,2-dioleoyl-sn-glycero-3-phospholipids. PC, phosphatidylcholine, PE, phosphatidylethanolamine, PG, phosphatidylglycerol, PS, phosphatidylserine and PA, phosphatidic acid. λ^{max} and ω are the wavelengths of maximum emission and the peak width at half height respectively, determined by fitting intensity corrected fluorescence emission spectra to Equation 3.8.

EcMscL Mutant	Fatty Acyl Chain C14:1		C18:1		C24:1	
	λ^{max} (nm)	ω (nm)	λ^{max} (nm)	ω (nm)	λ^{max} (nm)	ω (nm)
I79W	332.9 ± 0.1	54.9 ± 0.2	332.9 ± 0.1	54.2 ± 0.3	332.9 ± 0.1	54.5 ± 0.2
F85W	333.6 ± 0.2	55.5 ± 0.2	333.3 ± 0.2	53.4 ± 0.3	333.1 ± 0.1	55.0 ± 0.2
L86W	326.8 ± 0.1	53.7 ± 0.1	326.2 ± 0.1	53.4 ± 0.1	327.5 ± 0.1	53.7 ± 0.2
F93W	328.1 ± 0.1	52.0 ± 0.1	328.0 ± 0.1	51.6 ± 0.2	328.9 ± 0.1	53.9 ± 0.2
N100W	335.3 ± 0.1	57.7 ± 0.2	334.4 ± 0.2	58.1 ± 0.2	334.4 ± 0.2	61.6 ± 0.3

Table 5.3 Fluorescence properties of Trp mutants of EcMscL reconstituted with phosphatidylcholines. λ^{max} and ω are the wavelengths of maximum emission and the peak width at half height respectively, determined by fitting intensity corrected fluorescence emission spectra to Equation 3.8.

TbMscL Mutant	F/F_o	n
Q51W	0.61 ± 0.01	1.32 ± 0.06
T66W	0.75 ± 0.01	1.51 ± 0.07
L69W	0.51 ± 0.01	1.86 ± 0.17
L73W	0.49 ± 0.01	1.91 ± 0.12
I77W	0.43 ± 0.01	1.94 ± 0.10
F79W	0.52 ± 0.01	2.39 ± 0.19
F80W	0.20 ± 0.01	2.44 ± 0.13
F84W	0.13 ± 0.01	2.32 ± 0.09
Y87W	0.34 ± 0.01	1.75 ± 0.08
V91W	0.52 ± 0.01	1.51 ± 0.04
Y94W	0.50 ± 0.01	1.61 ± 0.11
V103W	0.81 ± 0.01	1.36 ± 0.13

Table 5.4 Fluorescence quenching of Trp mutants of TbMscL by 1,2-di(9,10-dibromostearoyl) phosphatidylcholine. F_0 and F are fluorescence intensities for TbMscL reconstituted in di(C18:1)PC and di(Br_2C18:0)PC respectively, measured at pH 7.2. The value of n is the value obtained by fitting the data in Figure 5.13 to Equation 3.11.

TbMscL Mutant	F/F_o	K_{SV} (M^{-1})	K_{SV}^{-1} (M)
Q51W	0.72 ± 0.04	0.81 ± 0.02	123
T66W	0.75 ± 0.02	0.65 ± 0.01	154
L69W	0.73 ± 0.01	0.76 ± 0.01	132
L73W	0.70 ± 0.01	0.89 ± 0.02	112
I77W	0.68 ± 0.02	0.95 ± 0.01	105
F79W	0.71 ± 0.03	0.86 ± 0.01	116
F80W	0.49 ± 0.04	2.07 ± 0.03	48
F84W	0.57 ± 0.05	1.46 ± 0.02	68
Y87W	0.56 ± 0.06	1.56 ± 0.01	64
V91W	0.70 ± 0.04	0.87 ± 0.02	115
Y94W	0.74 ± 0.03	0.71 ± 0.01	141
V103W	0.80 ± 0.05	0.51 ± 0.01	196

Table 5.5 Fluorescence quenching of Trp mutants of TbMscL by 1,2-diiodobenzene. F_o and F are fluorescence intensities for TbMscL reconstituted in di(C18:1)PC and with a mole ratio of di(C18:1)PC:1,2-diiodobenzene of 1:1 respectively. The Stern-Volmer quenching constant, K_{SV}, was determined by fitting the data in Figure 5.15 to Equation 3.1. The inverse of the Stern-Volmer quenching constant is the quencher concentration that will quench 50 % of the fluorescence.

TbMscL Mutant	F_o/F	K_{SV} (M^{-1})	K_{SV}^{-1} (M)
Q51W	1.80 ± 0.01	2.63 ± 0.02	0.38
T66W	2.04 ± 0.01	3.57 ± 0.04	0.28
L69W	1.72 ± 0.02	2.41 ± 0.02	0.41
L73W	1.65 ± 0.01	2.15 ± 0.02	0.47
I77W	1.60 ± 0.01	2.01 ± 0.03	0.50
F79W	1.71 ± 0.02	2.43 ± 0.04	0.41
F80W	1.34 ± 0.01	1.09 ± 0.03	0.92
F84W	1.41 ± 0.04	1.40 ± 0.02	0.71
Y87W	1.61 ± 0.01	1.98 ± 0.03	0.51
V91W	1.65 ± 0.01	2.17 ± 0.02	0.46
Y94W	1.76 ± 0.01	2.51 ± 0.02	0.40
V103W	2.29 ± 0.01	4.20 ± 0.04	0.24

Table 5.6 Fluorescence quenching of Trp mutants of TbMscL by acrylamide. F and F_0 are fluorescence intensities for TbMscL reconstituted in di(C18:1)PC in the presence and absence of 0.3 M acrylamide respectively, measured at pH 7.2. The Stern-Volmer quenching constant, K_{SV}, was determined by fitting the data in Figure 5.16 to Equation 3.1. The inverse of the Stern-Volmer quenching constant is the quencher concentration that will quench 50 % of the fluorescence.

TbMscL Mutant	F_o/F	K_{SV} (M^{-1})	K_{SV}^{-1} (M)
Q51W	1.32 ± 0.02	0.72 ± 0.04	1.39
T66W	1.67 ± 0.04	1.56 ± 0.08	0.64
L69W	1.29 ± 0.02	0.67 ± 0.02	1.49
L73W	1.24 ± 0.02	0.53 ± 0.01	1.89
I77W	1.13 ± 0.03	0.30 ± 0.01	3.33
F79W	1.42 ± 0.04	0.98 ± 0.05	1.02
F80W	1.02 ± 0.03	0.06 ± 0.01	16.67
F84W	1.07 ± 0.02	0.16 ± 0.01	6.25
Y87W	1.32 ± 0.03	0.73 ± 0.03	1.37
V91W	1.17 ± 0.02	0.39 ± 0.02	2.56
Y94W	1.19 ± 0.02	0.42 ± 0.02	2.38
V103W	1.80 ± 0.04	1.79 ± 0.05	0.56

Table 5.7 Fluorescence quenching of Trp mutants of TbMscL by iodide. F and F_0 are fluorescence intensities for TbMscL reconstituted in di(C18:1)PC in the presence and absence of 0.45 M iodide respectively, measured at pH 7.2. The Stern-Volmer quenching constant, K_{SV}, was determined by fitting the data in Figure 5.17 to Equation 3.1. The inverse of the Stern-Volmer quenching constant is the quencher concentration that will quench 50 % of the fluorescence.

TbMscL Mutant	Fatty acyl chains	Lifetimes (ns)			Preexponential factors			Fractional Intensities			Average fluorescence lifetime $\bar{\tau}$ (ns)	Chi^2
		τ_1	τ_2	τ_3	α_1	α_2	α_3	f_1	f_2	f_3		
L69C	C14:1	6.009	1.990	0.537	0.104	0.711	1.147	0.236	0.533	0.232	2.60	1.127
	C14:1	6.213	2.246	0.765	0.091	0.622	1.216	0.195	0.483	0.322	2.54	1.017
	C18:1	9.079	2.219	0.625	0.054	0.655	1.543	0.168	0.500	0.332	2.84	1.002
	C18:1	8.908	2.062	0.501	0.057	0.689	1.602	0.186	0.520	0.294	2.87	1.125
	C24:1	5.848	2.064	0.599	0.093	0.530	1.660	0.206	0.416	0.378	2.29	0.971
	C24:1	8.693	2.062	0.542	0.063	0.593	1.542	0.211	0.469	0.321	2.97	0.992
Y87C	C14:1	5.390	1.092		0.240	0.610		0.660	0.340		3.92	1.096
	C14:1	4.810	0.951		0.260	0.600		0.680	0.320		3.58	1.277
	C14:1	5.020	1.091		0.280	0.720		0.640	0.360		3.62	1.122
	C18:1	6.558	2.481	0.564	0.180	0.593	1.192	0.355	0.443	0.203	3.54	1.010
	C18:1	6.158	1.941	0.189	0.217	0.363	1.954	0.455	0.420	0.125	3.64	0.965
	C18:1	5.030	0.879		0.200	0.490		0.700	0.300		3.78	1.043
	C18:1	5.000	0.841		0.200	0.540		0.690	0.310		3.70	1.116
	C24:1	5.140	0.855		0.270	0.620		0.720	0.280		3.95	1.003
	C24:1	5.610	1.077		0.250	0.610		0.680	0.320		4.18	1.099

Table 5.8 Fluorescence lifetimes of NBD-labelled Cys mutants of TbMscL reconstituted into bilayers of phosphatidylcholines containing the given fatty acyl chains. The average fluorescence life time, $\bar{\tau}$ was calculated using Equation 3.10 and the preexponential factors (α) and lifetimes (τ) of each individual lifetime.

TbMscL Mutant	Fatty acyl chains	Lifetimes (ns)			Preexponential factors			Fractional Intensities			Average fluorescence lifetime $\bar{\tau}$ (ns)	Chi^2
		τ_1	τ_2	τ_3	α_1	α_2	α_3	f_1	f_2	f_3		
V91C	C14:1	0.493	5.507	2.044	0.894	0.283	0.598	0.137	0.484	0.379	3.51	1.045
	C18:1	9.744	2.070	0.494	0.035	0.393	1.711	0.171	0.406	0.423	2.71	1.013
	C18:1	6.304	2.365	0.680	0.148	0.419	0.768	0.381	0.405	0.213	3.51	1.001
	C24:1	2.350	5.711	0.789	0.454	0.200	0.798	0.376	0.402	0.222	3.36	0.975
	C24:1	3.267	8.763	0.973	0.425	0.072	0.806	0.494	0.266	0.280	3.87	0.959
Y94C	C14:1	4.665	1.568	0.518	0.101	0.458	1.381	0.248	0.377	0.375	1.94	1.005
	C14:1	6.165	1.957	0.526	0.056	0.418	1.681	0.169	0.399	0.432	2.05	0.944
	C18:1	1.533	7.087	0.376	0.246	0.013	2.006	0.308	0.077	0.615	1.25	0.991
	C18:1	5.479	1.795	0.449	0.081	0.430	2.033	0.207	0.363	0.430	1.98	1.047
	C18:1	6.518	1.860	0.438	0.058	0.474	2.14	0.175	0.404	0.421	2.07	1.002
	C24:1	9.207	2.161	0.459	0.020	0.227	1.491	0.135	0.361	0.504	2.25	0.988
	C24:1	13.100	2.132	0.468	0.019	0.246	1.603	0.167	0.343	0.490	3.15	1.128

Table 5.9 Fluorescence lifetimes of NBD-labelled Cys mutants of TbMscL reconstituted into bilayers of phosphatidylcholines containing the given fatty acyl chains. The average fluorescence lifetime, $\bar{\tau}$ was calculated using Equation 3.10 and the preexponential factors (α) and lifetimes (τ) of each individual lifetime.

TbMscL Mutant	Emission maximum (nm)	Dielectric constant*	Average fluorescence lifetime $\bar{\tau}$ (ns)	Dielectric constant†
L69C	536.2 ± 0.13	7.4	2.86 ± 0.02	3.0
Y87C	534.1 ± 0.15	5.0	3.67 ± 0.10	2.5
V91C	536.1 ± 0.07	7.2	3.51 ± 0.10	2.5
Y94C	537.1 ± 0.16	8.8	2.03 ± 0.07	4.0

Table 5.10 Fluorescence properties of NBD-labelled TbMscL. The concentration of TbMscL was 0.6 μM and the molar ratio of lipid to TbMscL was 100:1. The buffer was 20 mM Hepes, 100 mM KCl, 1 mM EGTA, pH 7.2. * Calculated from the emission maximum obtained by fitting the data in Figure 5.20 to Equation 3.8 and the using the data plotted in Figure 5.19. † Calculated from the average fluorescence lifetime using the data plotted in Figure 5.19 and the values in Tables 5.8 and 5.9.

TbMscL Mutant	Fatty acyl chains	Average fluorescence lifetime $\bar{\tau}$ (ns)†
L69C	C14:1	2.57 ± 0.04
	C24:1	2.63 ± 0.48
Y87C	C14:1	3.71 ± 0.07
	C24:1	4.06 ± 0.16
V91C	C14:1	3.51 ± 0.10
	C24:1	3.61 ± 0.36
Y94C	C14:1	2.03 ± 0.07
	C24:1	2.70 ± 0.63

Table 5.11 The effect of bilayer thickness on the fluorescence properties of NBD-labelled TbMscL in bilayers of phosphatidylcholine. The table lists average fluorescence lifetimes of NBD-labelled Cys mutants of TbMscL reconstituted into bilayers of phosphatidylcholines containing the given fatty acyl chains. The concentration of TbMscL was 0.6 μM and the molar ratio of lipid to TbMscL was 100:1. The buffer was 20 mM Hepes, 100 mM KCl, 1 mM EGTA, pH 7.2. † Calculated from the average fluorescence lifetime data in Tables 5.8 and 5.9.

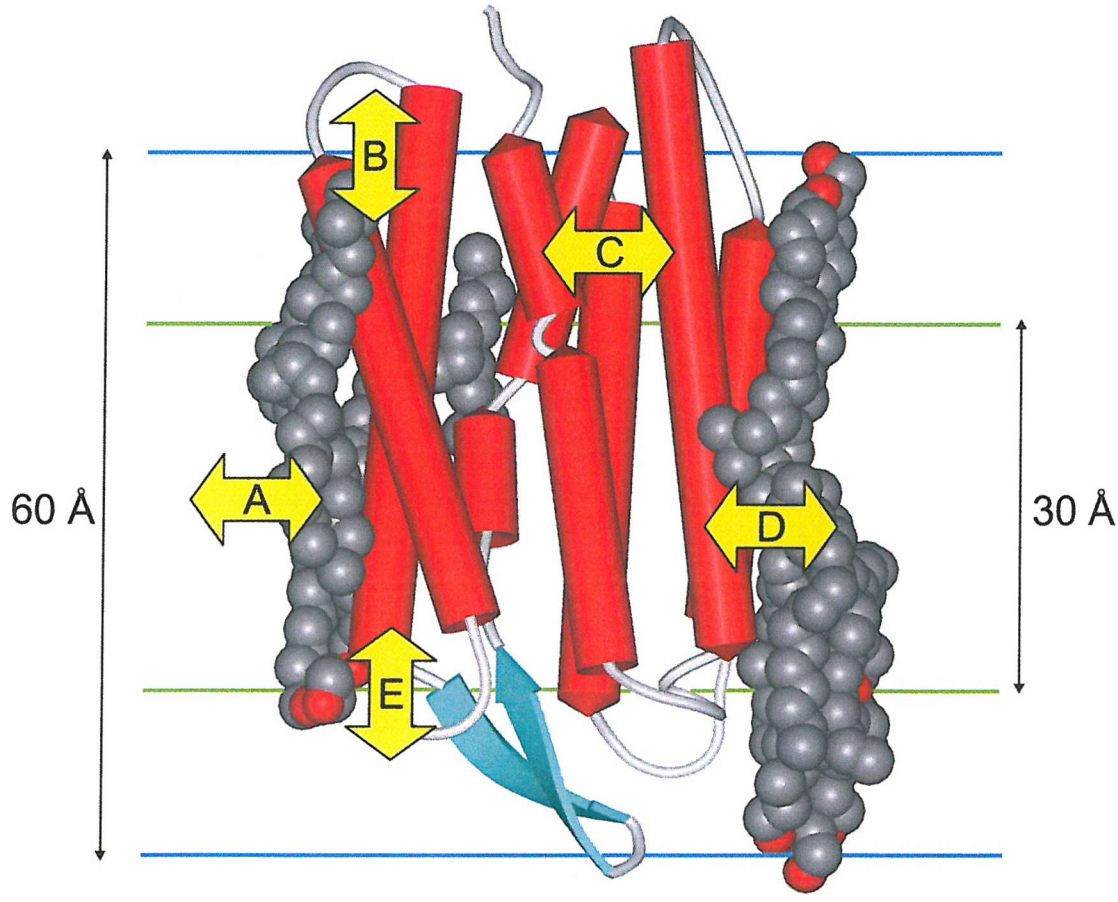

Figure 5.1 Interactions between an integral membrane protein and membrane lipids. The blue lines represent the total membrane thickness (60 Å), and the green lines the hydrocarbon core of the membrane (30 Å). The structure and thermodynamic stability of a membrane protein is determined by the extent to which: (A), the protein is embedded in the bulk bilayer matrix, and therefore exposed to global bilayer effects; (B), the ability of the protein to form a maximum number of intermolecular interactions that include protein side chain interactions with water; (C), internal protein-protein interactions; (D), protein-lipid interactions with annular lipids that include both hydrocarbon and (E), interfacial head group regions. PDB 1C3W. Adapted from White et al. (2001).

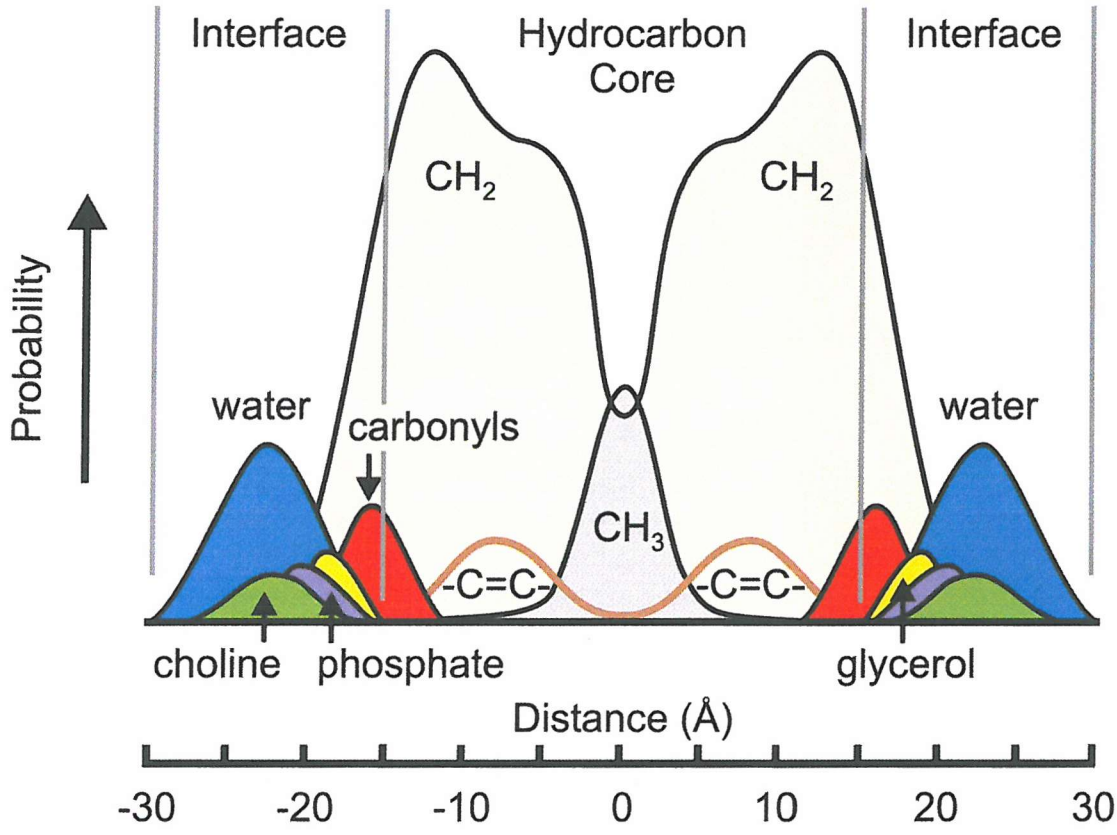

Figure 5.2 The structure of a fluid lipid bilayer of di(C18:1)PC at 23 °C and low hydration. The time-averaged Gaussian distribution profiles illustrate the extent of thermal motion along the bilayer normal for the principal structural components. The most rigid part of the bilayer corresponds to the glycerol backbone (bright yellow), the most disordered region being the fatty acyl chains. The bilayer interface is located at the position of the carbonyls of the glycerol backbone, and water is unable to penetrate past this marker. Modified from White et al. (2001).

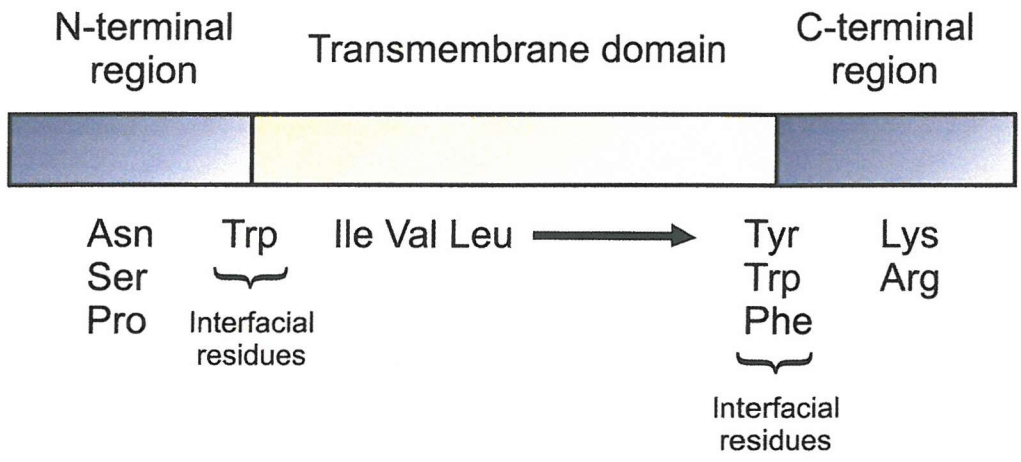

Figure 5.3 Amino acid consensus sequence for human type I bitopic transmembrane proteins. The distribution of specific residues within the membrane spanning segments is non-random. Transmembrane segments contain hydrophobic residues with aliphatic side chains, flanked by aromatic groups (Trp and Tyr) at the lipid-water interface, where these residues are believed to have a functional analogy to buoys on either side of the membrane. The extreme ends of transmembrane helices contain polar groups, which are able to form charge interactions with the lipid head group-water interface. Adapted from Landolt-Marticorena et al. (1993).

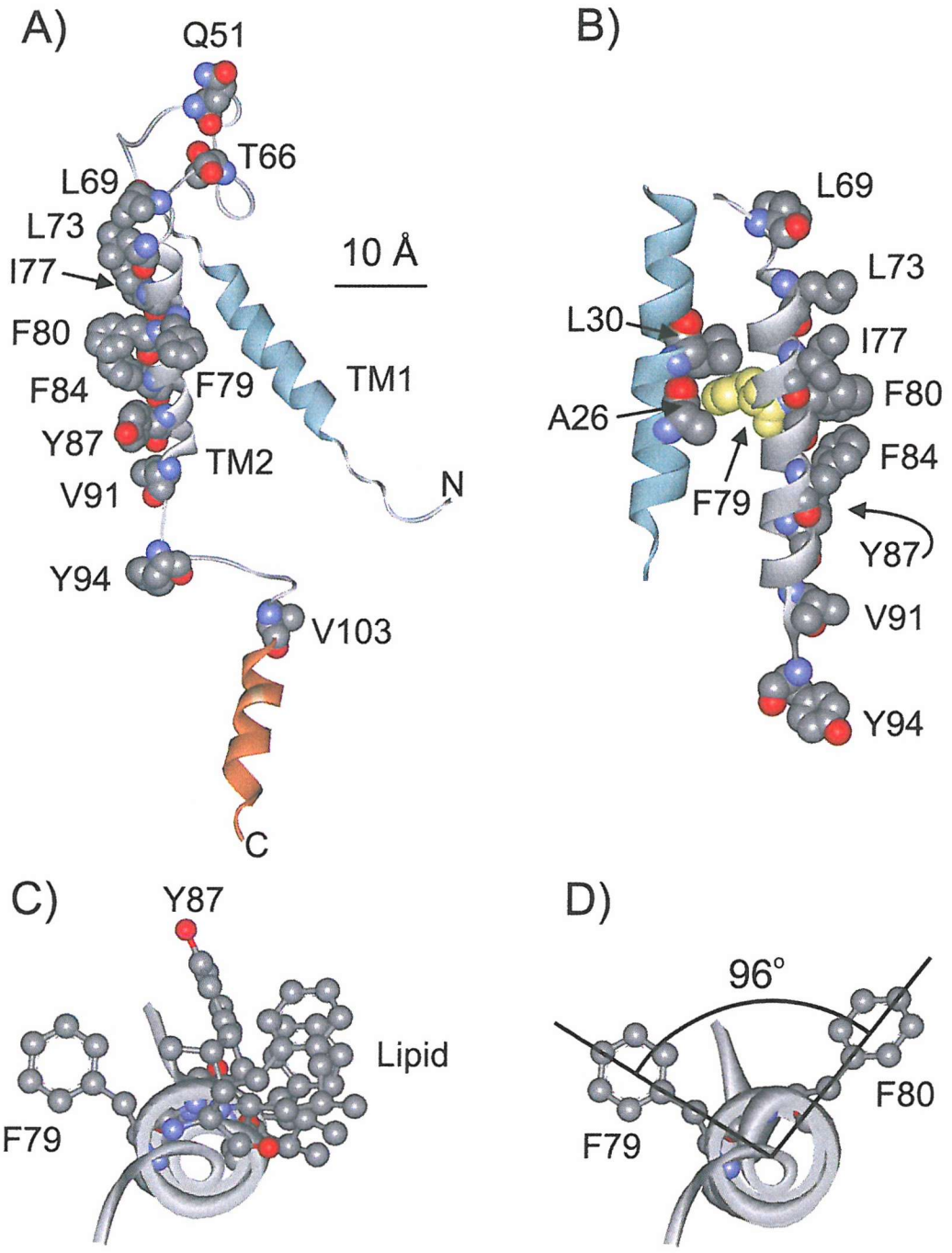

Figure 5.4 Locations of the mutated residues in a single chain from the homopentameric TbMscL homologue and their relationship to residue Phe-80. In (A) the mutated residues are shown in CPK representation and viewed from the side. In (B) the knobs-into-holes interaction of TM2 Phe-79 residue (yellow) with TM1 residues Ala-26 and Leu-30 is shown. In (C) the mutated residues are shown in ball and stick representation and viewed from the periplasm, along TM2 helical axis, and in (D) a simplified view of C) is shown, highlighting the spatial relationship of lipid exposed Phe-80 and protein exposed residue Phe-79 only. PDB file 1MSL.

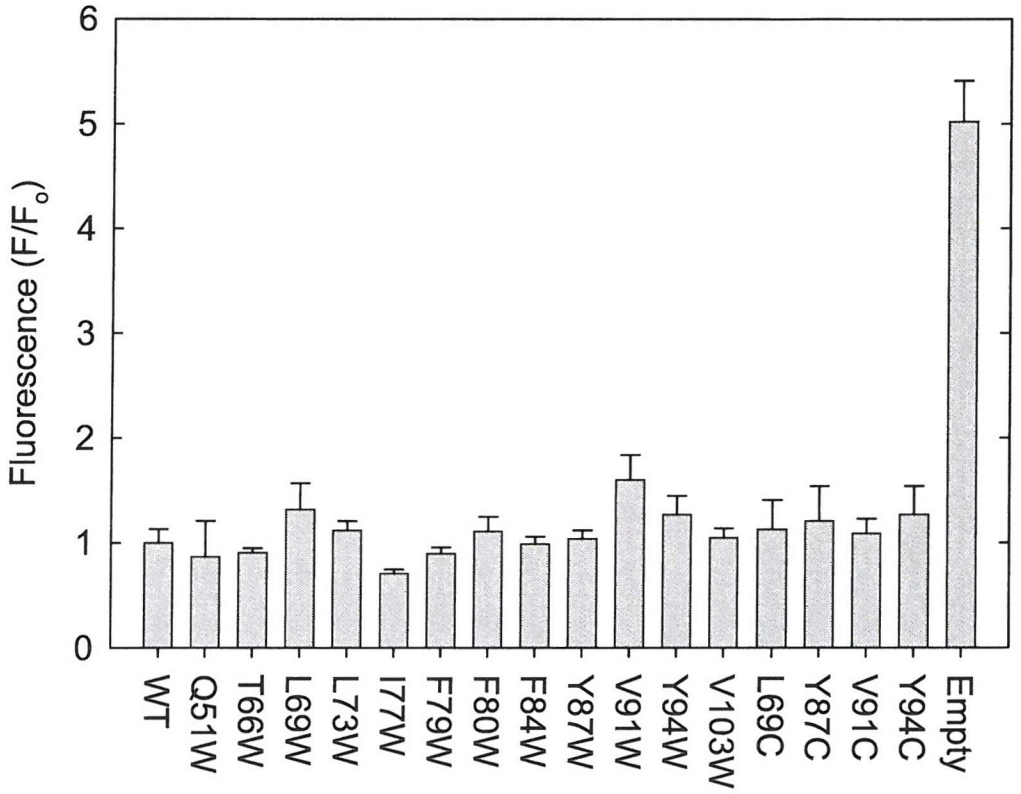

Figure 5.5 Viability of mechanosensitive-null *E. coli* expressing the *TbmscL* genes on an inducible plasmid. *E. coli* MJF465 transformants carrying the pET-19b plasmid with the *TbmscL* gene were grown in the presence of 0.4 M NaCl and induced for 4 h with 1 mM IPTG, followed by a hypoosmotic stress via a 60-fold dilution into water containing ethidium bromide (0.5 μg ml^{-1}). The fluorescence intensity of the supernatant was analysed for the release of DNA at 632 nm. Fluorescence intensities are expressed as a ratio with the fluorescence for MJF465 harbouring the WT-*TbmscL* gene. The fluorescence intensity for the release of DNA from the empty MJF465 cell line (no plasmid) is also shown. Intensities are the average of three colonies, and the error bars correspond to the standard deviation.

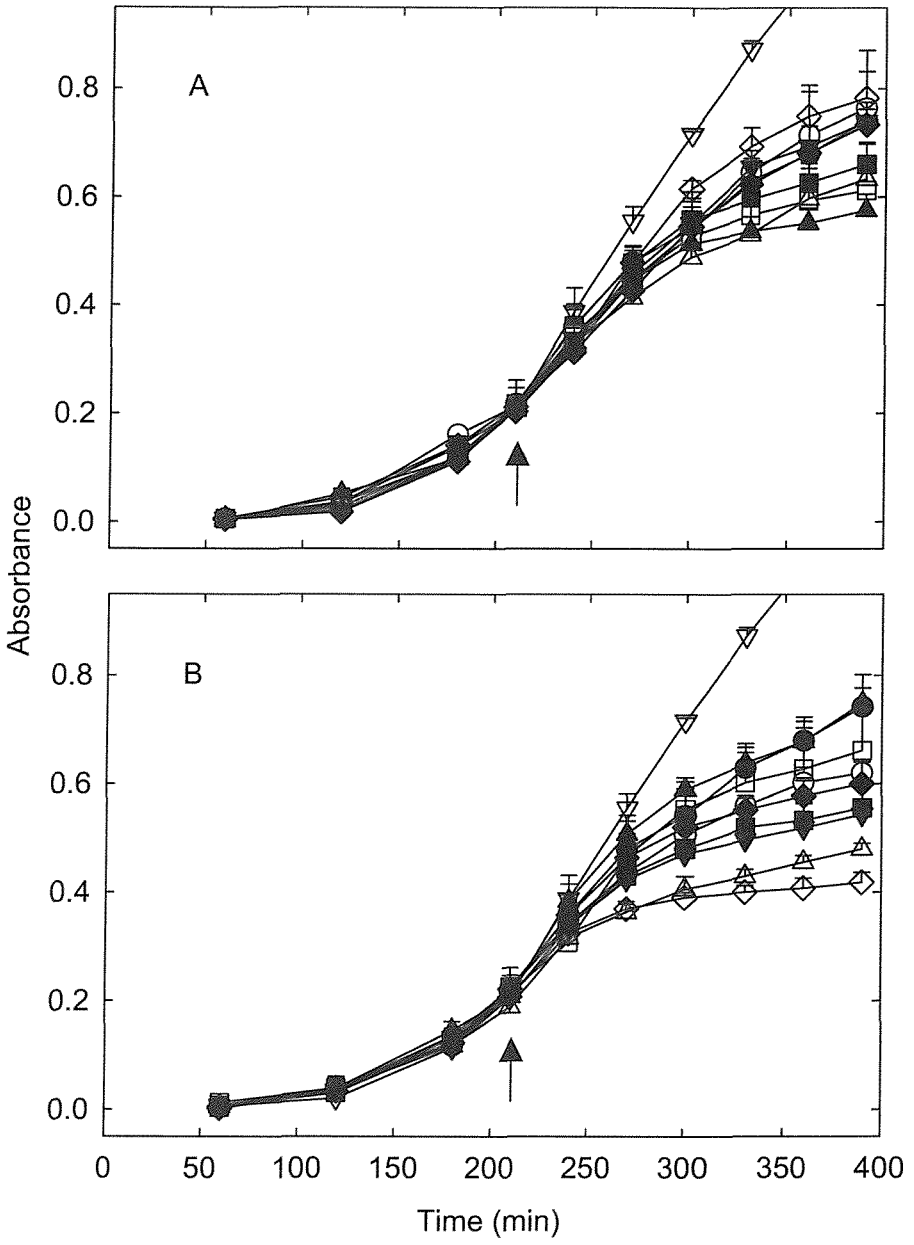

Figure 5.6 Growth of *E. coli* in liquid media expressing the *TbmscL* genes. *E. coli* BL21(DE3)pLysS transformants carrying the pET-19b plasmid with the *TbmscL* genes: (A) (●), WT; (○), Q51W; (■), T66W; (□), L69W; (▲), L69C; (△), L73W; (◆), I77W; (◇), F79W; and (▼), F80W. (B) (●), WT; (○), F84W; (■), Y87W; (□), Y87C; (▲), V91W; (△), V91C; (◆), Y94W; (◇), Y94C; and (▼), V103W, were grown at 37 °C in Luria broth medium supplemented with ampicillin (100 μg ml^{-1}). The non-induced growth of (▽), *E. coli* BL21(DE3)pLysS host strain (empty) is also shown in (A) and (B). Cells were induced with 1 mM IPTG at an absorbance at 600 nm of ~0.2 (arrow). Data points are the average of five colonies, the error bars correspond to the standard deviation.

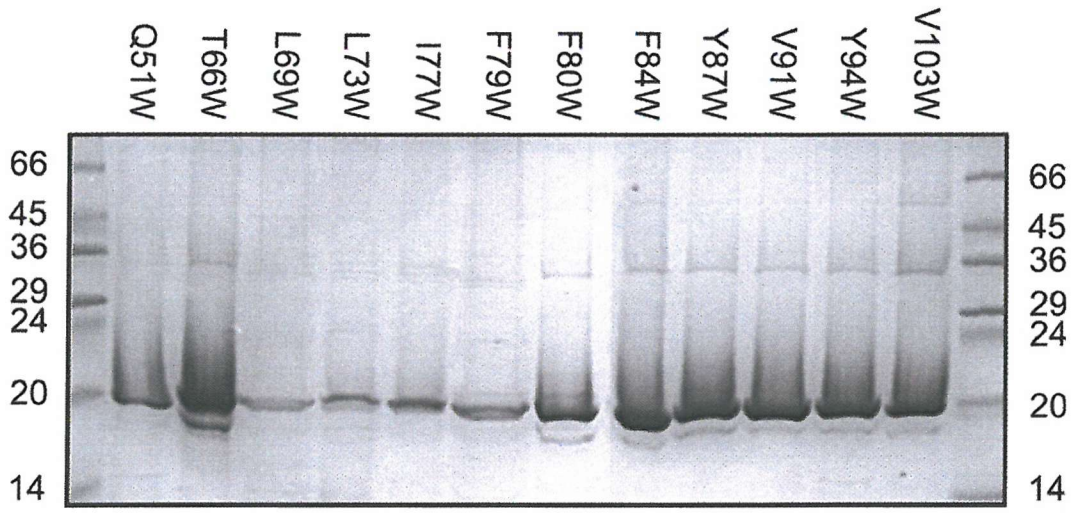

Figure 5.7 15 % Sodium dodecyl sulphate polyacrylamide gel electrophoresis of Trp mutants of TbMscL purified from 6 l liquid cultures in OG detergent. Protein bands were visualised by Coomassie brilliant blue staining. 5 µl of pooled and purified protein from each 6 l preparation were loaded into the gel lanes. The unreconstituted TbMscL samples consist largely of monomeric protein (M_r 18.6 kDa) with small amounts of dimeric species. The numbers above the lanes correspond to the TbMscL residue mutated. The lanes on either side of the gel contain 10 µl of low molecular weight range protein standards (Sigma).

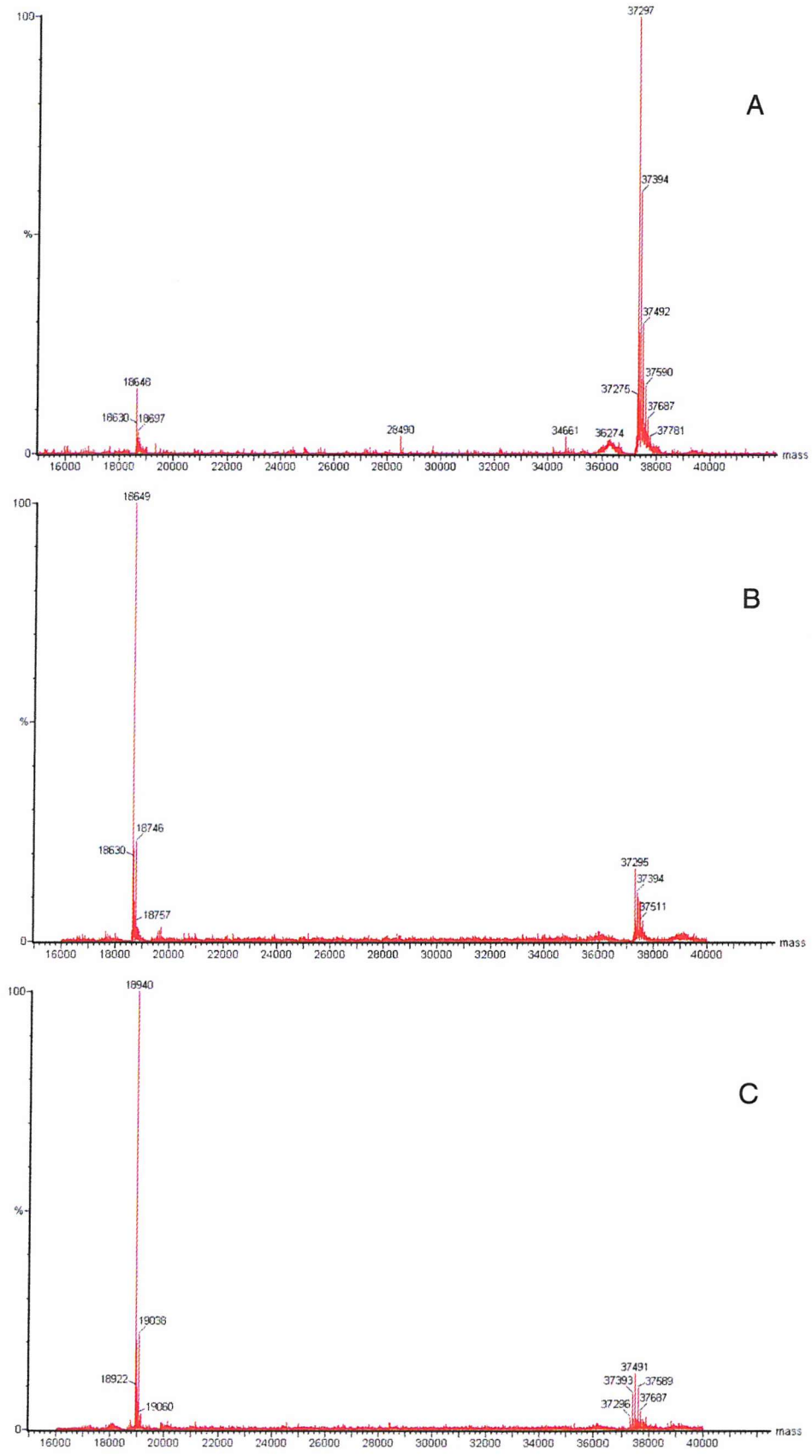

Figure 5.8 Electrospray mass spectrometry time of flight spectra of L69C-TbMscL. (A), unlabelled L69C-TbMscL consisting largely of dimeric protein (M_r 37.3 kDa). (B), incubation in the presence of 3 mM TCEP as reducing agent resulted in formation of monomer. (C) monomeric L69C-TbMscL (M_r 18.6 kDa) was labelled with NBD for 1.5 h at 25 ^{o}C generating monomeric NBD-L69C-TbMscL (M_r 18.9 kDa).

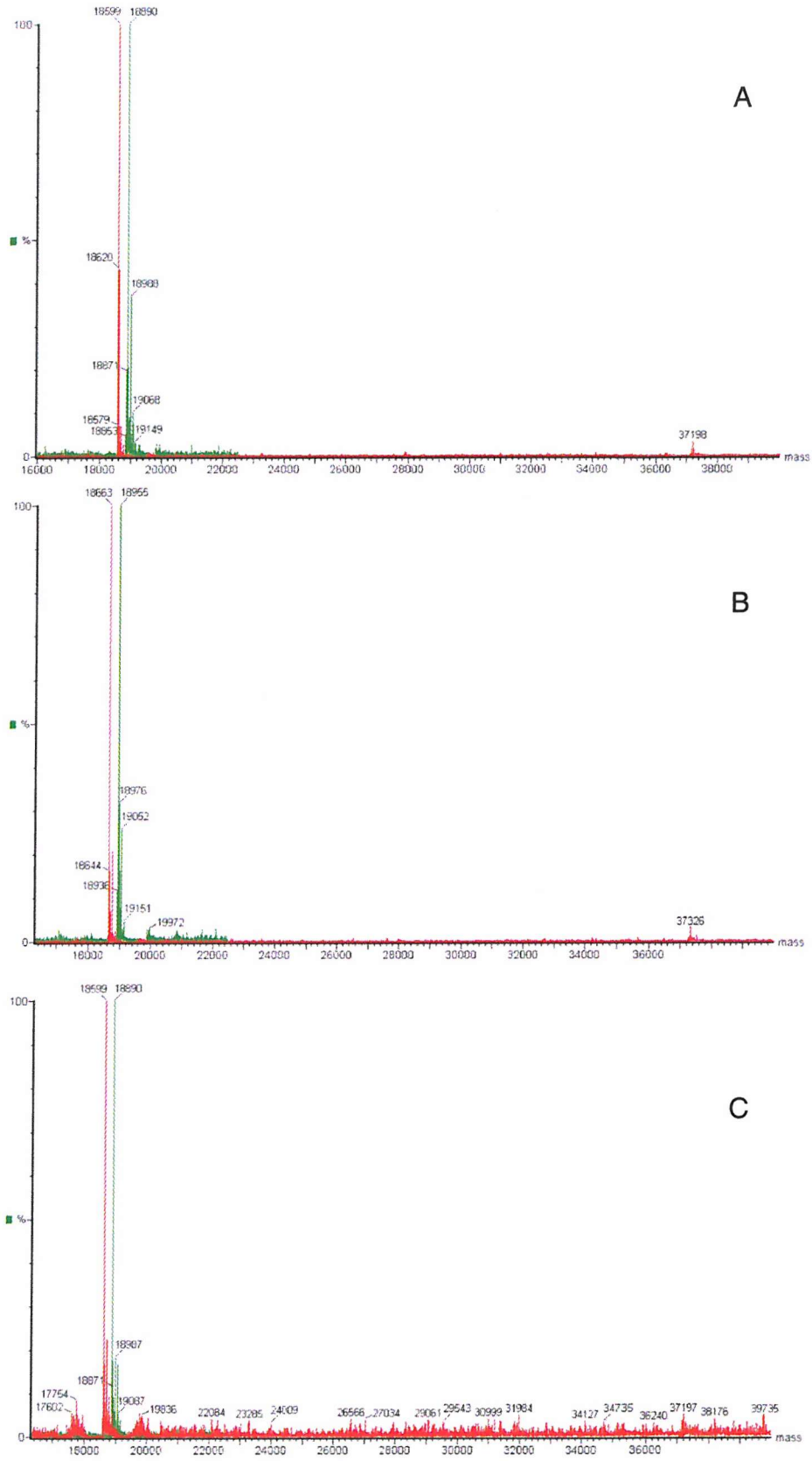

Figure 5.9 Electrospray mass spectrometry time of flight spectra for Cys mutants of TbMscL. Mass spectrometry spectra are shown for (A) Y87C-TbMscL, (B) V91C-TbMscL and (C) Y94C-TbMscL. Cys mutants of TbMscL were reduced with 3 mM TCEP (red) and then labelled with NBD (M_r 291 Da) (green).

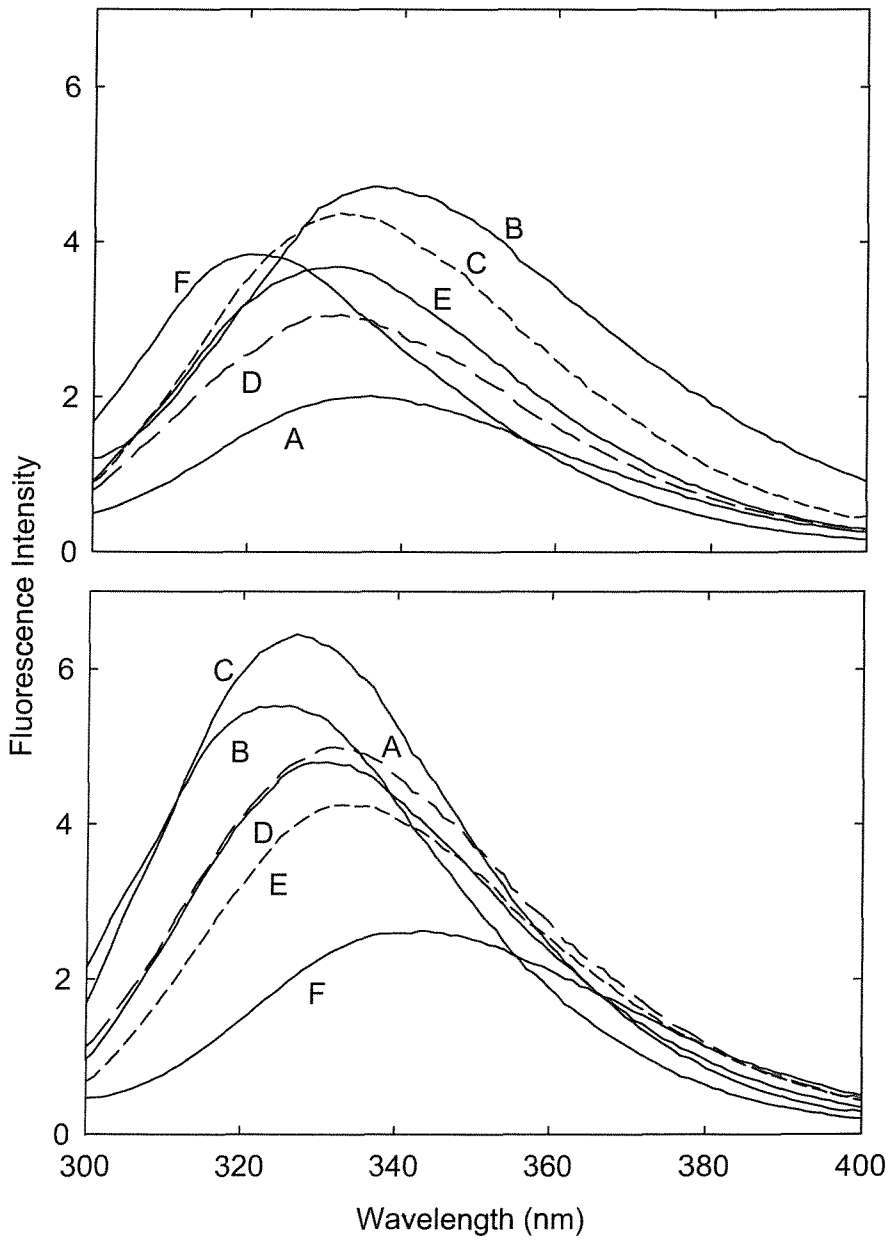

Figure 5.10 Fluorescence emission spectra for Trp mutants of TbMscL in bilayers of di(C18:1)PC. Fluorescence emission spectra are shown for Top panel: (A), Q51W; (B), T66W; (C), L69W; (D), L73W; (E), I77W; and (F), F80W. Lower panel: (A), F79W; (B), F84W; (C), Y87W; (D), V91W; (E), Y94W; and (F), V103W. The concentration of TbMscL was 0.98 μM and the molar ratio of lipid to TbMscL was 100:1. The excitation wavelength was 280 nm and the buffer was 20 mM Hepes, 100 mM KCl, 1 mM EGTA, pH 7.2.

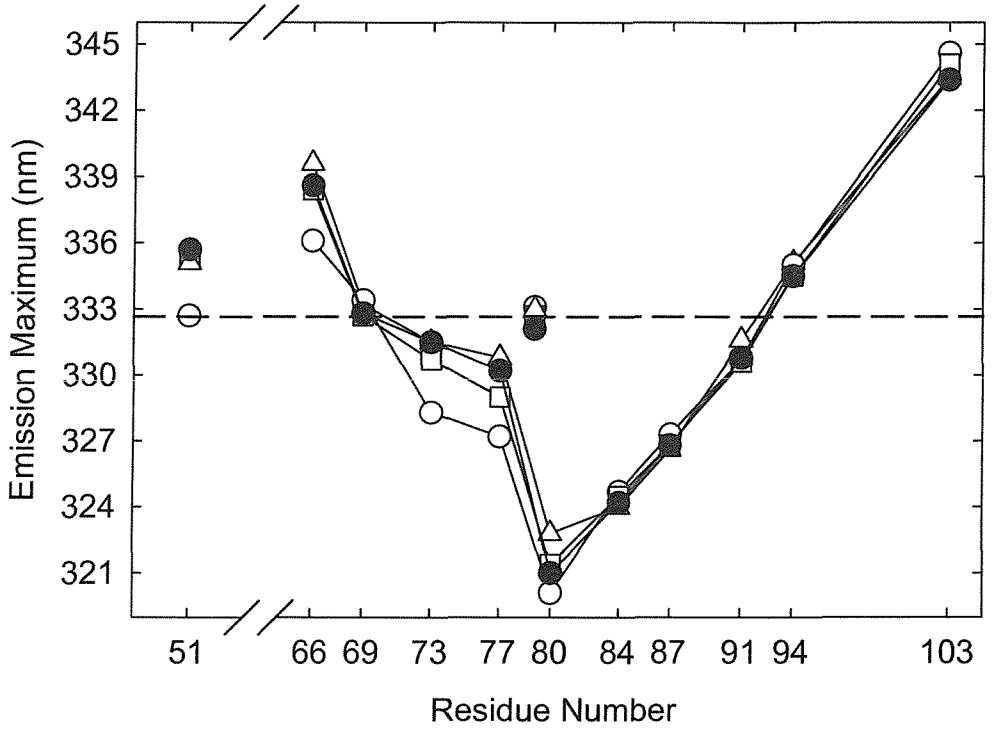

Figure 5.11 Fluorescence properties of Trp mutants of TbMscL. The Trp fluorescence emission maxima (nm) from Figure 5.10 and Table 5.1 for Trp mutants are plotted as a function of position, for TbMscL reconstituted in: (○), di(C12:0)PC; (□), di(C14:1)PC; (●), di(C18:1)PC; (Δ), di(C24:1)PC. The dotted line at 332.6 nm marks the expected fluorescence emission maximum for a Trp residue immediately below the glycerol backbone region of the bilayer.

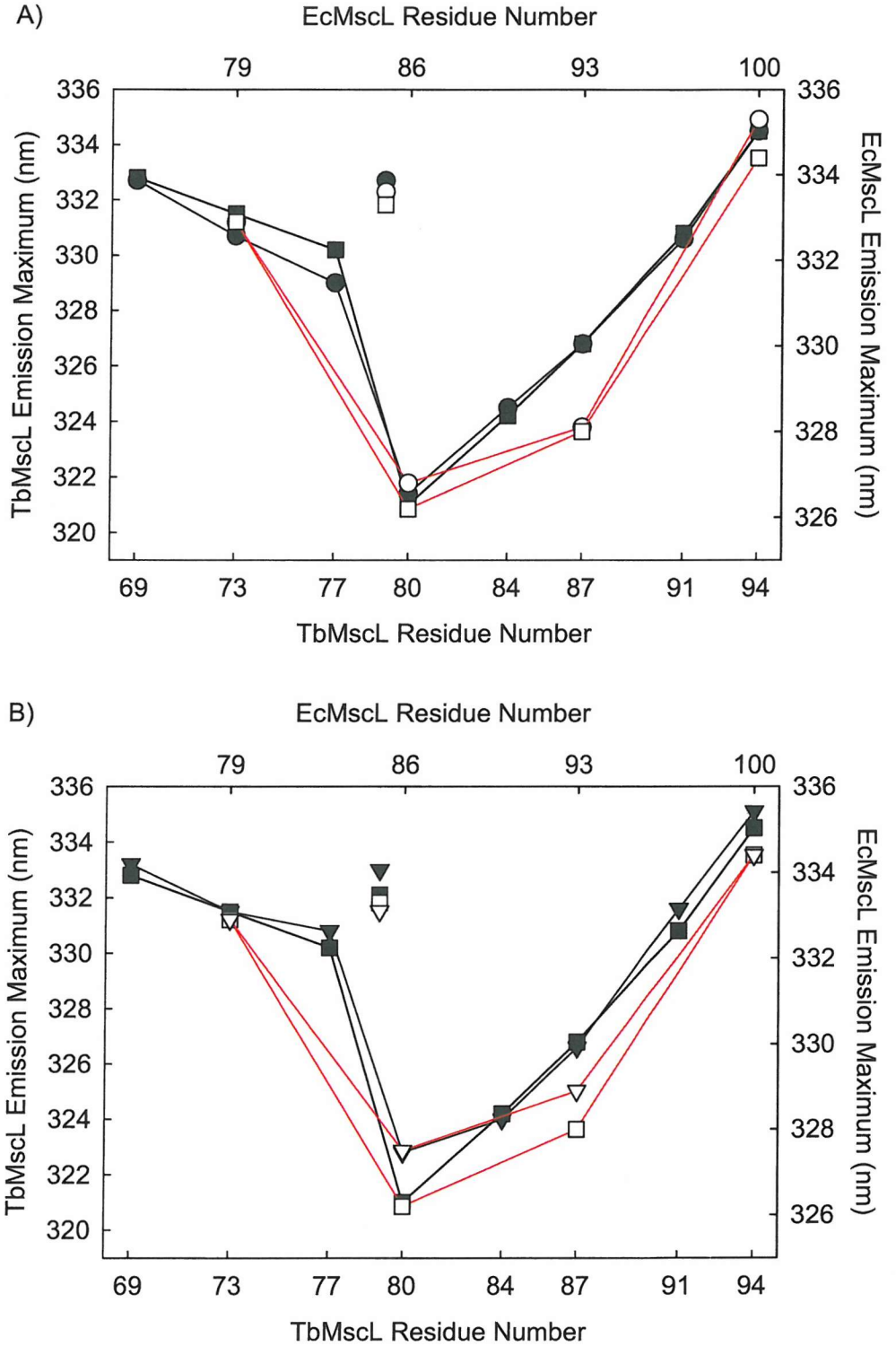

Figure 5.12 Fluorescence properties of Trp mutants of MscL. The Trp fluorescence emission maxima (nm) from Tables 5.1 and 5.3 for Trp mutants are plotted as a function of position, for TbMscL (filled symbols, black lines) and EcMscL (open symbols, red lines) reconstituted in: A) (●,○), di(C14:1)PC; (■,□), di(C18:1)PC and B) (■,□), di(C18:1)PC; (▼,▽), di(C24:1)PC.

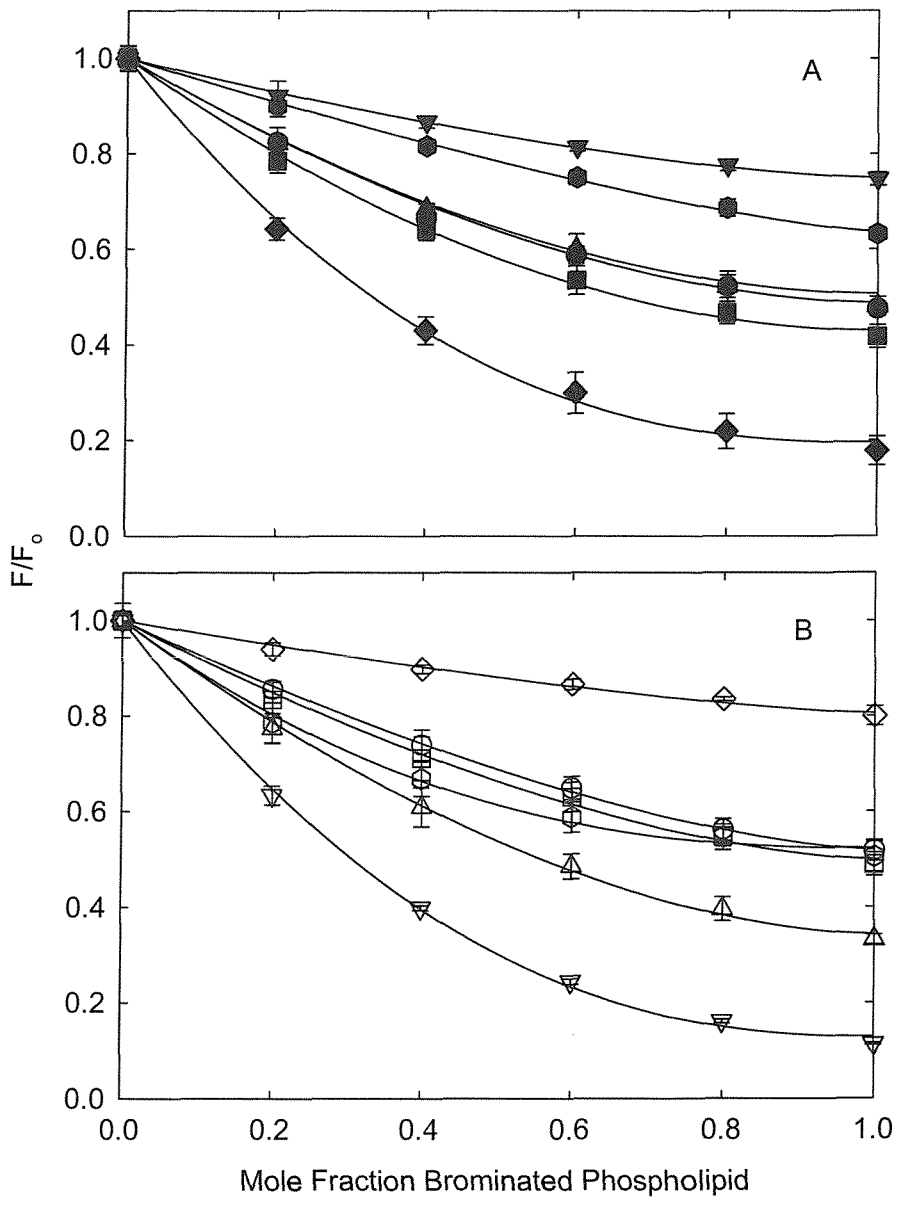

Figure 5.13 Quenching of the fluorescence of Trp mutants of TbMscL by brominated phosphatidylcholine. Trp mutants of TbMscL were reconstituted into bilayers containing mixtures of di(C18:1)PC and di(Br_2C18:0)PC. Fluorescence intensities are expressed as a fraction of the fluorescence for the TbMscL mutant reconstituted in the nonbrominated lipid. Trp mutants are as follows: (A) (⬢), Q51W; (▼), T66W; (▲), L69W; (●), L73W; (■), I77W; and (◆), F80W. (B) (⬡), F79W; (▽), F84W; (△), Y87W; (○), V91W; (□), Y94W; and (◇), V103W. The solid lines show fits to Equation 3.11, giving the values for *n* listed in Table 5.4. The concentration of TbMscL was 0.98 μM, and the molar ratio of lipid to TbMscL was 100:1. Data points are the average of three determinations.

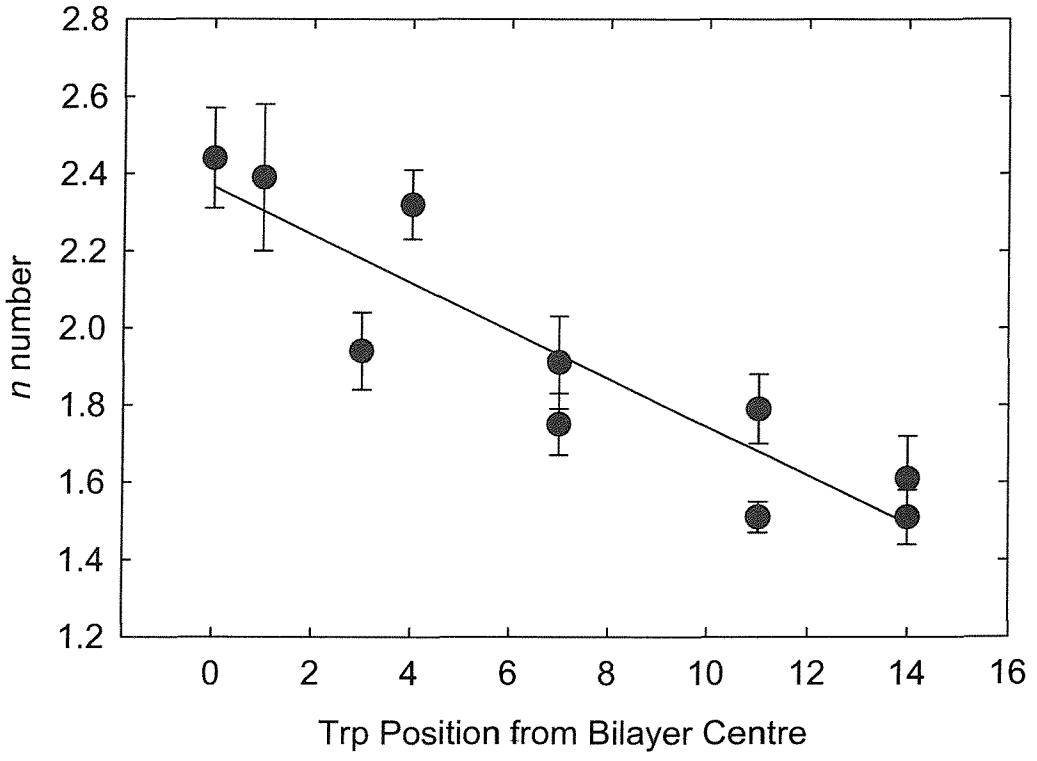

Figure 5.14 Variation of the value of n with the position of the Trp from the centre of the bilayer. The values of n are the values obtained by fitting the data in Figure 5.13 to Equation 3.11. The centre of the bilayer is taken as residue 80 in the second transmembrane α-helix of TbMscL. The x-axis represents the separation in amino acid residue number from position 80.

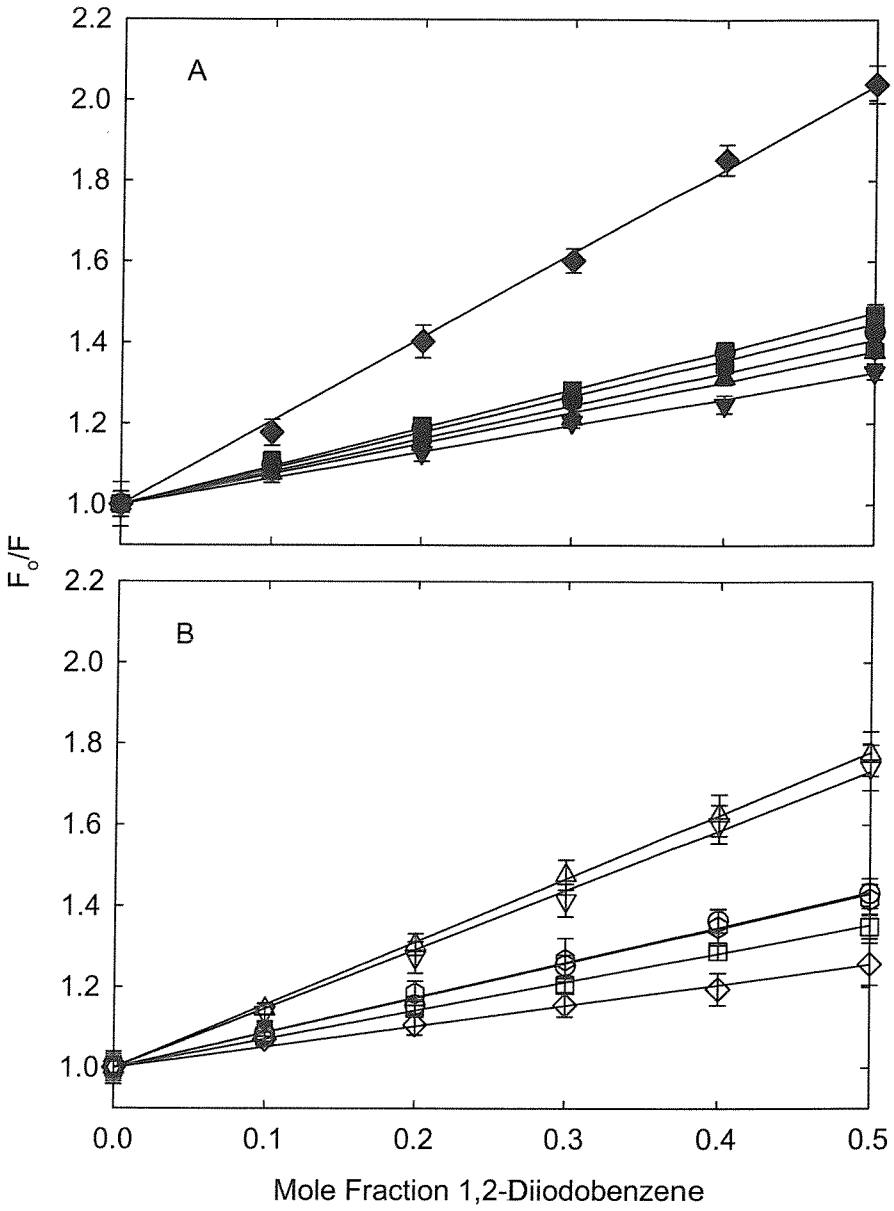

Figure 5.15 Stern-Volmer plots for quenching of the Trp fluorescence of mutants of TbMscL by 1,2-diiodobenzene. Trp mutants of TbMscL were reconstituted into bilayers containing mixtures of di(C18:1)PC and 1,2-diiodobenzene. Fluorescence intensities are expressed as a fraction of the fluorescence intensity for the TbMscL mutants reconstituted in phospholipid alone. Trp mutants are as follows: (A) (⬢), Q51W; (▼), T66W; (▲), L69W; (●), L73W; (■), I77W; and (◆), F80W. (B) (⬡), F79W; (▽), F84W; (△), Y87W; (○), V91W; (□), Y94W; and (◇), V103W. The solid lines show fits to Equation 3.1, giving the values for K_{SV} listed in Table 5.5. The concentration of TbMscL was 0.98 μM, and the molar ratio of lipid to TbMscL was 100:1. Data points are the average of three determinations.

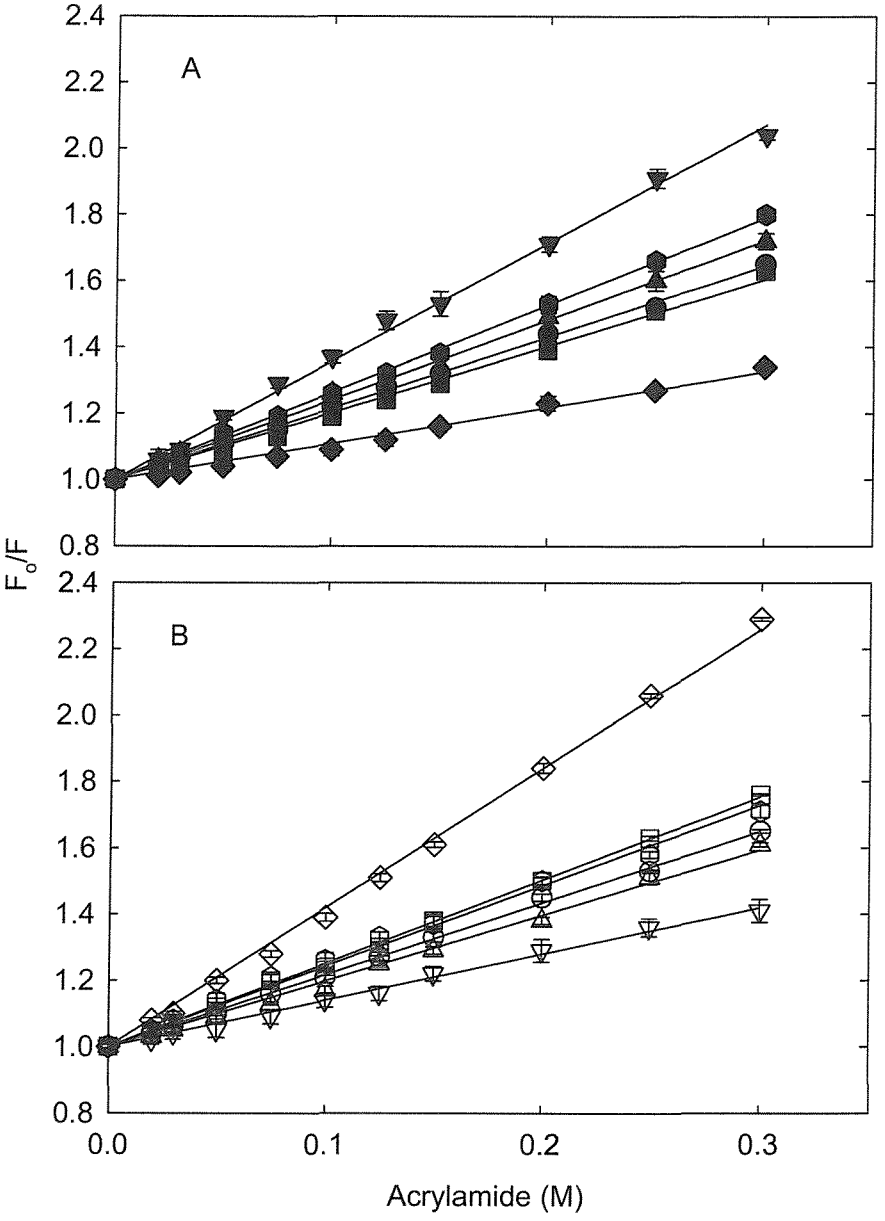

Figure 5.16 Stern-Volmer plots for quenching of the Trp fluorescence of mutants of TbMscL by acrylamide. Trp mutants of TbMscL were reconstituted into bilayers of di(C18:1)PC in the presence of the quencher acrylamide. Fluorescence intensities are expressed as a fraction of the fluorescence intensity for the TbMscL mutants in phospholipid alone. Trp mutants are as follows: (A) (⬢), Q51W; (▼), T66W; (▲), L69W; (●), L73W; (■), I77W; and (◆), F80W. (B) (⬡), F79W; (▽), F84W; (△), Y87W; (○), V91W; (□), Y94W; and (◇), V103W. The solid lines show fits to Equation 3.1, giving the values for K_{SV} listed in Table 5.6. The concentration of TbMscL was 0.98 μM, and the molar ratio of lipid to TbMscL was 100:1. Data points are the average of three determinations and corrected for the inner-filter effect.

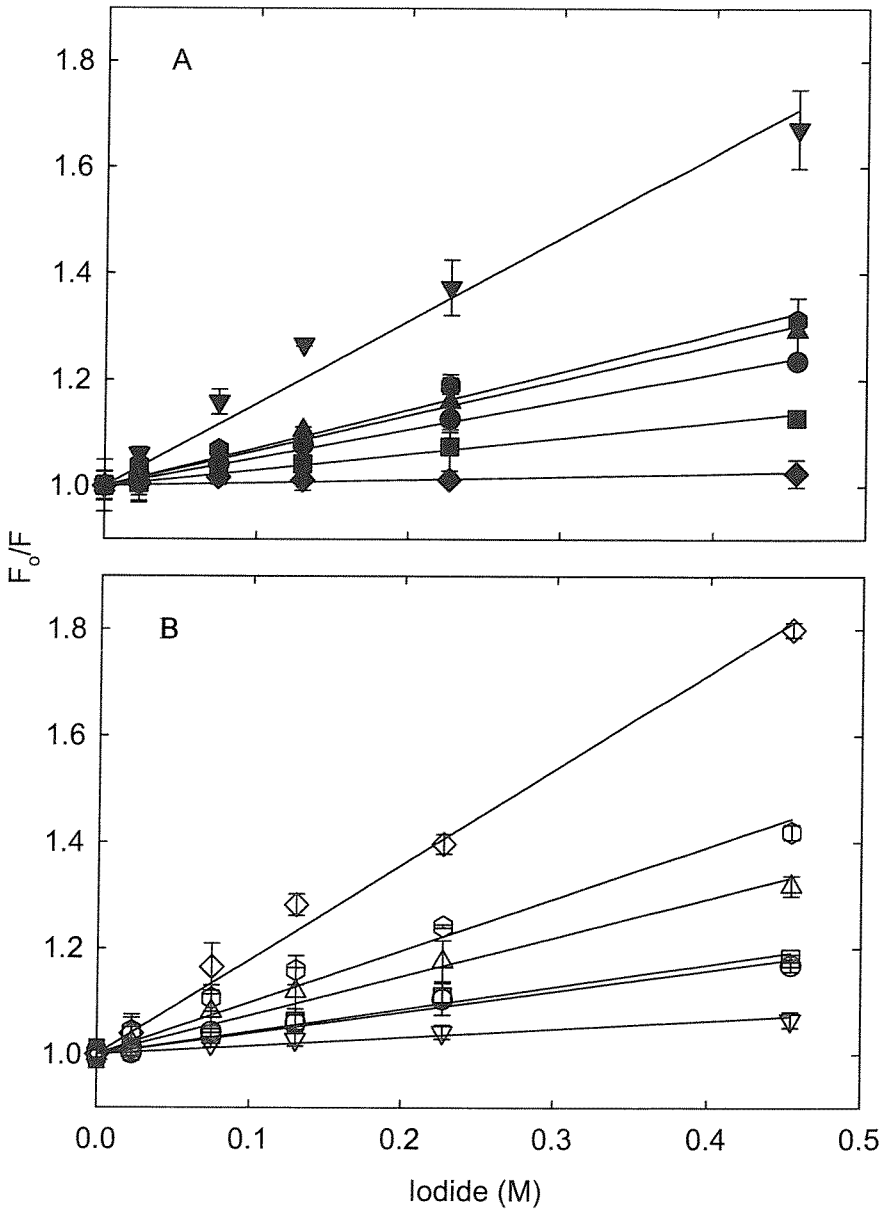

Figure 5.17 Stern-Volmer plots for quenching of the Trp fluorescence of mutants of TbMscL by iodide. Trp mutants of TbMscL were reconstituted into bilayers of di(C18:1)PC in the presence of the quencher iodide. Fluorescence intensities are expressed as a fraction of the fluorescence intensity for the TbMscL mutants in phospholipid alone. Trp mutants are as follows: (A) (⬢), Q51W; (▼), T66W; (▲), L69W; (●), L73W; (■), I77W; and (◆), F80W. (B) (⬡), F79W; (▽), F84W; (△), Y87W; (○), V91W; (□), Y94W; and (◇), V103W. The solid lines show fits to Equation 3.1, giving the values for K_{SV} listed in Table 5.7. The concentration of TbMscL was 0.98 μM, and the molar ratio of lipid to TbMscL was 100:1. Data points are the average of three determinations and corrected for the inner-filter effect.

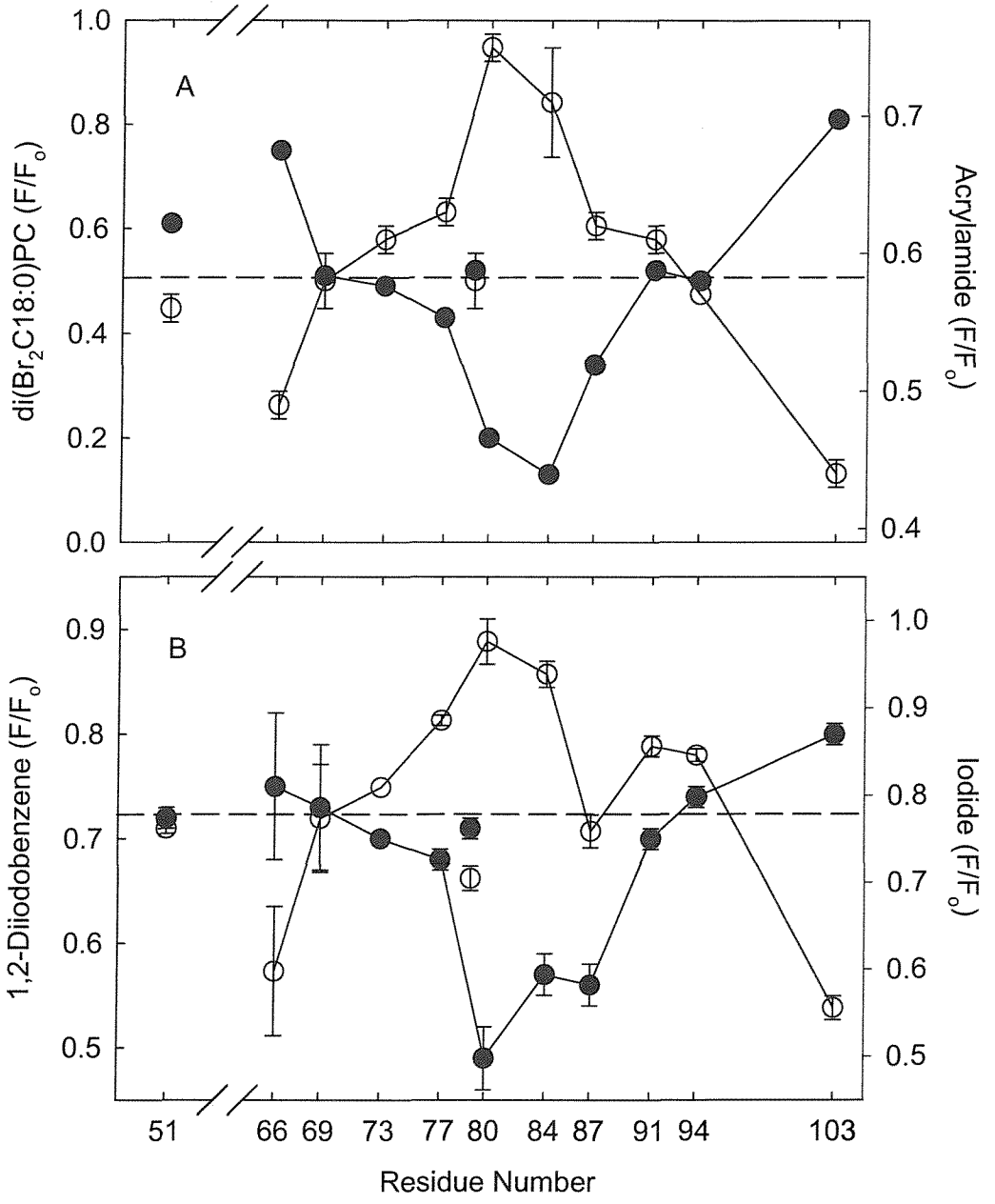

Figure 5.18 Fluorescence quenching of Trp mutants of TbMscL. Values of F/F_o are plotted as a function of Trp position, where F_o and F are fluorescence intensities in the absence and presence of quencher, respectively. (A) (●), TbMscL reconstituted in di(Br_2C18:0)PC; (○), TbMscL reconstituted in di(C18:1)PC in the presence of 0.25 M acrylamide. (B) (●), TbMscL reconstituted in di(C18:1)PC in the presence of 50 μM 1,2-diiodobenzene; (○), TbMscL reconstituted in di(C18:1)PC in the presence of 0.45 M iodide. In A and B the dotted lines have been drawn through the points for L69W. The concentration of TbMscL monomer was 0.98 μM, and the molar ratio of lipid to TbMscL monomer was 100:1.

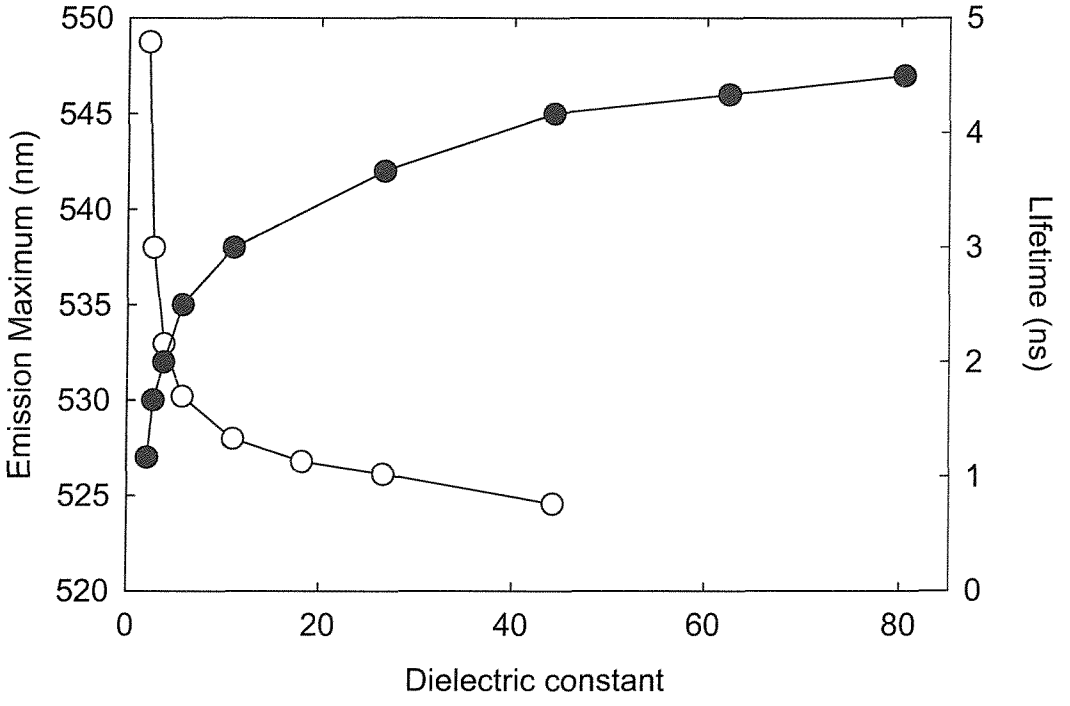

Figure 5.19 Fluorescence properties of IANBD in dioxane/water mixtures. Fluorescence emission maxima (●) and average fluorescence lifetimes (○) are plotted against dielectric constants for dioxane/water mixtures (Åkerlöf and Short, 1936).

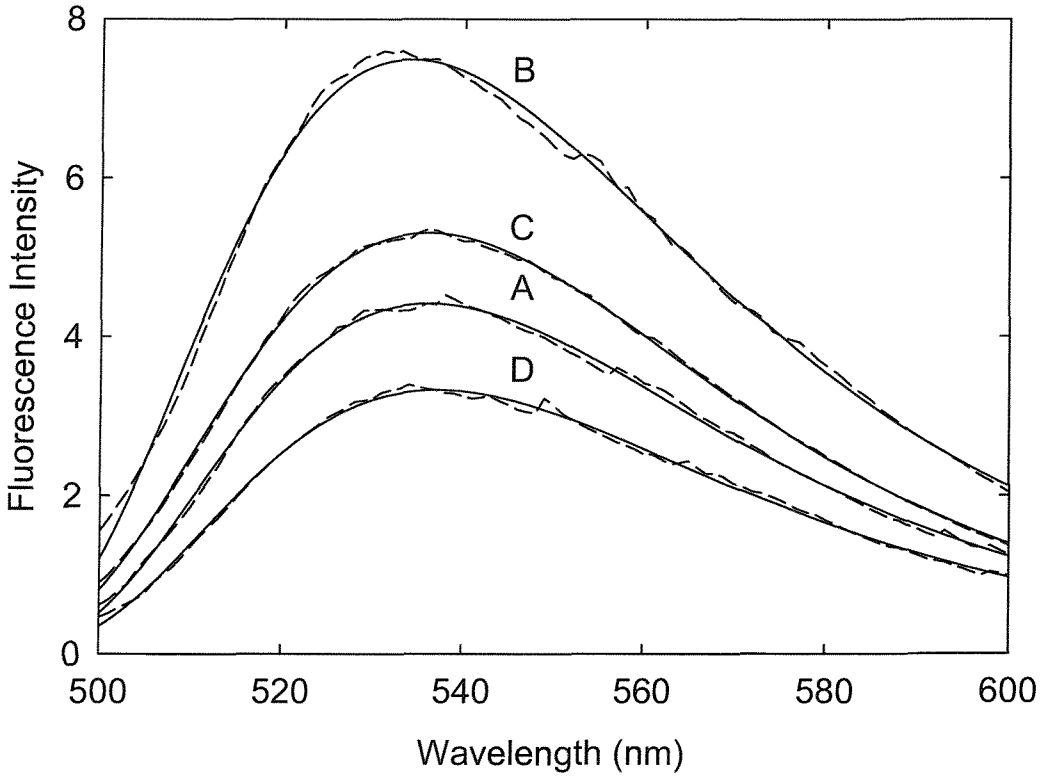

Figure 5.20 Fluorescence emission spectra of NBD-labelled Cys mutants of TbMscL in bilayers of di(C18:1)PC. Fluorescence emission spectra are shown for: (A), NBD-L69C-TbMscL; (B), NBD-Y87C-TbMscL; (C), NBD-V91C-TbMscL; and (D), NBD-Y94C-TbMscL. The solid lines show fits to Equation 3.8, giving the values of maximum emission listed in Table 5.10. The concentration of TbMscL was 11.9 μM and the molar ratio of lipid to TbMscL was 100:1. The excitation wavelength was 478 nm and the buffer was 20 mM Hepes, 100 mM KCl, 1 mM EGTA, pH 7.2.

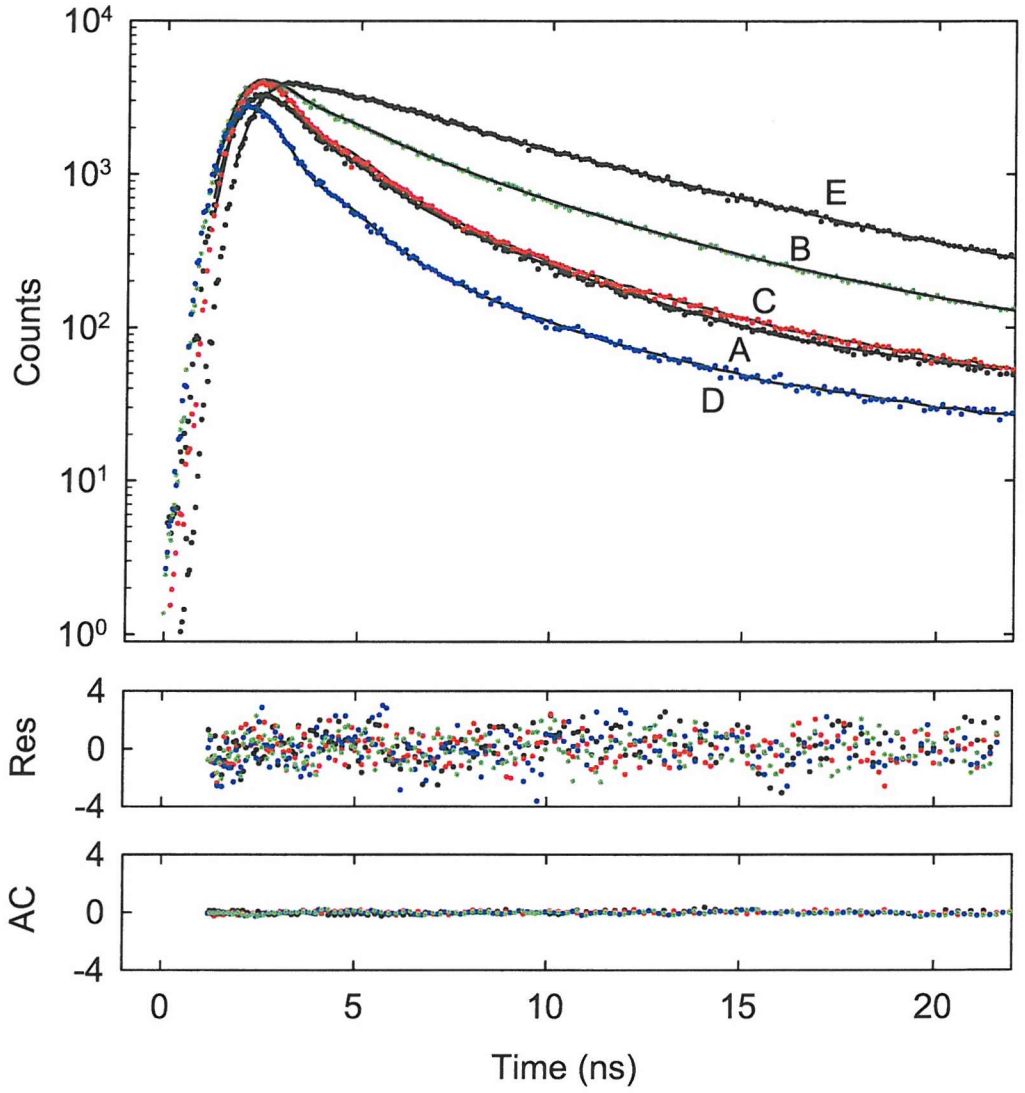

Figure 5.21 Time-resolved fluorescence decays of NBD-labelled Cys mutants of TbMscL in bilayers of di(C18:1)PC. Fluorescence decays are shown for: (A), NBD-L69C-TbMscL; (B), NBD-Y87C-TbMscL; (C), NBD-V91C-TbMscL; (D), NBD-Y94C-TbMscL; and (E), IANBD in dioxane. The solid lines through each decay are the multiexponential fits to the data; the lower panels show the autocorrelation and residuals for the fits. The concentration of TbMscL was between 0.2 and 2.0 μM and the molar ratio of lipid to TbMscL was 100:1. The excitation wavelength was 478 nm and the buffer was 20 mM Hepes, 100 mM KCl, 1 mM EGTA, pH 7.2

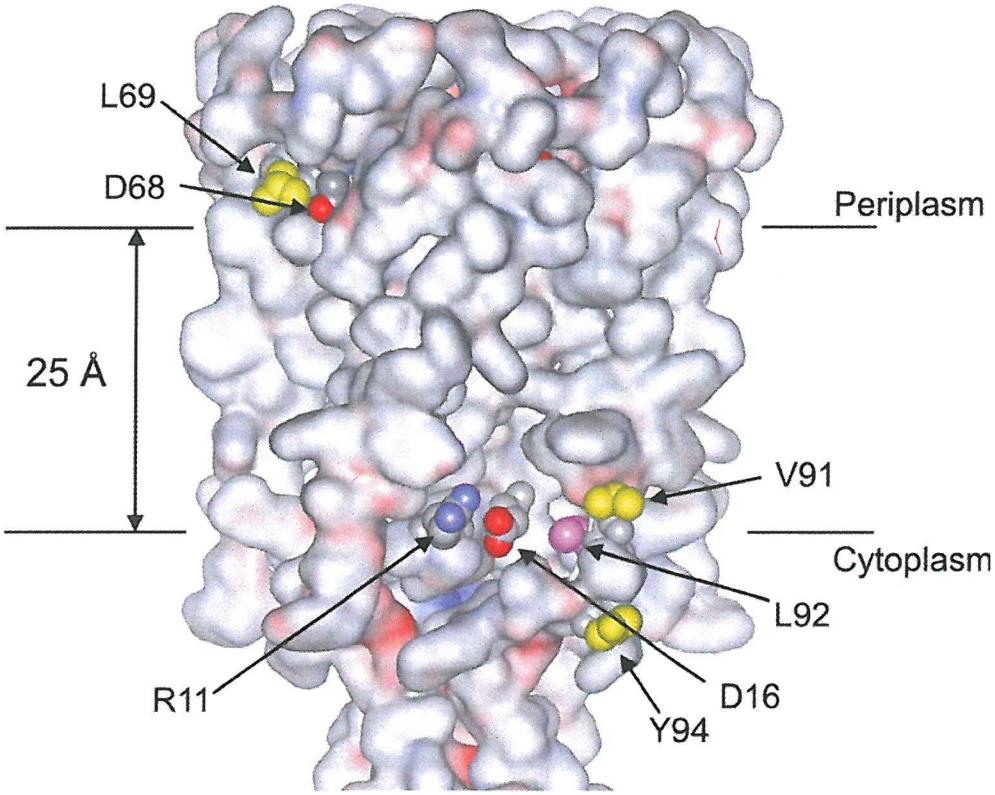

Figure 5.22 Structure of TbMscL. The surface of TbMscL is coloured by electrostatic charge, showing the exposed carboxyl groups on Asp-68 and Asp-16, and their relationship to Leu-69, Val-91, Leu-92 and Tyr-94, shown in yellow. PDB file 1MSL.

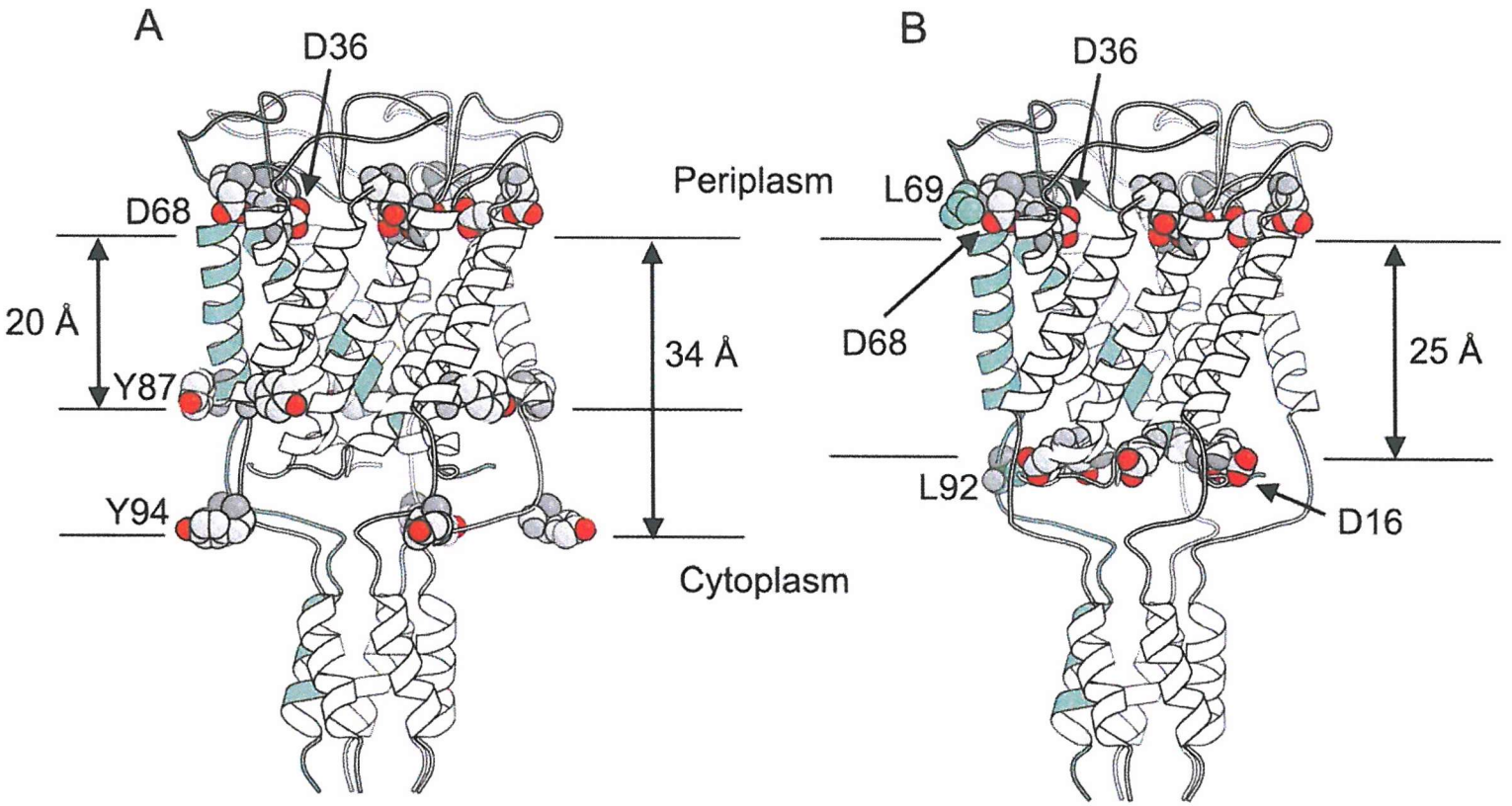

Figure 5.23 Structure of MscL. (A) Possible locations for the hydrophobic domain of MscL, defined by the positions of Asp-36 and Asp-68 on the periplasmic side of the membrane and either Tyr-87 or Tyr-94 on the cytoplasmic side. (B) The hydrophobic domain of MscL defined by the positions of Leu-69 and Leu-92 in TM2, showing the location of Asp-16 in TM1. One subunit of the pentameric channel is shown in green. Prepared using Bobscript (Esnouf, 1999) and the coordinates in PDB IMSL.

5.4 Conclusions

Measuring fluorescence emission spectra for Trp mutants of TbMscL reconstituted into bilayers of di(C18:1)PC show that the mutant with the lowest emission maximum is F80W (Figure 5.11), consistent with a location for residue 80 at the centre of the bilayer. However, the emission maximum (λ^{max}) for the mutant with a Trp residue at position 79 (F79W) is red shifted, suggesting a polar environment for residue 79. Analysis of the crystal structure of TbMscL reveals that Phe-79 is rotated some 96° further round the helix than lipid exposed residue Phe-80, and that Phe-79 in TbMscL is likely to be involved in protein-protein interactions (Figure 5.4). A molecular dynamics simulation of TbMscL in bilayers of (C16:0,C18:1)PC supports the experimental observation, and confirms that Phe-79 is involved in intersubunit interactions (Elmore and Dougherty, 2003). All the other residues mutated to Trp lie along the lipid exposed face of transmembrane helix two or are in regions of the protein exposed to the aqueous medium. A different location for the Trp residue in F79W than in the other mutants is also suggested by fluorescence quenching data.

Quenching of Trp fluorescence by brominated phospholipids requires either contact between the Trp residue and the dibrominated quencher or close proximity to allow Förster transfer (East and Lee, 1982; Mall et al., 2001). Fluorescence quenching by di(Br_2C18:0)PC with F80W-TbMscL channel is greater than the fluorescence quenching observed with F79W-TbMscL (Table 5.4). This is consistent with a reduced accessibility of the dibrominated quencher for F79W. Conversely, fluorescence quenching by water-soluble quenchers with F79W-TbMscL is greater than the fluorescence quenching observed with F80W-TbMscL (Tables 5.6 and 5.7). The quenching data obtained for Phe-79 (Figure 5.18, Tables 5.5 and 5.6), therefore suggests that F79W is located in a more polar environment.

The fluorescence emission spectra for Trp mutants of the EcMscL channel reconstituted into bilayers of di(C18:1)PC, show that the mutant with the lowest λ^{max} is L86W (Table 5.3). ESR studies with the closed EcMscL channel have previously identified residues 86-87 to be located at the centre of the bilayer (Perozo et al., 2001). Therefore, the observation that L86W has the lowest λ^{max} is consistent with a location for residue 86 deep within the hydrophobic bilayer core. A pair-wise,

primary sequence alignment of the *E. coli* and *M. tuberculosis* channels (See Figure 1.8) confirms that L86-EcMscL and F80-TbMscL are aligned, and gives confidence in the analysis that both of these residues are located at the centre of the bilayer.

Using the primary amino acid sequence alignment shown in Figure 1.8 *E. coli* residues Ile-79 and Asn-100 are shown to align to Leu-73 and Tyr-94 respectively, from *M. tuberculosis*. In Figure 5.12 the λ^{max} for EcMscL residues I79W and N100W overlay well with their corresponding TbMscL residues L73W and Y94W, respectively. Perozo et al. (2001) have shown that *E. coli* residue Phe-93 interacts with the lipid bilayer; the λ^{max} for F93W is around 328 nm, confirming a hydrophobic location for this residue. The primary sequence alignment suggests that EcMscL Phe-93 could be aligned with either Tyr-87 or Phe-88 in TbMscL (Figure 1.8). Alternatively, Phe-93 in EcMscL may occupy a position not observed in the TbMscL channel; a novel location for Phe-93 in the *E. coli* channel would explain why the λ^{max} shown in Figure 5.12 for Y87W-TbMscL and F93W-EcMscL do not overlap as well as the other residues. The molecular dynamics simulation of Elmore and Dougherty (2003) with TbMscL suggest that both Tyr-87 and Phe-88 interact with the lipid bilayer and collectively occupy a position taken up by Phe-93 in the EcMscL channel, thereby supporting the experimental observation reported here for Y87W-TbMscL and F93W-EcMscL.

The λ^{max} for the EcMscL mutant with a Trp residue at position 85 (F85W) is red shifted, suggesting a polar environment for residue Phe-85, despite this residue being located next to Leu-86 in the primary amino acid sequence (Figure 1.8). F85-EcMscL and F79-TbMscL are sequence aligned, and therefore *E. coli* residues Phe-85 and Leu-86 are likely to have the same relationship to residues Phe-79 and Phe-80 in the *M. tuberculosis* channel, occupying a similar position and with F85-EcMscL and F79-TbMscL being involved in similar protein-protein interactions in the two separate channels. This observation is supported by the fact that the Trp fluorescence emission profiles overlay well for these four residues (Figure 5.12).

5.4.1 Locating the Bilayer Interfaces on TbMscL

The environmental sensitivities of the Trp and NBD groups can be used to determine which residues in a membrane protein are located at the hydrophobic-polar interfaces on the two sides of a membrane. The fact that the same conclusions are reached with both probes suggests that any perturbations of structure resulting from mutation or labelling are small. Experiments with KcsA, where the Trp residues are located at the ends of the transmembrane α-helices, suggests that a Trp residue located immediately below the glycerol backbone region of the lipid bilayer will emit at 332.6 nm (Williamson et al., 2002) as shown in Figure 5.11. The results with the Trp mutants suggest that the hydrophobic domain of TbMscL is marked by the position of Leu-69 on the periplasmic side of the membrane and a residue between Val-91 and Tyr-94 on the cytoplasmic side (Figure 5.22). Similarly, the fluorescence lifetime data with NBD-labelled TbMscL suggest that Leu-69 is located at the bilayer interface and a residue between Val-91 and Tyr-94 marks the position of the bilayer interface on the opposite side of the membrane. Leu-69 is close to Asp-68, an exposed residue in TbMscL (Figure 5.22); Asp-36 is located at a distance from the bilayer centre similar to that of Asp-68, but is not surface exposed (Figure 5.23). If, as suggested, the position of Leu-69 marks the interface between the hydrophobic core of the bilayer and the lipid head group region, then the carboxyl oxygens of Asp-68 must be located close to the glycerol backbone region of the lipid bilayer. An analysis of a number of other membrane protein crystal structures suggests that this might be a common feature of membrane protein structure; for example Glu-9 in the first transmembrane α-helix of bacteriorhodopsin is close to the backbone of the neighbouring lipid molecules resolved in the crystal structure (Lee, 2003).

The only charged residues on the cytoplasmic side of the membrane located at a distance from the bilayer centre between those of Val-91 and Tyr-94 are Arg-11 and Asp-16 at the N-terminal end of TM1, both surface-exposed residues, located close to Leu-92 in TM2 (Figure 5.22). The hydrophobic thickness of TbMscL estimated assuming that Asp-16 is located at the glycerol backbone region is ca. 25 Å (Figures 5.22 and 5.23B). This agrees well with the observation that the phosphatidylcholine that binds most strongly to TbMscL is that with C16 chains, giving a bilayer of hydrophobic thickness ca. 24 Å (Chapter 4). Perozo et al. (2001) have previously

located the transmembrane domain of MscL of *E. coli* from studies of the effects of oxygen and a water-soluble Ni^{2+} chelate on the electron spin resonance spectra of Cys mutants of EcMscL labelled with a methanethiosulphonate spin label. Assuming that the transmembrane domain identified in the experiments of Perozo et al. (2001) corresponds to the hydrophobic domain identified here, then the His-74 to Leu-98 region of TM2 in *E. coli* identified by Perozo et al. (2001) as spanning the hydrophobic core of the lipid bilayer agrees well with the Leu-69 to Leu-92 region identified above for TM2 in *M. tuberculosis*, and the hydrophobic regions of TM2 of MscL of *E. coli* and *M. tuberculosis* have very similar lengths (25 and 24 residues, respectively). This is consistent with the observation that the phosphatidylcholine that binds most strongly to *E. coli* MscL also has a chain length of C16 (Chapter 4).

These results suggest that the region of TM2 that spans the hydrophobic core of the lipid bilayer cannot be determined by consideration of TM2 alone. Although the N-terminal end of TM2 is well marked by Asp-68, there are no charged residues close to the C-terminal end of TM2. Tyr residues are often found at the ends of transmembrane α-helices (Figure 5.3) and, although Tyr-87 is located at the C-terminal end of the α-helical region of TM2, this is unlikely to define the hydrophobic thickness of MscL, as this would give a thickness of ca. 20 Å (Figure 5.23A), unusually thin for a protein in a bacterial cytoplasmic membrane (Lee, 2003). Conversely, the position of Tyr-94 would define a too great hydrophobic thickness for MscL (Figure 5.23A). If the glycerol backbone region of the bilayer is located at a distance from the bilayer centre close to that of Leu-92, then the hydrophobic residues in TM2 between Leu-92 and Tyr-94 would be located in the head group region of the bilayer (Figures 5.22 and 5.23B), possible since the head group region of a bilayer of phosphatidylcholine has a thickness of about 15 Å (White et al., 2001).

It is noticeable that the plot of fluorescence emission maxima against residue number is not symmetrical about the middle of the membrane (ca. residue 80), emission maxima for L73W and I77W being at longer wavelengths than those of F84W and Y87W respectively (Figure 5.11). The structure of the MscL pentamer is such that the first and second of the transmembrane α-helices come together on the periplasmic side of the membrane (Figure 5.23), so that residues Phe-84 and Tyr-87 are more lipid exposed than residues Leu-77 and Ile-73. This is also apparent in molecular

dynamics simulations of MscL in bilayers of phosphatidylethanolamines where lipid-residue interaction energies are stronger for residues Phe-84 and Tyr-87 than for Leu-77 and Ile-73 (Elmore and Dougherty, 2003). A similar asymmetry is seen in fluorescence quenching plots with di(Br_2C18:0)PC and with 1,2-diiodobenzene (Figure 5.18), the levels of quenching of L73W and I77W being markedly less than those of F84W and Y87W, respectively, the shapes of the plots being very similar to that of the plot of emission maxima shown in Figure 5.11. The greater quenching observed for F84W and Y87W is consistent with greater lipid exposure of positions 84 and 87 than of positions 77 and 73. The asymmetry is less apparent in plots of quenching by the water-soluble quenchers acrylamide and iodide (Figure 5.18); quenching of Y87W by iodide is higher than might have been expected, which could be because Tyr-87 is located close to the positively charged guanidinium group of Arg-11.

5.4.2 The Efficiency of Hydrophobic Matching for MscL

Fluorescence emission maxima for TbMscL mutants L69W, V91W and Y94W reconstituted into bilayers of di(C12:0)PC or di(C24:1)PC are not significantly different to those reconstituted in di(C18:1)PC (Figure 5.11, Table 5.1) suggesting that the Trp residues maintain their locations close to the interface, despite a ca. 21 Å change in bilayer thickness. Similarly, λ^{max} for EcMscL mutants I79W, F93W and N100W reconstituted into bilayers of di(C14:1)PC or di(C24:1)PC are not significantly different to those reconstituted in di(C18:1)PC (Figure 5.12, Table 5.3), despite a ca. 17 Å change in bilayer thickness. The results obtained with the Trp fluorescence emission maxima are consistent with studies of the fluorescence lifetime of NBD-labelled TbMscL, which also show no significant changes in lifetime with bilayer thickness for any of the mutants (Table 5.11). Thus the efficiency of hydrophobic matching between MscL of *E. coli* and *M. tuberculosis* and the surrounding lipid bilayer is high.

5.4.3 Structural Rearrangements in MscL

Studies of spin-labelled EcMscL reported significant changes between closed and open states of the channel, consistent with changes in rotation and tilt for the transmembrane α-helices. Smaller changes in ESR spectra were also observed when the closed channel was reconstituted into short-chain lipids such as di(C14:1)PC. Since the pressure required to open EcMscL channels in thin bilayers is less than in thick bilayers, it has been suggested that the structure of MscL observed in a thin bilayer could be part way to the open structure (Perozo et al., 2002a,b).

A significant shift in Trp fluorescence emission maximum for TbMscL from di(C14:1)PC to di(C24:1)PC is observed only for I77W (Figure 5.11, Table 5.1); the 2 nm shift to longer wavelength with increasing bilayer thickness is consistent with a slight increase in polarity at position 77, but not with any significant rotation of TM2. The changes observed in di(C14:1)PC for TbMscL are smaller than might have been expected from the ESR results with EcMscL. However, TbMscL channels are known to required higher levels of membrane tension to gate under patch clamp techniques than EcMscL channels (Moe et al., 2000); the results in Figure 5.11 for TbMscL reconstituted into bilayers of di(C12:0)PC instead of di(C14:1PC, may therefore provide a better comparison between the two homologues.

Perozo et al. (2002a) reported that the largest changes in TM2 of EcMscL were seen on the periplasmic side of the membrane, between residues 76 and 79, with these residues generally becoming more lipid exposed when forming the open channel. These results are also consistent with the data shown in Figure 5.11 and Table 5.1 for TbMscL moving from bilayers of di(C24:1)PC to di(C12:0)PC; residues Thr-66, Leu-73 and Ile-77 located on the periplasmic side of TM2, together with residue Gln-51 in the periplasmic loop of TbMscL show a 3 nm shift in fluorescence emission maxima to shorter wavelengths with decreasing bilayer thickness. The emission maximum for residues at the bilayer interfaces remains unchanged, suggesting that TM2 must tilt to match the bilayer thickness. Residues 80 to 103 hardly change with changing bilayer thickness. This suggests that TM2 does not rotate as a whole, but that only the N-

terminal end rotates. The fact that the emission maximum of Phe-79 does not shift also suggests no rotation of the whole TM2 helix. Overall, the data indicates that the conformation adopted in short-chain lipids could represent an intermediate on the way to the fully open form.

Reconstitution of TbMscL channels into bilayers of di(C12:0)PC, would therefore be expected to result in significant tilting of the transmembrane α-helices in order to match the hydrophobic thickness of the bilayer; this tilting could also be accompanied by rotation of the helix. Tilting and rotation of the transmembrane α-helices in EcMscL has been observed by Perozo et al. (2002a); TM2 of EcMscL was reported to tilt 17° towards the bilayer plane and rotate by at least 70° in an anticlockwise direction upon forming an open channel.

Chapter 6:
Lipid Head Group Interactions with TbMscL: Hot-Spots for Anionic Lipids and Effects on Conformation

6 LIPID HEAD GROUP INTERACTIONS WITH TbMscL: HOT SPOTS FOR ANIONIC LIPIDS AND EFFECTS ON CONFORMATION

6.1 Introduction

A striking feature of biological membranes is that the membrane components are asymmetrically distributed between the two surfaces. For proteins, the asymmetry is generally absolute; every copy has the same orientation in the membrane (Janmey, 1995). Similarly, there is an asymmetry in the distribution of lipid molecules between the two layers of the cytoplasmic membrane. Generally, lipids with neutral or negative polar head groups, such as phosphatidylethanolamine (PE), phosphatidylserine (PS) and the phosphatidylinositols (PI) are preferentially located in the cytoplasmic leaflet. In contrast the zwitterionic lipid, phosphatidylcholine (PC) and sphingomyelin are located preferentially in the extracellular leaflet (Figure 6.1) (Cullis et al., 1996).

Membrane asymmetry is regulated by several factors including membrane voltage, electrostatic binding to intracellular protein and components of the cytoskeleton, and through the cooperative activities of three transporter proteins; the ATP-dependent aminophospholipid-specific translocase, ATP-dependent lipid flippase which slowly transports mainly PC and sphingomyelin from the inner-to-outer leaflet of the cell, and the Ca^{2+}-dependent non-specific lipid-scramblase which allows lipids to move randomly between the two leaflets (Maksymiw et al., 1987; Janmey, 1995). The role of lipid asymmetry is not completely understood; one possibility is that PE and PS may be required to maintain a fusion competent surface for exo and endocytosis, organelle fusion and cell division (Cullis et al., 1996; Epand, 1998), whereas the appearance of PS in the external leaflet of the cell membrane is diagnostic of cells entering apoptotic pathways (Dowhan and Bogdanov, 2002).

The cell membrane contains many different species of lipid and lipid asymmetry could have important effects on the function of transmembrane-spanning proteins, which are sensitive to and can be regulated by properties of the lipid bilayer such as bilayer thickness, acyl chain composition and head group interactions. The bilayer interfaces are approximately 15 Å thick on either side of the membrane and possess a

steep gradient in hydrophobicity from the highly apolar hydrocarbon core of the bilayer to the highly polar, aqueous region (White et al., 2001). Possibilities for many complex interactions, including hydrogen bonding and dipole-dipole interactions, are provided by the ester carbonyls of the lipid molecules, the lipid head groups and water bound ions located around the head groups (Dowhan and Bogdanov, 2002). Electrostatic interactions are also possible between negatively charged head groups and positively charged amino acid residues. Some membrane proteins also contain specific binding pockets for lipid head groups (Lee, 2003). More than 50 membrane proteins have been shown to require a specific phospholipid for optimal function following purification and reconstitution; lipid head groups are known to alter the activity of transmembrane proteins such as receptors, transporters and ion channels, in addition to cytoskeletal proteins and peripheral proteins (Fairman et al., 1998; Lee, 1998; van der Heide et al., 2001; Valiyaveetil et al., 2002).

Bilayer asymmetry has also been shown to have important affects on the gating properties of EcMscL *in vivo*, since incorporation of lysophosphatidylcholine (LPC) to one side of the membrane only causes the channel to open; the effects being reversed on incorporation of LPC into the opposite side of the membrane (Martinac et al., 1990). In addition, gating of both EcMscL and TbMscL is easier when the proteins are reconstituted into asolectin vesicles instead of spheroplasts, with the channels requiring lower patch clamp pressures to open (Moe et al., 2000); bilayer thickness has also been shown to alter channel gating, EcMscL gating at lower threshold when reconstituted into thinner membranes (Perozo et al., 2002b). The data from these experiments suggest that interactions between the channel and surrounding lipid are central to gating of MscL.

6.1.1 Chapter 6 Overview

Fluorescence quenching studies with brominated phospholipids will provide information only about lipid interactions in the vicinity of that Trp residue; thus changing the location of the Trp residue will provide information about lipid interactions with a variety of sites on the protein, depending on the location of the Trp residue. In order to study the lipid-protein interactions for the TbMscL channel on

either side of the bilayer, a Trp residue was introduced at residue Leu-69, located towards the periplasmic end of TM2 and a Trp residue was also introduced at residue Tyr-87, located towards the cytoplasmic end of TM2, thereby providing two TbMscL channels with Trp reporter groups at different locations of the protein and on either side of the bilayer leaflet (Figure 6.2).

A cluster of three positively charged residues, Arg-98, Lys-99 and Lys-100, is located on the cytoplasmic side of TbMscL (Figure 6.2), in a position where they could interact with the head group of an anionic phospholipid. These residues were mutated to Gln on F80W-TbMscL. The lipid binding constants were determined for single and triple charge mutants and compared to the data obtained with the F80W channel alone, which retains the Arg-98, Lys-99 and Lys-100 charge cluster (Chapter 4).

6.2 Materials and Methods

All chemicals were obtained from Sigma or BDH with the following exceptions:

Avanti Polar Lipids

1,2-dioleoyl-sn-glycero-3-phosphatdic acid (di(C18:1)PA)
1,2-dioleoyl-sn-glycero-3-phosphatidylcholine (di(C18:1)PC)
1,2-dioleoyl-sn-glycero-3-phosphatidylethanolamine (di(C18:1)PE)
1,2-dioleoyl-sn-glycero-3-phosphatidylserine (di(C18:1)PS)
1,1'2,2'-tetraoleoyl cardiolipin (tetra(C18:1)CL)

Anatrace, Anagrade®

n-Octyl-β-D-glucopyranoside (Octylglucoside)

Calbiochem, Ultrol® Grade

N-(2-hydroxyethyl)piperazine-N'-(2-ethyanesulphonic acid) (Hepes)
1,3-diaza-2,4-cyclopentadiene (Imidazole)

6.2.1 *TbmscL* Mutation

The pET-19b plasmid containing the *Mycobacterium tuberculosis* F80W-*mscL* gene was used as a template for site directed mutagenesis, using the QuickChange™ protocol, as outlined in Section 2.2.5.2, and the synthetic oligonucleotide primers in Table 2.7. The mutation of Leu-69 and Tyr-87 to Trp residues has previously been described in Section 5.2.1.

6.2.2 Bioassay

6.2.2.1 *In vivo Channel Function Assay*

Loss of function (LOF) mutants were detected through a reduced or total inability to rescue *E. coli* knock-out strain MJF465 from hypoosmotic stress, following induction of TbMscL production with IPTG, as described in Section 5.2.2.1.

6.2.2.2 *Growth Curve Studies*

Gain of function (GOF) mutants were detected by a reduced rate of growth after induction of TbMscL production with IPTG, as described in Section 5.2.2.2.

6.2.3 Protein Expression and Purification

E. coli BL21(λDE3)pLysS transformants carrying the pET-19b plasmid (Novagen) with the mutated *TbmscL* gene were grown in 6 l Luria broth to mid-log phase (absorbance at 600 nm of 0.6) and then induced for 3 h in the presence of isopropyl-β-D-thiogalactopyranoside (1.0 mM). *E. coli* BL21(λDE3)pLysS transformants harbouring GOF mutants of TbMscL, identified through growth curve studies, were grown in large scale, typically 60 l Luria broth to late-log phase (absorbance at 600 nm of 1.1) and then induced for 80 min in the presence of isopropyl-β-D-thiogalactopyranoside (1.0 mM). TbMscL was purified as described in Section 2.2.4.

6.2.4 Reconstitution

Purified TbMscL was reconstituted into lipid bilayers by mixing lipid and TbMscL in cholate, followed by dilution into buffer, as described in Section 4.2.10.1.

6.2.5 Steady-State Fluorescence Measurements

Trp fluorescence was recorded for 0.98 μM TbMscL in buffer (20 mM Hepes, 100 mM KCl, 1 mM EGTA, pH 7.2) at 25 °C, using an SLM 8100 fluorimeter, with excitation at 280 nm, as described in Section 3.5. Emission intensity corrected fluorescence spectra were fitted to skewed Gaussian curves, also described in Section 3.5.

6.3 Results

6.3.1 Bioassays

6.3.1.1 *Downshock Assay*

The osmotic downshock assay developed in Chapter 5 was used to confirm functionality of the mutated TbMscL channels. WT and mutant TbMscL channels were expressed in the mechanosensitive channel free bacterial strain MJF465 (Section 2.2.1.4). As shown in Figure 6.3, all mutated *TbmscL* genes rescue the *E. coli* strain from the effects of hypoosmotic stress following induction of the channels with IPTG, confirming that the channels are active.

6.3.1.2 *Growth Curve Assay*

GOF mutants are detected by a reduced rate of growth of *E. coli* expressing the *TbmscL* genes, causing a change in the shape of the growth curve and a reduced optical density when the cells reach steady state, compared to WT channel (Yoshimura et al., 1999; Moe et al., 2000). Figure 6.4 shows the growth profiles of *E. coli* expressing mutated TbMscL channels. Growth curves for F80W, F80W:K99Q and F80W:K100Q are clustered at the top of the graph together with WT channel, confirming that growth rates are unaffected by expression of the mutant TbMscLs. Similarly, the growth curves for F80W:R98Q and the double charge mutant F80W:K99Q:K100Q are located towards the top of the graph, although the rate of growth appears slightly affected. However, double charge mutants F80W:R98Q:K99Q and F80W:R98Q:K100Q show a reduced rate of growth following induction with IPTG, suggesting that F80W:R98Q:K99Q and F80W:R98Q:K100Q are forming channels that could be slightly easier to open than the WT channel and that the effect of removing the charge cluster is cumulative. Removing all three positively charged groups from the cytoplasmic region of the protein, giving the mutant F80W:R98Q:K99Q:K100Q, causes a marked reduction in the growth of rate, consistent with a channel in an open or open-intermediate state, requiring lower levels of membrane tension to become fully open (Yoshimura et al., 1999). In all cases, mutant channels containing the R98Q charge neutralisation show

the greatest affect on the rate of growth, suggesting that R98 has a dominant role. A possible explanation is the fact that the guanidinium group of Arg is able to form a bidentate interaction compared to the single interaction formed by the amino group of a Lys residues, and therefore loss of a single Arg would be more severe than loss of a single Lys residue.

Y87W-TbMscL shows a slightly altered growth profile from that of the F80W-TbMscL, but the growth curve is still located towards the top of the graph (Figure 6.5); expression and purification of the Y87W was unaffected (See Figure 5.7). In contrast to F80W which has no effect on growth curves, Y87W contributes a slight GOF profile. The single and double site charge mutants of Y87W shown in Figure 6.5 had a greater affect on the rate of growth of *E. coli*, than the equivalent charge mutants made using the F80W-*TbmscL* template. Therefore, Y87W-*TbMscL* could not be used as a template for the charge mutations, as the single charge mutants of Y87W may represent open-intermediates of the channel and so analysis and interpretation of the lipid binding data for the surface of TbMscL would be complicated, and expression and purification of these mutant channels in milligram quantities would be impractical. However, the data obtained with Y87W and the charge mutants of the Y87W channel, further supports the accumulative effect observed with double and triple charge mutants of the F80W channel.

6.3.2 Fluorescence Spectroscopy

TbMscL was reconstituted into bilayers of di(C18:1)PC to give a 100:1 molar ratio of phospholipid to TbMscL, and the intensity corrected emission spectra (Figure 6.6) were fitted to skewed Gaussian curves to give the parameters listed in Table 6.1. The Trp residue in F80W-TbMscL is located in the middle of the bilayer with an emission maximum (λ^{max}) in di(C18:1)PC of 321.0 ± 0.1. Charge mutants of F80W-TbMscL, where positively charged residues were clustered on the cytoplasmic region of TbMscL were replaced with uncharged Gln residues, show a red shift (Table 6.1). The biggest red shift was observed for F80W:R98Q:K99Q:K100Q, suggesting that removal of these positively charged residues, individually or collectively, causes the Trp residue at position 80 to move to a more polar environment (Figure 6.6 and Table 6.1).

6.3.3 Fluorescence Quenching of TbMscL by Brominated Phospholipids

TbMscL was reconstituted into bilayer fragments by the dilution method as described Section 4.2.10.1, using the detergent cholate, at a molar ratio of lipid-protein of 100:1. Fluorescence quenching curves for Trp mutants of TbMscL in mixtures of a brominated and the corresponding non-brominated phospholipid were determined and the results are shown in Figures 6.7-6.9. The fluorescence intensity is plotted as F/F_o, where F is the fluorescence intensity at intermediate fractions of brominated phospholipid and F_o is the fluorescence intensity when the mole fraction of non-brominated phospholipid is 1. The data shown in these figures were fitted to Equation 3.11, giving the values of n listed in Tables 6.2 and 6.3. The results in Figures 6.7-6.9 show that fluorescence intensities decrease with increasing mole fraction of brominated lipid. The maximum levels of fluorescence quenching of mutants of TbMscL in brominated anionic phospholipids, in particular di(Br_2C18:0)PA, are slightly greater than in di(Br_2C18:0)PC; the values for n for all phospholipids are very similar except for PA and CL where the small head group and number of chains, respectively, effect the values of n for these lipids, as described in Section 4.3.7.

6.3.4 Relative Phospholipid Binding Constants for TbMscL

6.3.4.1 *Bilayer Interfaces*

In Section 4.3.8 the binding constants for phospholipids were measured using F80W-TbMscL. The Trp reporter group in the F80W-TbMscL channel is located in the centre of the bilayer and therefore provides information about how phospholipids interact with the overall hydrophobic surface of the protein. By moving the Trp reporter group to either side of the membrane, phospholipid binding constants can be determined selectively for each side of the membrane leaflet. Residues Leu-69 and Tyr-87 located on the periplasmic and cytoplasmic regions of TbMscL were mutated

to Trp residues (See Chapter 5), and the phospholipid binding constants were determined for each mutant.

Fluorescence quenching curves for L69W-TbMscL and Y87W-TbMscL in mixtures of phosphatidylcholine and phosphatidylethanolamine are shown in Figure 6.10. The binding constants for di(C18:1)PE relative to di(C18:1)PC are close to 1 for both L69W and Y87W TbMscL channels (Figure 6.10, Table 6.4); consistent with the binding affinity of 1 determined using F80W-TbMscL channel (Table 4.7), and confirms simple competitive binding of phosphatidylcholine and phosphatidylethanolamine to the lipid binding sites on TbMscL.

Binding constants for the anionic lipids phosphatidylserine and phosphatidic acid on the periplasmic surface of the TbMscL (L69W) obtained from experiments with di(Br_2C18:0)PC and nonbrominated anionic phospholipids are the same and are also close to 1 (Figure 6.11, Table 6.4). The reciprocal nature of the binding constants obtained using L69W are consistent with simple competition between phosphatidylcholines and anionic lipids for the periplasmic surface of TbMscL. For cardiolipin, a smaller binding constant was obtained from experiments with mixtures of di(C18:1)PC and tetra(Br_2C18:0)CL than with di(Br_2C18:0)PC and tetra(C18:1)CL (Figure 6.11, Table 6.4), but interpretation of this effect is complicated by the fact that cardiolipin contains for fatty acyl chains compared to the two in phosphatidylcholine.

Results obtained with Y87W are significantly different to those obtained with L69W. Binding constants for anionic lipids on the cytoplasmic surface of the TbMscL (Y87W) obtained from experiments with mixtures of di(Br_2C18:0)PC and nonbrominated anionic lipids are significantly different from those obtained from experiments with mixtures of di(C18:1)PC and brominated anionic lipid (Figure 6.11, Table 6.4). The marked quenching observed in mixtures with brominated anionic lipids suggests that brominated anionic lipids bind strongly to the cytoplasmic surface of TbMscL, but the experiments with nonbrominated anionic lipids suggest that nonbrominated anionic lipids are unable to displace di(Br_2C18:0)PC from around TbMscL with the efficiency expected from the experiments with brominated anionic lipids. The strongest binding for anionic lipids with the cytoplasmic surface of

TbMscL using Y87W was observed for di(Br_2C18:0)PA with a binding constant of 4.42 (Table 6.4).

In Chapter 4, lipid binding affinities were determined as a function of lipid head groups for F80W-TbMscL; anionic lipids were shown to bind with greater affinity than the zwitterionic lipids PC or PE. The binding constants determined with F80W-TbMscL are smaller than those determined with Y87W-TbMscL, since F80W is located deep within the membrane and therefore the binding constant reported by F80W represents an average for the two sides of the membrane.

The nonreciprocal binding constants determined for anionic lipids with Y87W-TbMscL are consistent with those obtained for anionic lipids with F80W-TbMscL (Table 4.7). The most obvious explanation for this result is that there are two classes of binding sites around TbMscL for anionic phospholipid, one class of sites showing a higher affinity for anionic lipids than the other. Since quenching by brominated lipids on the cytoplasmic side of the membrane fits to a value of n close to 2 (Table 6.2), the data were also analysed in terms of a two site model with equal quenching of Trp fluorescence from the two sites (Section 3.7.2). The data shown in Figure 6.12 were fitted to Equation 3.22 by an iterative procedure using the nonlinear least-squares routine in the SigmaPlot, to give the values for the relative binding constants at the two sites given in Table 6.5. The data obtained with cardiolipin cannot be fitted to the two site model, since, as a four-chain molecule, cardiolipin will bind simultaneously to both sites, as shown by its value for n close to 1 (Table 6.2).

6.3.4.2 *Charge Mutants*

The three cationic residues Arg-98, Lys-99, and Lys-100 in each monomer of TbMscL form a cluster on the cytoplasmic side of the membrane in a position where they could interact strongly with an anionic lipid head group. These three residues were mutated individually in F80W to Gln, and a triple mutant was also prepared. Trp fluorescence emission spectra were recorded for the mutants reconstituted into bilayers of di(C18:1)PC, using the environmental sensitivity of Trp fluorescence emission to look for possible changes in conformation. The fluorescence emission maximum for F80W reconstituted into bilayer of di(C18:1)PC is 321 nm,

characteristic of a very hydrophobic environment for the Trp residue (Table 6.1). In contrast, the fluorescence emission maximum for F80W:V21K is shifted ca. 11 nm to longer wavelength, suggesting a major conformation change between the closed and open forms of MscL, affecting the location of the Trp residue introduced at position 80. Mutation of Arg-98, Lys-99 or Lys-100 in F80W resulted in 5–8 nm increases in fluorescence emission maxima (Table 6.1), suggesting that these single charge mutations also result in significant structural changes in the channel, even though the growth studies shown in Figure 6.4 suggest that the mutations do not result in a gain of function phenotype. The observation of a fairly constant peak width for the mutants (Table 6.4) suggests that the mutated protein adopts one major conformational state in di(C18:1)PC, since a mixture of conformations, each with different Trp fluorescence emission characteristics, would have resulted in a broader peak (Ladokhin et al., 2000).

Replacing these three residues with uncharged Gln residues, either individually or collectively has little effect on the value of n (Table 6.3). Values of n are very similar for all the lipids and all the mutants except for tetra(Br_2C18:0)CL for which the value of n is about half that for the other phospholipids, consistent with the four-chain structure of cardiolipin compared to the two-chain structure of the other phospholipids.

As discussed in Chapter 4, binding constant obtained from experiments with di(Br_2C18:0)PA are greater than that obtained from experiments with di(Br_2C18:0)PC (Table 6.6), consistent with the presence of at least two classes of binding site on TbMscL from which the fluorescence of Trp-80 can be quenched, one with a higher relative binding constant for phosphatidic acid than the other. Mutation of Arg-98, Lys-99 or Lys-100 results in a ca. 50 % decrease in affinity for phosphatidic acid, now with no significant difference between the affinities measured with di(Br_2C18:0)PC and with di(Br_2C18:0)PA (Figure 6.13 and Table 6.6). Simultaneous mutation of all three charged residues results in a reduction of the relative binding constant for phosphatidic acid to a value of close to 1, showing a loss of selectivity for phosphatidic acid, and that these lipids now bind through a simple competitive binding model (Figure 6.13 and Table 6.6). Selectivity of F80W for phosphatidylserine is less than that for phosphatidic acid but again mutation of

charged residues, particularly Lys-99 and Lys-100, results in a loss of specificity for phosphatidylserine (Figure 6.13 and Table 6.6). Results with cardiolipin are again, more difficult to interpret since cardiolipin will occupy two two-chain lipid binding sites on MscL, but any specificity in binding cardiolipin is less than for the other anionic phospholipids (Figure 6.13C and Table 6.6).

TbMscL Mutant	Phospholipid					
	PC		PS		PA	
	λ^{max} (nm)	ω (nm)	λ^{max} (nm)	ω (nm)	λ^{max} (nm)	ω (nm)
F80W	321.0 ± 0.1	45.9 ± 0.2	321.1 ± 0.1	40.8 ± 0.2	320.9 ± 0.1	43.2 ± 0.2
F80W:R98Q	328.5 ± 0.1	52.6 ± 0.1	326.0 ± 0.1	54.1 ± 0.2	324.2 ± 0.1	55.4 ± 0.3
F80W:K99Q	326.9 ± 0.1	49.4 ± 0.2	323.7 ± 0.1	52.2 ± 0.2	323.9 ± 0.1	54.0 ± 0.3
F80W:K100Q	325.7 ± 0.2	46.4 ± 0.2	323.8 ± 0.1	49.5 ± 0.2	321.6 ± 0.1	49.2 ± 0.3
F80W:R98Q:K99Q:K100Q	332.4 ± 0.1	58.2 ± 0.2	-	-	-	-

Table 6.1 Fluorescence properties of TbMscL Trp mutants reconstituted with 1,2-dioleoyl-sn-glycero-3-phospholipids. PC, phosphatidylcholine, PS, phosphatidylserine and PA, phosphatidic acid. λ^{max} and ω are the wavelength of maximum emission and the peak width at half height respectively, determined by fitting the fluorescence emission spectra shown in Figure 6.6 to Equation 3.8. The values for F80W-TbMscL are taken from Table 5.2.

Phospholipid	F/F_o	n
	Periplasmic: L69W	
di(C18:1)PC	0.49 ± 0.01	1.79 ± 0.09
di(C18:1)PE	0.56 ± 0.02	1.80 ± 0.23
di(C18:1)PS	0.42 ± 0.01	2.29 ± 0.14
di(C18:1)PA	0.33 ± 0.01	2.26 ± 0.14
tetra(C18:1)CL	0.39 ± 0.02	1.10 ± 0.09
	Cytoplasmic: Y87W	
di(C18:1)PC	0.34 ± 0.01	1.75 ± 0.08
di(C18:1)PE	0.38 ± 0.02	1.35 ± 0.12
di(C18:1)PS	0.16 ± 0.01	1.93 ± 0.10
di(C18:1)PA	0.23 ± 0.02	2.05 ± 0.19
tetra(C18:1)CL	0.29 ± 0.01	1.01 ± 0.04

Table 6.2 Fluorescence quenching of Trp mutants of TbMscL in brominated phospholipids as a function of lipid head group. F_0 and F are fluorescence intensities for TbMscL reconstituted in nonbrominated phospholipid and the corresponding brominated phospholipid respectively, measured at pH 7.2. The value of n is the value obtained by fitting the data in Figure 6.7 to Equation 3.11.

Phospholipid	F/F_o	n
	F80W	
di(C18:1)PC	0.19 ± 0.01	2.54 ± 0.10
di(C18:1)PS	0.12 ± 0.01	2.95 ± 0.22
di(C18:1)PA	0.11 ± 0.01	3.62 ± 0.27
tetra(C18:1)CL	0.09 ± 0.01	1.25 ± 0.02
	F80W:R98Q	
di(C18:1)PC	0.37 ± 0.02	2.40 ± 0.22
di(C18:1)PS	0.28 ± 0.02	2.39 ± 0.19
di(C18:1)PA	0.25 ± 0.02	2.41 ± 0.17
tetra(C18:1)CL	0.25 ± 0.02	1.14 ± 0.08
	F80W:K99Q	
di(C18:1)PC	0.32 ± 0.02	2.19 ± 0.16
di(C18:1)PS	0.31 ± 0.02	2.88 ± 0.24
di(C18:1)PA	0.24 ± 0.02	2.76 ± 0.21
tetra(C18:1)CL	0.28 ± 0.02	1.34 ± 0.09
	F80W:K100Q	
di(C18:1)PC	0.25 ± 0.01	2.33 ± 0.06
di(C18:1)PS	0.24 ± 0.01	2.96 ± 0.15
di(C18:1)PA	0.16 ± 0.02	2.84 ± 0.24
tetra(C18:1)CL	0.20 ± 0.03	1.32 ± 0.11
	F80W:R98Q:K99Q:K100Q	
di(C18:1)PC	0.27 ± 0.02	2.33 ± 0.20
di(C18:1)PS	0.25 ± 0.02	2.29 ± 0.16
di(C18:1)PA	0.13 ± 0.01	3.12 ± 0.19
tetra(C18:1)CL	0.24 ± 0.02	1.23 ± 0.07

Table 6.3 Fluorescence quenching of TbMscL mutants in brominated phospholipids as a function of lipid head group. F_o and F are fluorescence intensities for TbMscL reconstituted in nonbrominated phospholipid and the corresponding brominated phospholipid respectively, measured at pH 7.2. The value of n is the value obtained by fitting the data in Figures 6.7 and 6.8 to Equation 3.11. Data for F80W-TbMscL is taken from Table 4.5.

Phospholipid	Relative binding constant measured using di(Br_2C18:0)PC	Relative binding constant measured using di(C18:1)PC
	Periplasmic: L69W	
di(C18:1)PE	1.16 ± 0.24	0.90 ± 0.17
di(C18:1)PS	1.30 ± 0.06	1.00 ± 0.15
di(C18:1)PA	1.03 ± 0.14	1.12 ± 0.08
tetra(C18:1)CL	0.83 ± 0.04	0.52 ± 0.05
	Cytoplasmic: Y87W	
di(C18:1)PE	0.92 ± 0.05	1.21 ± 0.20
di(C18:1)PS	1.79 ± 0.13	2.96 ± 0.27
di(C18:1)PA	2.60 ± 0.20	4.42 ± 0.17
tetra(C18:1)CL	2.46 ± 0.14	1.91 ± 0.15

Table 6.4 Relative lipid binding constants for the periplasmic and cytoplasmic surface of TbMscL as a function of lipid head group. Binding constants relative to di(C18:1)PC were calculated from quenching data for TbMscL mutants in mixtures of di(Br_2C18:0)PC with non-brominated lipid or di(C18:1)PC with brominated lipid, at pH 7.2, using the values for n given in Table 6.2. For tetra(C18:1)CL the mole fraction was calculated based on the number of moles of fatty acyl chains to account for the fact that tetra(C18:1)CL contains four chains and di(C18:1)PC contains two chains, and correspondingly the value for n used in the analysis was consequently double that given in Table 6.2.

Phospholipid	Relative Lipid Binding Constant	
	Site 1	Site 2
di(C18:1)PS	1.23 ± 0.11	5.02 ± 0.61
di(C18:1)PA	1.69 ± 0.14	8.41 ± 0.54

Table 6.5 Relative lipid binding constants on the cytoplasmic side of the membrane. Binding constants relative to di(C18:1)PC were obtained by fitting the quenching data shown in Figure 6.11 for Y87W-TbMscL in mixtures of di(Br_2C18:0)PC with non-brominated lipid or di(C18:1)PC with brominated lipid to Equation 3.22 using the values for n given in Table 6.2.

Phospholipid	Relative binding constant measured using di(Br_2C18:0)PC	Relative binding constant measured using di(C18:1)PC
	F80W	
di(C18:1)PS	1.66 ± 0.16	1.69 ± 0.10
di(C18:1)PA	1.81 ± 0.21	3.49 ± 0.25
tetra(C18:1)CL	1.52 ± 0.21	0.96 ± 0.06
	F80W:R98Q	
di(C18:1)PS	1.90 ± 0.26	1.20 ± 0.18
di(C18:1)PA	1.16 ± 0.26	1.69 ± 0.28
tetra(C18:1)CL	1.40 ± 0.15	0.73 ± 0.04
	F80W:K99Q	
di(C18:1)PS	1.06 ± 0.06	1.00 ± 0.09
di(C18:1)PA	1.10 ± 0.09	1.38 ± 0.19
tetra(C18:1)CL	1.01 ± 0.08	0.60 ± 0.07
	F80W:K100Q	
di(C18:1)PS	1.35 ± 0.12	1.06 ± 0.16
di(C18:1)PA	1.25 ± 0.22	1.51 ± 0.21
tetra(C18:1)CL	0.94 ± 0.05	0.61 ± 0.03
	F80W:R98Q:K99Q:K100Q	
di(C18:1)PS	1.30 ± 0.10	0.91 ± 0.10
di(C18:1)PA	1.08 ± 0.08	1.07 ± 0.05
tetra(C18:1)CL	1.01 ± 0.09	0.44 ± 0.04

Table 6.6 Relative lipid binding constants for charge mutants of F80W-TbMscL as a function of lipid head group. Binding constants relative to di(C18:1)PC were calculated from quenching data for TbMscL mutants in mixtures of di(Br_2C18:0)PC with non-brominated lipid or di(C18:1)PC with brominated lipid, at pH 7.2, using the values for *n* given in Table 6.3. For tetra(C18:1)CL the mole fraction was calculated based on the number of moles of fatty acyl chains to account for the fact that tetra(C18:1)CL contains four chains and di(C18:1)PC contains two chains, and correspondingly the value for *n* used in the analysis was consequently double that given in Table 6.3. Data for F80W-TbMscL is taken from Table 4.7.

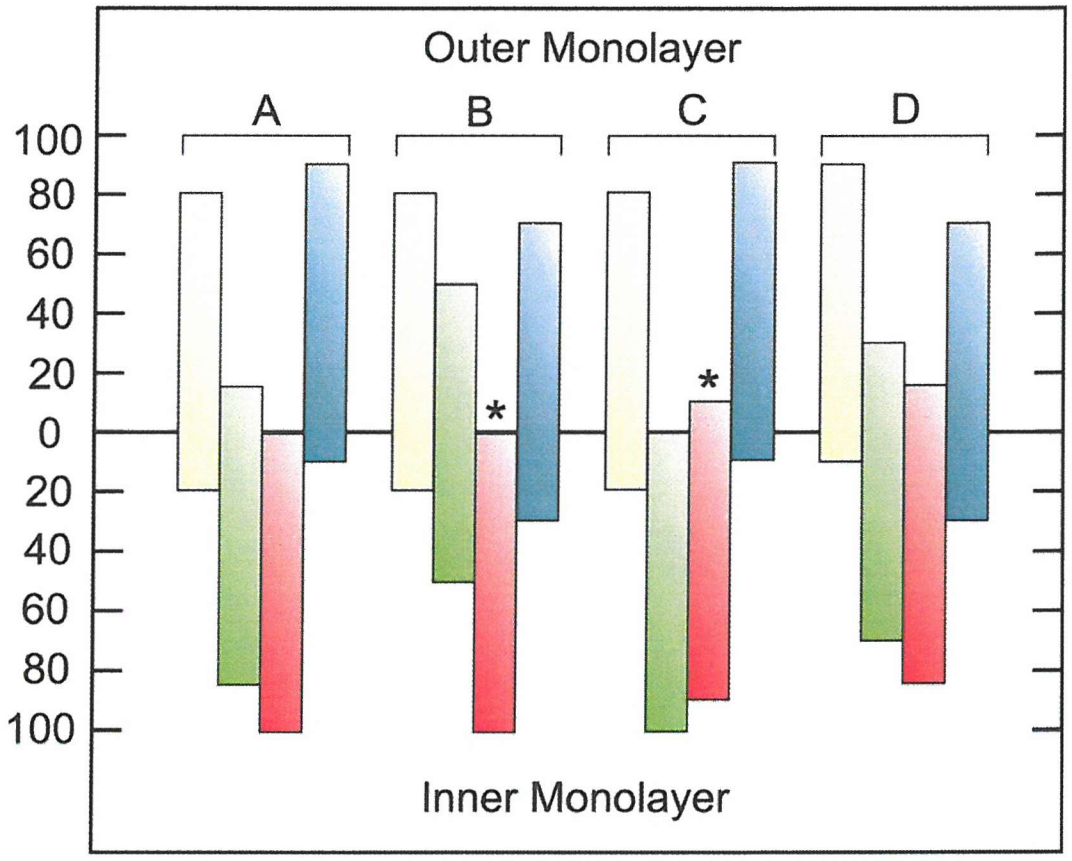

Figure 6.1 Phospholipid asymmetry in plasma membranes. The lipid composition and distribution in the human erythrocyte membrane (A), rat liver blood sinusoidal plasma membrane (B), rat liver plasma membrane (D) and VSV envelope derived from hamster kidney BHK-21 cells are shown. PC (yellow), PE (green), PS (red) where * corresponds to a combination of PS and PI, and sphingomyelin (blue). Taken from Cullis et al. (1996).

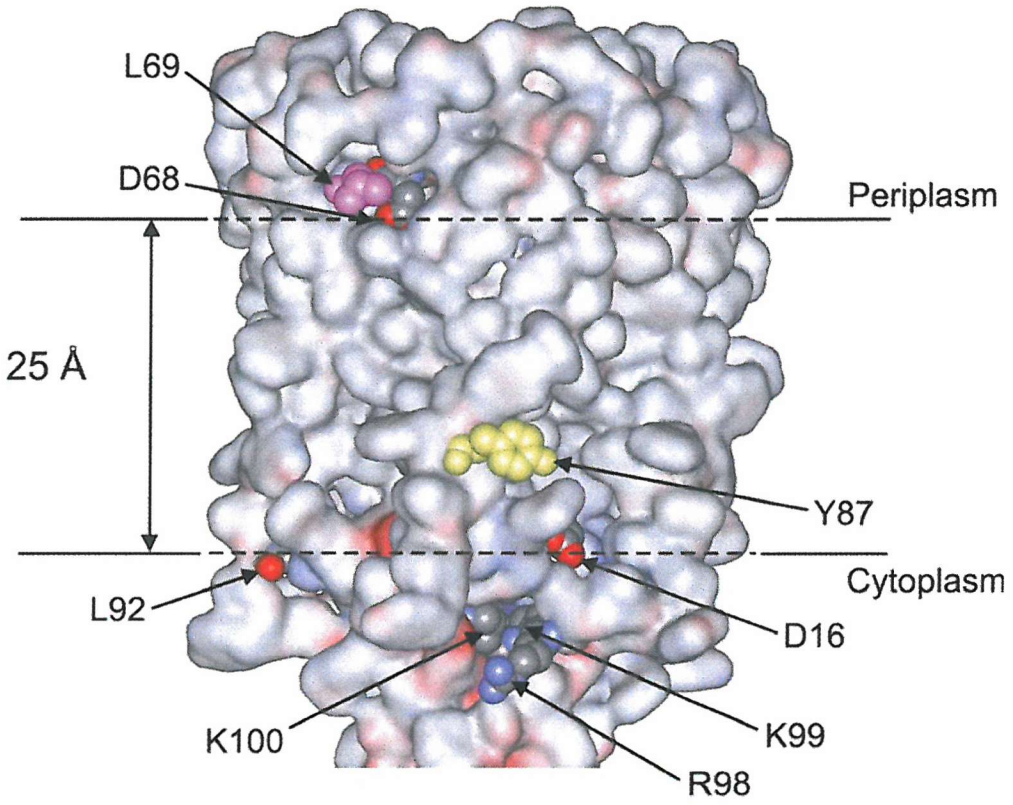

Figure 6.2 Structure of TbMscL viewed from the membrane. The surface of TbMscL is coloured by electrostatic charge, showing the locations of the bilayer interfaces as determined in Chapter 5, marked by the positions of exposed carboxyl groups on Asp-68, Asp-16 and Leu-92. Leu-69 (lilac) and Tyr-87 (yellow) were mutated to Trp residues and used as a reporter groups for the periplasmic and cytoplasmic sides of the channel respectively. Residues forming the conserved charge cluster, Arg-98, Lys-99 and Lys-100 located on the cytoplasmic side of the channel are shown in CPK. The side chain of Lys-100 is not resolved in the crystal structure, and has been modelled in for illustrative purposes. PDB file 1MSL.

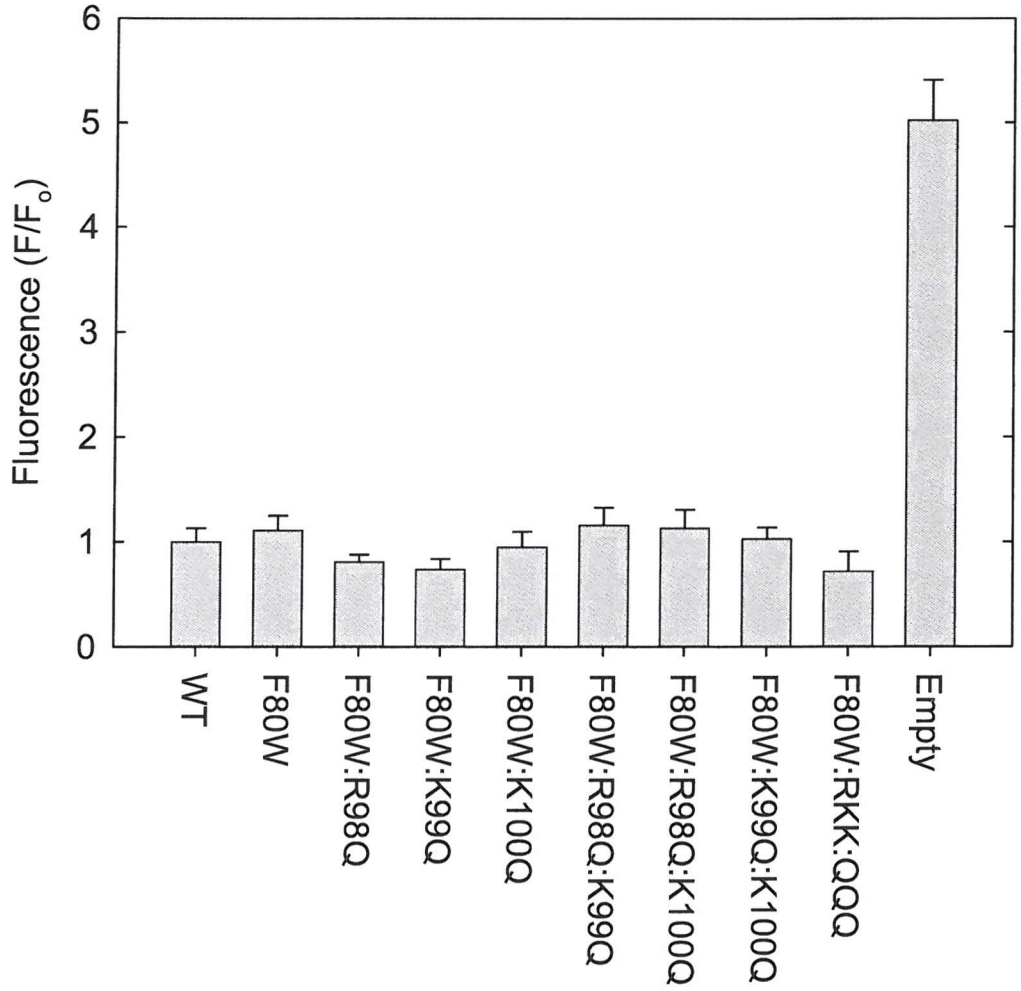

Figure 6.3 Viability of mechanosensitive-null *E. coli* expressing the *TbmscL* genes on an inducible plasmid. *E. coli* MJF465 transformants carrying the pET-19b plasmid with the *TbmscL* gene were grown in the presence of 0.4 M NaCl and induced for 4 with 1 mM IPTG, followed by a hypoosmotic stress via a 60-fold dilution into water containing ethidium bromide (0.5 μg ml^{-1}). The fluorescence intensity of the supernatant was analysed for the release of DNA at 632 nm. Fluorescence intensities are expressed as a ratio with the fluorescence for MJF465 harbouring the WT-*TbmscL* gene. The fluorescence intensity for the release of DNA from the empty MJF465 cell line (no plasmid) is also shown. Intensities are the average of three colonies, the error bars correspond to the standard deviation.

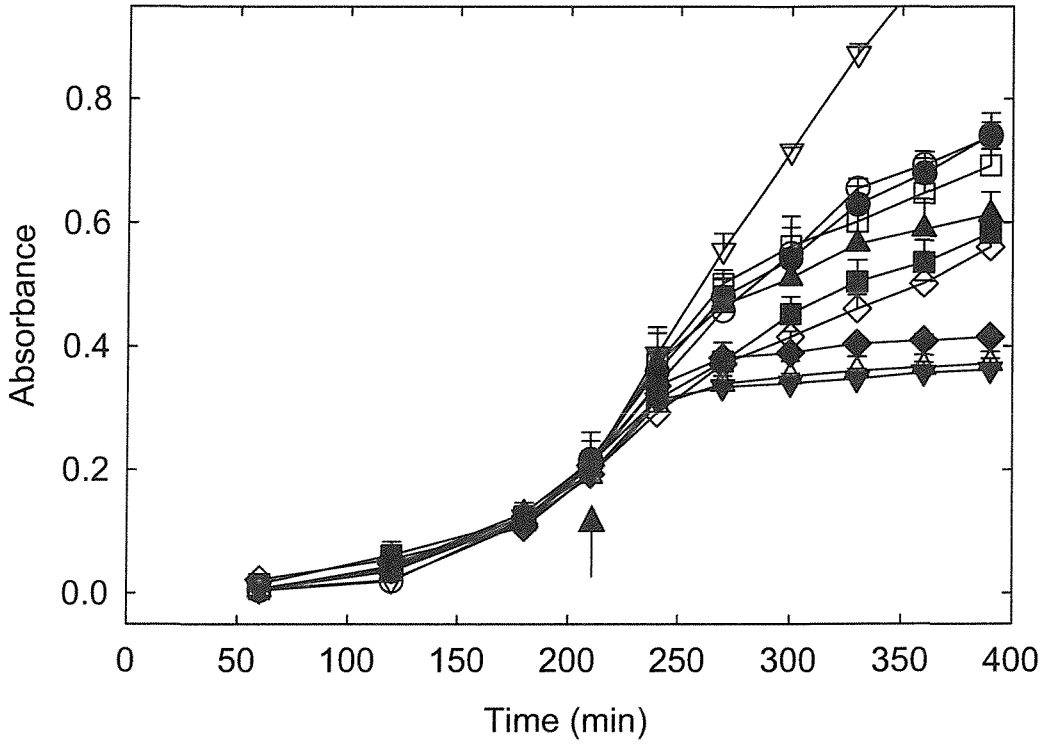

Figure 6.4 Growth of *E. coli* in liquid media expressing the *TbmscL* genes. *E. coli* BL21(DE3)pLysS transformants carrying the pET-19b plasmid with the *TbmscL* genes: (●), WT; (○), F80W; (■), F80W:R98Q; (□), F80W:K99Q; (▲), F80W:K100Q; (△), F80W:R98Q:K99Q; (◆), F80W:R98Q:K100Q; (◇), F80W:K99Q:K100Q; and (▼), F80W:R98Q:K99Q:K100Q were grown at 37 °C in Luria broth medium supplemented with ampicillin (100 μg ml^{-1}). The non-induced growth of (▽), *E. coli* BL21(DE3)pLysS host strain (empty) is also shown. Cells were induced with 1 mM IPTG at an absorbance at 600 nm of ~0.2 (arrow). Data points are the average of five colonies, and the error bars correspond to the standard deviation.

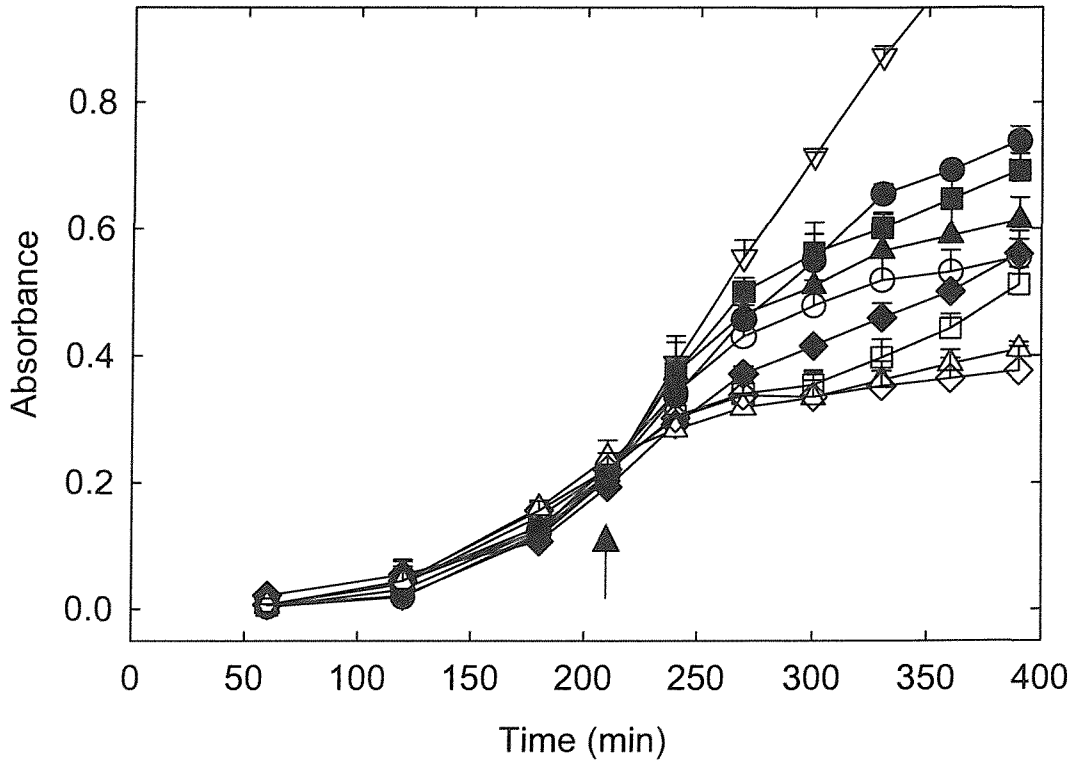

Figure 6.5 Growth of *E. coli* in liquid media expressing the *TbmscL* genes. *E. coli* BL21(DE3)pLysS transformants carrying the pET-19b plasmid with the *TbmscL* genes: (●), F80W; (■), F80W:K99Q; (▲), F80W:K100Q; (◆), F80W:K99Q:K100Q; (○), Y87W; (□), Y87W:K99Q; (△), Y87W:K100Q; and (◇), Y87W:K99Q:K100Q were grown at 37 °C in Luria broth medium supplemented with ampicillin (100 μg ml^{-1}). The non-induced growth of (▽), *E. coli* BL21(DE3)pLysS host strain (empty) is also shown. Cells were induced with 1 mM IPTG at an absorbance at 600 nm of ~0.2 (arrow). Data points are the average of five colonies, and the error bars correspond to the standard deviation.

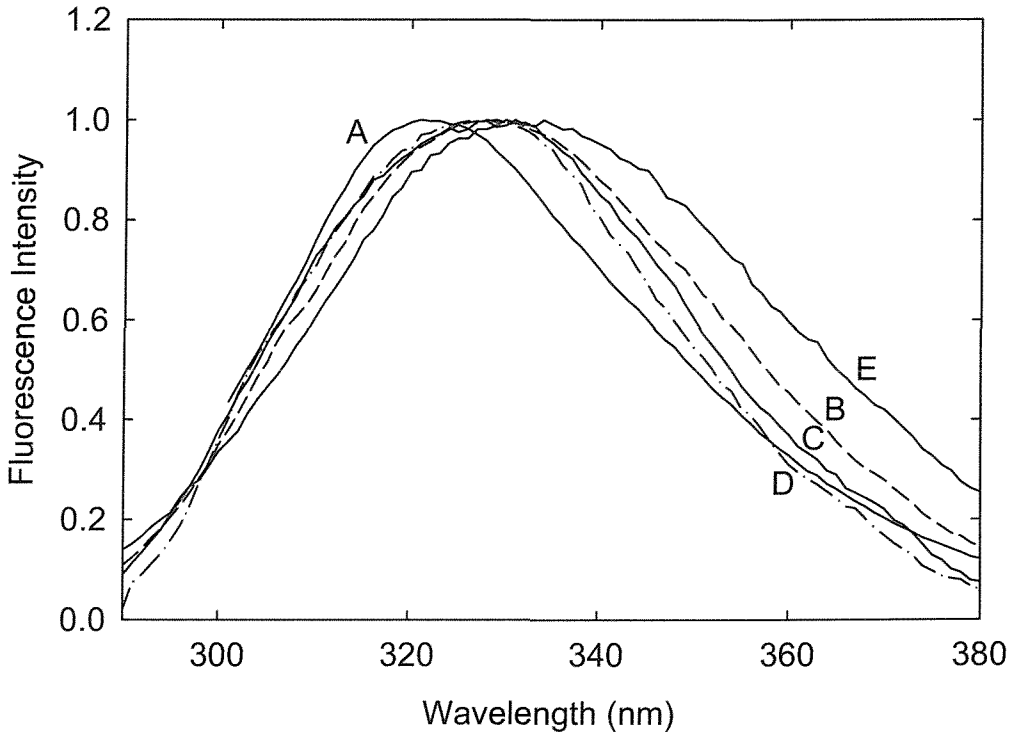

Figure 6.6 Fluorescence emission spectra for charge mutants of F80W-TbMscL in phospholipid bilayers. Intensity corrected fluorescence emission spectra are shown for: (A), F80W; (B), F80W:R98Q; (C), F80W:K99Q; (D), F80W:K100Q; and (E), F80W:R98Q:K99Q:K100Q in di(C18:1)PC. The concentration of TbMscL was 0.98 μM and the molar ratio of lipid to TbMscL was 100:1. The excitation wavelength was 280 nm and the buffer was 20 mM Hepes, 100 mM KCl, 1 mM EGTA, pH 7.2.

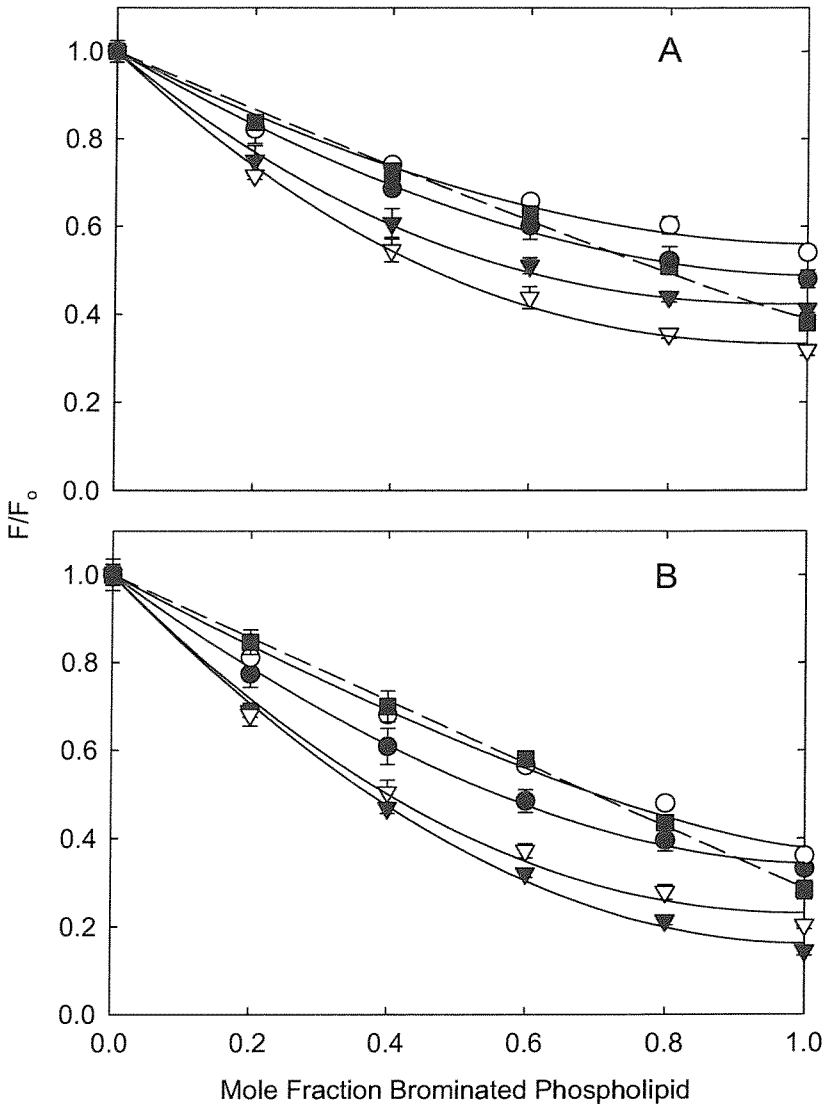

Figure 6.7 Quenching of the fluorescence of Trp mutants of TbMscL by brominated phospholipids. L69W-TbMscL (A) and Y87W-TbMscL (B) were reconstituted into bilayers containing mixtures of nonbrominated lipid and the corresponding brominated lipid, all the lipids having C18 chains. Fluorescence intensities are expressed as a fraction of the fluorescence for TbMscL reconstituted in the nonbrominated lipid. Lipid head groups were as follows: (●), di(C18:1)PC; (○), di(C18:1)PE; (▼), di(C18:1)PS; (▽), di(C18:1)PA; and (■), tetra(C18:1)CL. Data points are the average of three determinations. The lines show fits to Equation 3.11 giving the values for *n* listed in Table 6.2. The concentration of TbMscL was 0.98 μM and the molar ratio of lipid to TbMscL was 100:1.

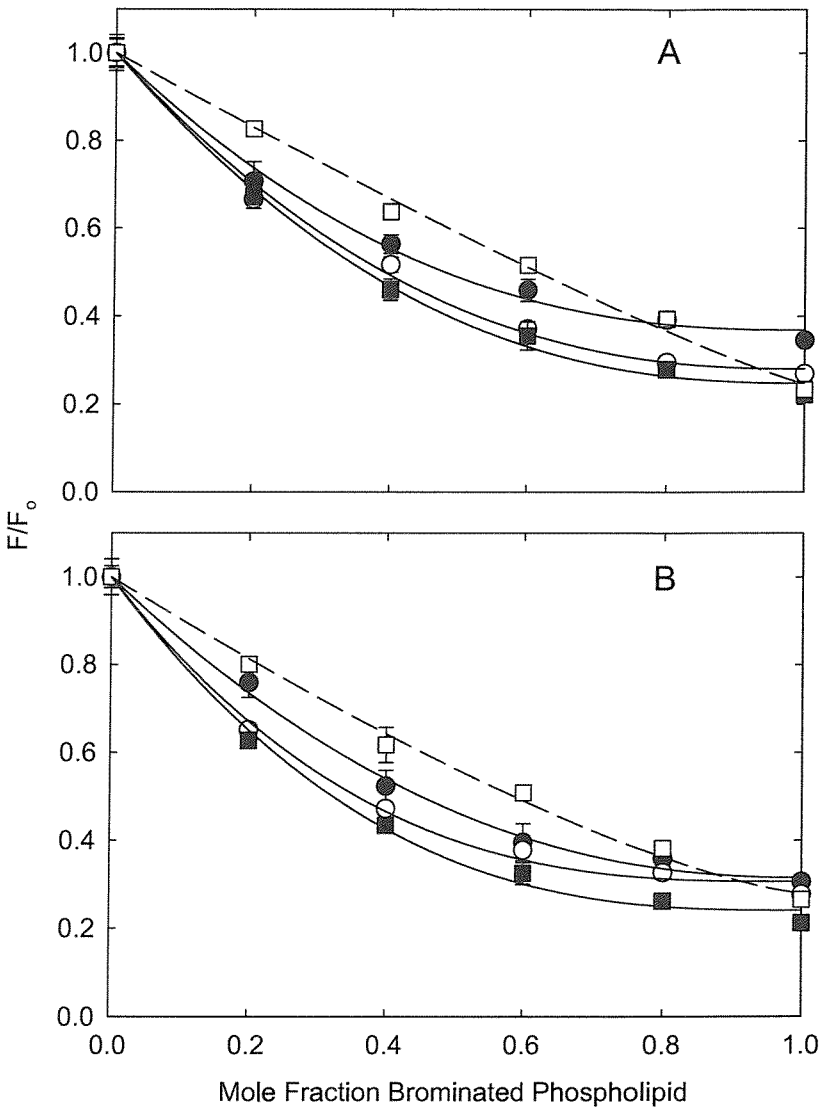

Figure 6.8 Quenching of the fluorescence of charge mutants of F80W-TbMscL by brominated phospholipids. F80W:R98Q-TbMscL (A) and F80W:K99Q-TbMscL (B) were reconstituted into bilayers containing mixtures of nonbrominated lipid and the corresponding brominated lipid, all the lipids having C18 chains. Fluorescence intensities are expressed as a fraction of the fluorescence for TbMscL reconstituted in the nonbrominated lipid. Lipid head groups were as follows: (●), di(C18:1)PC; (○), di(C18:1)PS; (■), di(C18:1)PA; and (□), tetra(C18:1)CL. The lines show fits to Equation 3.11 giving the values for *n* listed in Table 6.3. The concentration of TbMscL was 0.98 μM and the molar ratio of lipid to TbMscL was 100:1.

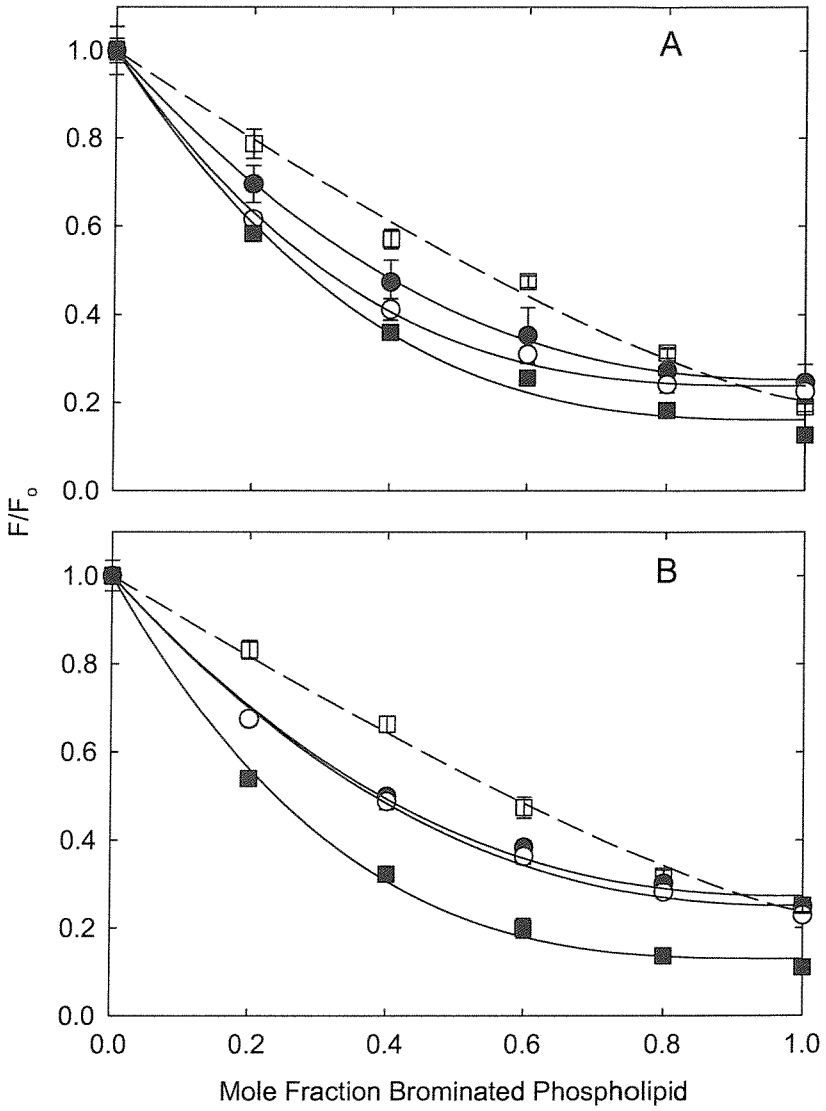

Figure 6.9 Quenching of the fluorescence of charge mutants of F80W-TbMscL by brominated phospholipids. F80W:K100Q-TbMscL (A) and F80W:R98Q:K99Q:K100Q-TbMscL (B) were reconstituted into bilayers containing mixtures of nonbrominated lipid and the corresponding brominated lipid, all the lipids having C18 chains. Fluorescence intensities are expressed as a fraction of the fluorescence for TbMscL reconstituted in the nonbrominated lipid. Lipid head groups were as follows: (●), di(C18:1)PC; (○), di(C18:1)PS; (■), di(C18:1)PA; and (□), tetra(C18:1)CL. Data points are the average of three determinations. The lines show fits to Equation 3.11 giving the values for n listed in Table 6.3. The concentration of TbMscL was 0.98 μM and the molar ratio of lipid to TbMscL was 100:1.

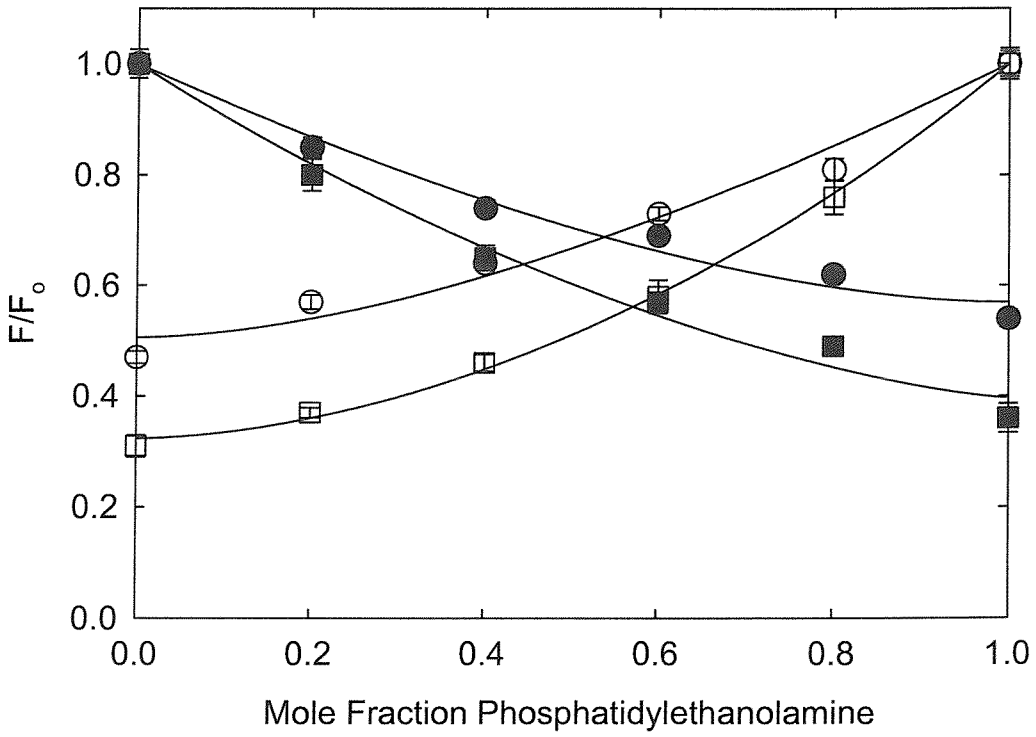

Figure 6.10 Quenching of the fluorescence of Trp mutants of TbMscL in mixtures of phosphatidylethanolamine and phosphatidylcholine. TbMscL mutants L69W (circles) and Y87W (squares) were reconstituted into mixtures containing di(C18:1)PC and (Br_2C18:0)PE (filled), or di(C18:1)PE and di(Br_2C18:0)PC (open). Data points are the average of three determinations. The solid lines show best fits to Equation 3.15 giving the relative binding constants listed in Table 6.4.

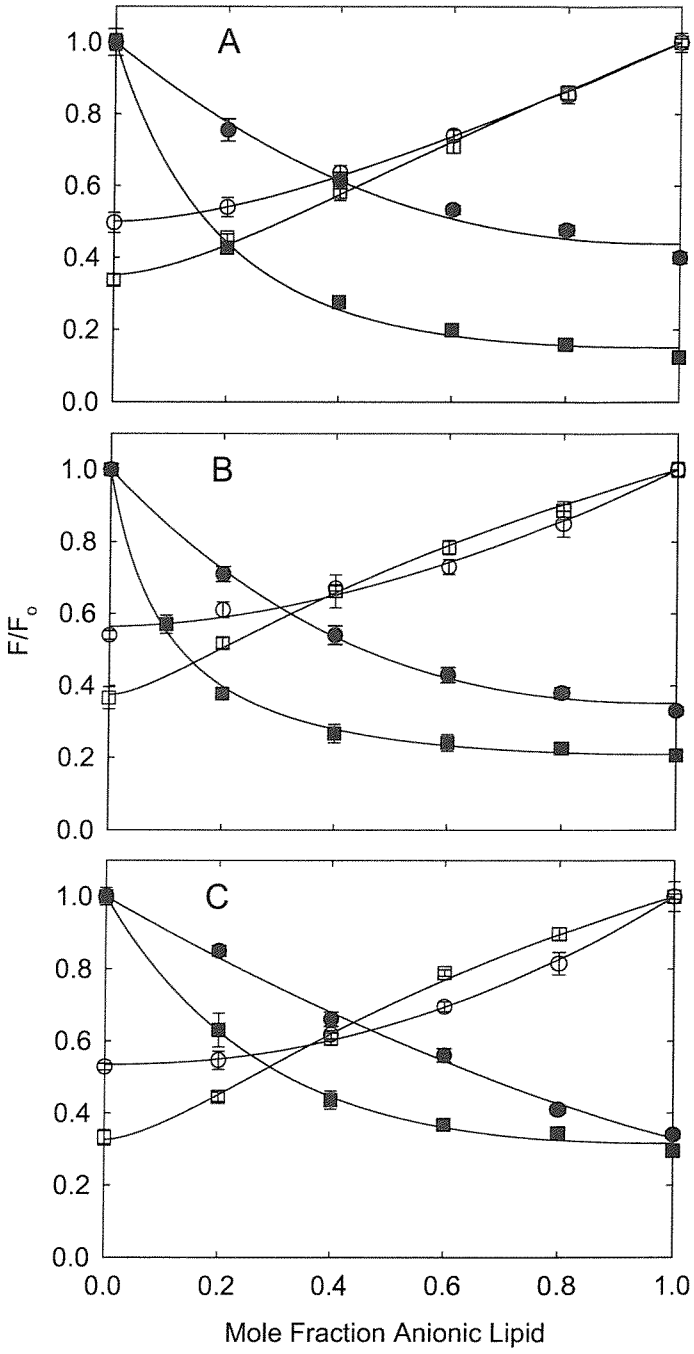

Figure 6.11 Quenching of the fluorescence of Trp mutants of TbMscL in mixtures of anionic lipid and phosphatidylcholine. TbMscL mutants L69W (circles) and Y87W (squares) were reconstituted into mixtures containing di(C18:1)PC and brominated anionic phospholipid (filled), or non-brominated anionic phospholipid and di(Br_2C18:0)PC (open): (A), phosphatidylserine; (B), phosphatidic acid; and (C), cardiolipin. The mole fraction is determined on a lipid chain basis. Levels of fluorescence quenching were corrected for the effect of the anionic head group. The solid lines show best fits to Equations 3.15 for both L69W and Y78W, giving the relative binding constants listed in Table 6.4.

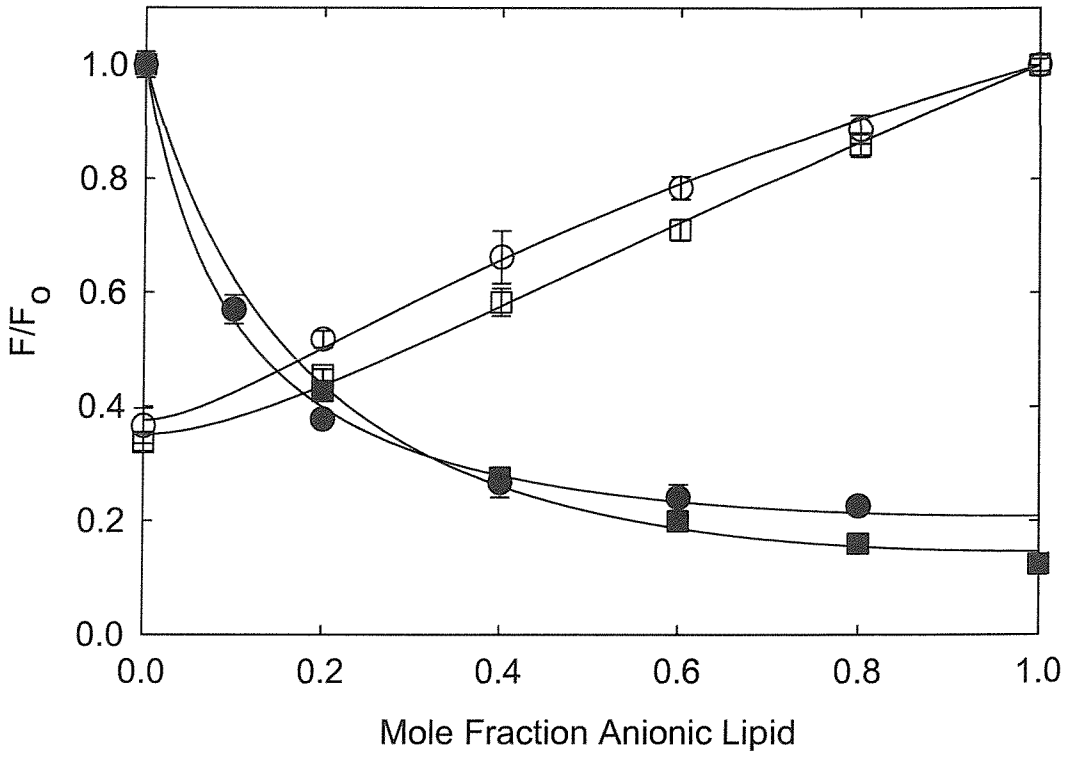

Figure 6.12 Quenching of Trp fluorescence of Y87W in mixtures of phosphatidylcholine and phosphatidylserine or phosphatidic acid. Y87W was reconstituted into mixtures containing di(C18:1)PC and di(Br_2C18:0)PS (■) or di(Br_2C18:0)PA (●), or into mixtures containing di(Br_2C18:0)PC and di(C18:1)PS (□), or di(C18:1)PA (○). The solid lines show best fits to Equation 3.22 giving the relative binding constants listed in Table 6.5.

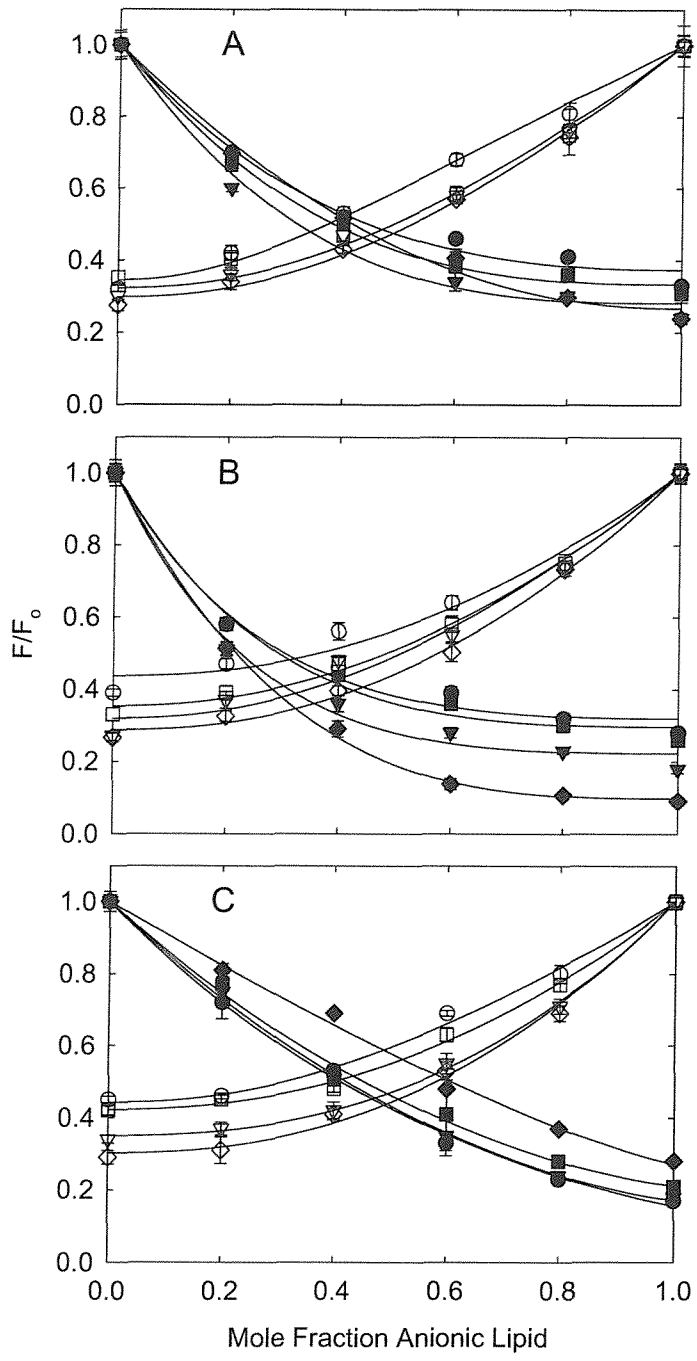

Figure 6.13 Quenching of the fluorescence of charge mutants of F80W-TbMscL in mixtures of anionic lipid and phosphatidylcholine. F80W-TbMscL charge mutants: (●,○), R98Q; (■,□), K99Q; (▼,▽), K100Q; and (◆,◇), R98Q:K99Q:K100Q were reconstituted into mixtures containing di(C18:1)PC and brominated anionic phospholipid (filled), or non-brominated anionic phospholipid and di(Br_2C18:0)PC (open): (A), phosphatidylserine; (B), phosphatidic acid; and (C), cardiolipin. The mole fraction is determined on a lipid chain basis. Data points are the average of three determinations. The solid lines show best fits to Equation 3.15 giving the relative binding constants listed in Table 6.6.

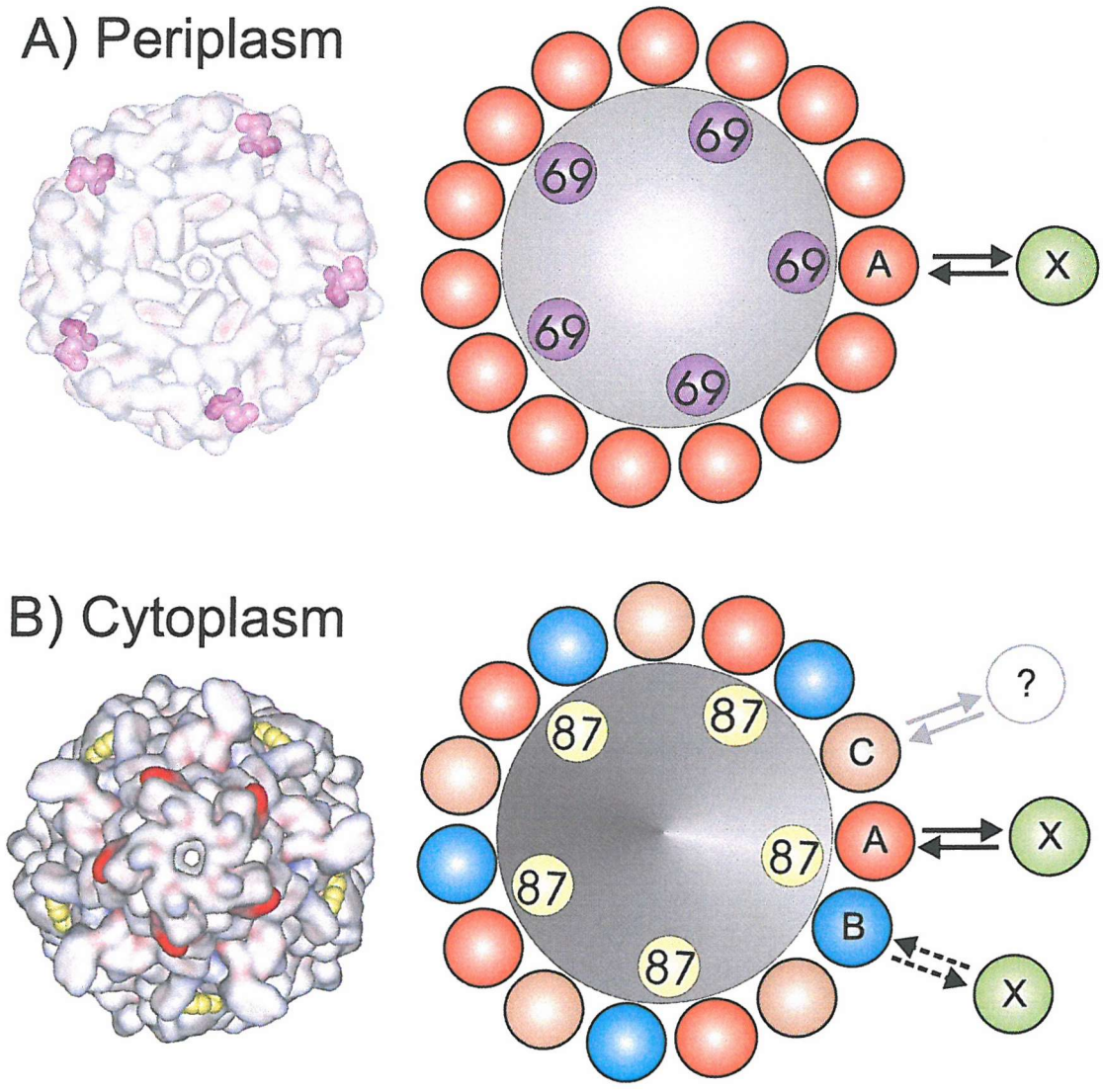

Figure 6.14 Cartoon representation of the two site binding model for phospholipids interacting with the surface of TbMscL. The high-resolution structure shown in Figure 6.2 is viewed from A) the periplasmic surface of the membrane with Leu-69 shown in lilac and B) the cytoplasmic surface of the membrane with Tyr-87 shown in yellow. In A) all lipid binding sites on the periplasmic surface of the protein are equivalent and exchange of two lipids A and X at a given site on the protein is shown. Lipid binding at ca. three sites per monomer (lipids A, B and C) on the cytoplasmic surface of the protein is shown in B); one site has high affinity for anionic lipid (lipid B) and the second site is much less specific (lipid A). The third site is too far away from Tyr-87, to report on the nature of lipid binding, however site three is unlikely to show specificity for anionic lipid (lipid C).

6.4 Conclusions

6.4.1 Mutated TbMscL Structure and Function

TbMscL channels with Trp residues at positions 69 or 87, located at or close to the periplasmic and cytoplasmic interfaces respectively (Chapter 5), were used to obtain lipid binding constants for phospholipids on each side of the bilayer leaflet. Residues Leu-69 and Tyr-87 are lipid exposed residues, on the second transmembrane α-helix of TbMscL. Introduction of a Trp residue at position Leu-69 was shown not to perturb the secondary structure or block the function of the channel. Introduction of a Trp at position Tyr-87 did not block channel function, and although the rate of growth of *E. coli* was slightly reduced, the level of protein expression was unaffected, consistent with a closed channel structure (Chapter 5). Similarly, F80W channels with the Trp reporter group located in the centre of the second transmembrane α-helix of TbMscL has also been shown to retain WT channel activity (Chapter 4).

Replacing the Arg-98, Lys-99 and Lys-100 charge cluster with Gln residues, does not affect the ability of these mutant channels to rescue *E. coli* knock out strain MJF465 from hypoosmotic stress (Figure 6.3). However, expression of these mutated channels caused a reduced rate of growth following induction with IPTG, the effect appearing cumulative, with single charge mutations having little or no effect and double charge mutants or total neutralisation of the charge cluster having the most severe effect (Figure 6.4). The cumulative nature of the charge mutations were also confirmed from experiments with Y87W (Figure 6.5). Although the Y87W mutation alone has a small affect on the rate of growth of *E. coli*, single and double mutations of Lys-99 and Lys-100 using the Y87W-*TbmscL* template resulted in more severe affects on the rate of growth, than the equivalent charge mutants made using the F80W-*TbmscL* template. The effect on growth of *E. coli* is consistent with these charge mutants occupying open or open-intermediate states (Yoshimura et al., 1999). Studies with EcMscL have shown that deletion of the last 27 residues at the carboxyl terminus of the channel (EcMscLΔ110-136) has no affect on channel activity, but removal of an additional six residues in EcMscLΔ104-136 abolished channel activity (Blount et al., 1996). These additional six residues in EcMscL contain the charge cluster Arg-104, Lys-105 and Lys-106, which align with the Arg-98, Lys-99 and

Lys-100 cluster in TbMscL, suggesting this conserved charged region in the protein could have important roles in channel function.

6.4.2 Fluorescence Properties

As discussed in Chapter 5, F80W in TbMscL is located deep within the membrane, whereas residues Leu-69 and Tyr-87 are located at or close to the bilayer interfaces (Figure 6.2). Fluorescence intensities of L69W and Y87W reconstituted into di(C18:1)PS and di(C18:1)PA are lower than in di(C18:1)PC (Figure 6.7, Table 6.2). This could be a quenching effect of the anionic lipid head group; acidic groups quench Trp fluorescence, by a mechanism involving electron or proton transfer when the Trp and the acidic groups are in close contact. For example, oleic acid has been shown to quench the Trp fluorescence of the Ca^{2+}-ATPase (Froud et al., 1986).

Mutation of the charged residues Arg-98, Lys-99 or Lys-100 to Gln residues in F80W-TbMscL, leads to altered fluorescence properties of the Trp reporter group; fluorescence emission spectra are shifted to longer wavelengths (Figure 6.6, Table 6.1). The shift in Trp fluorescence emission observed in di(C18:1)PC for the single charge mutants was reversed when the mutated protein was reconstituted into bilayers of di(C18:1)PA or di(C18:1)PS, suggesting that the conformational change induced by mutation of one of the three charged residues is reversed by binding of anionic lipid. This could be the reason why the single charge mutations did not result in a gain of function phenotype (Figure 6.4); the *E. coli* cell membrane contains ca. 30 mol % anionic lipid (Harwood and Russell, 1984). Single mutations of Arg-104, Lys-105, or Lys-106 in *E. coli*, equivalent to Arg-98, Lys-99 and Lys-100 in *M. tuberculosis* MscL, also result in no effect on growth rate (Maurer and Dougherty, 2003). In contrast to the results with the single charge mutants, simultaneous mutation of Arg-98, Lys-99 and Lys-100 results in a larger shift of Trp fluorescence emission in di(C18:1)PC. These results suggest that the conformational change induced by the triple mutation cannot be reversed by interaction with anionic lipid, and hence when expressed in *E. coli* result in a gain of function phenotype (Figure 6.4).

Rotation of the TM2 helix, as suggested with TbMscL reconstituted into di(C12:0)PC bilayers (Chapter 5) and suggested by Perozo et al. (2002a) for EcMscL in the open form, could cause movement of residue F80W towards a protein-protein interface and therefore account for a red shift in the emission. Fluorescence quenching by brominated phospholipids of F80W-TbMscL is greater than the fluorescence quenching observed with charge mutants of the F80W channel (R98Q, K99Q and K100Q) (Table 6.3). This would be consistent with a reduced accessibility of the dibrominated quencher for the Trp group. The fluorescence properties of F80W in the charge mutants are similar to the fluorescence properties of residue F79W reported in Chapter 5. Collectively, these data, together with the growth curves, suggest that F80W in the R98Q:K99Q:K100Q mutant moves towards the polar environment of the protein-protein interface, occupying a position more characteristic of F79W in the closed channel (See Figure 5.3) and in doing so becomes protected from the dibrominated lipid quencher, possibly through a steric shielding mechanism.

6.4.3 Lipid Binding Affinities at TbMscL Interfaces

6.4.3.1 *Periplasmic Interface*

By introducing Trp residues at positions 69 and 87 on the periplasmic and cytoplasmic sides of the membrane respectively, lipid binding constants can be measured for the two halves of the bilayer. The relative lipid binding constants for the periplasmic surface of L69W-TbMscL are shown in Table 6.4. Lipid binding on the periplasmic side of TbMscL is independent of lipid head group, with both zwitterionic and anionic phospholipids binding equally well to L69W-TbMscL. PE is an unusual lipid favouring the H_{II} phase when in isolation (Dowhan and Bogdanov, 2002) that has been suggested to alter the lateral pressure profile of the membrane, an effect suggested to be translated to the protein (Cantor, 1997b; Epand, 1998). The observation that di(C18:1)PE and di(C18:1)PC bind to the periplasmic side of TbMscL with equal affinity provides no evidence for the idea that di(C18:1)PE is in some way 'special'. It is also interesting that the very different hydrogen bonding potential of the di(C18:1)PE and di(C18:1)PC head groups does not give rise to a

difference in binding constant for the two lipids. In fact, the molecular dynamics simulations suggest that total lipid-residue interaction energies are very similar for (C16:0,C18:1)PE and (C16:0,C18:1)PC on the periplasmic side (Elmore and Dougherty, 2003).

The quenching data shown in Figure 6.11 for the anionic lipids di(C18:1)PS, di(C18:1)PA and tetra(C18:1)CL are also consistent with a single class of binding site on the periplasmic surface of TbMscL. The equal binding affinities obtained for anionic lipids and di(C18:1)PC to L69W-TbMscL is surprising, given that proteins usually have a net positive surface charge and therefore may be expected to show preference for phospholipids with anionic head groups. However, the lack of selectivity for anionic lipids on the periplasmic side of the membrane is consistent with the distribution of charged residues in TbMscL on the periplasmic side. The only positively charged residues on the periplasmic side are Arg-45 and Arg-58, on the top surface of the protein, pointing away from the lipid head group region. Furthermore, surface exposed oxygens from Asp-68 located towards the periplasmic end of TM2 (Figure 6.2) may generate unfavourable charge-charge interactions with the anionic lipids resulting in the low binding constants observed experimentally.

6.4.3.2 *Cytoplasmic Interface*

Lipid binding constants for phospholipids on the cytoplasmic surface of TbMscL were determined using Y87W. As on the periplasmic surface of TbMscL, no selectivity between di(C18:1)PE and di(C18:1)PC on the cytoplasmic surface of TbMscL was observed, with di(C18:1)PE and di(C18:1)PC binding equally well. Elmore and Dougherty (2003) have used molecular dynamics simulations of TbMscL to show that the cytoplasmic domain of the protein undergoes conformational changes upon transition from a PC to PE bilayer, with some lipid-protein contacts favoured in one conformation but not the other. These simulations suggest that the equal binding affinities observed experimentally for di(C18:1)PE and di(C18:1)PC to F80W-TbMscL could be the result of a compensatory mechanism, in which the protein changes its structure from a bilayer of di(C18:1)PC to a bilayer of di(C18:1)PE.

Results for the anionic lipids obtained with Y87W-TbMscL are significantly different to those described for L69W-TbMscL. The cytoplasmic side of the membrane shows a marked selectivity for anionic lipid (Table 6.4). As for the experiments with F80W, a higher binding constant is obtained from analysis of quenching data for Y87W with di(Br_2C18:0)PA or di(Br_2C18:0)PS than with di(Br_2C18:0)PC (Table 6.4). In this case, an analysis is possible in terms of a two site model in which binding of brominated lipid to either of two sites close to the Trp residue at position 87 causes fluorescence quenching, the two sites having different relative affinities for anionic lipid (Equation 3.22). The data fit well to this model (Figure 6.12) giving the binding constants listed in Table 6.5. Binding at one of the two sites shows a marked preference for anionic lipid, whereas binding at the other site shows a slight preference for phosphatidic acid and phosphatidylserine over phosphatidylcholine (Table 6.5). On the cytoplasmic side of the membrane the only positively charged residues in a position to interact with an anionic phospholipid head group are Arg-98, Lys-99 and Lys-100. The number of lipid molecules required to form a complete bilayer shell around the MscL pentamer is ca. 29, since the circumference of MscL is about 135 Å and the diameter of a lipid molecule is ca. 9.4 Å. Thus the total number of lipid molecules in contact with each MscL monomer on the cytoplasmic side of the membrane is ca. 3. Given the distribution of charged residues on the cytoplasmic side of the protein, it is likely that the only site of high affinity for anionic lipids is that detected in the fluorescence quenching experiments described below.

6.4.4 Lipid Binding Affinities with Charge Mutants of TbMscL

From the results obtained with L69W and Y87W, it was establish that specificity in binding anionic lipids observed using F80W-TbMscL (Chapter 4) was a result of three sites all located on the cytoplasmic side of TbMscL, showing a high specificity for anionic lipid (Figure 6.14). Using the X-ray crystal structure of TbMscL and sequence alignments, a sequence of positively charge residues (Arg-98, Lys-99 and Lys-100) at the cytoplasmic end of TM2 were identified and targeted for site directed mutagenesis, neutralising the charge cluster by replacing these residues with Gln (Figure 6.2). Furthermore, sequence alignments revealed that this charge cluster was conserved throughout the MscL homologues and aligned with Arg-104, Lys-105 and

Lys-106 in the EcMscL channel (See Figure 1.8). To determine if the high affinity binding site involved the cluster of charged residues Arg-98, Lys-99 and Lys-100, these residues were mutated individually to Gln. As shown in Table 6.6, this resulted in a reduced affinity for phosphatidic acid, with smaller differences between the experiments with di(Br_2C18:0)PA and those with di(Br_2C18:0)PC. Simultaneous mutation of all three charged residues led to complete loss of selectivity for phosphatidic acid (Table 6.6). Mutation of Arg-98, Lys-99 or Lys-100 also results in a reduced affinity for phosphatidylserine. Results with cardiolipin are difficult to interpret because cardiolipin contains four fatty acyl chains compared to the two in phosphatidylcholine, but again mutation of Arg-98, Lys-99 or Lys-100 results in reduced affinity for the anionic lipid (Table 6.6).

The shift in Trp fluorescence emission observed in di(C18:1)PC for the single charge mutants was reversed when the mutated protein was reconstituted into bilayers of di(C18:1)PA or di(C18:1)PS (Section 6.4.2). Although these results are consistent with a role for these charged residues in high affinity binding of phosphatidic acid, an alternative explanation could be that mutation of the charged residues results in a significant change in conformation for MscL, and in this new conformation there is no high affinity binding site for phosphatidic acid.

When all three positively charged residues are removed (F80W:R98Q:K99Q:K100Q), and the binding constants for the anionic lipids determined from experiments with di(Br_2C18:0)PC and from experiments with di(C18:1)PC and brominated anionic lipid, all the lipid binding constants are around 1 and are reciprocal (Figures 6.11B and 6.11C, Table 6.6). These data suggests that binding of anionic lipids to the second class of binding site has been totally disrupted in the R98Q:K99Q:K100Q mutant. However, loss of binding could be the result of two possibilities; either the binding site is formed by residues Arg-98, Lys-99 or Lys-100 in TbMscL and that replacing these groups with Gln simply removes the charge interaction, or alternatively by disrupting the charge cluster the channel may become open and the lipids may no longer be able to bind to the surface of the open channel by the same mechanism as with the closed channel, due to a change in conformation of the channel and/or repositioning of side chains in this area.

Chapter 7:
Characterisation of the Open MscL Channel

7 CHARACTERISATION OF THE OPEN MscL CHANNEL

7.1 Introduction

Lipid bilayers have a very low compressibility, therefore the volume of the bilayer will not change significantly when the pressure across the bilayer is increased (Lee, 2004); an osmotic downshift will therefore lead to an increase in membrane area and a decrease in membrane thickness (Hamill and Martinac, 2001). The cost of exposing hydrophobic fatty acyl chains or protein residues to water is such that the hydrophobic thickness of the membrane protein should match the hydrophobic thickness of the bilayer (Tanford, 1980). The data in Chapter 5 suggests that hydrophobic matching for MscL is very efficient, even when the hydrophobic thickness of the bilayer changes by ca. 21 Å; hydrophobic matching could be achieved by a distortion of the lipid bilayer around the protein, by a distortion of the membrane protein, or by some combination of both (Lee, 2004). Changes in the thickness of the bilayer are therefore associated with an energetic cost.

Most theories of hydrophobic mismatch assume that the lipid chains in the vicinity of a membrane protein adjust their length to the hydrophobic thickness of the protein, with the protein acting as a rigid body (Fattal and Ben-Shaul, 1993). When the thickness of the bilayer is less than the hydrophobic thickness of the protein, the lipid chains must be stretched around the protein (Figure 7.1). Conversely, when the thickness of the bilayer is greater than the hydrophobic thickness of the protein, the lipid chains must be compressed around the protein. Either stretching or compressing the fatty acyl chains of the lipid requires work, so a lipid molecule that has to change its hydrophobic thickness to bind to a membrane protein would be expected to bind less strongly to the protein than a lipid for which no stretching or compressing is required. Thus, the possibility that hydrophobic matching between a membrane protein and the surrounding lipid bilayer is achieved by distortion of the lipid bilayer can be tested by measuring lipid binding constants as a function of lipid fatty acyl chain length.

Alternatively if the transmembrane helices of a membrane protein were too long to match the surrounding lipid bilayer, tilting of the helices could reduce their effective length across the bilayer (Webb et al., 1998). The possibility that membrane proteins distort to help match the hydrophobic thickness of the surrounding lipid bilayer is suggested by the fact that the membrane proteins such as Ca^{2+}-ATPase (East and Lee, 1982), Na^{+},K^{+}-ATPase (Cornelius, 2001), diacylglycerol kinase (Pilot et al., 2001) and rhodopsin (Baldwin and Hubbell, 1985) all show highest activities in bilayers of phospholipids with a particular fatty acyl chain length, generally C18, activities decreasing as the chain length increases or decreases from this optimal value.

MscL has the largest channel conductance of any ion channel characterised to date (Batiza et al., 1999); *in vitro* sieving experiments and conductivity measurements suggest that the open MscL channel may reach 30-40 Å in diameter (Cruickshank et al., 1997; Sukharev et al., 1999b), and ESR studies with EcMscL in the open state suggest an open pore size of at least 25 Å in diameter (Perozo et al., 2002a). An increase in channel radius is likely to be linked to a reduction in the hydrophobic thickness of the channel; studies with the spin-labelled EcMscL channel have shown a correlation between changes in the conformation of EcMscL and bilayer thickness, with significant changes in TM1 for EcMscL reported between reconstitution into bilayers of di(C14:1)PC and di(C18:1)PC (Perozo et al., 2002b). Hydrophobic mismatch was also reported to have a significant effect on the function of EcMscL; in di(C16:1)PC EcMscL opened with a significantly lower activation threshold than in di(C18:1)PC, whereas in di(C20:1)PC the threshold was higher, so that thin bilayers favour channel opening and thick bilayers stabilise the closed form, although changes in bilayer thickness alone are insufficient to open the channel (Perozo et al., 2002b).

7.1.1 Chapter 7 Overview

In order to study the lipid interactions with the open form of TbMscL in model bilayer systems, a channel locked in the open form is required. A large amount of mutational information is available about single and double point mutations of MscL that alter the gating kinetics (Blount et al., 1996c; Ou et al., 1998; Yoshimura et al., 1999; Maurer and Dougherty, 2003; Bartlett et al., 2004). From these studies it has

been established that the main channel gate is formed by a region consisting of five valines located above five glycines in EcMscL (Gly-22 and Val-23), one pair being provided by each TM1, consistent with channel gating being most severely affected by mutation of Gly-22 and Val-23. Using sequence alignments, Gly-22 and Val-23 have been mapped onto the high resolution structure of the TbMscL homologue and shown to be equivalent to residues Ala-20 and Val-21 (See Figure 1.8). Severe GOF mutants have been reported for G22K-EcMscL and V21D-TbMscL by Yoshimura et al. (1999) and Moe et al. (2000) respectively. A Lys residue was therefore introduced at position Val-21 in the F80W-TbMscL mutant, generating a GOF phenotype with altered gating properties. The lipid-protein interactions of the open channel were then determined and allowed not only chain length dependencies but also the head group interactions for both the open and closed channels to be characterised.

7.2 Materials and Methods

All chemicals were obtained from Sigma or BDH with the following exceptions:

Avanti Polar Lipids

1,2-dimyristoleoyl-sn-glycero-3-phosphatidylcholine (di(C14:1)PC)
1,2-dipalmitoleoyl-sn-glycero-3-phosphatidylcholine (di(C16:1)PC)
1,2-dioleoyl-sn-glycero-3-phosphatidylcholine (di(C18:1)PC)
1,2-dieicosenoyl-sn-glycero-3-phosphatidylcholine (di(C20:1)PC)
1,2-dierucoyl-sn-glycero-3-phosphatidylcholine (di(C22:1)PC)
1,2-dinervonyl-sn-glycero-3-phosphatidylcholine (di(C24:1)PC)
1,2-dioleoyl-sn-glycero-3-phosphatdic acid (di(C18:1)PA)
1,2-dioleoyl-sn-glycero-3-phosphatidylethanolamine (di(C18:1)PE)

Anatrace, Anagrade®

n-Octyl-β-D-glucopyranoside (Octylglucoside)

Calbiochem, Ultrol® Grade

N-(2-hydroxyethyl)piperazine-N'-(2-ethyanesulphonic acid) (Hepes)
1,3-diaza-2,4-cyclopentadiene (Imidazole)

Pierce

Disuccinimidyl suberate (DSS)

7.2.1 *TbmscL* Mutation

The pET-19b plasmid containing the *Mycobacterium tuberculosis* F80W-*mscL* gene was used as a template for site directed mutagenesis, using the QuickChange™ protocol, as outlined in Section 2.2.5.2, and the synthetic oligonucleotide primers in Table 2.7.

7.2.2 Protein Expression and Purification

E. coli BL21(λDE3)pLysS transformants carrying the pET-19b plasmid (Novagen) with the mutated *TbmscL* gene were grown in 60 l Luria broth to late-log phase (absorbance at 600 nm of 1.1) and then induced for 80 min in the presence of isopropyl-β-D-thiogalactopyranoside (1.0 mM). MscL was purified as described in Section 2.2.4.

7.2.3 Bioassay

7.2.3.1 *In vivo Channel Function Assay*

Loss of function mutants are detected through a reduced or total inability to rescue *E. coli* knock-out strain MJF465 from hypoosmotic stress following induction of MscL production with IPTG, as described in Section 5.2.2.1.

7.2.3.2 *Growth Curve Studies*

The gain of function mutant was detected by a marked reduction in the growth rate after induction of MscL production with IPTG, as described in Section 5.2.2.2.

7.2.4 Reconstitution

Purified V21K:F80W-TbMscL was reconstituted into lipid bilayers by mixing lipid and TbMscL in cholate, followed by dilution into buffer to decrease the concentration of cholate below its critical micelle concentration, as described in Section 4.2.10.1.

7.2.5 Cross-linking of MscL

MscL (0.34 mg) was reconstituted by dialysis to give a molar ratio of lipid to MscL ratio of 100:1 (Section 4.2.10.2). MscL was cross-linked using disuccinimidyl suberate (DSS; Pierce) and subsequently resolved on 12.5 % SDS-PAGE, as described in Section 4.2.12.

7.2.6 Steady-State Fluorescence Measurements

Trp fluorescence was recorded for 0.35 μM V21K:F80W-TbMscL in buffer (20 mM Hepes, 100 mM KCl, 1 mM EGTA, pH 7.2) at 25 °C, using an SLM 8100 fluorimeter, with excitation at 280 nm, as described in Section 3.5. Emission intensity corrected fluorescence spectra were fitted to skewed Gaussian curves, as described in Section 3.5.

Quenching of Trp fluorescence by acrylamide was studied by addition of an aliquot of a freshly prepared stock solution of acrylamide (1M) in Hepes buffer (20 mM Hepes, 100 mM KCl, 1 mM EGTA, pH 7.2) to TbMscL (0.35 μM). Fluorescence quenching by acrylamide and iodide was measured at an excitation wavelength of 295 nm and corrected for the inner filter effect, as described in Section 3.5.

7.3 Results

7.3.1 Bioassays

7.3.1.1 *Downshock Assay*

The osmotic downshock assay described in Chapter 5 was used to confirm functionality of V21K:F80W-TbMscL. WT and mutant TbMscL channels were expressed in the mechanosensitive channel free bacterial strain MJF465 (Section 2.2.1.4). As shown in Figure 7.2, all mutated *TbmscL* genes are able to rescue the *E. coli* cells from the effects of hypoosmotic stress following induction of the channels with IPTG, confirming that the channels are active.

7.3.1.2 *Growth Curve Assay*

The growth profiles of *E. coli* expressing mutated TbMscL channels are shown in Figure 7.3. The growth curve for F80W is located at the top of the graph together with WT channel, confirming that F80W does not affect the growth of the *E. coli*. However, introducing a Lys residue into the primary hydrophobic gate at position Val-21 dramatically slows the rate of growth of *E. coli* expressing the mutant channel. The large effect observed with V21K:F80W-TbMscL will therefore be due to the Lys-21 residue alone and hence V21K:F80W is considered a pseudo-single site mutation, as described by Maurer and Dougherty (2003). Reduced cell viability was also reported for G22K-EcMscL and V21D-TbMscL by Yoshimura et al. (1999) and Moe et al. (2000) respectively. Patch clamp recordings revealed that G22K-EcMscL and V21D-TbMscL required lower levels of membrane patch suction to gate, were 'flickery' in the fully open state and occupied a stable open/subconducting state (Yoshimura et al., 1999; Moe et al., 2000). These data would suggest that the mutant V21K:F80W-TbMscL generated in this study, is likely to be in an open or open-intermediate state of the channel, requiring lower levels of membrane tension to become fully open.

7.3.2 Cross-linking Studies

As described in Section 4.3.5.3, MscL crystallises as a pentamer and cross linking MscL in the native membrane results in a ladder-like pattern on SDS gels, corresponding to multiples of the monomeric protein up to a pentamer or higher; before cross-linking, TbMscL runs predominantly as a monomeric species, with small amounts of dimer (Figures 7.4 and 4.9). SDS gels of V21K:F80W-TbMscL following reconstitution into bilayers of di(C18:1)PC and cross-linking with DSS, show the presence of predominantly pentameric species, with small amounts of monomer (Figure 7.4). These results suggest that the pentamer of V21K:F80W-TbMscL would be more stable in SDS than that of F80W-TbMscL.

7.3.3 Fluorescence Properties

Intensity corrected emission spectra for TbMscL reconstituted into bilayers of di(C18:1)PC and di(C18:1)PA are shown in Figure 7.5; the spectra were fitted to skewed Gaussian curves to give the parameters in Table 7.1. The closed F80W-TbMscL channel has a Trp emission maximum (λ^{max}) in di(C18:1)PC of 321.0 ± 0.1, characteristic of a very hydrophobic environment for the Trp residue. The mutant channel V21K:F80W-TbMscL, shows a large red shift with a Trp λ^{max} in di(C18:1)PC of 331.8 ± 0.2, suggesting a major conformation change between the closed and open forms of MscL, affecting the location of the Trp residue introduced at position 80 (Table 7.1). A similar observation was made with the triple charge mutant of F80W-TbMscL (R98Q:K99Q:K100Q), described in Chapter 6. On reconstitution into di(C18:1)PA, there is a very small shift in fluorescence emission for V21K:F80W to shorter wavelengths, with no significant sift for F80W.

7.3.4 Acrylamide Quenching of MscL

Stern-Volmer plots for quenching of the Trp fluorescence of TbMscL mutants in bilayers of di(C18:1)PC by acrylamide were determined and the results are shown in Figure 7.6. The fluorescence intensity is plotted as F_o/F, where F_o is the fluorescence

intensity in the absence of quencher and F is the fluorescence intensity at intermediate concentrations of quencher. The results in Figure 7.6 show that fluorescence quenching was linearly dependent on acrylamide concentration and that the level of quenching for V21K:F80W-TbMscL is higher than that observed for F80W-TbMscL. Quenching of V21K:F80W-TbMscL is similar to that observed for F79W (Table 7.2).

7.3.4 Relative Phospholipid Binding Constants for MscL

MscL was reconstituted into bilayer fragments by the dilution method at a molar ratio of lipid:protein of 100:1. Fluorescence quenching curves for Trp mutants of TbMscL in mixtures of a brominated and the corresponding non-brominated phospholipid were determined and the results are shown in Figure 7.7. The fluorescence intensity is plotted as F/F_o, where F is the fluorescence intensity at intermediate fractions of brominated phospholipid and F_o is the fluorescence intensity when the mole fraction of non-brominated phospholipid is 1. The data shown in Figure 7.7 were fitted to Equation 3.11 using the nonlinear least-squares programme in SigmaPlot, giving the values of *n* listed in Table 7.3.

Fluorescence quenching curves for V21K:F80W-TbMscL in mixtures of di(Br_2C18:0)PC and phosphatidylcholines with chain lengths between C12 and C24 are shown in Figure 7.8. Relative binding constants obtained for the shortest chain and longest chain phosphatidylcholines, di(C12:0)PC and di(C24:1)PC are 0.71 and 0.42 respectively (Table 7.4). In contrast, di(C14:1)PC and di(C16:1)PC bind with greater affinity than di(C18:1)PC to V21K:F80W-TbMscL, with binding constants of 1.28 and 1.15 respectively (Table 7.4). The binding constant determined with di(C14:1)PC for V21K:F80W-TbMscL is greater than the binding constant observed for di(C14:1)PC with F80W-TbMscL (Table 7.4).

The relative binding constants are plotted as a function of fatty acyl chain length in Figure 7.9. The results show that V21K:F80W-TbMscL has a greater affinity for di(C14:1)PC than for di(C18:1)PC. The relative binding constants for V21K:F80W-TbMscL decrease for phosphatidylcholines with fatty acyl chain lengths longer or shorter than C14, particularly those with fatty acyl chains longer than C18. The total

change in lipid binding affinity for V21K:F80WMscL was three-fold for phosphatidylcholines over the C14-C24 range.

Fluorescence quenching curves for V21K:F80W-TbMscL in mixtures of phosphatidylcholine and phosphatidylethanolamine are shown in Figure 7.10. The binding constants obtained for phosphatidylethanolamine from experiments with mixtures of di(C18:1)PC and di(Br_2C18:0)PE or di(Br_2C18:0)PC and di(C18:1)PE are the same and are ca. 1.3 for V21K:F80W-TbMscL (Figure 7.10, Table 7.5); the binding constants determined for V21K:F80W are slightly higher than those determined for F80W-TbMscL (Table 7.5).

Binding constants for the anionic lipid phosphatidic acid with V21K:F80W-TbMscL obtained from experiments with di(C18:1)PC and di(Br_2C18:0)PA or di(Br_2C18:0)PC and di(C18:1)PA are the same and are ca. 1.3 (Figure 7.11, Table 7.5). The small and reciprocal nature of the binding constants obtained using V21K:F80W is consistent with simple competition between phosphatidylcholines and phosphatidic acid for the surface of V21K:F80W-TbMscL.

TbMscL Mutant	Phospholipid	λ^{max} (nm)	ω (nm)
F80W	di(C18:1)PC	321.0 ± 0.1	45.9 ± 0.2
	di(C18:1)PA	320.9 ± 0.1	43.2 ± 0.2
V21K:F80W	di(C18:1)PC	331.8 ± 0.2	51.6 ± 0.3
	di(C18:1)PA	329.9 ± 0.2	50.4 ± 0.2

Table 7.1 Fluorescence properties of reconstituted TbMscL mutants. λ^{max} and ω are the wavelength of maximum emission and the peak width at half height respectively, determined by fitting the fluorescence emission spectra shown in Figure 7.5 to Equation 3.8. The values for F80W-TbMscL are taken from Table 5.2.

TbMscL Mutant	F/F_o	K_{SV} (M^{-1})	K_{SV}^{-1} (M)
F79W	1.72 ± 0.02	2.44 ± 0.04	0.41
F80W	1.34 ± 0.01	1.09 ± 0.03	0.92
V21K:F80W	1.73 ± 0.01	2.47 ± 0.03	0.40

Table 7.2 Fluorescence quenching of Trp mutants of TbMscL by acrylamide. F and F_0 are fluorescence intensities for TbMscL reconstituted in di(C18:1)PC in the presence and absence of 0.3 M acrylamide respectively, measured at pH 7.2. The Stern-Volmer quenching constant, K_{SV}, was determined by fitting the data in Figure 7.6 to Equation 3.1. The inverse of the Stern-Volmer quenching constant is the quencher concentration that will quench 50 % of the fluorescence.

Phospholipid	F_o/F	n
	F80W	
di(C18:1)PC	0.19 ± 0.01	2.46 ± 0.05
di(C18:1)PE	0.25 ± 0.02	2.59 ± 0.29
di(C18:1)PA	0.11 ± 0.01	3.62 ± 0.27
	V21K:F80W	
di(C18:1)PC	0.52 ± 0.01	2.15 ± 0.21
di(C18:1)PE	0.52 ± 0.01	1.23 ± 0.07
di(C18:1)PA	0.42 ± 0.01	2.88 ± 0.13

Table 7.3 Fluorescence quenching of TbMscL mutants in brominated phospholipids as a function of lipid head group. F_o and F are fluorescence intensities for MscL reconstituted in nonbrominated phospholipid and the corresponding brominated phospholipid respectively, measured at pH 7.2. The value of n is the value obtained by fitting the data in Figure 7.7 to Equation 3.11. Data for F80W-TbMscL is taken from Table 4.5.

Fatty acyl chain	Relative binding constant measured using di(Br_2C18:0)PC	
	F80W	**V21K:F80W**
C12:0	0.78 ± 0.08	0.71 ± 0.09
C14:1	1.05 ± 0.10	1.28 ± 0.15
C16:1	1.13 ± 0.11	1.15 ± 0.10
C18:1	1	1
C20:1	0.85 ± 0.07	0.78 ± 0.11
C22:1	0.79 ± 0.08	0.56 ± 0.08
C24:1	0.72 ± 0.05	0.42 ± 0.04

Table 7.4 Relative lipid binding constants for F80W-TbMscL and V21K:F80W-TbMscL as a function of phosphatidylcholine fatty acyl chain length. Binding constants were calculated from quenching data for F80W-TbMscL and V21K:F80W-MscL in mixtures of di(Br_2C18:0)PC with non-brominated lipid, at pH 7.2, using values for n of 2.54 and 2.15 respectively.

Phospholipid	Relative binding constant measured using di(Br_2C18:0)PC	Relative binding constant measured using di(C18:1)PC
	F80W	
di(C18:1)PE	1.04 ± 0.07	1.14 ± 0.01
di(C18:1)PA	1.81 ± 0.21	3.49 ± 0.25
	V21K:F80W	
di(C18:1)PE	1.44 ± 0.10	1.34 ± 0.15
di(C18:1)PA	1.30 ± 0.12	1.24 ± 0.16

Table 7.5 Relative lipid binding constants for F80W-TbMscL and V21K:F80W-TbMscL channels as a function of lipid head group. Binding constants relative to di(C18:1)PC were calculated from quenching data for TbMscL mutants in mixtures of di(Br_2C18:0)PC with non-brominated lipid or di(C18:1)PC with brominated lipid, at pH 7.2, using the values for *n* given in Table 7.5.

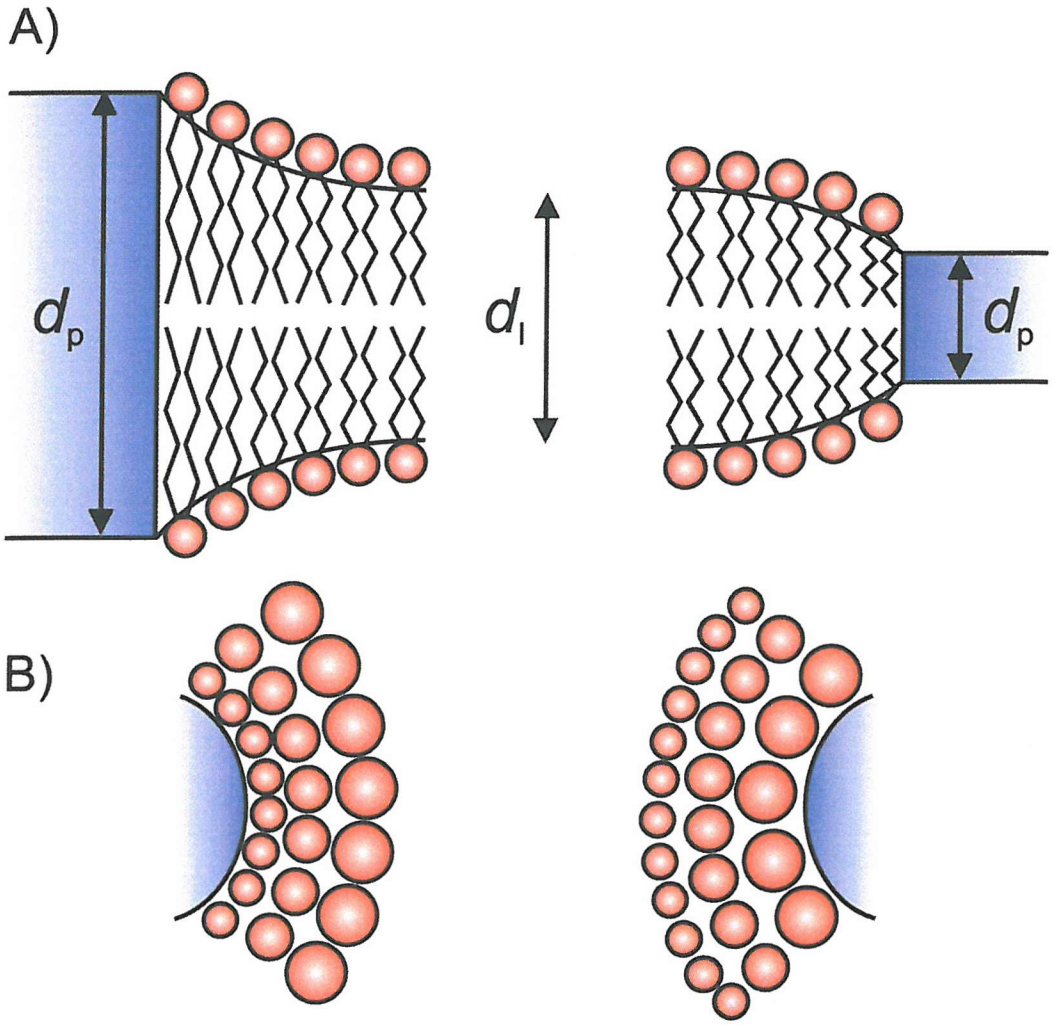

Figure 7.1 The model of Fattal and Ben-Shaul (1993) for hydrophobic mismatch for a rigid protein. The diagram shows how a lipid bilayer could distort around a membrane protein whose hydrophobic thickness is greater than that of the lipid bilayer (left, $d_p > d_l$) or less than that of the lipid bilayer (right, $d_p < d_l$). (A) shows a side view of the membrane and (B) shows a view down onto the surface of the membrane. When the hydrophobic thickness of the protein is greater than the hydrophobic thickness of the bilayer, the lipid chains must be stretched so that the surface area occupied by a lipid molecule will be less in the vicinity of the protein than for bulk lipid. Conversely, to match a protein with a thin transmembrane region, the fatty acyl chains of neighbouring lipids will be compressed and will therefore occupy a greater surface area (Lee, 2004).

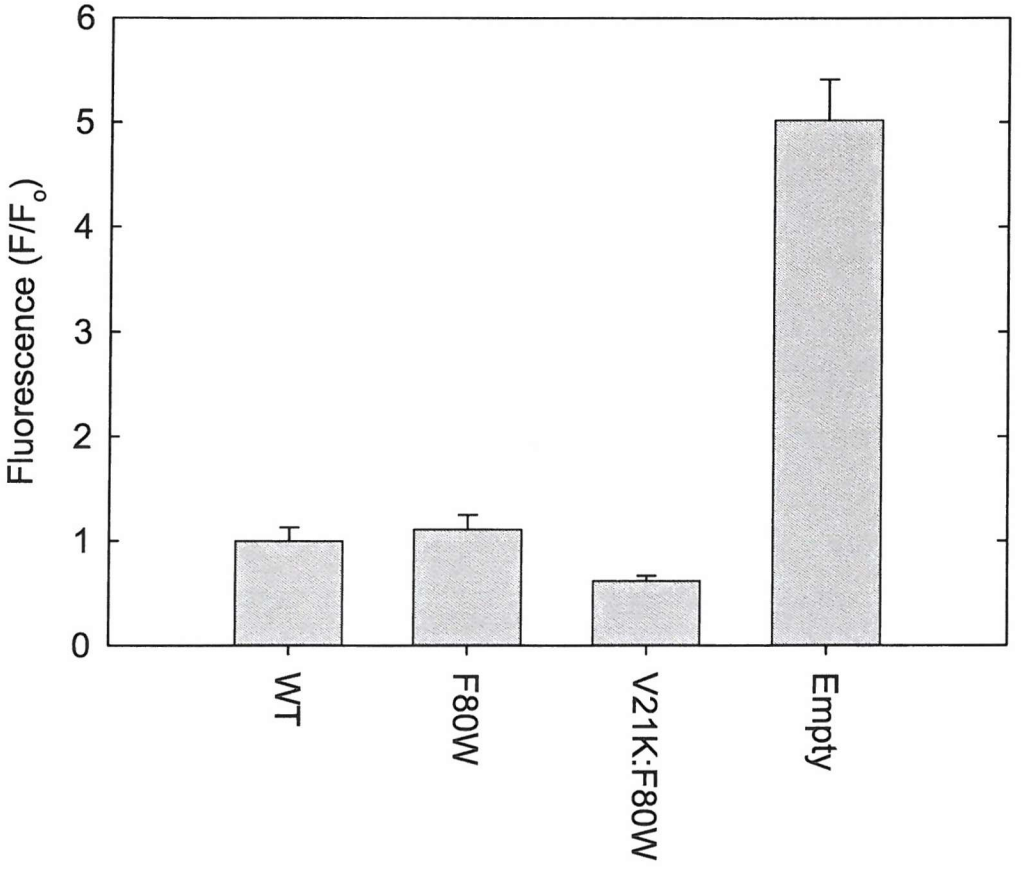

Figure 7.2 Viability of mechanosensitive-null *E. coli* expressing the *TbmscL* genes on an inducible plasmid. *E. coli* MJF465 transformants carrying the pET-19b plasmid with the *TbmscL* gene were grown in the presence of 0.4 M NaCl and induced for 4 h with 1 mM IPTG, followed by a hypoosmotic stress via a 60-fold dilution into water containing ethidium bromide (0.5 μg ml^{-1}). The fluorescence intensity of the supernatant was analysed for the release of DNA at 632 nm. Fluorescence intensities are expressed as a ratio with the fluorescence for MJF465 harbouring the WT-*TbmscL* gene. The fluorescence intensity for the release of DNA from the empty MJF465 cell line (no plasmid) is also shown. Intensities are the average of three colonies, the error bars correspond to the standard deviation.

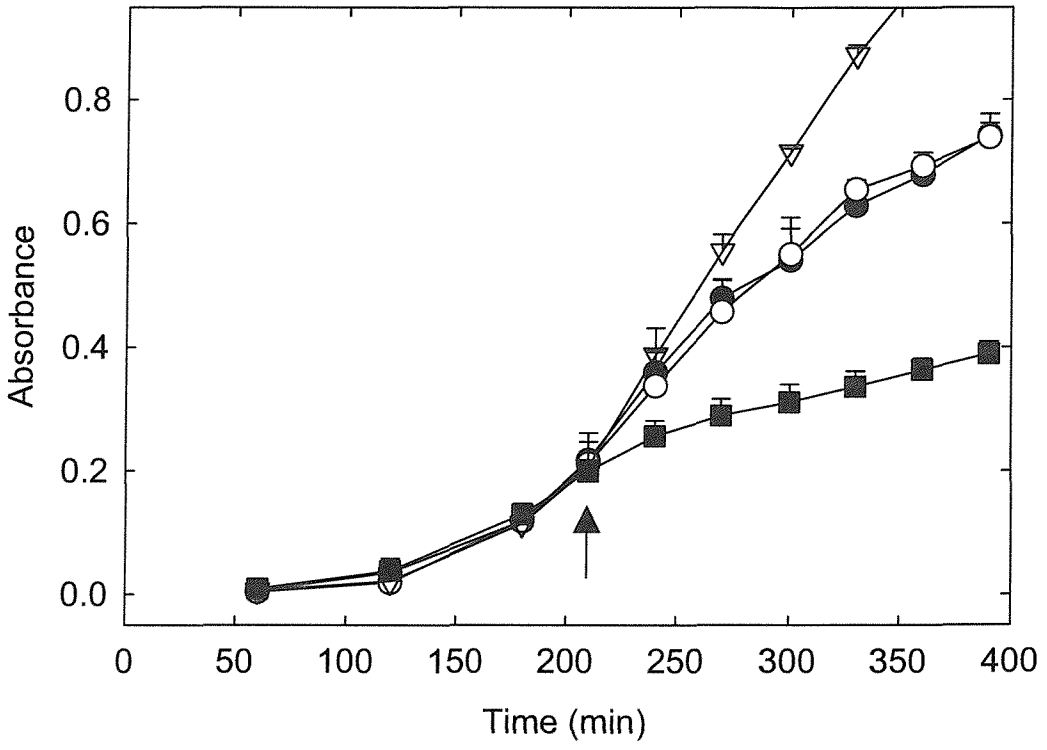

Figure 7.3 Growth of *E. coli* in liquid media expressing the *TbmscL* genes. *E. coli* BL21(DE3)pLysS transformants carrying the pET-19b plasmid with the *TbmscL* genes: (●), WT; (○), F80W; and (■), V21K:F80W were grown at 37 °C in LB medium supplemented with ampicillin (100 μg ml^{-1}). The non-induced growth of (▽), *E. coli* BL21(DE3)pLysS host strain (empty) is also shown. Cells were induced with 1 mM IPTG at an absorbance at 600 nm of ~0.2 (arrow). Data points are the average of five colonies, the error bars correspond to the standard deviation.

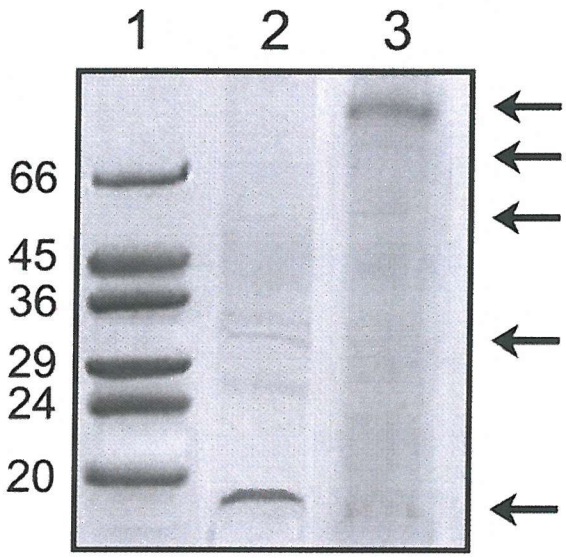

Figure 7.4 12.5 % Sodium dodecyl sulphate polyacrylamide gel electrophoresis of reconstituted V21K:F80W-TbMscL after cross-linking with DSS (2.18 mM) for 30 min at room temperature. Protein bands were visualised by Coomassie brilliant blue staining. Lane 1 contains molecular weight markers (Sigma). Lane 2 contains unreconstituted V21K:F80W-TbMscL, consisting largely of monomeric protein (M_r of 18.6 kDa) with a small amount of dimeric species. Lane 3 contains cross linked V21K:F80W-TbMscL following reconstitution into di(C18:1)PC. The arrows show the expected positions of monomeric TbMscL and of dimeric, trimeric, tetrameric and pentameric species. In the reconstituted systems the molar ratio of phospholipid to MscL was 100:1.

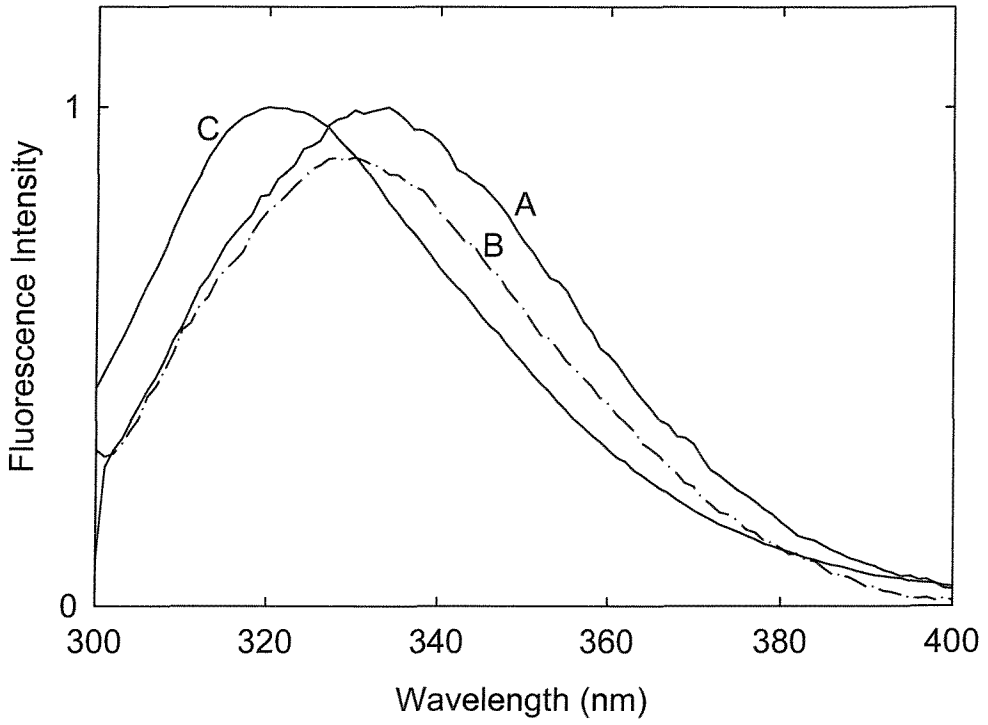

Figure 7.5 Intensity corrected fluorescence emission spectra for V21K:F80W-TbMscL in phospholipid bilayers. Fluorescence emission spectra are shown for V21K:F80W-TbMscL in di(C18:1)PC (A) and di(C18:1)PA (B). The fluorescence emission spectrum is also shown for F80W-TbMscL in di(C18:1)PC (C). The concentration of MscL was 0.35 μM and the molar ratio of lipid to MscL was 100:1. The excitation wavelength was 280 nm and the buffer was 20 mM Hepes, 100 mM KCl, 1 mM EGTA, pH 7.2.

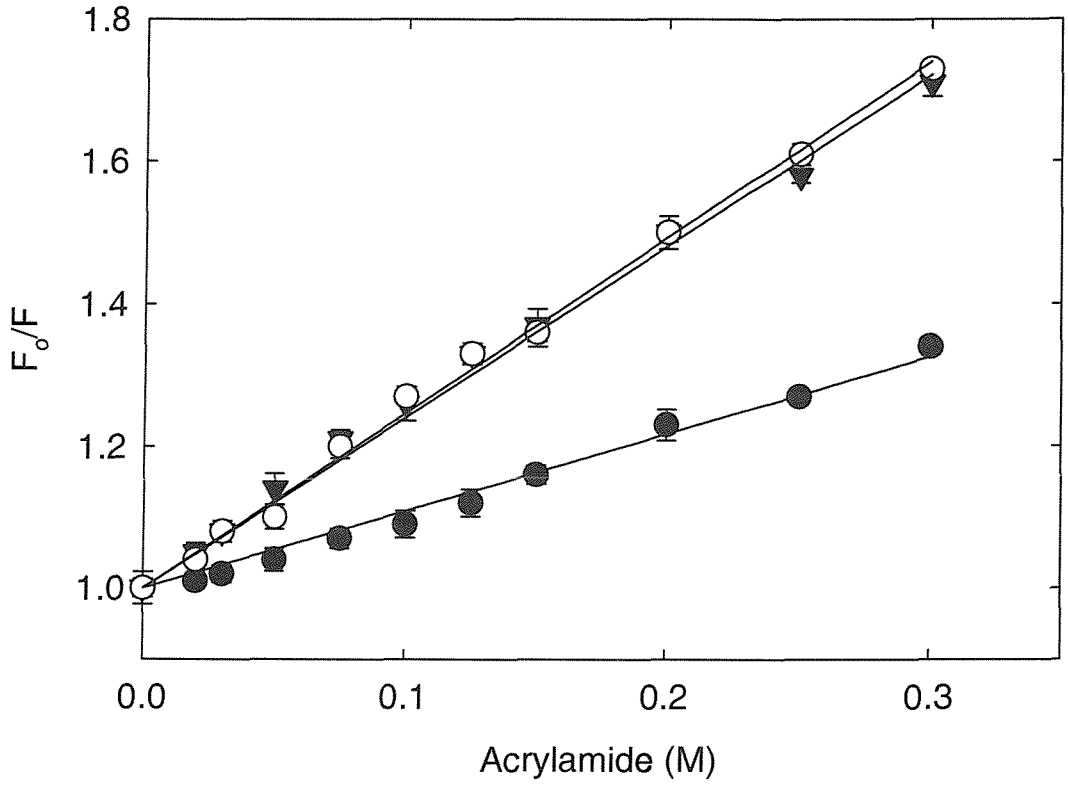

Figure 7.6 Stern-Volmer plots for quenching of the Trp fluorescence of mutants of TbMscL by acrylamide. Trp mutants of TbMscL were reconstituted into bilayers of di(C18:1)PC in the presence of the quencher acrylamide. Fluorescence intensities are expressed as a fraction of the fluorescence intensity for the TbMscL mutants in phospholipid alone. Trp mutants are as follows: (●), F80W; (○), V21K:F80W; and (▼), F79W. The solid lines show fits to Equation 3.1, giving the values for K_{SV} listed in Table 7.2. The concentration of V21K:F80W-TbMscL was 0.35 μM, the concentration of all other Trp mutants of TbMscL was 0.98 μM, and the molar ratio of lipid to TbMscL was 100:1. Data points are the average of three determinations and corrected for the inner-filter effect.

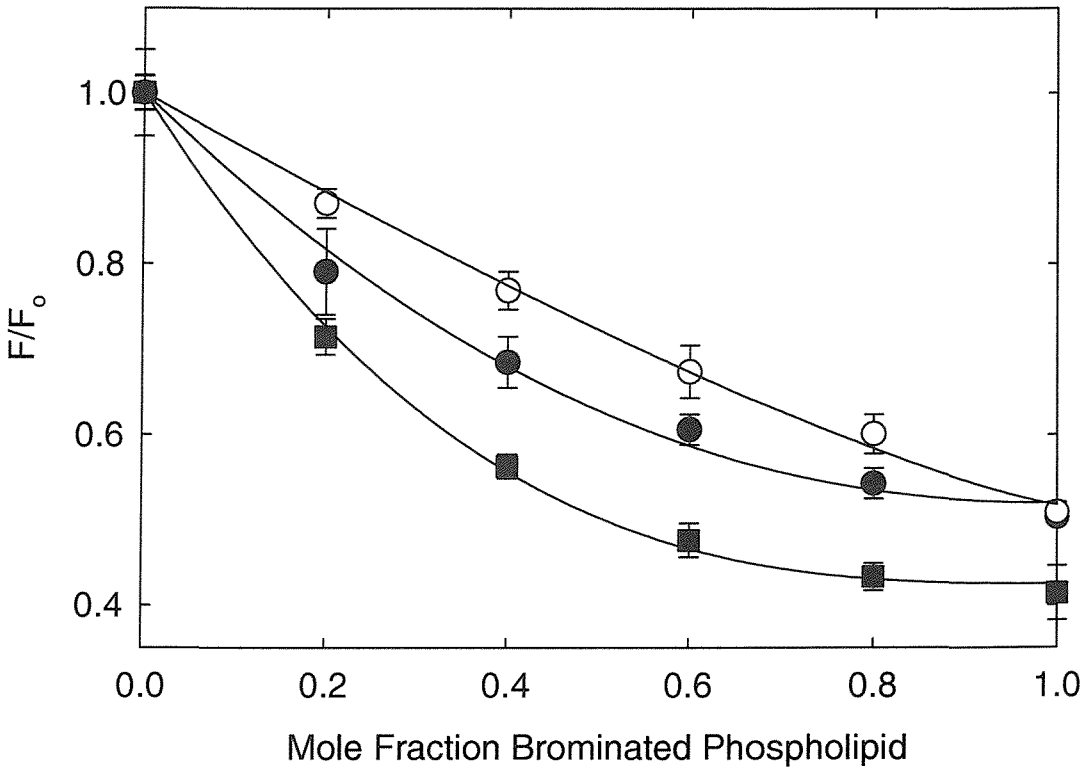

Figure 7.7 Quenching of V21K:F80W-TbMscL fluorescence by brominated phospholipids. V21K:F80W-TbMscL was reconstituted into bilayers containing mixtures of nonbrominated lipid and the corresponding brominated lipid. Fluorescence intensities are expressed as a fraction of the fluorescence for V21K:F80W-TbMscL reconstituted in the nonbrominated lipid. Lipid head groups were as follows: (●), di(C18:1)PC; (○), di(C18:1)PE; and (■), di(C18:1)PA. The line is the fit to Equation 3.11 giving the values for n listed in Table 7.3. The concentration of TbMscL was 0.35 μM and the molar ratio of lipid to TbMscL was 100:1.

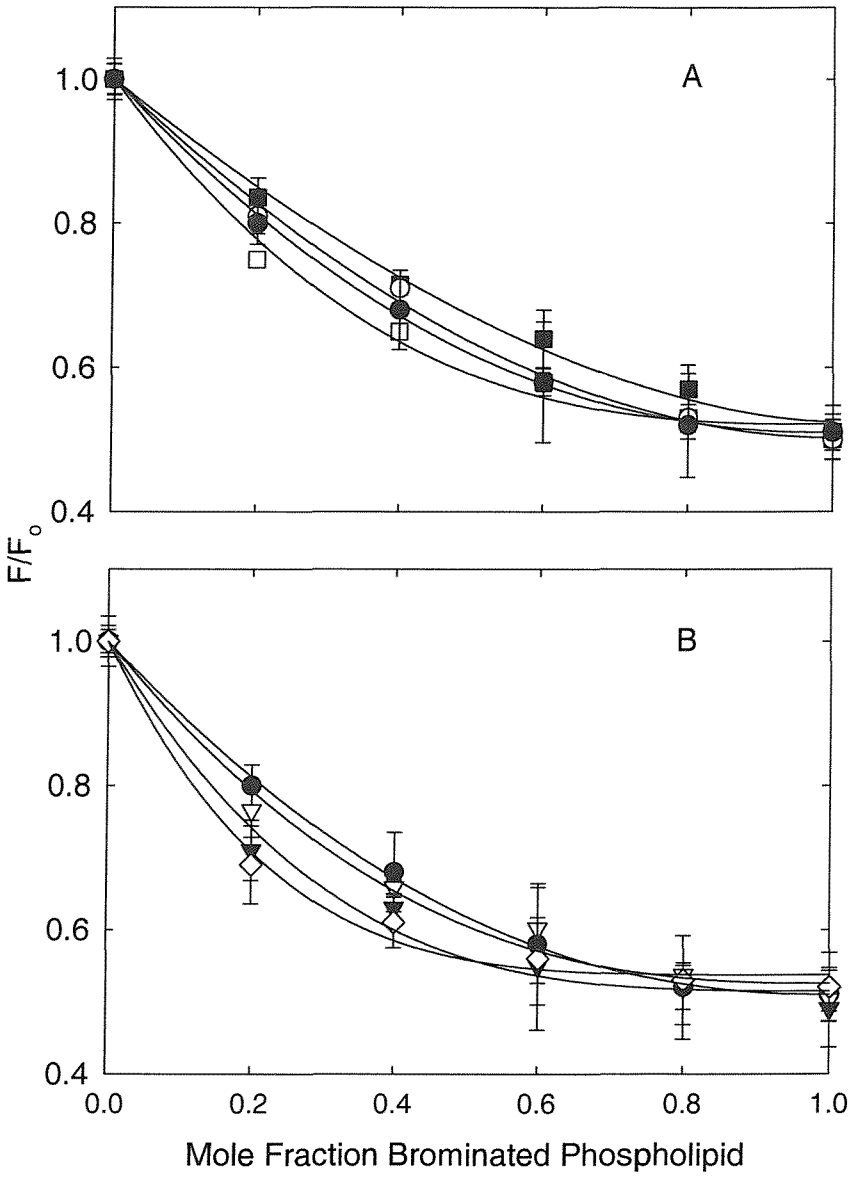

Figure 7.8 Quenching of V21K:F80W-TbMscL in mixtures of phosphatidylcholines with di(Br_2C18:0)PC. V21K:F80W-TbMscL was reconstituted into mixtures of di(Br_2C18:0)PC and A) (□), di(C12:0)PC; (■), di(C14:1)PC; (○), di(C16:1)PC; (●), di(C18:1)PC; and B) (●), di(C18:1)PC; (▽), di(C20:1)PC; (▼), di(C22:1)PC; (◇), di(C24:1)PC. Data points are the average of three determinations. The solid lines show best fits to Equation 3.15 giving the relative binding constants listed in Table 7.4.

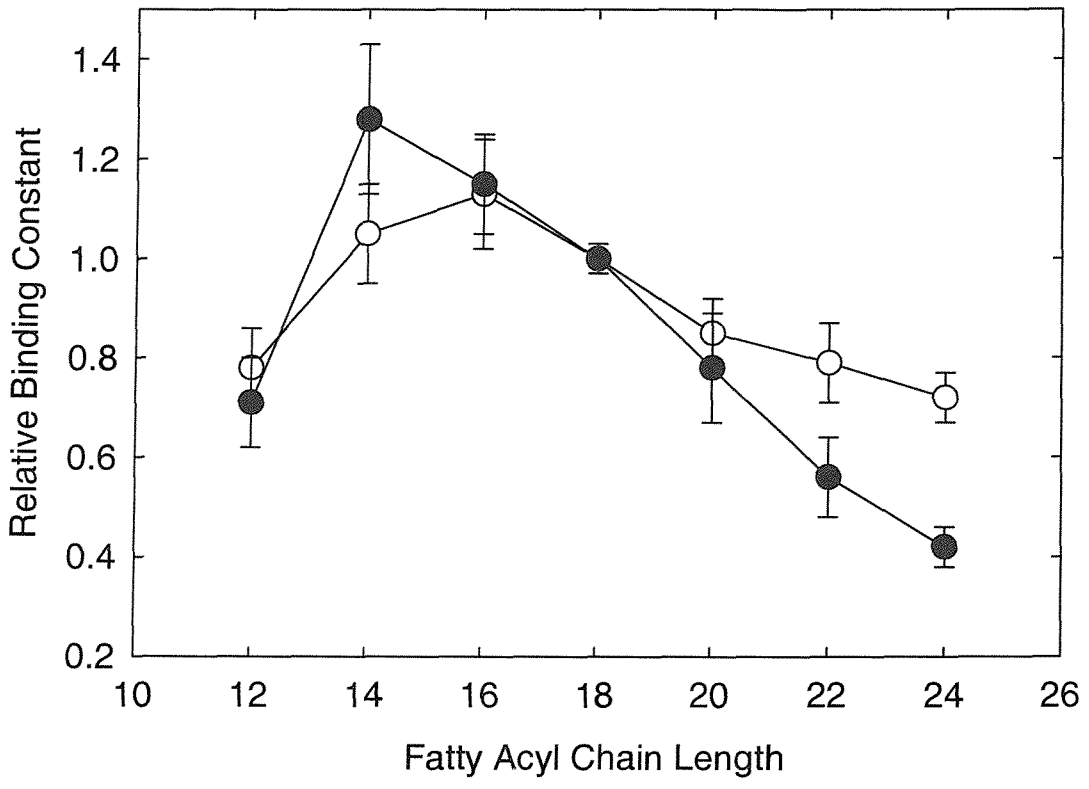

Figure 7.9 The dependence of lipid binding constants on chain length. The chain length dependencies of the binding constants for phosphatidylcholines relative to di(C18:1)PC are plotted for: (●), V21K:F80W-TbMscL; and (○), F80W-TbMscL.

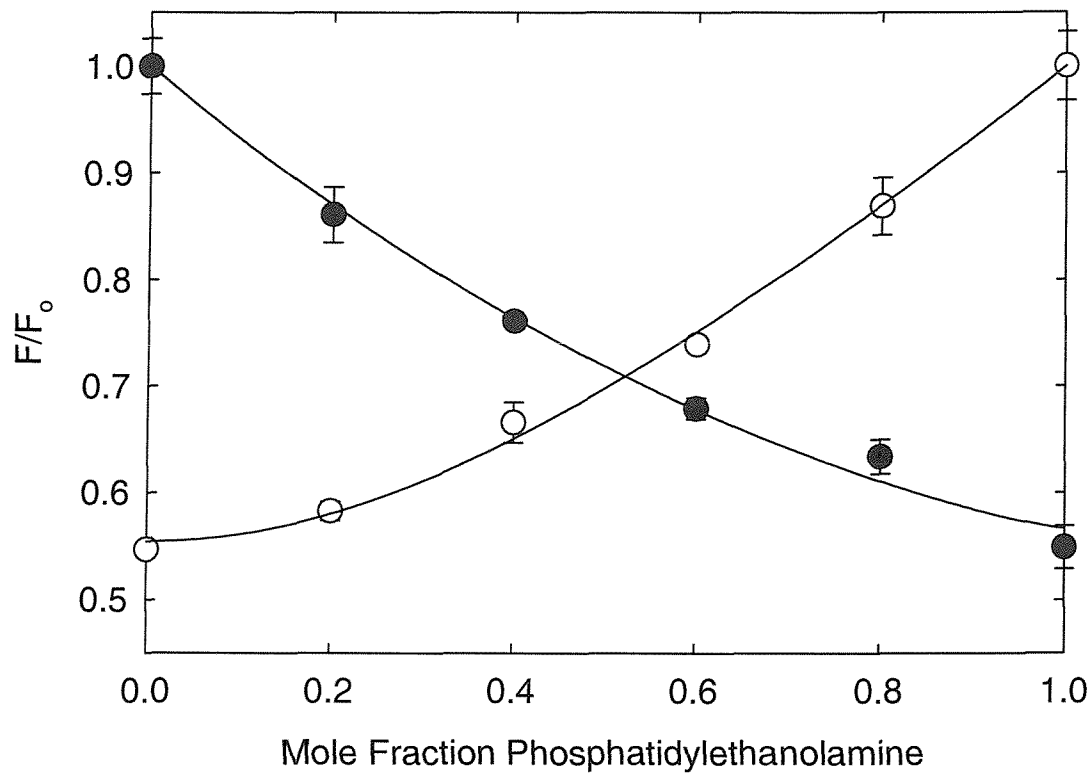

Figure 7.10 Quenching of V21K:F80W-TbMscL in mixtures of phosphatidylethanolamine and phosphatidylcholine. V21K:F80W-TbMscL was reconstituted into mixtures containing di(C18:1)PC and (Br_2C18:0)PE (●), or di(C18:1)PE and di(Br_2C18:0)PC (○). Data points are the average of three determinations. The solid lines show best fits to Equation 3.15 giving the relative binding constants listed in Table 7.5.

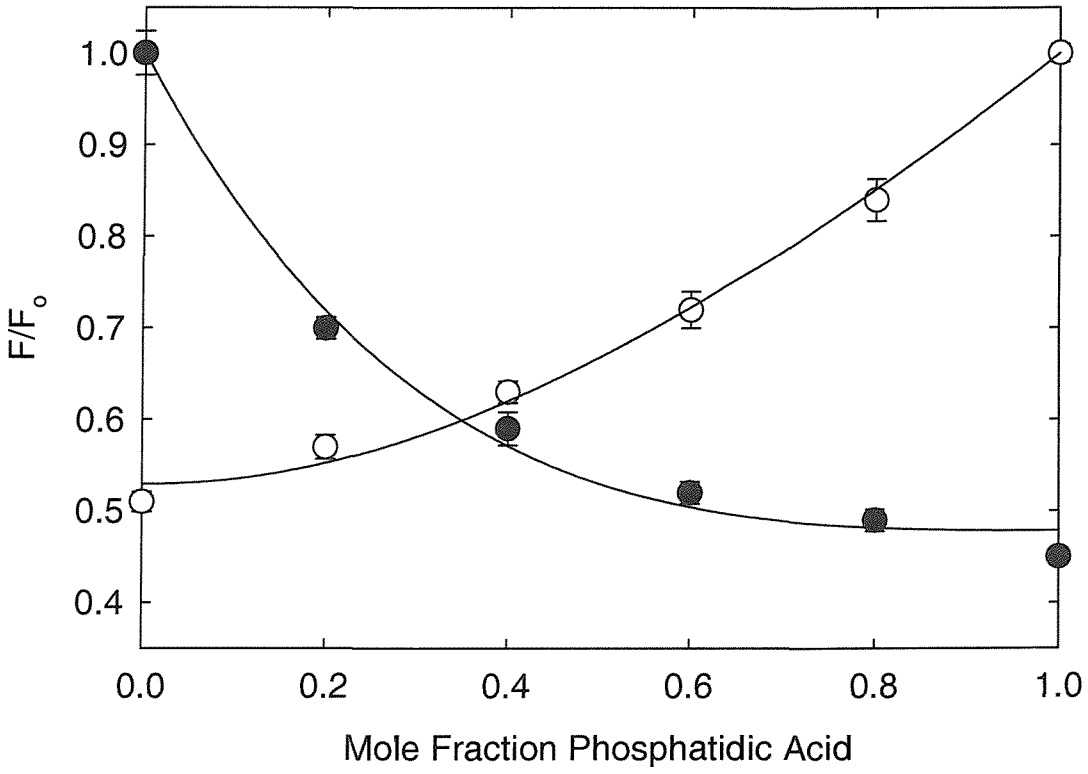

Figure 7.11 Quenching of V21K:F80W-TbMscL in mixtures of phosphatidic acid and phosphatidylcholine. V21K:F80W-TbMscL was reconstituted into mixtures containing di(C18:1)PC and (Br_2C18:0)PA (●), or di(C18:1)PA and di(Br_2C18:0)PC (○). Data points are the average of three determinations. The solid lines show best fits to Equation 3.15 giving the relative binding constants listed in Table 7.5.

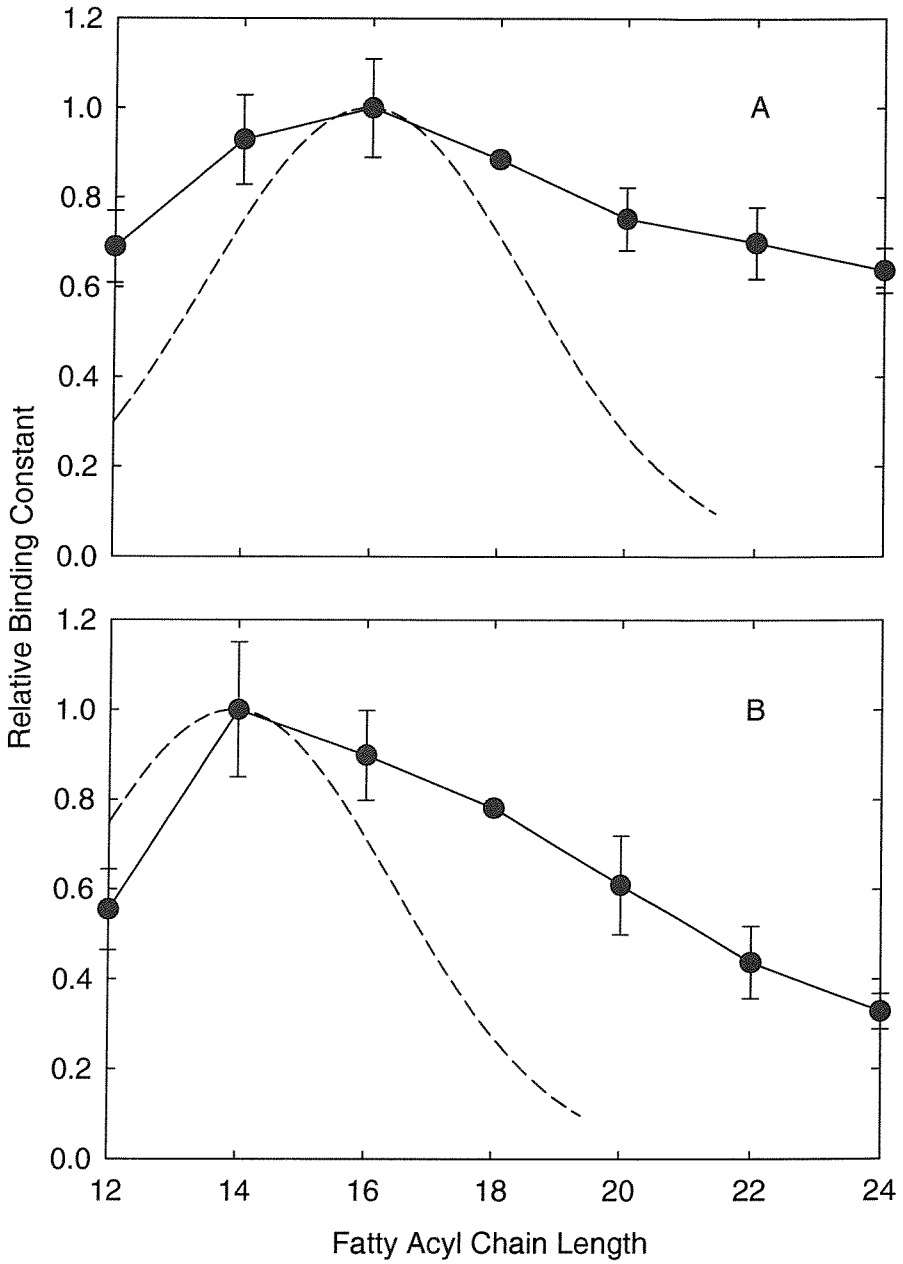

Figure 7.12 The dependence of lipid binding constants on chain length. The chain length dependencies of the binding constants for phosphatidylcholines relative to di(C18:1)PC are plotted for: A) the closed F80W-TbMscL channel scaled to a value of 1 for di(C16:1)PC; and B) the open V21K:F80W-TbMscL channel scaled to a value of 1 for di(C14:1)PC. The dotted line in A and B show the theoretical dependence of lipid binding constant determined from the data of Fattal and Ben-Shaul (1993), shifted along the chain length axis to match the experimental optimum binding at di(C16:1)PC and di(C14:1)PC for F80W and V21K:F80W-TbMscL channels respectively.

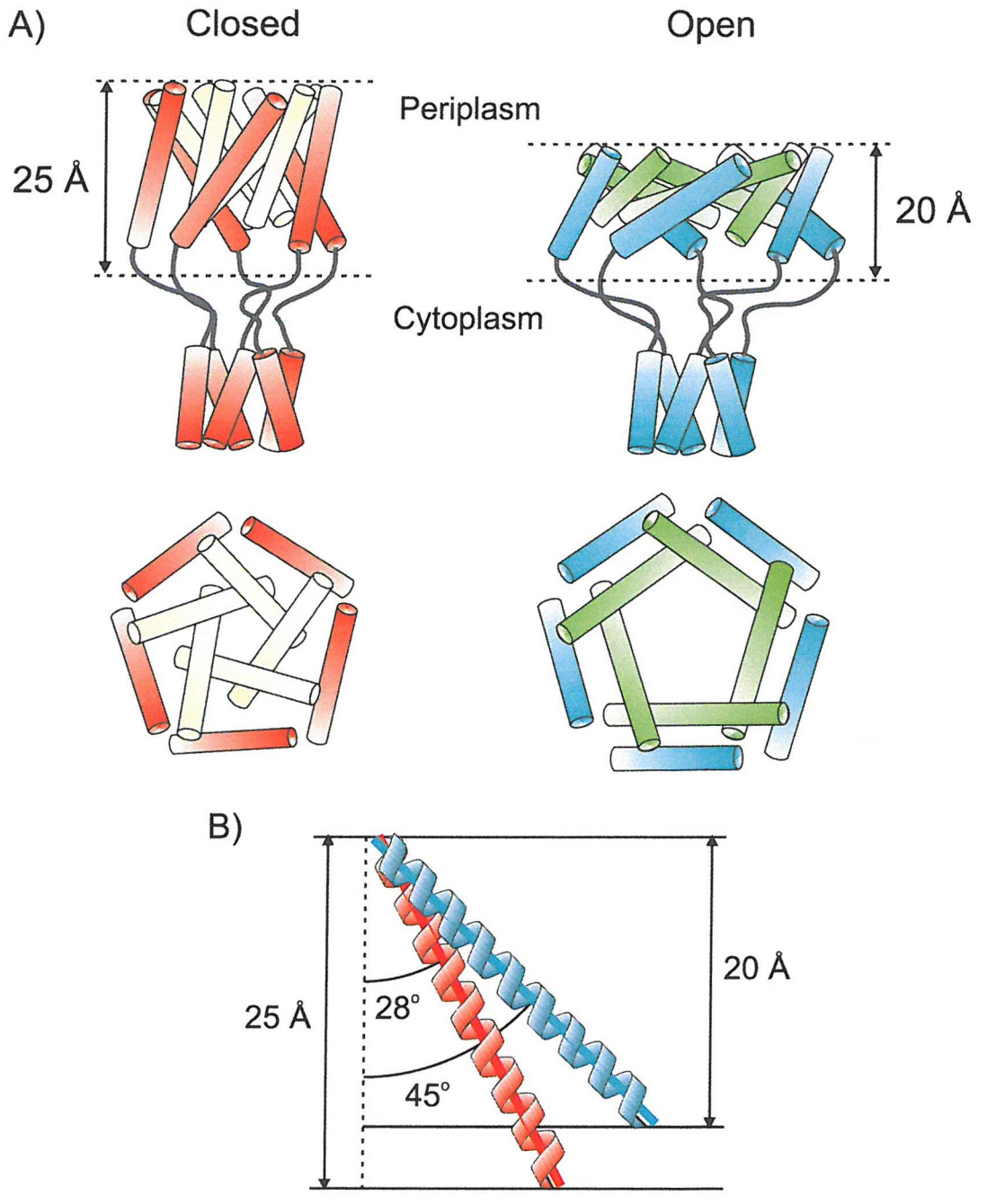

Figure 7.13 Model for hydrophobic matching of the open TbMscL channel by tilting TM2 α-helices. A) cartoon representation of the closed (red-yellow) and open TbMscL channels (blue-green), viewed from the side and the cytoplasmic surface of the membrane. B) schematic representation of TM2 α-helices showing the position of the α-helices in the closed (red) and open channels (blue). TM2 α-helices are tilted 28° to the bilayer normal and have a hydrophobic thickness of 25 Å in the closed channel. In the open EcMscL channel, TM2 α-helices tilt by an additional 17°, consistent with a reduction in hydrophobic length by ~5 Å to a hydrophobic thickness of 20 Å. The model for the open channel is adapted from Sukharev and Anishkin (2004) and Sukharev and Guy (2004).

7.4 Conclusions

7.4.1 Mutating TbMscL to an Open Channel

Mutational studies have previously identified the main channel gate of TbMscL to be formed by residues Ala-20 and Val-21 on TM1 of TbMscL; severe GOF mutants have been reported for G22K-EcMscL and V21D-TbMscL by Yoshimura et al. (1999) and Moe et al. (2000) respectively. Replacing Val-21 with a Lys residue in F80W-TbMscL did not prevent the mutated channel from rescuing *E. coli* strain MJF465 from the effects of hypoosmotic stress (Figure 7.2). However, V21K:F80W-TbMscL severely reduced the rate of growth of *E. coli* following induction of the mutant channel (Figure 7.3). These data confirm that V21K:F80W-TbMscL is a GOF phenotype and consistent with other GOF phenotypes (G22K-EcMscL, V21D-TbMscL) is likely to represent an open or open intermediate of the channel.

Cross-linking experiments with V21K:F80W-TbMscL channels in bilayers of phosphatidylcholine does not result in the characteristic ladder-like pattern of bands (see Figure 4.9), instead SDS-PAGE gels of cross-linked V21K:F80W-TbMscL following reconstitution into bilayers of di(C18:1)PC show the presence of predominantly pentameric species, with small amounts of monomer (Figure 7.4). Although, the cross-linking data suggests that V21K:F80W-TbMscL maintains a pentameric structure in bilayers of phosphatidylcholines, confirming that reconstitution does not denature the protein, the data also suggests that the pentameric species formed by V21K:F80W-TbMscL may be more stable in SDS than that formed by F80W-TbMscL.

7.4.2 Fluorescence Properties

Mutation of Val-21 to a Lys residue in F80W-TbMscL leads to altered fluorescence properties of the Trp reporter group at position 80 in TbMscL; fluorescence emission spectra are shifted to longer wavelengths (Figure 7.5, Table 7.1). The red shifted emission spectrum for V21K:F80W-TbMscL suggests a more polar environment for

residue 80 in V21K:F80W than in the closed channel F80W-TbMscL. A similar observation was made with the Trp residue in the charge mutant F80W:R98Q:K99Q:K100Q-TbMscL (Chapter 6). In contrast to the results with the single charge mutants, where reconstitution of these channels into bilayers of di(C18:1)PA and di(C18:1)PS reversed the shift in Trp fluorescence emission (See Table 6.1), the results with V21K:F80W reconstituted into bilayers of di(C18:1)PA suggest that the conformational change induced by introducing the Lys residue at position 21 cannot be reversed by interaction with anionic lipid (Table 7.1).

A different location for residue 80 in the open channel than in the closed channel is also suggested by fluorescence quenching data. Fluorescence quenching by the water soluble quencher acrylamide with V21K:F80W-TbMscL is greater than the fluorescence quenching observed with the closed F80W-TbMscL channel, and approximately equal to that observed with F79W-TbMscL (Figure 7.6, Table 7.2). Furthermore, fluorescence quenching of F80W by di(Br_2C18:0)PC is greater than the fluorescence quenching observed with V21K:F80W-TbMscL (Figure 7.7, Table 7.3). A similar observation was made by comparison of residues F79W and F80W in the closed channel (Chapter 5). The lower levels of Trp fluorescence quenching of V21K:F80W-TbMscL in the open state is consistent with a reduced accessibility of the dibrominated quencher for F80W. Collectively, the quenching data obtained for F80 (Tables 7.2 and 7.3), therefore suggests that F80W in the open channel is located in a more polar environment than F80W in the closed channel. This could be achieved, for example, by a rotation of TM2.

7.4.3 Lipid Binding to the Open form of TbMscL

7.4.3.1 *Chain Length*

Lipid binding constants for phosphatidylcholines with chain lengths between C12-C24 for V21K:F80W-TbMscL are shown in Figure 7.8 and Table 7.4. From this data it can be seen that binding constants vary by a factor of three for V21K:F80W-TbMscL, with weak binding observed for phosphatidylcholines with short or long fatty acyl chains, the highest affinity being observed for an acyl chain length of C14.

The hydrophobic thickness of a di(C14:1)PC bilayer can be calculated using Equation 4.1, to be about 20 Å. The lipid binding with greatest affinity to the closed F80W-TbMscL channel was a phosphatidylcholine with an acyl chain length of C16, corresponding to a hydrophobic thickness of 24 Å (Chapter 4). The fact that di(C14:1)PC is the lipid binding most strongly to the open V21K:F80W-TbMscL channel, whereas di(C16:1)PC binds with greatest affinity to the closed F80W-TbMscL channel suggests that the hydrophobic thickness for TbMscL has decreased by 4 Å on transforming from the closed to open channel structure.

7.4.3.2 *Protein vs Bilayer Distortion as a Result of Hydrophobic Matching*

The efficiency of hydrophobic matching between the lipid bilayer and MscL is high. For example, in Chapter 5 the fluorescence emission maxima of single Trp mutants of TbMscL were shown to maintain their locations when the fatty acyl chain lengths of the phosphatidylcholines were varied between C12 and C24 (Table 5.1), suggesting highly efficient matching of the hydrophobic thickness of MscL to that of the lipid bilayer, despite a ca. 21 Å change in bilayer thickness (Chapter 5).

Fattal and Ben-Shaul (1993) calculated the membrane deformation energy due to the inclusion in the bilayer of a rigid protein, over a range of bilayer hydrophobic thicknesses from 20-40 Å. The resulting profile of energy of interaction as a function of hydrophobic mismatch was fairly symmetrical about the point of zero mismatch. The basis of the model is that the protein is a fixed rigid structure whereas the hydrophobic lipid chains are flexible, able to stretch, compress and tilt (Figure 7.1). As shown in Figure 7.12, the model of Fattal and Ben-Shaul (1993) predicts a much steeper dependence of the relative binding constant on chain length than observed experimentally for either the closed or open TbMscL channels. Roughly, it can be estimated that the effect of varying lipid chain length is about half that expected from the model of Fattal and Ben-Shaul (1993). Thus, again roughly, it can be said that about half of any hydrophobic mismatch is made up by distortion of the lipid bilayer, the remaining half being accounted for by distortion of the protein. This conclusion is in agreement with molecular dynamic simulations of MscL in thin bilayers, about half the hydrophobic mismatch in a C12 bilayer is made up by stretching of the chains (Elmore and Dougherty, 2003). However, complete hydrophobic matching is

not achieved in the simulations, possibly because of the relatively short time scale of the simulations did not allow any large changes in the conformation of the protein (Elmore and Dougherty, 2003).

If distortion of the lipid bilayer does not provide full hydrophobic matching with MscL, then MscL must distort to match the hydrophobic thickness of the lipid bilayer. This is supported by the fact that the approach of Fattal and Ben-Shaul (1993) works reasonably well for a β-barrel protein OmpF, since β-barrel proteins cannot distort to match the surrounding lipid bilayer (O'Keeffe et al., 2000). However α-helical membrane proteins should not be considered to be rigid in the sense of Fattal and Ben-Shaul as they can distort to match the surrounding lipid bilayer (Lee, 2004). Possible distortions of the membrane protein include changes in the tilt of the transmembrane α-helices, changes in the packing of the transmembrane α-helices, and rotation of side chains about the Cα-Cβ bond linking the side chain to the polypeptide backbone; for a residue at the end of a helix such a rotation would change the effective length of the helix (Lee, 2003).

The crystal structure of Chang et al. (1998) showed that both transmembrane α-helices in each monomer are tilted 28° with respect to the bilayer normal in the closed structure; the hydrophobic thickness for TbMscL was determined in Chapters 4 and 5 to be ca. 25 Å (Figure 7.13), thereby allowing the hydrophobic length of TM2 to be calculated from simple trigonometry using the following equation:

$$cos\theta = a/h \qquad \text{Equation 7.1}$$

where a is the adjacent and h is the hypotenuse. Using equation 7.1 with a value of 25 Å for a, and an angle of 28°, the hydrophobic length of TM2 is 28 Å. Webb et al. (1998) have suggested that transmembrane α-helices can reduce their effective length across the bilayer and therefore apparent hydrophobic thickness by tilting. Tilting and rotation of the transmembrane α-helices in EcMscL has been observed by Perozo et al. (2002a); TM2 of EcMscL was reported to tilt an additional 17° towards the bilayer plane and rotate by at least 70° in an anticlockwise direction upon forming an open channel. Using these data and Equation 7.1, a model for TM2 α-helices of the TbMscL channel in the open form can be developed (Figure 7.13). Assuming the

gating mechanism is conserved throughout the MscL channels, a similar 17° tilt of TM2 towards the bilayer plane would also be observed for TbMscL; this increased tilt for the TM2 α-helices would reduce their effective hydrophobic length along the bilayer normal by ~5 Å, giving a hydrophobic thickness for the open form of the channel of 20 Å. Thus, the experimental observation that di(C14:1)PC is the lipid binding most strongly to the open V21K:F80W-TbMscL channel (Table 7.4) is in excellent agreement with a 5 Å reduction in the apparent hydrophobic thickness of the open channel (Figure 7.13).

Effects of hydrophobic matching on protein structure will be highly cooperative (Lee, 1998, Lee 2003). Reconstitution of F80W-TbMscL into di(C14:1)PC bilayers was shown not to alter the emission maximum for the Trp group (Table 5.1), the emission maximum remaining centred around 321 nm. In contrast, V21K:F80W-TbMscL has an emission maximum centred at 332 nm (Table 7.1), suggesting that the F80W-TbMscL chanel reconstituted into di(C14:1)PC bilayers remains closed, despite the open channel structure best matching the hydrophobic thickness of a bilayer containing di(C14:1)PC. This observation is supported by the fact that although thin bilayers favour channel opening of the EcMscL homologue and thick bilayers stabilise the closed form of the channel, changes in bilayer thickness alone were insufficient to open the channel (Perozo et al., 2002b).

7.4.3.3 *Head Groups*

The relative binding constants for V21K:F80W-TbMscL as a function of phospholipid head group are shown in Table 7.5. The data for V21K:F80W shows a slight preference for di(C18:1)PE over di(C18:1)PC, an effect not seen in F80W (Table 7.5). The effect is small, but could represent an effect of channel opening, with more possibilities for hydrogen bonding between di(C18:1)PE and the open form of the channel than between di(C18:1)PE and the closed channel.

Results obtained with di(C18:1)PA for the open V21K:F80W-TbMscL channel are significantly different from the results obtained with the closed F80W-TbMscL channel, in two ways (Table 7.5). First, the open channel shows less selectivity for di(C18:1)PA over di(C18:1)PC than the closed channel. Second, whereas the binding

constant for di(C18:1)PA and the closed channel obtained from experiments with di(C18:1)PC and di(Br_2C18:0)PA mixtures, for the open form of the channel, the binding constants obtained from the two sets of experiments were equal (Table 7.5). Thus whereas the data obtained for the closed channel was consistent with two classes of binding site, one of which had a high affinity for di(C18:1)PA, the data obtained for the open channel is consistent with simple competitive binding of di(C18:1)PA to a single class of site. As discussed in Chapter 6, the high affinity site for di(C18:1)PA on F80W-TbMscL probably involves the charge cluster Arg-98, Lys-99 and Lys-100. Thus in forming the open channel, this cluster must be disrupted or repositioned, so that high affinity binding of di(C18:1)PA is no longer observed.

Chapter 8:

General Discussion

8 GENERAL DISCUSSION

Membrane proteins such as receptors and transporters are responsible for the specific functions of biological membranes. The interaction between membrane proteins and lipids is important, since membrane lipids not only serve as solvent for the integral membrane protein, but also have the ability to significantly affect the activity of the protein. Membrane lipids could affect membrane proteins in many ways, through effects of bulk properties of the membrane such as membrane thickness, and through more specific interactions between individual lipids and the protein, for example, through hydrogen bonding, charge, and van der Waals interactions.

Interactions between the lipid bilayer and the mechanosensitive channel of large conductance, MscL, are particularly important since MscL opens on increasing tension in model systems containing just lipid and MscL, so that membrane tension must be transduced directly from the lipid molecules to the protein (Sukharev et al., 1999b).

These studies have shown that MscLs from *E. coli* and *M. tuberculosis* can be successfully purified from *E. coli* membranes using a range of detergents, the most effective detergents being dodecylmaltoside and octylglucoside. A reconstitution protocol was developed for MscL allowing successful reconstitution into synthetic bilayers by dilution or by dialysis (Chapter 4). MscLs were shown to retain their pentameric structures in phospholipids of various fatty acyl chain lengths and lipid head groups (Figure 4.9), confirming that reconstitution does not denature the proteins. Reconstitution then allowed the important features of the surrounding membrane to be defined.

Single Trp residues were introduced into the membrane regions of EcMscL and TbMscL, which allowed lipid binding constants to be measured for MscL (Chapter 4). Trp residues introduced into the bilayer interface regions of TbMscL were shown to maintain their locations, despite a change in bilayer thickness of ca. 21 Å (Section 5.4.2). Similarly, Trp residues in EcMscL were also shown to maintain their locations with respect to the membrane interface despite a ca. 17 Å change in bilayer thickness. These

data confirm that the efficiency of hydrophobic matching between both MscLs and the surrounding lipid bilayer is high.

A technique was developed to identify the hydrophobic thickness of a membrane protein (Chapter 5). Scanning Trp mutagenesis on TM2 of MscL combined with fluorescence spectroscopy, was used to map the membrane profile onto the protein. The results obtained with the Trp mutants were confirmed by measuring the fluorescence lifetime of NBD-labelled Cys mutants of MscL. Both methods revealed that residues Leu-69 and Leu-92, respectively located next to or close to surface-exposed oxygens of Asp-68 and Asp-16, represent the location of the bilayer interfaces in MscL. The hydrophobic thickness of TbMscL estimated from the crystal structure assuming that Leu-69 and Leu-92 are located at the glycerol backbone region is ca. 25 Å (Figures 5.22 and 5.23B).

Binding of phospholipids to EcMscL and TbMscL was shown to be selective (Chapter 4). The phosphatidylcholine with the highest binding constant for both MscLs was that with a chain of length C16, corresponding to a bilayer of hydrophobic thickness ca. 24 Å, consistent with the hydrophobic thickness of TbMscL of about 25 Å determined from the scanning Trp mutagenesis data. The native *M. tuberculosis* membrane will have a hydrophobic thickness close to 24 Å since the predominant phospholipids of *M. tuberculosis* contain C18:1 and C16:0 chains at the *sn*-1 and *sn*-2 positions, respectively (Coren, 1984). Lipid binding constants change by only a factor of 1.5 for TbMscL and by a factor of 3 for EcMscL in the chain length range from C12 to C24, much less than expected from theories of hydrophobic mismatch in which the protein is treated as a rigid body. The variation in lipid binding constant with varying lipid chain length suggests that approximately half of any hydrophobic mismatch between the membrane and MscL is made up by distortion of the lipid bilayer; the remaining half must be accounted for by distortion of the protein. This is supported by the molecular dynamic simulations of Elmore and Dougherty (2003).

An *in vivo* channel function assay was developed to ensure the mutant channels generated in these studies were not loss of function mutants, and confirmed that introducing Trp residues into MscL did not block activity. Furthermore, measuring the

rate of growth of *E. coli* expressing these mutant channels was used to ensure that the channels were not gain of function (GOF) mutants, and hence remained closed under normal cell growth conditions (Chapter 5).

Introducing a Lys residue into the hydrophobic gate of MscL at position Val-21 generated a GOF phenotype, as shown by the effects on the rate of growth of *E. coli* expressing these channels (Chapter 7). Lipid binding constants were determined for V21K-TbMscL. The highest binding constant for V21K-TbMscL was observed with a chain of length C14, corresponding to a bilayer of hydrophobic thickness of ca. 20 Å, compared to the value of ca. 24 Å obtained from the same lipid binding studies with the closed channel. This suggests that the hydrophobic thickness for TbMscL is reduced by 4 Å on transforming from the closed to open channel structure consistent with the ESR results obtained for EcMscL by Perozo et al. (2002a,b)

Previous studies with membrane proteins have shown that phospholipid binding constants exhibit a dependence on head group structure (Starling et al., 1996; O'Keeffe et al., 2000). Selectivity in binding was also observed with respect to the lipid head group for MscL (Chapter 4). Quenching experiments with the closed TbMscL channel labelled with a Trp reporter group in the centre of the bilayer (F80W) revealed a single class of binding sites for phosphatidylcholine and phosphatidylethanolamine on TbMscL. Binding constants for anionic lipids were greater than that for phosphatidylcholine, but quenching experiments suggest two classes of lipid binding sites on TbMscL for phosphatidic acid.

The nature of the lipid binding sites was investigated in more detail, by moving the position on the Trp residue from the centre of the bilayer to the bilayer interfaces, so that lipid-protein interactions for the protein on either side of the membrane could be studied (Chapter 6). This is important for two main reasons, the first being that lipids are asymmetrical distributed between the two bilayer leaflets in living cells (Cullis et al., 1996), and the second being that Martinac et al. (1990) have previously shown that bilayer asymmetry affects the activity of MscL. Single Trp mutants of TbMscL, L69W and Y87W were used to measure lipid binding constants on the periplasmic and

cytoplasmic sides of the membrane, respectively. This appears to be the first reported measurement of this type for a membrane protein, primarily because the presence of multiple Trp residues in membrane proteins complicates the analysis of the fluorescence quenching data; MscL channels from *Escherichia coli* and *Mycobacterium tuberculosis* contain no Trp residues.

Quenching data for L69W on the periplasmic side of the membrane is consistent with simple competitive binding of lipids at a single class of site (Section 6.4.3.1). No selectivity was observed for anionic phospholipids. This is consistent with the distribution of charged residues in TbMscL. Lipid binding constants measured for the cytoplasmic side of the membrane using Trp mutant Y87W-TbMscL were very different to those obtained for the periplasmic side of the membrane. Quenching data for Y87W reveals two binding sites for anionic lipid close to residue 87, binding to one of these sites showing a marked preference for anionic lipid over zwitterionic lipid, whereas binding at the second site shows a small preference for anionic lipid over zwitterionic lipid. The size of the MscL channel is such that ca. 3 lipid binding sites in all will exist per monomer on the cytoplasmic side. The major membrane lipids of the *Mycobacteria* are the anionic phospholipids cardiolipin and phosphatidylinositolmannosides (Coren, 1984). Thus, given the stronger binding of anionic than zwitterionic phospholipids to TbMscL to two of the three sites on the cytoplasmic side, the majority of the lipids surrounding TbMscL in the native membrane on the cytoplasmic side are likely to be anionic phospholipids. On the cytoplasmic side of the membrane the only positively charged residues in a position to interact with an anionic phospholipid headgroup are Arg-98, Lys-99 and Lys-100.

Sequence alignments confirmed that residues Arg-98, Lys-99 and Lys-100 belong to a conserved charge cluster (equivalent to Arg-104, Lys-105, and Lys-106 in EcMscL). Single mutations of these charged residues in F80W result in a decreased affinity for phosphatidic acid (Section 6.4.4). Simultaneous mutation of all three charged residues results in total loss of selectivity in binding phosphatidic acid. However, the triple charge mutation severely affected the rate growth of *E. coli* expressing the channel, consistent with a GOF phenotype. The V21K mutant was used to determine binding

constants to a GOF channel that retains the Arg-98, Lys-99 and Lys-100 charge cluster. Lipid binding measurements show that di(C18:1)PC and di(C18:1)PA bind with equal affinity, suggesting that the conformational change caused by the V21K mutation results in a break-up of the cluster of three positive charges, and that the loss of binding of anionic lipids observed with the Arg-98, Lys-99 and Lys-100 charge mutants is not simply due to loss of the charge interaction. Interestingly deletion of the charge cluster in the C-terminal region from the *E. coli* protein leads to loss of function, providing additional evidence that this region of MscL has an important role in channel function (Blount et al., 1996c).

In all lipid binding measurements di(C18:1)PE was shown to bind with the same affinity to MscL as di(C18:1)PC, except for V21K where it bound slightly more strongly. The equal binding affinities measured in this study provide no evidence for the idea that di(C18:1)PE is in some way 'special', despite the very different hydrogen bonding potential of the PE and PC head groups. Molecular dynamics simulations of Elmore and Dougherty (2003) show that the cytoplasmic domain of the protein undergoes conformational changes upon transition from a PC to PE bilayer. Therefore, the equal binding affinities for PE and PC to TbMscL on the cytoplasmic side could be the result of a compensatory mechanism, in which the protein changes its structure from a bilayer of PC to a bilayer of PE.

Trp fluorescence spectroscopy is a powerful tool to study the structures of membrane proteins, and the results presented in this thesis show that Q51W, T66W, L73W and I77W located towards the periplasmic end of TM2 of TbMscL, undergo a 3 nm shift to a shorter wavelength on changing the surrounding lipid from di(C24:1)PC to di(C12:0)PC; the fluorescence emission maxima of all other Trp residues remains constant (Section 5.4.3). The emission maximum for residues at the bilayer interfaces remains unchanged, suggesting that TM2 must tilt to match the bilayer thickness. The fact that residues 80 to 103 on the cytoplasmic half of TM2 hardly change with changing bilayer thickness, whereas 73 and 77 have a small change in fluorescence suggests that any rotation of TM2 does not occur as a whole, but that only the N-terminal end rotates upon changes in bilayer thickness.

Trp-80 in the closed TbMscL channel has a fluorescence emission maximum of 321 nm, whereas the same Trp residue in the V21K channel emits at ca. 332 nm (Section 7.3.3). The other severe GOF phenotype generated in these studies, F80W:R98Q:K99Q:K100Q also has a fluorescence emission maximum around 332 nm. Thus, the data suggests that a major conformation change between the closed and open forms of MscL affects the location of the Trp residue introduced at position 80.

In conclusion, the closed structures of both *E. coli* and *M. tuberculo*sis MscL have a hydrophobic thickness of ca. 25 Å, which best match a phosphatidylcholine bilayer with a fatty acyl chain of C16. The bilayer interfaces have been defined for TbMscL as being at positions Leu-69 and Leu-92 on the two sides of the bilayer. Hydrophobic matching for both MscL proteins is very high upon changes in bilayer thickness, with interfacial residues remaining at the bilayer interfaces. These data together with the chain length dependency data reveal that both MscLs are flexible proteins, and that hydrophobic matching for TbMscL involves tilting of the TM2 together with small changes in the position of some residues located towards the periplasmic end of the helix. It appears that all lipid head groups bind equally well to TbMscL on the periplasmic side of the membrane. In contrast, anionic lipids bind with significantly greater affinity on the cytoplasmic side of TbMscL, with two classes of binding site involving the conserved charge cluster Arg-98, Lys-99 and Lys-100. This binding site is broken up when the channel forms an open structure. In the open channel the protein thins by 4 Å.

References

REFERENCES

Ajouz, B., Berrier, C., Garrigues, A., Besnard, M. & Ghazi, E. 1998. *Journal of Biological Chemistry* 273: 26670-26674.

Ajouz, B., Berrier, C., Besnard, M., Martinac, B. & Ghazi, A. 2000. *Journal of Biological Chemistry* 275: 1015-1022.

Åkerlöf, G. & Short, O. A. 1936. *Journal of American Chemical Society* 58: 1241-1243.

Alberts, B., Johnson, A., Lewis, J., Raff, M., Roberts, K. & Walter, P. 2002. Molecular Biology Of The Cell. New York: Garland Science.

Anishkin, A., Gendel, V., Sharifi, N. A., Chiang, C. S., Shirinian, L., Guy, H. R. & Sukharev, S. I. 2003. *Journal of General Physiology* 121: 227-244.

Baldwin, P. A. & Hubbell, W. L. 1985. *Biochemistry* 24: 2633-2639.

Bartlett, G. R. 1952. *Journal of Biological Chemistry* 234: 466-468.

Bass, R. B., Strop, P., Barclay, M. T. & Rees, D. C. 2002. *Science* 298: 1582-1587.

Batiza, A. F., Rayment, I. & Kung, C. 1999. *Structure with Folding & Design* 7: R99-R103.

Ben-Shaul, A. 1995. In Lipowsky, R. & Sackmann, E. (Eds) Structure and Dynamics of Membranes *From Cells to Vesicles* (pp. 359-401). Amsterdam: Elsevier.

Berg, J. M., Tymoczko, J. L. & Stryer, L. 2002. Biochemistry. New York: W.H. Freeman and Company.

Berrier, C., Coulombe, A., Houssin, C. & Ghazi, A. 1989. Pressure-activated channels are located in the inner membrane. *Febs Letters* 259: 27-32.

Berrier, C., Coulombe, A., Szabo, I., Zoratti, M. & Ghazi, A. 1992. *European Journal of Biochemistry* 206: 559-565.

Berrier, C., Besnard, M., Ajouz, B., Coulombe, A. & Ghazi, A. 1996. *Journal of Membrane Biology* 151: 175-187.

Berrier, C., Garrigues, A., Richarme, G. & Ghazi, A. 2000. *Journal Of Bacteriology* 182: 248-251.

Betanzos, M., Chiang, C. S., Guy, H. R. & Sukharev, S. I. 2002. *Nature Structural Biology* 9: 704-710.

Bezrukov, S. M. 2000. *Current Opinion in Colloid & Interface Science* 5: 237-243.

Biggin, P. C. & Sansom, M. S. P. 2001. *Current Biology* 11: R364-R366.

Bligh, E. G. & Dyer, W. J. 1959. *Canadian Journal of Biochemistry and Physiology* 37: 911-915.

Blount, P., Sukharev, S. I., Moe, P. C., Nagle, S. K. & Kung, C. 1996a. *Biochemistry* 87: 1-8.

Blount, P., Sukharev, S. I., Moe, P. C., Schroeder, M. J., Guy, H. R. & Kung, C. 1996b. *Embo Journal* 15: 4798-4805.

Blount, P., Sukharev, S. I., Schroeder, M. J., Nagle, S. K. & Kung, C. 1996c. *Proceedings of the National Academy of Sciences of the United States of America* 93: 11652-11657.

Blount, P., Schroeder, M. J. & Kung, C. 1997. *Journal of Biological Chemistry* 272: 32150-32157.

Blount, P. 2003. *Neuron* 37: 731-734.

Booth, I. R. & Louis, P. 1999. *Current Opinion in Microbiology* 2: 166-169.

Booth, I. R., Edwards, M. D. & Miller, S. 2003. *Biochemistry* 42: 10045-10053.

Bowie, J. U. 1997. *Journal of Molecular Biology* 272: 780-789.

Campbell, I. D. & Dwek, R. A. 1986. In Campbell, I. D. & Dwek, R. A. (Eds) Biological Spectroscopy (pp. 91). London: The Bejamin/Cummings Publishing Company, Inc.

Cantor, R. S. 1997a. *Journal of Physical Chemistry B* 101: 1723-1725.

Cantor, R. S. 1997b. *Biochemistry* 36: 2339-2344.

Cantor, R. S. 1999. *Biophysical Journal* 76: 2625-2639.

Caputo, G. A. & London, E. 2003. *Biochemistry* 42: 3265-3274.

Chang, G., Spencer, R. H., Lee, A. T., Barclay, M. T. & Rees, D. C. 1998. *Science* 282: 2220-2226.

Chothia, C., Levitt, M. & Richardson, D. 1981. *Journal Of Molecular Biology* 145: 215-250.

Clark, E. H., East, J. M. & Lee, A. G. 2003. *Biochemistry* 42: 11065-11073.

Colombo, G., Marrink, S. J. & Mark, A. E. 2003. *Biophysical Journal* 84: 2331-2337.

Coren, M. B. 1984. In Kubica, G. P. & Wayne, L. G. (Eds) The Mycobacteria (pp. 379-415). New York: Marcel Dekker.

Cornelius, F. 2001. *Biochemistry* 40: 8842-8851.

Cruickshank, C. C., Minchin, R. F., Le Dain, A. C. & Martinac, B. 1997. *Biophysical Journal* 74: 2889-2902.

Csonka, L. N. 1989. *Microbiological Reviews* 53: 121-147.

Cullis, P. R., Fenske, D. B. & Hope, M. J. 1996. In Vance, D. E. & Vance, J. (Eds) Biochemistry of Lipids, Lipoproteins and Membranes (pp. 1-33). Amsterdam: Elsevier.

de Kruijff, B. 1997. *Nature* 386: 129-130.

de Planque, M. R. R., Boots, J. W. P., Rijkers, D. T. S., Liskamp, R. M. J., Greathouse, D. V. & Killian, J. A. 2002. *Biochemistry* 41: 8396-8404.

Dixon, G. S., Black, S. G., Butler, C. T. & Jain, A. K. 1982. *Analytical Biochemistry* 121: 55-61.

Dowhan, W. & Bogdanov, M. 2002. In Vance, D. E. & Vance, J. (Eds) Biochemistry of Lipids, Lipoproteins and Membranes (pp. 1-36). Amsterdam: Elsevier.

Doyle, D. A., Cabral, J. M., Pfuetzner, R. A., Kuo, A. L., Gulbis, J. M., Cohen, S. L., Chait, B. T. & MacKinnon, R. 1998. *Science* 280: 69-77.

East, J. M. & Lee, A. G. 1982. *Biochemistry* 21: 4144-4151.

Edwards, M. D., Booth, I. R. & Miller, S. 2004. *Current Opinion in Microbiology* 7: 163-167.

Eftink, M. R. 1991. In Dewey, T. G. (Ed) Biophysical and Biochemical Aspects of Fluorescence Spectroscopy (pp. 1-41). New York: Plenum Press.

Elmore, D. E. & Dougherty, D. A. 2001. *Biophysical Journal* 81: 1345-1359.

Elmore, D. E. & Dougherty, D. A. 2003. *Biophysical Journal* 85: 1512-1524.

Engelman, D. M., Steitz, T. A. & Goldman, A. 1986. *Annual Review of Biophysics and Biophysical Chemistry* 15: 321-353.

Epand, R. M. 1998. *Biochimica et Biophysica Acta-Reviews On Biomembranes* 1376: 353-368.

Esnouf, R. M. 1999. *Acta Crystallography* 55: 938-940.

Fairman, W. A., Sonders, M. S., Murdoch, G. H. & Amara, S. G. 1998. *Nature Neuorscience* 1: 105-113.

Fattal, D. R. & Ben-Shaul, A. 1993. *Biophysical Journal* 65: 1795-1809.

Froud, R. J., East, J. M., Rooney, E. K. & Lee, A. G. 1986. *Biochemistry* **25**: 7535-7544.

Garavito, R. M. & Ferguson-Miller, S. 2001. *Journal of Biological Chemistry* 276: 32403-32406.

Glaasker, E., Konings, W. N. & Poolman, B. 1996. *Journal of Bacteriology* 271: 10060-10065.

Gould, G. W., McWhirter, J. M., East, J. M. & Lee, A. G. 1987. *Biochemical Journal* 245: 751-755.

Guharay, F. & Sachs, F. 1984. *Journal of Physiology* 352: 685-701.

Gullingsrud, J., Kosztin, D. & Schulten, K. 2001. *Biophysical Journal* 80: 2074-2081.

Hamill, O. P. & McBride, D. 1993. *Biophysical Journal* 65: 17-18.

Hamill, O. P. & Martinac, B. 2001. *Physiological Reviews* 81: 685-740.

Harwood, J. L. & Russell, N. J. 1984. Lipids in Plants and Microbes. London: George Allen and Unwin.

Häse, C. C., Le Dain, A. C. & Martinac, B. 1995. *Journal of Biological Chemistry* 270: 18329-18334.

Higuchi, R., Krummel, B. & Saiki, R. K. 1988. *Nucleic Acids Research* 16: 7351-7367.

Ingraham, J. L., Low, K. B., Magasanik, B., Schaechter, M. & Umbarger, H. E. 1987. *Escherichia coli* and *Salmonella typhimurium*: Cellular and Molecular Biology. Washington DC: American Society for Microbiology.

Janmey, P. 1995. In Lipowsky, R. & Sackmann, E. (Eds) Handbook of Biological Physics (pp. 805-849). New York: Elsevier Science.

Jormakka, M., Tornroth, S., Byrne, B. & Iwata, S. 2002. *Science* 295: 1863-1868.

Kong, Y. F., Shen, Y. F., Warth, T. E. & Ma, J. P. 2002. *Proceedings of the National Academy of Sciences of the United States of America* 99: 5999-6004.

Ladokhin, A. S. 1999. *Biophysical Journal* 76: 946-955.

Ladokhin, A. S. 2000. Fluorescence Spectroscopy in Peptide and Protein Analysis. In Meyers, R. A. (Ed) Encyclopedia of Analytical Chemistry (pp. 5762-5779). Chichester: John Wiley & Sons Ltd.

Ladokhin, A. S., Jayasinghe, S. & White, S. H. 2000. *Analytical Biochemistry* 285: 235-245.

Laemmli, U. K. 1970. *Nature* 227: 680-685.

Lakowicz, J. R. 1999. Principles of Fluorescence Spectroscopy. New York: Kluwer Academic/Plenum Publishers.

Landau, E. M. & Rosenbusch, J. P. 1996. *Proceedings of the National Academy of Sciences of the United States of America* 93: 14532-14535.

Landolt-Marticorena, C., Williams, K. A., Deber, C. M. & Reithmeier, R. A. F. 1993. *Journal Of Molecular Biology* 229: 602-608.

Lee, A. G. 1998. *Biochimica et Biophysica Acta-Reviews on Biomembranes* 1376: 381-390.

Lee, A. G. 2000. *Current Biology* 10: R377-R380.

Lee, A. G. 2003. *Biochimica et Biophysica Acta-Biomembranes* 1612: 1-40.

Lee, A. G. 2004. *Biochimica et Biophysica Acta-Reviews on Biomembranes* 1666: 62-87.

Levina, N., Totemeyer, S., Stokes, N. R., Louis, P., Jones, M. A. & Booth, I. R. 1999. *Embo Journal* 18: 1730-1737.

Lewis, B. A. & Engelman, D. M. 1983. *Journal of Molecular Biology* 166: 211-217.

Li, Y. Z., Moe, P. C., Chandrasekaran, S., Booth, I. R. & Blount, P. 2002. *Embo Journal* 21: 5323-5330.

London, E. & Feigenson, G. W. 1981. *Biochemistry* 20: 1939-1948.

Lotan, R. & Nicholson, G. L. 1981. Advanced Cell Biology. New York.

Maksymiw, R., Sui, S. F., Gaub, H. & Sackmann, E. 1987. *Biochemistry* 26: 2983-2990.

Mall, S., Sharma, R. P., East, J. M. & Lee, A. G. 1998. *Faraday Discussions* 127-136.

Mall, S., Broadbridge, R., Sharma, R. P., Lee, A. G. & East, J. M. 2000. *Biochemistry* 39: 2071-2078.

Mall, S., Broadbridge, R., Sharma, R. P., East, J. M. & Lee, A. G. 2001. *Biochemistry* 40: 12379-12386.

Mall, S., East, J. M. & Lee, A. G. 2002. *Peptide-Lipid Interactions* 52: 339-370.

Marsh, D. 1993. In Watts, A. (Ed) Protein-Lipid Interactions (pp. 41-66). London: Elsevier.

Marsh, D. 1996. *Biochimica et Biophysica Acta-Biomembranes* 1286: 183-223.

Martinac, B., Buechner, M., Delcour, A. H., ADLER, J. & Kung, C. 1987. *Proceedings of the National Academy of Sciences of the United States of America* 84: 2297-2301.

Martinac, B., ADLER, J. & Kung, C. 1990. *Nature* 348: 261-263.

Martinac, B. & Kloda, A. 2003. *Progress in Biophysics & Molecular Biology* 82: 11-24.

Maurer, J. A., Elmore, D. E., Lester, H. A. & Dougherty, D. A. 2000. *Journal of Biological Chemistry* 275: 22238-22244.

Maurer, J. A. & Dougherty, D. A. 2003. *Journal of Biological Chemistry* 278: 21076-21082.

McKee, T. & McKee, J. R. 1999. Biochemistry: an introduction. The McGraw-Hill Companies, Inc.

Miller, S., Bartlett, W., Chandrasekaran, S., Simpson, S., Edwards, M. D. & Booth, I. R. 2003a. *Embo Journal* 22: 36-46.

Miller, S., Edwards, M. D., Ozdemir, C. & Booth, I. R. 2003b. *Journal of Biological Chemistry* 278: 32246-32250.

Moe, P. C., Blount, P. & Kung, C. 1998. *Molecular Microbiology* 28: 583-592.

Moe, P. C., Levin, G. & Blount, P. 2000. *Journal of Biological Chemistry* 275: 31121-31127.

Morris, J. G. 1978.In Morris, J. G. (Ed) A Biologist's Physical Chemistry (pp. 181-211). London: Edward Arnold Ltd.

Munkonge, F., Michelangeli, F., Rooney, E. K., East, J. M. & Lee, A. G. 1988. *Biochemistry* 27: 6800-6805.

Nakamaru, Y., Takahashi, Y., Unemoto, T. & Nakamura, T. 1999. *Febs Letters* 444: 170-172.

O'Keeffe, A. H., East, J. M. & Lee, A. G. 2000. *Biophysical Journal* 79: 2066-2074.

Ou, X. R., Blount, P., Hoffman, R. J. & Kung, C. 1998. *Proceedings of the National Academy of Sciences of the United States of America* 95: 11471-11475.

Pérochon, E., Lopez, A. & Tocanne, J. F. 1992. *Biochemistry* 31: 7672-7682.

Perozo, E., Kloda, A., Cortes, D. M. & Martinac, B. 2001. *Journal of General Physiology* 118: 193-205.

Perozo, E., Cortes, D. M., Sompornpisut, P., Kloda, A. & Martinac, B. 2002a. *Nature* 418: 942-948.

Perozo, E., Kloda, A., Cortes, D. M. & Martinac, B. 2002b. *Nature Structural Biology* 9: 696-703.

Perozo, E. & Rees, D. C. 2003. *Current Opinion in Structural Biology* 13: 432-442.

Peter, H., Burkovski, R. & Krämer, R. 1998. *Journal of Biological Chemistry* 273: 2567-2574.

Pilot, J. D. Effects of Lipid on Membrane Protein Function. 1-257. 2001. University of Southampton. PhD Thesis.

Pilot, J. D., East, J. M. & Lee, A. G. 2001. *Biochemistry* 40: 14891-14897.

Poolman, B. & Glaasker, E. 1998. *Molecular Microbiology* 29: 397-407.

Poolman, B., Blount, P., Folgering, J. H. A., Friesen, R. H. E., Moe, P. C. & van der Heide, T. 2002. *Molecular Microbiology* 44: 889-902.

Poolman, B., Spitzer, J. J. & Wood, J. M. 2004. *Biochimica et Biophysica Acta-Reviews on Biomembranes* 1666: 88-104.

Racanksy, V., Valachovic, D. & Balgavy, P. 1987. *Acta Physica Slovaca* 37: 166-176.

Rooney, E. K. & Lee, A. G. 1986. *Journal of Biochemical and Biophysical Methods* 120: 175-189.

Roseman, M. A. 1988. *Journal Of Molecular Biology* 201: 621-623.

Rübenhagen, R., Rönsch, H., Jung, H. & Krämer, R. 2000. *Journal of Biological Chemistry* **275**: 735-741.

Rübenhagen, R., Morbach, S. & Krämer, R. 2001. *Embo Journal* 20: 5412-5420.

Sackin, H. 1995. *Annual Review of Physiology* 57: 333-353.

Sackmann, E. 1984. In Chapman, D. (Ed) Biological Membranes (pp. 105-143). London: Academic Press.

Schumann, U., Edwards, M. D., Li, C. & Booth, I. R. 2004. *Febs Letters* 572: 233-237.

Seddon, J. M. 1990. *Biochimica et Biophysica Acta* 1031: 1-69.

Seddon, J. M. & Templer, R. H. 1995. In Lipowsky, R. & Sackmann, E. (Eds) Structure and Dynamics of Membranes *From Cells to Vesicles* (pp. 97-160). Amsterdam: Elsevier.

Shepard, L. A., Heuck, A. P., Hamman, B. D., Rossjohn, J., Parker, M. W., Ryan, K. R., Johnson, A. E. & Tweten, R. K. 1998. *Biochemistry* 37: 14563-14574.

Simidjiev, I., Stoylova, S., Amenitsch, H., Javorfi, T., Mustardy, L., Laggner, P., Holzenburg, A. & Garab, G. 2000. *Proceedings of the National Academy of Sciences of the United States of America* 97: 1473-1476.

Simmonds, A. C., East, J. M., Jones, O. T., Rooney, E. K., McWhirter, J. M. & Lee, A. G. 1982. *Biochimica et Biophysica Acta* 693: 398-406.

Singer, S. J. & Nicholson, G. L. 1972. *Science* 175: 720-731.

Sprong, H., van der Sluijs, P. & van Meer, G. 2001. *Nature Reviews Molecular Cell Biology* 2: 504-513.

Starling, A. P., Dalton, K. A., East, J. M., Oliver, S. & Lee, A. G. 1996. *Biochemical Journal* 320: 309-314.

Stokes, N. R., Murray, H. D., Subramaniam, C., Gourse, R. L., Louis, P., Bartlett, W., Miller, S. & Booth, I. R. 2003. *Proceedings of the National Academy of Sciences of the United States of America* 100: 15959-15964.

Strandberg, E. & Killian, J. A. 2003. *Febs Letters* 544: 69-73.

Sukharev, S. I., Martinac, B., Arshavsky, V. Y. & Kung, C. 1993. *Biophysical Journal* 65: 1-7.

Sukharev, S. I., Blount, P., Martinac, B., Blattner, F. R. & Kung, C. 1994. *Nature* 368: 265-268.

Sukharev, S. I., Blount, P., Martinac, B. & Kung, C. 1997. *Annual Review of Physiology* 59: 633-657.

Sukharev, S. I., Schroeder, M. J. & McCaslin, D. R. 1999a. *Journal of Membrane Biology* 171: 183-193.

Sukharev, S. I., Sigurdson, W. J., Kung, C. & Sachs, F. 1999b. *Journal of General Physiology* 113: 525-539.

Sukharev, S. I. 2000. *Trends in Microbiology* 8: 12-13.

Sukharev, S. I., Betanzos, M., Chiang, C. S. & Guy, H. R. 2001a. *Nature* 409: 720-724.

Sukharev, S. I., Durell, S. R. & Guy, H. R. 2001b. *Biophysical Journal* 81: 917-936.

Sukharev, S. I. & Anishkin, A. 2004. *Trends in Neurosciences* 27: 345-351.

Sukharev, S. I. & Guy, H. R. Research snapshots: models of the *E. coli* MscL in the closed, expanded and open states. 2004. http://www.life.umd.edu/biology/sukharevlab/research.htm

Tanford, C. 1980. The Hydrophobic Effect: Formation of Micelles and Biological Membranes. New York: John Wiley & Sons.

Thompson, J. D., Plewnial, F., Thierry, J. C. & Poch, O. 2000. *Nucleic Acids Research* 28: 2919-2926.

Ulmschneider, M. B. & Sansom, M. S. P. 2001. *Biochimica et Biophysica Acta-Biomembranes* 1512: 1-14.

Valiyaveetil, F. I., Zhou, Y. F. & MacKinnon, R. 2002. *Biochemistry* 41: 10771-10777.

van der Heide, T. & Poolman, B. 2000. *Proceedings of the National Academy of Sciences of the United States of America* 97: 7102-7106.

van der Heide, T., Stuart, M. C. A. & Poolman, B. 2001. *Embo Journal* 20: 7022-7032.

van Voorst, F. & de Kruijff, B. 2000. *Biochemical Journal* 347: 601-612.

von Heijne, G. 1994. *Annual Review of Biophysics and Biomolecular Structure* 23: 167-192.

Webb, R. J., East, J. M., Sharma, R. P. & Lee, A. G. 1998. *Biochemistry* 37: 673-679.

White, D. 2000. In White, D. (Ed) The Physiology and Biochemistry of Prokaryotes (pp. 384-397). New York: Oxford University Press.

White, S. H., Ladokhin, A. S., Jayasinghe, S. & Hristova, K. 2001. *Journal of Biological Chemistry* 276: 32395-32398.

Wiener, M. C. & White, S. H. 1992. *Biophysical Journal* 61: 428-433.

Williamson, I. M., Alvis, S. J., East, J. M. & Lee, A. G. 2002. *Biophysical Journal* 83: 2026-2038.

Wood, J. M. 1999. *Microbiology and Molecular Biology Reviews* 63: 230-262.

Wood, J. M., Bremer, E., Csonka, L. N., Krämer, R., Poolman, B., van der Heide, T. & Smith, L. T. 2001. *Comparative Biochemistry and Physiology A-Molecular & Integrative Physiology* 130: 437-460.

Yoshimura, K., Batiza, A. F., Schroeder, M., Blount, P. & Kung, C. 1999. *Biophysical Journal* 77: 1960-1972.

Yoshimura, K., Batiza, A. F. & Kung, C. 2001. *Biophysical Journal* 80: 2198-2206.

Zelent, B., Kusba, J., Gryczynski, I., Johnson, M. L. & Lakowicz, J. R. 1996. *Journal of Physical Chemistry* 100: 18592-18602.